(12) INTERNATIONAL APPLICATION PUBLISHED UNDER THE PATENT COOPERATION TREATY (PCT)

(19) World Intellectual Property Organization
International Bureau

(43) International Publication Date
22 August 2019 (22.08.2019)

WIPO | PCT

(10) International Publication Number
WO 2019/161136 A1

(51) International Patent Classification:
A61F 2/28 (2006.01) *A61L 27/00* (2006.01)
A61K 35/32 (2015.01) *A61L 27/54* (2006.01)
A61K 38/18 (2006.01) *A61P 19/08* (2006.01)

(21) International Application Number:
PCT/US2019/018115

(22) International Filing Date:
14 February 2019 (14.02.2019)

(25) Filing Language: English

(26) Publication Language: English

(30) Priority Data:
62/630,557 14 February 2018 (14.02.2018) US

(71) Applicant: **CORNELL UNIVERSITY** [US/US]; 395 Pine Tree Road, Suite 310, Ithaca, New York 14850 (US).

(72) Inventors: **GREENBLATT, Matthew**; 1161 York Avenue, Apt. 1a, New York, New York 10065 (US). **XU, Ren**; 465 Main Street, Apt. 7C, New York, New York 10044 (US). **GLIMCHER, Laurie H.**; 100 Beacon St., Unit 3A, Boston, Massachusetts 02116 (US).

(74) Agent: **PERDOK, Monique M.** et al.; Schwegman, Lundberg & Woessner, P.A., P.O. Box 2938, Minneapolis, Minnesota 55402 (US).

(81) Designated States *(unless otherwise indicated, for every kind of national protection available)*: AE, AG, AL, AM, AO, AT, AU, AZ, BA, BB, BG, BH, BN, BR, BW, BY, BZ, CA, CH, CL, CN, CO, CR, CU, CZ, DE, DJ, DK, DM, DO, DZ, EC, EE, EG, ES, FI, GB, GD, GE, GH, GM, GT, HN, HR, HU, ID, IL, IN, IR, IS, JO, JP, KE, KG, KH, KN, KP, KR, KW, KZ, LA, LC, LK, LR, LS, LU, LY, MA, MD, ME, MG, MK, MN, MW, MX, MY, MZ, NA, NG, NI, NO, NZ, OM, PA, PE, PG, PH, PL, PT, QA, RO, RS, RU, RW, SA, SC, SD, SE, SG, SK, SL, SM, ST, SV, SY, TH, TJ, TM, TN, TR, TT, TZ, UA, UG, US, UZ, VC, VN, ZA, ZM, ZW.

(84) Designated States *(unless otherwise indicated, for every kind of regional protection available)*: ARIPO (BW, GH, GM, KE, LR, LS, MW, MZ, NA, RW, SD, SL, ST, SZ, TZ, UG, ZM, ZW), Eurasian (AM, AZ, BY, KG, KZ, RU, TJ, TM), European (AL, AT, BE, BG, CH, CY, CZ, DE, DK, EE, ES, FI, FR, GB, GR, HR, HU, IE, IS, IT, LT, LU, LV, MC, MK, MT, NL, NO, PL, PT, RO, RS, SE, SI, SK, SM, TR), OAPI (BF, BJ, CF, CG, CI, CM, GA, GN, GQ, GW, KM, ML, MR, NE, SN, TD, TG).

Published:
— *with international search report (Art. 21(3))*
— *with sequence listing part of description (Rule 5.2(a))*

(54) Title: SLIT AND BONE GROWTH MODULATION

(57) Abstract: Methods and compositions are described herein that promote bone formation. Such methods and compositions include SLIT3 or SLIT2 agents that can be administered to a subject (e.g., one in need thereof). Methods are also described herein that reduce or prevent unwanted bone formation. Such methods can involve administering an inhibitor of SLIT3 or SLIT2 to a subject.

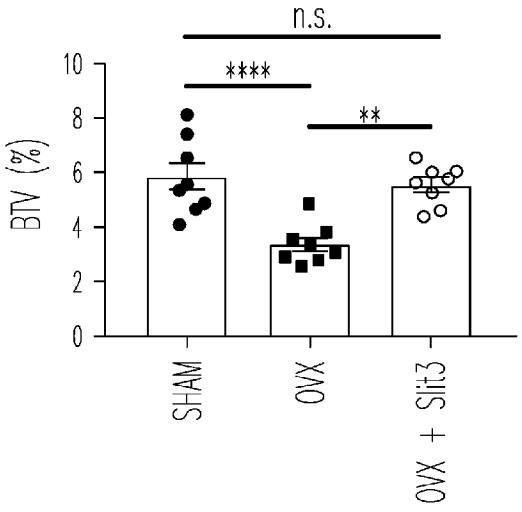

Fig. 28B-1

WO 2019/161136 A1

SLIT and Bone Growth Modulation

[0001] This application claims benefit of priority to the filing date of U.S. Provisional Application Ser. No. 62/630,557, filed February 14, 2018, the contents of which are specifically incorporated by reference herein in their entirety.

Background

[0002] There is an urgent need to develop improved methods to treat osteoporosis and other disorders of low bone mass. One in two women and one in four men will experience a fracture due to osteoporosis during their lifetimes. In total, osteoporosis kills as many women each year as breast cancer. Moreover, medical systems are vastly undertreating osteoporosis, and one factor in this undertreatment is a concern regarding the highly publicized side effects of existing drugs, such as the atypical femoral fractures or osteonecrosis of the jaw occurring with bisphosphonate, the most commonly used class of anti-osteoporosis drugs.

[0003] Drugs for the treatment of osteoporosis typically fall into one of two categories. They function either to block bone resorption by osteoclasts or to augment bone formation by osteoblasts. Such different categories of anti-osteoporosis medications can have distinct uses. For instance, augmenting bone formation during the repair of bones, as may occur after a traumatic fracture, tumor resection, or after surgical management of other orthopedic problems, is desirable, as substantial secondary morbidity can be associated with prolonged convalescence from these injuries. Complete failure of bone healing is a common occurrence in patients with other comorbid conditions including vascular diseases such as diabetes or disorders causing ongoing inflammation. Impaired healing is commonly noted when optimal physical stabilization of the injury site cannot be achieved by orthopedic surgical approaches or when the injury size is too large (so-called critical-sized defects). However, so far, no existing anabolic agent has demonstrated clear activity in clinical studies to enhance bone healing across any of these indications.

[0004] It is increasingly appreciated that the ancillary cell types present in bone tissue actively participate in osteogenesis. For example, a subset of $CD31^{hi}$, $endomucin^{hi}$ ($EMCN^{hi}$) vascular endothelium has been recently identified as residing in the bone marrow (BM) near the growth plate. $CD31^{hi}EMCN^{hi}$ endothelium, also known as "type H endothelium", is believed to actively direct bone formation, as alterations in $CD31^{hi}EMCN^{hi}$ endothelium impact bone architecture, bone formation, and numbers of osteoprogenitors present in the marrow (Kusumbe, Ramasamy, and Adams 2014, Ramasamy et al. 2014). $CD31^{hi}EMCN^{hi}$ endothelium levels can be altered by platelet-derived growth factor type BB (PDGF-BB), providing a potential link between bone

resorption activity by osteoclasts and CD31^{hi}EMCN^{hi} endothelium (Xie et al. 2014). However, it is currently unclear if and how levels of CD31^{hi}EMCN^{hi} endothelium are coupled with the physiologic need for bone formation and whether osteoblasts participate in this regulation.

[0005] The inventors and coworkers have previously shown that the adaptor protein Schnurri3 (SHN3) is a suppressor of osteoblast activity, as mice lacking SHN3 display a progressive increase in postnatal bone mass due to augmented bone formation (Shim et al. 2013, Jones et al. 2006). As deletion of *Shn3* in osteoblast-lineage cells is sufficient to greatly enhance bone formation, it appears that osteoblasts can coordinate the various tissue activities beyond osteoblast-mediated matrix secretion needed to form mature bone.

Summary

[0006] Described herein are methods for prevention of bone loss or for promoting bone growth, bone-strengthening, or bone healing in a subject in need thereof, comprising administering a composition that included a SLIT3 or SLIT2 agent to said subject. It may be in the form of a protein or an expression vector that can express the SLIT3 or SLIT2 protein. The composition can be delivered locally and may be targeted to bone. It may be delivered by injection or in combination with a carrier or medical device. The bone formation may involve promoting the formation or growth of CD31^{hi}EMCN^{hi} endothelium.

[0007] Also described herein are methods of preventing bone growth in a subject in need thereof, comprising administering a SLIT3 or SLIT2 inhibiting agent to said subject. The SLIT3 or SLIT2 inhibiting agent may be targeted to bone or delivered locally. The SLIT3 or SLIT2 inhibiting agent is a small interfering RNA or an antibody.

[0008] As shown herein, CD31^{hi}EMCN^{hi} skeletal vasculature is increased in mice with an inducible deletion of *Shn3* in osteoblasts and CD31^{hi}EMCN^{hi} endothelium is regulated by osteoblasts. More significantly, the secreted ligand SLIT3 as a novel SHN3-controlled, osteoblast-derived regulator of CD31^{hi}EMCN^{hi} endothelium levels. SLIT3 belongs to a conserved family of SLIT ligands that were initially discovered in the context of CNS development, where they mediate axonal guidance through ROBO receptors (Robo1-4) (Nguyen Ba-Charvet et al. 1999, Jaworski and Tessier-Lavigne 2012). Subsequent studies showed SLITs are widely expressed, and the SLIT/ROBO pathway has been implicated in multiple physiological functions outside of the nervous system such as angiogenesis/vasculogenesis (Jones et al. 2008, Rama et al. 2015, Vasam et al. 2017), stem cell regulation (Geutskens et al. 2012, Zhou et al. 2013) and cancer development (Mehlen, Delloye-Bourgeois, and Chedotal 2011). Additionally, SLIT3 has been identified as a proangiogenic factor in mouse models and human engineered

tissue (Zhang et al. 2009, Paul et al. 2013). However, the role of SLIT3 in bone metabolism was largely unclear until this work. Herein, we used genetic models to demonstrate that osteoblast-derived SLIT3 controls levels of skeletal $CD31^{hi}EMCN^{hi}$ endothelium and bone mass accrual. Furthermore, we provide proof-of principle that exogenous SLIT3 administration is a novel class of vascular-targeted therapeutics for the treatment of disorders of low bone mass or for enhancing fracture healing.

Brief Description of the Drawings

[0009] FIG. 1A-1F illustrate that *Shn3*$^{-/-}$ mice have increased skeletal vasculature and $CD31^{hi}EMCN^{hi}$ endothelium. FIG. 1A shows representative images of 2-week-old mouse femurs stained with CD31 and 4',6-diamidino-2-phenylindole (DAPI) (n=4 per group) (Top, lower power; Bottom, higher power). Growth plate (GP) and cortical bone (CB) are marked. Scale bars, 300μm (lower power) and 100μm (higher power). FIG. 1B shows representative images of 2-week-old mouse femurs stained with Endomucin (EMCN) and 4',6-diamidino-2-phenylindole (DAPI) (n=4 per group) (Top, lower power; Bottom, higher power). FIG. 1C-1 graphically illustrates relative CD31-positive in the bone marrow cavity (n=4 per group). FIG. 1C-2 graphically illustrates relative EMCN-positive vessel area in the bone marrow cavity (n=4 per group). FIG. 1D shows representative image of CD31 and EMCN dual-immunostained femur sections from the femur in 2-week-old mice. Scale bars, 100μm, n=3 per group. FIG. 1E shows representative flow cytometry plots of $CD31^{hi}Emcn^{hi}$ endothelial cells in $Ter119^{-}$ and $CD45^{-}$ cell population from the femur in 2-week-old mice (n=4 per group). FIG. 1F illustrates the relative frequency of $CD31^{hi}Emcn^{hi}$ endothelial cells in $Ter119^{-}$ and $CD45^{-}$ cell population from the femur in 2-week-old mice (n=4 per group). Values represent mean ± s.e.m.; $^{**}P < 0.01$ and $^{***}P < 0.001$ by an unpaired two-tailed Student's *t*-test in all panels.

[0010] FIG. 2A-2L illustrate that ablation of *Shn3* in osteoblasts selectively enhances osteogenesis and angiogenesis *in vivo*. FIG. 2A-1 shows representative micro-CT (μCT) images of trabecular bone in the distal femurs of *Shn3*$^{f/f}$ (n=7) and *Shn3* conditional knockout *Shn3*^{dmp1} mice (n=8) at 8-weeks of age. Scale bars, 1mm. FIG. 2A-2 graphically illustrates relative quantitative analysis of bone volume/total volume (BV/TV) in *Shn3*$^{f/f}$ (n=7) and *Shn3*^{dmp1} mice (n=8) at 8-weeks of age. Scale bars, 1mm. FIG. 2B-1 shows representative histomorphometry images of the L3 vertebrae in *Shn3*$^{f/f}$ (n=6) and *Shn3*^{dmp1} mice (n=5) at 8-weeks of age. Scale bars, 500μm. FIG. 2B-2 graphically illustrates quantitative analysis of bone volume/total volume in *Shn3*$^{f/f}$ (n=6) and *Shn3*^{dmp1} mice (n=5) at 8-weeks of age. FIG. 2C shows representative calcein double labeling images of the L3 vertebrae in *Shn3*$^{f/f}$ mice (n=6) and *Shn3*^{dmp1} mice (n=6) at 8-weeks of age. FIG. 2D graphically illustrates quantification of histomorphometric

parameters of the L3 vertebrae in *Shn3*$^{f/f}$ mice (n=6) and *Shn3*^{dmp1} mice (n=6) at 8-weeks of age. Trabecular mineral apposition rate (MAR, mm day^{-1}), bone formation rate/bone surface (BFR/BS, mm^3 mm^{-2} yr^{-1}), osteoclast number/bone perimeter (No. Oc./B. Pm) and osteoblast surface/bone surface (Ob.S/BS, %). FIG. 2E shows representative confocal images of femurs from 2-week old mice with EMCN and CD31 n=3, per group. GP, growth plate. Scale bars, 100 μm. FIG. 2F shows representative flow cytometry plots of CD31^{hi}Emcn^{hi} endothelial cells from the femur of 2-week-old *Shn3*^{dmp1} (n=6) and *Shn3*$^{f/f}$ littermate control (n=5) mice. FIG. 2G graphically illustrates relative frequency of CD31^{hi}Emcn^{hi} endothelial cells in the femur of 2-week-old *Shn3*^{dmp1} (n=6) and *Shn3*$^{f/f}$ littermate control (n=5) mice. FIG. 2H shows representative μCT images of the trabecular bone in the distal femur metaphysis of *Shn3*$^{f/f}$ (oil =7; tamoxifen =7) and in mice exhibiting tamoxifen-inducible inhibition of *Shn3* (*Shn3*$^{ocn-ert2}$ mice) (oil =6; tamoxifen =8) twelve-weeks after tamoxifen injection or corn oil injection at 4-weeks of age. FIG. 2I graphically illustrates relative quantitative analysis of bone volume/total volume in *Shn3*$^{f/f}$ mice (oil =7; tamoxifen =7) and in mice exhibiting tamoxifen-inducible inhibition of *Shn3* (*Shn3*$^{ocn-ert2}$ mice) (oil =6; tamoxifen =8) twelve-weeks after tamoxifen injection or corn oil injection at 4-weeks of age. FIG. 2J shows representative confocal images of endomucin (red) immunostained femur sections from *Shn3*$^{f/f}$ (n=3) and *Shn3*$^{ocn-ert2}$ mice (n=3) at 4-weeks after tamoxifen injection into 4-week old mice. GP, growth plate. Scale bars, 300 μm. FIG. 2K shows representative flow cytometry plots of CD31^{hi}Emcn^{hi} endothelial cells from the femurs of *Shn3*$^{f/f}$ (n=5) and *Shn3*$^{ocn-ert2}$ mice (n=5) 6-weeks after tamoxifen injection at 4-weeks of age. FIG. 2L graphically illustrates relative frequency of CD31^{hi}Emcn^{hi} endothelial cells from the femurs of *Shn3*$^{f/f}$ (n=5) and *Shn3*$^{ocn-ert2}$ mice (n=5) 6-weeks after tamoxifen injection at 4-weeks of age. Values represent mean ± s.e.m.; n.s., not significant and *, $P < 0.05$; **, $P < 0.01$; ***, $P < 0.001$ all by an unpaired two-tailed Student's *t*-test or by one-way ANOVA followed by a Tukey's posttest in all panels.

[0011] FIG. 3A-3M illustrate that inhibition of *Shn3* enhances *Slit3* expression in osteoblasts. FIG. 3A shows representative images of bone marrow-derived endothelial progenitor outgrowth cells (EPOCs) from a transwell migration assay. FIG 3B graphically illustrates migrated cells per field from a transwell migration assay of bone marrow-derived endothelial progenitor outgrowth cells (EPOCs). Basal medium, (BM); Conditioned medium, (CM). n=5 per group. FIG 3C shows representative images of tube branches from a Matrigel tube formation assay of EPOCs. FIG. 3D graphically illustrates relative quantification of tube branch numbers from a Matrigel tube formation assay with EPOCs. n=5 per group. FIG. 3E illustrates gene ontology (GO) enrichment analysis of differentially expressed genes between *Shn3*$^{-/-}$ mice and littermate control

mice. Each bar is colored and labeled according to p-value of enrichment analysis, where darker colors indicate greater differential expression than lighter colors. FIG. 3F illustrates a heatmap of proangiogenic gene expression from three independently derived sets of primary osteoblasts from *Shn3*$^{+/+}$and *Shn3*$^{-/-}$ mice. FIG. 3G graphically illustrates relative RNA expression as detected by real-time PCR analysis of *Slit3* expression in *Shn3*$^{+/+}$and *Shn3*$^{-/-}$ osteoblasts. FIG. 3H-1 graphically illustrates *Slit3* mRNA expression in human mesenchymal stromal cells (hMSCs) expressing a control vector or *Shn3* shRNAs cultured under osteogenic conditions. n=4 per group. FIG. 3H-2 shows a protein blot illustrating protein levels of *Slit3* in human mesenchymal stromal cells (hMSCs) expressing a control vector or *Shn3* shRNAs cultured under osteogenic conditions. n=4 per group. FIG. 3I-1 graphically illustrates mRNA levels of *Slit3* in hMSCs transgenically expressing *Shn3* and mRNA levels of *Slit3* in hMSCs transformed with a control vector where the hMSCs were cultured in osteogenic conditions. n=4, per group. FIG. 3I-2 shows a protein blot illustrating protein levels of *Slit3* in hMSCs having a control vector or a vector encoding *Shn3* when the hMSCs were cultured under osteogenic conditions. n=4, per group. FIG. 3J graphically illustrates results of an ELISA for SLIT3 in osteoblast conditioned media (CM). n=6 per group. FIG. 3K graphically illustrates results of quantitative real-time PCR analysis of *Slit3* in *Shn3*$^{+/+}$ osteoblasts and in osteoblasts expressing a defective Shn3 (resulting from knock-in of a mutation in 3 amino acids within the ERK interacting motif of Shn3, *Shn3*$^{KI/KI}$) osteoblasts. FIG. 3L graphically illustrates results of quantitative real-time PCR analysis of *Slit3* in hMSCs treated with the indicated doses of trametinib (TTNB). n=4 per group. FIG. 3M shows representative confocal images of CD31 and endomucin (red) dual immunostained sections from the femur of 2-week-old *Shn3*$^{KI/KI}$ mice or controls n=3 per group. GP, growth plate. Scale bars, 100μm. Values represent mean ± s.e.m.; n.s., not significant, $*P < 0.05$, $**P < 0.01$, $***P < 0.001$ and $****P < 0.0001$ by an unpaired two-tailed Student's *t*-test or one-way ANOVA followed by a Tukey's posttest in all panels.

[0012] FIG. 4A-4L illustrate that *Slit3*$^{-/-}$ mice have decreased skeletal vasculature and bone mass. FIG. 4A shows representative images of tube branches formed in a Matrigel tube formation assay of endothelial progenitor outgrowth cells (EPOCs) in varying concentrations of Slit3. Scale bars, 200μm. FIG. 4B graphically illustrates that the quantity of tube branch numbers increases with increased Slit3 as measured in a Matrigel tube formation assay with endothelial progenitor outgrowth cells (EPOCs). n=5 per group. FIG. 4C shows representative images of endothelial progenitor outgrowth cells (EPOCs) of various genotypes cultured under different conditions in a Matrigel tube formation assay. Where indicated, a SLIT3-neutralizing antibody or a

related isotype control was added. n=5 per group. Scale bars, 200μm. FIG. 4D graphically illustrates relative quantification of tube branch numbers in a Matrigel tube formation assay of endothelial progenitor outgrowth cells (EPOCs) of various genotypes cultured under different conditions in a Matrigel tube formation assay. Where indicated, a SLIT3-neutralizing antibody or a related isotype control was added. n=5 per group. FIG. 4E shows representative confocal images of CD31-immunostained sections of the bone marrow cavity from the femur of 2-week-old mice. n=4 per group. Scale bars, 300μm (lower power) and 100μm (higher power). FIG. 4F shows representative confocal images of endomucin-immunostained sections of the bone marrow cavity from the femur of 2-week-old mice. n=4 per group. Scale bars, 300μm (lower power) and 100μm (higher power). FIG. 4G-1 graphically illustrates quantification of relative CD31-postive vessel area in the bone marrow cavity from the femur of 2-week-old mice. n=4 per group. 4G-2 graphically illustrates quantification of relative endomucin-positive vessel area in the bone marrow cavity from the femur of 2-week-old mice. n=4 per group. Scale bars, 300μm (lower power) and 100μm (higher power). FIG. 4H-1 shows representative images of the L3 vertebrae in *Slit3*$^{+/+}$ mice and *Slit3*$^{-/-}$ mice. Scale bars, 500μm. FIG. 4H-2 graphically illustrates quantitative analysis of bone volume/total volume in *Slit3*$^{+/+}$ mice and *Slit3*$^{-/-}$ mice at 6-weeks of age. n=7 per group. FIG. 4H-3 graphically illustrates quantitative analysis of cortical bone thickness in *Slit3*$^{+/+}$ mice and *Slit3*$^{-/-}$ mice at 6-weeks of age. n=7 per group. FIG. 4I-1 shows representative μCT images of trabecular bone in the distal femur metaphysis in *Slit3*$^{+/+}$ mice (n=8) and *Slit3*$^{-/-}$ mice. Scale bars, 1mm. FIG. 4I-2 graphically illustrates quantitative analysis of bone volume/total volume in *Slit3*$^{+/+}$ mice (n=8) and *Slit3*$^{-/-}$ mice (n=6) at 12-weeks of age. FIG. 4H-3 graphically illustrates quantitative analysis of cortical bone thickness in *Slit3*$^{+/+}$ mice (n=8) and *Slit3*$^{-/-}$ mice (n=6) at 12-weeks of age. FIG. 4J shows representative confocal images of CD31 (top) immunostained, and CD31 and endomucin dual-immunostained, bone sections from the femurs of 2-week-old *OSX-cre* and *Slit3*^{osx} mice. n=4 per group. Scale bars, 300μm (lower power) and 100μm (higher power). FIG. 4K-1 shows representative μCT images of trabecular bone in the distal femur metaphysis of *OSX-cre* (n=6) and *Slit3*^{osx} mice (n=6) at 3-weeks of age. Scale bars, 1mm. FIG. 4K-2 graphically illustrates quantitative analysis of bone volume/total volume in *OSX-cre* (n=6) and *Slit3*^{osx} mice (n=6) at 3-weeks of age. FIG. 4L-1 shows representative μCT images of cortical bone in the distal femur metaphysis of *OSX-cre* (n=6) and *Slit3*^{osx} mice (n=6) at 3-weeks of age. Scale bars, 1mm. FIG. 4L-2 graphically illustrates quantitative analysis of cortical bone thickness in *OSX-cre* (n=6) and *Slit3*^{osx} mice (n=6) at 3-weeks of age. Values represent mean ± s.e.m.; $^{*}P < 0.05$,

$^{**}P < 0.01$, $^{***}P < 0.001$ and $^{****}P < 0.0001$ by an unpaired two-tailed Student's *t*-test or one-way ANOVA followed by a Tukey's posttest in all panels.

[0013] FIG. 5A-5H illustrate that *Slit3* contributes to the ability of *Shn3* to control osteogenesis and $CD31^{hi}EMCN^{hi}$ endothelium *in vivo*. FIG. 5A shows representative confocal images of CD31 and endomucin dual-immunostained bone sections. GP, growth plate. Scale bars, 100μm. FIG. 5B-1 illustrates representative flow cytometry dot plots of $CD31^{hi}Emcn^{hi}$ endothelial cells (b, right) of the femur in 2-week-old $Shn3^{+/+}$ $Slit3^{+/+}$ (n=5), $Shn3^{+/+}$ $Slit3^{-/-}$ (n=3), $Shn3^{-/-}$ $Slit3^{+/+}$ (n=5) and $Shn3^{-/-}$ $Slit3^{-/-}$ mice (n=5). FIG. 5B-2 illustrates relative frequency of $CD31^{hi}Emcn^{hi}$ endothelial cells of the femur in 2-week-old $Shn3^{+/+}$ $Slit3^{+/+}$ (n=5), $Shn3^{+/+}$ $Slit3^{-/-}$ (n=3), $Shn3^{-/-}$ $Slit3^{+/+}$ (n=5) and $Shn3^{-/-}$ $Slit3^{-/-}$ mice (n=5). FIG. 5C-1 shows representative μCT images of the trabecular bone in the distal femur metaphysis of 6-week-old $Shn3^{+/+}$ $Slit3^{+/+}$(n=7), $Shn3^{+/+}$ $Slit3^{-/-}$ (n=7), $Shn3^{-/-}$ $Slit3^{+/+}$(n=7) and $Shn3^{-/-}$ $Slit3^{-/-}$ mice (n=6). Scale bar, 1mm. FIG. 5C-2 graphically illustrates percent BV/TV (bone volume/total volume) of 6-week-old $Shn3^{+/+}$ $Slit3^{+/+}$(n=7), $Shn3^{+/+}$ $Slit3^{-/-}$(n=7), $Shn3^{-/-}$ $Slit3^{+/+}$(n=7) and $Shn3^{-/-}$ $Slit3^{-/-}$ mice (n=6). FIG. 5D shows representative images of calcein labelling of 6-week-old $Shn3^{+/+}$ $Slit3^{+/+}$(n=5), $Shn3^{+/+}$ $Slit3^{-/-}$(n=6), $Shn3^{-/-}$ $Slit3^{+/+}$(n=4) and $Shn3^{-/-}$ $Slit3^{-/-}$ mice (n=5). Scale bars, 100μm. FIG. 5E graphically illustrates histomorphometric analysis of mineral apposition rate (MAR, mm day^{-1}) in 6-week-old $Shn3^{+/+}$ $Slit3^{+/+}$(n=5), $Shn3^{+/+}$ $Slit3^{-/-}$(n=6), $Shn3^{-/-}$ $Slit3^{+/+}$(n=4) and $Shn3^{-/-}$ $Slit3^{-/-}$ mice (n=5). FIG. 5F-1 graphically illustrates bone volume/ total volume in 6-week-old $Shn3^{+/+}$ $Slit3^{+/+}$(n=5), $Shn3^{+/+}$ $Slit3^{-/-}$ (n=6), $Shn3^{-/-}$ $Slit3^{+/+}$(n=4) and $Shn3^{-/-}$ $Slit3^{-/-}$ mice (n=5) in 6-week-old $Shn3^{+/+}$ $Slit3^{+/+}$(n=5), $Shn3^{+/+}$ $Slit3^{-/-}$(n=6), $Shn3^{-/-}$ $Slit3^{+/+}$(n=4) and $Shn3^{-/-}$ $Slit3^{-/-}$ mice (n=5). FIG. 5F-2 graphically illustrates bone formation rate/bone surface (BFR/BS, mm3 mm^{-2} yr^{-1}) in 6-week-old $Shn3^{+/+}$ $Slit3^{+/+}$(n=5), $Shn3^{+/+}$ $Slit3^{-/-}$(n=6), $Shn3^{-/-}$ $Slit3^{+/+}$(n=4) and $Shn3^{-/-}$ $Slit3^{-/-}$ mice (n=5). FIG. 5G-1 shows representative μCT images of the trabecular bone in the distal femur metaphysis in 12-week-old $Robo1^{+/+}$ (n=8) and $Robo1^{-/-}$ mice (n=6). Scale bars, 1mm. FIG. 5G-2 graphically illustrates bone volume / total volume in 12-week-old $Robo1^{+/+}$ (n=8) and $Robo1^{-/-}$ mice (n=6). Scale bars, 1mm. FIG. 5H shows representative confocal images of CD31-stained, endomucin-stained and DAPI immunostained femurs from 2-week-old $Robo1^{-/-}$ mice (n=3) and littermate controls (n=3). Arrows highlight the region containing $CD31^{hi}EMCN^{hi}$ endothelium near the growth plate (GP). Scale bars, 100μm. Values represent mean ± s.e.m.; $^{*}P < 0.05$, $^{**}P < 0.01$, $^{***}P < 0.001$ and $^{****}P < 0.0001$ by an unpaired two-tailed Student's *t*-test or by one-way ANOVA followed by a Tukey's posttest in all panels.

[0014] FIG. 6A-6N shows that administration of recombinant SLIT3 has therapeutic effects on bone fracture healing and ovariectomy-induced bone loss. FIG.

6A shows representative μCT images of mouse femurs 21 days after open femoral midshaft fracture in *Shn3*$^{+/+}$ *Slit3*$^{+/+}$, *Shn3*$^{+/+}$ *Slit3*$^{-/-}$, *Shn3*$^{-/-}$ *Slit3*$^{+/+}$ and *Shn3*$^{-/-}$ *Slit3*$^{-/-}$ mice. Scale bar = 1 mm in μCT. FIG. 6B shows representative μCT images of H&E stained and mouse femurs subjected to EMCN immunohistochemistry 21 days after open femoral midshaft fracture in *Shn3*$^{+/+}$ *Slit3*$^{+/+}$, *Shn3*$^{+/+}$ *Slit3*$^{-/-}$, *Shn3*$^{-/-}$ *Slit3*$^{+/+}$ and *Shn3*$^{-/-}$ *Slit3*$^{-/-}$ mice. Arrowheads highlight EMCN positive vessels located in the fracture callus. Scale bar = 200 μm in H&E and 100 μm in EMCN immunohistochemistry (IHC). FIG. 6C graphically illustrates non-union frequency of the fractured femora 4 weeks after open femoral midshaft fracture *Shn3*$^{+/+}$ *Slit3*$^{+/+}$, *Shn3*$^{+/+}$ *Slit3*$^{-/-}$, *Shn3*$^{-/-}$ *Slit3*$^{+/+}$ and *Shn3*$^{-/-}$ *Slit3*$^{-/-}$ mice (n≥4, per group). FIG. 6D graphically illustrates μCT measurement of BV/TV (bone volume/total volume) in callus area of the fractured femora 4 weeks after open femoral midshaft fracture *Shn3*$^{+/+}$ *Slit3*$^{+/+}$, *Shn3*$^{+/+}$ *Slit3*$^{-/-}$, *Shn3*$^{-/-}$ *Slit3*$^{+/+}$ and *Shn3*$^{-/-}$ *Slit3*$^{-/-}$ mice (n≥4, per group). FIG. 6E-1 graphically illustrates EMCN positive vessel number in the fractured femora 4 weeks after open femoral midshaft fracture *Shn3*$^{+/+}$ *Slit3*$^{+/+}$, *Shn3*$^{+/+}$ *Slit3*$^{-/-}$, *Shn3*$^{-/-}$ *Slit3*$^{+/+}$ and *Shn3*$^{-/-}$ *Slit3*$^{-/-}$ mice (n≥4, per group). FIG. 6E-2 graphically illustrates results maximum load as assessed by bio-mechanical testing of the maximum compressive load of the fractured femora 4 weeks after open femoral midshaft fracture *Shn3*$^{+/+}$ *Slit3*$^{+/+}$, *Shn3*$^{+/+}$ *Slit3*$^{-/-}$, *Shn3*$^{-/-}$ *Slit3*$^{+/+}$ and *Shn3*$^{-/-}$ *Slit3*$^{-/-}$ mice (n≥4, per group). FIG. 6F shows representative μCT images of mouse femurs 21 days post-fracture with IV injection of SLIT3 or PBS. Scale bar = 1 mm for μCT. FIG. 6G shows representative H&E stained and EMCN (insert) immunohistochemically stained images of mouse femurs 21 days post-fracture with IV injection of SLIT3 or PBS. Scale bar = 1 mm for μCT, 200 μm in H&E and 100μm in EMCN IHC. FIG. 6H graphically illustrates μCT measurement of BV/TV in callus area of femurs after IV injection of SLIT3 or PBS 21 days after fracture (n≥4, per group). FIG. 6I-1 graphically illustrates EMCN positive vessel number in femurs after IV injection of SLIT3 or PBS 21 days after fracture (n≥4, per group). FIG. 6I-2 graphically illustrates EMCN positive vessel volume in femurs after IV injection of SLIT3 or PBS 21 days after fracture (n≥4, per group). FIG. 6J-1 graphically illustrates results of bio-mechanical test of maximum compressive load of femurs after IV injection of SLIT3 or PBS 21 days after fracture (n≥4, per group). FIG. 6J-2 graphically illustrates results of bio-mechanical test of stiffness of femurs after IV injection of SLIT3 or PBS 21 days after fracture (n≥4, per group). FIG. 6K-1 graphically illustrates results of measurement of fracture callus BV/TV of mouse femurs harvested 21 days post-fracture with insertion of a gelatin sponge soaked with SLIT3 or vehicle. A no sponge control is included. FIG. 6K-2 graphically illustrates results of biomechanical testing of maximum load of mouse femurs harvested 21 days post-fracture with insertion of a gelatin sponge

soaked with SLIT3 or vehicle. A no sponge control is included. FIG. 6L shows representative images of CD31 and EMCN dual-immunostained callus sections of mouse femurs 21 days post-fracture with insertion of a gelatin sponge soaked with SLIT3 or vehicle at the time of fracture. Scale bars, 300μm, n=3 per group. FIG. 6M shows representative μCT images of the trabecular bone in the distal femur of mice after sham-operation (Sham), or in ovariectomized (OVX) mice, where the OVX mice were treated with vehicle, SLIT3, or parathyroid hormone (PTH) injection. Scale bars, 1mm. FIG. 6N graphically illustrates relative quantitative analysis of bone volume/total volume in trabecular bone in the distal femur of mice after sham-operation (Sham), or in ovariectomized (OVX) mice, where the OVX mice were treated with vehicle, SLIT3, or parathyroid hormone (PTH) injection. Values represent mean ± s.e.m; $*P < 0.05$, $**P < 0.01$, $***P < 0.001$ and $****P < 0.0001$ by a Fisher's exact test (FIG. 6C) unpaired two-tailed Student's *t*-test or by one-way ANOVA followed by a Tukey's posttest in all other panels.

[0015] FIG. 7A-7C illustrate that *Shn3*$^{-/-}$ mice have increased skeletal vasculature and CD31^{hi}EMCN^{hi} endothelium. FIG. 7A shows representative confocal images of heart, brain, lung and kidney from 2-week-old mice stained for endomucin and 4',6-diamidino-2-phenylindole (DAPI). Scale bars, 100μm, n=3 per group. FIG. 7B-1 shows representative images of CD31-postive (upper) and endomucin-positive (lower) vessel area of neonatal mice, n=4 per group. FIG. 7B-2 graphically illustrates quantification of CD31-postive (upper) and endomucin-positive (lower) vessel area of neonatal mice, n=4 per group. FIG. 7C shows a schematic representation of the strategy used for flow cytometry for analysis of CD31^{hi}EMCN^{hi} endothelial cells. Values represent mean ± s.e.m.; NS, $*P < 0.05$ and $**P < 0.01$ by an unpaired two-tailed Student's *t*-test in all panels.

[0016] FIG. 8A-8H illustrates that ablation of *Shn3* in osteoblasts enhances osteogenesis and angiogenesis in vivo. FIG. 8A-1 graphically illustrates percent BV/TV of trabecular bone in *Shn3*$^{f/f}$ and *Shn3*^{osx} mice at 8-weeks of age (male, n≥4). FIG. 8A-2 graphically illustrates cortical bone thickness in *Shn3*$^{f/f}$ and *Shn3*^{osx} mice at 8-weeks of age (male, n≥4). FIG. 8B-1 shows representative confocal images of DAPI stained metatarsals from OSX-Cre; R26-mT/mG mice at 7-days of age (male, n=3). Endosteal surface (ES), Cortical bone (CB) and Periosteal surface (PS). Scale bars, 100μm. FIG. 8B-2 shows representative confocal images of direct eGFP/tdTomato fluorescence in metatarsals from OSX-Cre; R26-mT/mG mice at 7-days of age (male, n=3). Red: membrane-targeted tdTomato; Green: membrane-targeted eGFP; Blue: DAPI. Endosteal surface (ES), Cortical bone (CB) and Periosteal surface (PS). Scale bars, 100μm. FIG. 8C-1 shows representative μCT images of bone in *Shn3*$^{f/f}$ and *Shn3*^{dmp1} mice at 8-weeks

of age (male, n≥5). Scale bars, 500 μm. FIG. 8C-2 graphically illustrates cortical bone thickness in *Shn3*$^{f/f}$ and *Shn3*^{dmp1} mice at 8-weeks of age (male, n≥5). Scale bars, 500 μm. FIG. 8D-1 graphically illustrates histomorphometric quantification of mineral apposition rate (MAR, mm day^{-1}) at the endosteal and periosteal bone surfaces of the L3 vertebrae in *Shn3*$^{f/f}$ (n=5) and *Shn3*^{dmp1} mice (n=5) at 8-weeks of age. FIG. 8D-2 graphically illustrates histomorphometric quantification of bone formation rate/bone surface (BFR/BS, mm^3 mm^{-2} yr^{-1}) at the endosteal and periosteal bone surfaces of the L3 vertebrae in *Shn3*$^{f/f}$ (n=5) and *Shn3*^{dmp1} mice (n=5) at 8-weeks of age. FIG. 8E-1 graphically illustrates histomorphometric quantification of osteoblast surface/bone surface (Ob. S/BS, %) at the endosteal bone surfaces of the L3 vertebrae in *Shn3*$^{f/f}$ mice (n=5) and *Shn3*^{dmp1} mice (n=5) at 8-weeks of age. FIG. 8E-2 graphically illustrates osteoclast number/bone perimeter (No. Oc./B. Pm) at the endosteal bone surfaces of the L3 vertebrae in *Shn3*$^{f/f}$ mice (n=5) and *Shn3*^{dmp1} mice (n=5) at 8-weeks of age. FIG. 8F shows representative confocal images of femurs from 2-week-old mice stained for CD31 (red) and DAPI (blue) (Top, low power; Bottom, high power). FIG. 8G representative confocal images of femurs from 2-week-old mice stained for Endomucin (red) and DAPI (blue) (Top, low power; Bottom, high power). GP, growth plate; CB, cortical bone. Scale bars, 300μm (lower power); 100μm (high power). FIG. 8H-1 graphically illustrates the percent of CD31-postive vessels in the bone marrow cavity in *Shn3*$^{f/f}$ and *Shn3*^{dmp1} mice (n=4). FIG. 8H-2 graphically illustrates the percent of endomucin-positive vessels in the bone marrow cavity in *Shn3*$^{f/f}$ and *Shn3*^{dmp1} mice (n=4). Values represent mean ± s.e.m.; ns, not significant, $*P < 0.05$, $**P < 0.01$, $***P < 0.001$ and $****P < 0.0001$ by an unpaired two-tailed Student's *t*-test in all panels.

[0017] FIG. 9A-9G illustrate that *Shn3* in endothelial cells is dispensable for osteogenesis and angiogenesis *in vivo*. FIG. 9A graphically illustrates *Shn3* expression in bone marrow derived endothelial cells sorted from *Shn3*$^{f/f}$ and *Shn3*^{cdh5} mice as quantified by quantitative real-time PCR analysis of (n=4). FIG. 9B shows representative confocal images of femurs from 2-week-old mice stained for CD31 and DAPI (top, lower power; bottom, high power). GP, growth plate; CB, cortical bone. Scale bars, 300μm (lower power); 100μm (high power). FIG. 9C shows representative confocal images of femurs from 2-week-old mice stained for endomucin and DAPI (top, lower power; bottom, high power). GP, growth plate; CB, cortical bone. Scale bars, 300μm (lower power); 100μm (high power). FIG. 9D-1 graphically illustrates quantification of the staining performed as described for FIG. 9B. FIG. 9D-2 graphically illustrates quantification of the staining performed as described for FIG. 9C. FIG. 9E shows representative confocal images of CD31 and endomucin immunostained sections from the femurs of 2-week-old mice (n=4 per group). GP, growth plate. FIG. 9F shows

representative μCT images of trabecular bone in the distal femur in *Shn3*$^{f/f}$ and *Shn3*^{cdh5} mice at 8-weeks of age (male, n≥6). FIG. 9G graphically illustrates results of relative quantitative analysis of bone volume/total volume (g) in *Shn3*$^{f/f}$ and *Shn3*^{cdh5} mice at 8-weeks of age (male, n≥6). Values represent mean ± s.e.m.; ns, not significant and ***$P < 0.001$ by an unpaired two-tailed Student's *t*-test in all panels.

[0018] FIG. 10 illustrates inducible inhibition of *Shn3* in osteoblasts increases cortical bone thickness. Quantitative μCT analysis of cortical bone thickness in *Shn3*$^{f/f}$ (oil =7; tamoxifen =7) and *Shn3*$^{ocn\text{-}cre}$ mice (oil =6; tamoxifen =8) at 12-weeks after tamoxifen injection or corn oil injection at 4-weeks of age. Values represent mean ± s.e.m.; n.s., not significant and **$P < 0.01$ by one-way ANOVA followed by a Tukey's posttest.

[0019] FIG. 11A-11F show that *Slit3* is expressed in osteoblasts. FIG. 11A graphically illustrates results of quantitative real-time PCR analysis of *Slit3* expression in mouse brain, lung, kidney, heart, liver, spleen, bone marrow, bones (femur and tibia after bone marrow flushing), primary osteoblasts and osteoclasts (n=4). FIG. 11B graphically illustrates results of quantitative real-time PCR analysis of *Slit3* expression during human CD14$^+$ cell differentiation with M-CSF and RANKL. Human brain cDNA (Clontech) as a positive control. FIG. 11C-1 graphically illustrates quantification of *Alpl* in human mesenchymal stem cells differentiation (n=4). FIG. 11C-2 graphically illustrates quantification of *Ibsp* in human mesenchymal stem cells differentiation (n=4). FIG. 11C-3 graphically illustrates quantification of *Slit3* in human mesenchymal stem cells differentiation (n=4). FIG. 11D-1 graphically illustrates quantification of mRNA (mRNA) levels of *Slit3* in murine primary osteoblasts (POBs) transduced with a control vector or a construct expressing SHN3 and subsequently cultured under osteogenic conditions. n=4 per group. FIG. 11D-2 graphically illustrates quantification of protein levels of *Slit3* in murine primary osteoblasts (POBs) transduced with a control vector or a construct expressing SHN3 and subsequently cultured under osteogenic conditions. n=4 per group. FIG. 11E graphically illustrates quantification of PDGF-BB in osteoblast CM and serum from *Shn3*$^{-/-}$ mice by ELISA analyses using littermate controls. FIG. 11F graphically illustrates quantification of *Slit3* expression as measured by quantitative real-time PCR analysis of in POBs treated with the indicated doses of trametinib (TTNB). n=6 per group. Values represent mean ± s.e.m.; n.s., not significant, **$P < 0.01$ and ****$P < 0.0001$ by an unpaired two-tailed Student's *t*-test or one-way ANOVA followed by a Tukey's posttest in all panels.

[0020] FIG. 12 illustrates *in vivo* expression of *Slit3* and *Robo1*. Representative confocal images of femurs from 2-week-old *Slit3*$^{+/-}$ or *Robo1*$^{+/-}$ mice with a lacZ knock-in and the control mice stained for beta-galactosidase, Endomucin and DAPI

(top, lower power; bottom, high power). GP, growth plate. Scale bars, 100μm (lower power); 40μm (high power). n=3 per group.

[0021] FIG. 13A-13B show that SLIT3 has proangiogenic activity *in vitro*. FIG. 13A-1 shows representative images from a wound healing assay of bone marrow-derived endothelial progenitor outgrowth cells (EPOCs) with SLIT3 stimulation. n=3 per group. FIG. 13A-2 graphically illustrates relative quantification results from a wound healing assay of bone marrow-derived endothelial progenitor outgrowth cells (EPOCs) with SLIT3 stimulation. n=3 per group. FIG. 13B graphically illustrates results of an Alamar blue based proliferation assay in EPOCs with SLIT3 treatment. n=5 per group. Values represent mean ± s.e.m.; $*P < 0.05$, $**P < 0.01$, $***P < 0.001$ and $****P < 0.0001$ by a two-way ANOVA followed by a Tukey's posttest in all panels.

[0022] FIG. 14A-14C show that SLIT1 and SLIT2 have proangiogenic activity. FIG. 14A-1 shows representative images of a Matrigel tube formation assay using EPOCs after SLIT1 treatment. n=5 per group. FIG. 14A-2 graphically illustrates relative quantification of tube branch numbers of a Matrigel tube formation assay in EPOCs after SLIT1 treatment. n=5 per group. FIG. 14B-1 shows representative images of a Matrigel tube formation assay using EPOCs after SLIT2 treatment. n=5 per group. FIG. 14B-2 graphically illustrates relative quantification of tube branch numbers of a Matrigel tube formation assay in EPOCs after SLIT2 treatment. n=5 per group. FIG. 14C-1 shows representative flow cytometry dot plots of $CD31^{hi}Emcn^{hi}$ endothelial cells from femurs of 8-week-old B6 mice after twice weekly IV injection of SLIT2 (1mg/kg) or vehicle initiated 21 days prior to sacrifice. FIG. 14C-2 graphically illustrates relative frequency of $CD31^{hi}Emcn^{hi}$ endothelial cells (right) in femurs of 8-week-old B6 mice after twice weekly IV injection of SLIT2 (1mg/kg) or vehicle initiated 21 days prior to sacrifice., Vehicle (n=5), SLIT2 (n=4). Values represent mean ± s.e.m.; $*P < 0.05$, $**P < 0.01$, $***P < 0.001$ and $****P < 0.0001$ by an unpaired two-tailed Student's *t*-test or a two-way ANOVA followed by a Tukey's posttest in all panels.

[0023] FIG. 15 illustrates that SLIT3 induces activation of Hippo and ERK MAPK pathway signaling in bone marrow derived endothelial cells. Effects of Slit3 treatment on YAP, AKT and ERK phosphorylation in mouse EPOCs after serum starvation are illustrated.

[0024] FIG. 16A-16B show that SLIT3 induces production of skeletal $CD31^{hi}EMCN^{hi}$ cells *in vitro* and *in vivo*. FIG. 16A shows representative flow cytometry plots (left) and relative frequency of $CD31^{hi}Emcn^{hi}$ endothelial cells (right) in cultures of EPOCs after SLIT3 stimulation, FGF2 as a positive control. FIG. 16B shows representative flow cytometry plots (left) and relative frequency of $CD31^{hi}Emcn^{hi}$ endothelial cells (right) in the $Ter119^-$, $CD45^-$ cell fraction isolated from the femurs of 8-

week-old B6 mice after twice weekly IV injection of SLIT3 (1mg/kg) or vehicle initiated 21 days prior to sacrifice. (Vehicle=5; SLIT3=4). Values represent mean ± s.e.m.; $*P < 0.05$ and $**P < 0.01$ by an unpaired two-tailed Student's *t*-test or by one-way ANOVA followed by a Tukey's posttest in all panels.

[0025] FIG. 17A-17G show that SLIT3 does not directly regulate osteoblast differentiation or activity. FIG. 17A-1 graphically illustrates body weight of 1-month old *Slit3*$^{-/-}$ mice and littermate controls (1M, n=4). FIG. 17A-2 graphically illustrates body weight of 3-month old *Slit3*$^{-/-}$ mice and littermate controls (3M, n≥5). FIG. 17B-1 graphically illustrates the trabecular osteoclast number/bone perimeter (No. Oc./B. Pm) of the L3 vertebrae in *Slit3*$^{-/-}$ mice (n=7) and littermate controls mice (n=7) at 6-weeks of age. FIG. 17B-2 graphically illustrates ELISA results for type I collagen carboxy-terminal telopeptide (CTX) levels in serum samples collected from *Slit3*$^{-/-}$ mice (n=8) and littermate controls (n=6) at 6 weeks of age. FIG. 17C-1 graphically illustrates quantitative real-time PCR analysis of *Sp7* expression levels in mouse primary osteoblasts derived from neonatal *Slit3*$^{-/-}$ mice and littermate controls (n=4 per group) after 6 days of culture under osteoblast differentiation conditions. FIG. 17C-2 graphically illustrates quantitative real-time PCR analysis of *Runx2* expression levels in mouse primary osteoblasts derived from neonatal *Slit3*$^{-/-}$ mice and littermate controls (n=4 per group) after 6 days of culture under osteoblast differentiation conditions. FIG. 17C-3 graphically illustrates quantitative real-time PCR analysis of *Ibsp* expression levels in mouse primary osteoblasts derived from neonatal *Slit3*$^{-/-}$ mice and littermate controls (n=4 per group) after 6 days of culture under osteoblast differentiation conditions. FIG. 17C-4 graphically illustrates quantitative real-time PCR analysis of *Bglap* expression levels in mouse primary osteoblasts derived from neonatal *Slit3*$^{-/-}$ mice and littermate controls (n=4 per group) after 6 days of culture under osteoblast differentiation conditions. FIG. 17D graphically illustrates alkaline phosphatase (ALP) activity in mouse primary osteoblasts derived from neonatal *Slit3*$^{-/-}$ and littermate control mice (n=5) after 6 days of culture under osteoblast differentiation conditions. FIG. 17E-1 shows a mineralization assay of mouse primary osteoblasts derived from neonatal *Slit3*$^{-/-}$ and littermate control mice (n=5) after 6 days of culture under osteoblast differentiation conditions. FIG. 17E-2 graphically illustrates results of a mineralization assay of mouse primary osteoblasts derived from neonatal *Slit3*$^{-/-}$ and littermate control mice (n=5) after 6 days of culture under osteoblast differentiation conditions. FIG. 17F graphically illustrates results of an ALP activity assay in human mesenchymal stromal cells treated with different doses of recombinant SLIT3 after 6 days of osteogenic culture. Values represent mean ± s.e.m.; n.s., not significant and $*P < 0.05$ by an unpaired two-tailed Student's *t*-test or by one-way ANOVA followed by a Tukey's

posttest in all panels. FIG. 17G graphically illustrates results of an ALP activity assay in human mesenchymal stromal cells treated with different doses of recombinant Robo1-Fc after 6 days of osteogenic culture. Values represent mean ± s.e.m.; n.s., not significant and $*P < 0.05$ by an unpaired two-tailed Student's *t*-test or by one-way ANOVA followed by a Tukey's posttest in all panels.

[0026] FIG. 18A-18E illustrate that ablation of *Slit3* in osteoblasts impairs osteogenesis and angiogenesis *in vivo*. FIG. 18A illustrates protein levels of SLIT3 in primary osteoblasts collected from $Slit3^{f/f}$ mice subsequently transduced with *Cre* expressing or control lentivirus. FIG. 18B shows representative μCT images of the trabecular bone in the distal femur in $Slit3^{f/f}$ (n=4) and $Slit3^{osx}$ mice (n=6) at 8-weeks of age. Scale bars, 1mm. FIG. 18C-1 graphically illustrates bone volume/total volume in $Slit3^{f/f}$ (n=4) and $Slit3^{osx}$ mice (n=6) at 8-weeks of age. FIG. 18C-2 graphically illustrates cortical bone thickness in $Slit3^{f/f}$ (n=4) and $Slit3^{osx}$ mice (n=6) at 8-weeks of age. FIG. 18D-1 shows representative μCT images of the trabecular bone in the distal femur in $Slit3^{f/f}$ (n=6) and $Slit3^{dmp1}$ mice (n=6) at 8-weeks of age. Scale bars, 1mm. FIG. 18D-2 graphically illustrates bone volume/total volume in $Slit3^{f/f}$ (n=6) and $Slit3^{dmp1}$ mice (n=6) at 8-weeks of age. FIG. 18E-1 shows representative flow cytometry plots within the $Ter119^-$, $CD45^-$ cell fraction isolated from the femur of 2-week-old $Slit3^{f/f}$ and $Slit3^{dmp1}$ mice (n=4 per group). Values represent mean ± s.e.m.; $*P < 0.05$ and $**P < 0.01$ by an unpaired two-tailed Student's *t*-test in all panels. FIG. 18E-2 graphically illustrates the relative frequency of $CD31^{hi}Emcn^{hi}$ endothelial cells within the $Ter119^-$, $CD45^-$ cell fraction isolated from the femur of 2-week-old $Slit3^{f/f}$ and $Slit3^{dmp1}$ mice (n=4 per group). Values represent mean ± s.e.m.; $*P < 0.05$ and $**P < 0.01$ by an unpaired two-tailed Student's *t*-test in all panels.

[0027] FIG. 19A-19B show that skeletal functions of *Slit3* do not map to endothelial cells or neurons. FIG. 19A-1 shows representative μCT images of the trabecular bone in the distal femur and quantitative analysis of bone volume/total volume in $Slit3^{f/f}$ (n=6) and $Slit3^{cdh5}$ mice (n=5) at 8-weeks of age. Scale bars, 1mm. FIG. 19A-2 graphically illustrates bone volume/total volume in $Slit3^{f/f}$ (n=6) and $Slit3^{cdh5}$ mice (n=5) at 8-weeks of age. FIG. 19B-1 shows representative μCT images of the trabecular bone in the distal femur of $Slit3^{f/f}$ (n=5) and $Slit3^{syn1}$ mice (n=6) at 8-weeks of age. Scale bars, 1mm. Values represent mean ± s.e.m.; n.s., not significant by an unpaired two-tailed Student's *t*-test in all panels. FIG. 19B-2 graphically illustrates bone volume/total volume in $Slit3^{f/f}$ (n=5) and $Slit3^{syn1}$ mice (n=6) at 8-weeks of age. Scale bars, 1mm. Values represent mean ± s.e.m.; n.s., not significant by an unpaired two-tailed Student's *t*-test in all panels.

[0028] FIG. 20A-20H illustrates that ROBO1 is a key receptor of SLIT3 signals regulating skeletal angiogenesis and bone mass accrual. FIG. 20A is a heatmap of SLIT/ROBO expression from three sets per genotype of independently derived $CD31^{hi}EMCN^{hi}$ endothelial cells sorted from *Slm3*$^{f/f}$ and *Slm3*^{dmp1} mice. FIG. 20B graphically illustrates results of quantitative real-time PCR analysis of *Robo1-4* expression in murine osteoblasts using a murine total brain mRNA preparation as a positive control, (n=4). FIG. 20C graphically illustrates results of quantitative real-time PCR analysis of *Robo1-4* expression in murine osteoclasts using a murine total brain mRNA preparation as a positive control, (n=4). FIG. 20D-1 shows representative μCT images of the trabecular bone in the distal femur metaphysis of trabecular bone mass (right) in *Robo1*$^{-/-}$ and *Robo1*$^{+/+}$ mice at 6-weeks of age (male, n≥6). FIG. 20D-2 graphically illustrates quantitative analysis of trabecular bone mass (right) in *Robo1*$^{-/-}$ and *Robo1*$^{+/+}$ mice at 6-weeks of age (male, n≥6). FIG. 20E-1 shows representative μCT images of the trabecular bone in the distal femur metaphysis of *Robo4*$^{-/-}$ and *Robo4*$^{+/+}$ mice at 6-weeks of age (male, n=6). FIG. 20E-2 graphically illustrates quantitative analysis of trabecular bone mass in *Robo4*$^{-/-}$ and *Robo4*$^{+/+}$ mice at 6-weeks of age (male, n=6). FIG. 20F shows representative flow cytometry plots of $CD31^{hi}EMCN^{hi}$ endothelial cells and a heatmap of SLIT/ROBO expression from two sets per genotype of independently derived $CD31^{hi}EMCN^{hi}$ endothelial cells sorted from *Robo1*$^{+/+}$ and *Robo1*$^{-/-}$mice. FIG. 20G-1graphically illustrates mRNA levels of *Robo1* in mouse EPOCs expressing a control vector or *Robo1* shRNA. Values represent mean ± s.e.m.; n.s., not significant and $^{*}P < 0.05$ by an unpaired two-tailed Student's *t*-test in all panels. FIG. 20G-2 shows protein levels of *Robo1* in mouse EPOCs expressing a control vector or *Robo1* shRNA. Values represent mean ± s.e.m.; n.s., not significant and $^{*}P < 0.05$ by an unpaired two-tailed Student's *t*-test in all panels. FIG. 20H-1graphically illustrates mRNA levels of *Robo2* in mouse EPOCs expressing a control vector or *Robo1* shRNA. Brain is included as a positive control for *Robo2* expression. Values represent mean ± s.e.m.; n.s., not significant and $^{*}P < 0.05$ by an unpaired two-tailed Student's *t*-test in all panels. FIG. 20H-2 illustrates protein levels of *Robo2* in mouse EPOCs expressing a control vector or *Robo1* shRNA. Brain is included as a positive control for *Robo2* expression. Values represent mean ± s.e.m.; n.s., not significant and $^{*}P < 0.05$ by an unpaired two-tailed Student's *t*-test in all panels.

[0029] FIG. 21A-21D shows that the hippo pathway is a key mediator of SLIT3/ROBO1- induced tube formation. FIG. 21A-1 shows representative images from EPOCs transduced with a *Robo1* or control shRNA, treated with SLIT3 or FGF2, and subjected to a Matrigel tube formation assay. n=5 per group. FIG. 21A-2 graphically illustrates tube branch numbers for EPOCs transduced with a *Robo1* or control shRNA,

treated with SLIT3 or FGF2, and subjected to a Matrigel tube formation assay. n=5 per group. FIG. 21B-1 shows an immunoblot of EPOC proteins after EPOCs were transduced with a control shRNA, where immunoblotting was conducted with the indicated antibodies after SLIT3 treatment. FIG. 21B-2 shows an immunoblot of EPOC proteins after EPOCs were transduced with a *Robo1* shRNA, where immunoblotting was conducted with the indicated antibodies after SLIT3 treatment. FIG. 21C illustrates protein levels of YAP as determined by immunoblotting of mouse EPOCs expressing a YAP or control shRNA. FIG. 21D-1 shows a Matrigel tube formation assay where EPOCs were first transduced with a Robo1 or control shRNA, then treated with SLIT3 or FGF2, and placed in a Matrigel tube formation assay; n=5 per group. Scale bars, 100μm. Values represent mean ± s.e.m.; n.s., not significant, $*P < 0.05$, $**P < 0.01$ and $***P < 0.001$ by a one-way ANOVA followed by a Tukey's posttest in all panels. FIG. 21D-2 graphically illustrates tube branch numbers formed in a Matrigel tube formation assay by EPOCs that were first transduced with a Robo1 or control shRNA, then treated with SLIT3 or FGF2, and placed in a Matrigel tube formation assay; n=5 per group. Scale bars, 100μm. Values represent mean ± s.e.m.; n.s., not significant, $*P < 0.05$, $**P < 0.01$ and $***P < 0.001$ by a one-way ANOVA followed by a Tukey's posttest in all panels.

[0030] FIG. 22A-22B illustrate that interaction between *Slit3* and *Shn3* null alleles is intrinsic to osteoblasts. FIG. 22A-1 shows representative μCT images of the trabecular bone in the distal femur metaphysis of 8-week-old *OSX cre* mice. Scale bar, 1mm. FIG. 22A-2 shows representative μCT images of the trabecular bone in the distal femur metaphysis of 8-week-old *OSX cre-Slit3*$^{f/+}$ mice. Scale bar, 1mm. FIG. 22A-3 shows representative μCT images of the trabecular bone in the distal femur metaphysis of 8-week-old *Osx cre-Shn3*$^{f/+}$ mice. Scale bar, 1mm. FIG. 22A-4 shows representative μCT images of the trabecular bone in the distal femur metaphysis of 8-week-old *OSX cre-Slit3*$^{f/+}$*Shn3*$^{f/+}$ mice. Scale bar, 1mm. FIG. 22B graphically illustrates BV/TV analysis of 8-week-old *OSX cre*, *OSX cre-Slit3*$^{f/+}$, *Osx cre-Shn3*$^{f/+}$ *and OSX cre-Slit3* $^{f/+}$*Shn3* $^{f/+}$ mice.

[0031] FIG. 23A-23B SLIT3 is expressed in osteoblasts present in human fracture callus tissue. FIG. 23A shows an image of a human fracture callus that was immunohistochemically stained for SLIT3. Scale bars, 100μm. FIG. 23B-1 shows an image of a human fracture callus that was H&E stained. Scale bars, 100μm. FIG. 23B-2 shows an image of a human fracture callus that was immunohistochemically stained for CD31. The images shown for FIG. 23B-1 and 23B-2 were from serial sections from human fracture callus tissue. Scale bars, 100μm.

[0032] FIG. 24A-24C illustrates that systemic administration of SLIT3 enhances bone-fracture healing. FIG. 24A graphically illustrates the quantity of EMCN-positive vessel volume/total volume (Relative vessel volume (%)) in a callus area as determined by histomorphometry of femurs 21 days after fracture in male $Shn3^{+/+}$ $Slit3^{+/+}$, $Shn3^{+/+}$ $Slit3^{-/-}$, $Shn3^{-/-}$ $Slit3^{+/+}$ and $Shn3^{-/-}$ $Slit3^{-/-}$ mice. FIG. 24B graphically illustrates the stiffness determined by bio-mechanical testing of femurs 21 days after fracture in male $Shn3^{+/+}$ $Slit3^{+/+}$, $Shn3^{+/+}$ $Slit3^{-/-}$, $Shn3^{-/-}$ $Slit3^{+/+}$ and $Shn3^{-/-}$ $Slit3^{-/-}$ mice. FIG. 24C shows images of fracture callus tissue in mice treated with IV injection of SLIT3 or vehicle and at 21 days post-fracture callus tissue was harvested and immunostained for CD31 and EMCN. Scale bars, 100μm, n=3 per group. Values represent mean ± s.e.m.; $^{**}P <$ 0.01 and $^{***}P < 0.001$ by one-way ANOVA followed by a Tukey's posttest in all panels.

[0033] FIG. 25A-25D illustrates that systemic administration of SLIT3 does not cause abnormalities in the amount or morphology of non-skeletal vasculature. FIG. 25A shows representative confocal images of retinal flat-mounts of 8-week-old mice stained with ve-cadherin (green) from mice 21 days post-fracture with IV injection of SLIT3 or Vehicle. Scale bars, 500μm, n=3 per group. FIG. 25B shows representative confocal images of heart, kidney and lung sections stained for endomucin (red) and 4',6-diamidino-2-phenylindole (DAPI, blue) from mice 21 days post-fracture with IV injection of SLIT3 or Vehicle. Scale bars, 100μm, n=3 per group. FIG. 25C shows representative images of the whole brain sections stained for neurofilament-M (NF-M, green) and Nissl (red) from mice 21 days post-fracture with IV injection of SLIT3 or Vehicle. Scale bars, 500μm, n=3 per group. FIG. 25D shows representative images of the whole brain sections stained for neurofilament-M (NF-M, green) and Nissl (red) from mice 21 days post-fracture with IV injection of SLIT3 or Vehicle, where the boxed areas of the upper images are shown with higher magnification below. Scale bars, 500μm, n=3 per group.

[0034] FIG. 26A-26F illustrates that local delivery of SLIT3 enhances bone-fracture healing. FIG. 26A shows representative μCT images of mouse femurs harvested 21 days post-fracture with insertion of a gelatin sponge soaked with SLIT3 or vehicle. A no sponge control is included. Scale bar = 1 mm. FIG. 26B shows representative image of CD31 and EMCN (red) dual immunostained callus sections of mouse femurs 21 days post-fracture with insertion of a gelatin sponge soaked with SLIT3 or vehicle at the time of fracture. Scale bars, 300μm, n=3 per group. FIG. 26C shows representative confocal images of retinal flat-mounts of 8-week-old mice stained with ve-cadherin (green). Retinas were harvested from mice 21 days post-fracture with implantation of a gelatin sponge soaked with SLIT3 or vehicle at the time of fracture.

Scale bars, 500μm, n=3 per group. FIG. 26D shows representative images of the whole brain sections stained for neurofilament-M (NF-M, green) and Nissl (red). Brains were harvested from mice 21 days post-fracture after implantation of a gelatin sponge soaked with SLIT3 or vehicle. Scale bars, 500μm, n=3 per group. FIG. 26E shows representative μCT images of mouse femurs. Mice were subjected to femoral fracture created by a midshaft osteotomy which was subsequently stabilized by an intramedullary rod. At the time of fracture, a hydrogel construct containing SLIT3 or a control gel construct only containing PBS vehicle were implanted at the periosteal surface near the site of fracture. FIG. 26F shows representative μCT images of mouse femurs. Mice were subjected to femoral fracture as described for FIG. 26E and a construct including a SLIT3-containing collagen sponge or a PBS vehicle containing control collagen sponge was similarly implanted at the fracture site. SLIT3-eluting collagen sponges were also supplemented with additional targeted injection of SLIT3 performed into collagen sponge 7 days after fracture (FIG. 26F, right)

[0035] FIG. 27A-27F illustrate that SLIT3 has preventive effects in the ovariectomized (OVX) mouse model. FIG. 27A shows representative images of the uterus from sham-operated (Sham) and ovariectomized (OVX) mice. Scale bar, 500μm. FIG. 27B graphically illustrates quantitative analysis of uterus weight in Sham and OVX mice. FIG. 27C-1 graphically illustrates cortical bone thickness of distal femoral metaphyseal regions from mice after sham operation, OVX and OVX with SLIT3 injection. FIG. 27C-2 graphically illustrates trabecular number (Tb. N) of distal femoral metaphyseal regions from mice after sham operation, OVX and OVX with SLIT3 injection. FIG. 27C-3 graphically illustrates trabecular thickness (Tb. Th) of distal femoral metaphyseal regions from mice after sham operation, OVX and OVX with SLIT3 injection. FIG. 27C-4 graphically illustrates trabecular bone space (Tb. Sp) of distal femoral metaphyseal regions from mice after sham operation, OVX and OVX with SLIT3 injection. FIG. 27D shows representative confocal images of CD31 (green) and endomucin (red) dual-immunostained bone sections of the L3 vertebrae from mice after sham operation, OVX or OVX with SLIT3 injection. GP, growth plate. Scale bars, 300μm. FIG. 27E-1 graphically illustrates periosteal bone formation rates/bone surface (BFR/BS, $mm^3\ mm^{-2}\ yr^{-1}$) of the L3 vertebrae from mice after sham operation, OVX or OVX with SLIT3 injection. FIG. 27E-2 graphically illustrates endosteal bone formation rates/bone surface (BFR/BS, $mm^3\ mm^{-2}\ yr^{-1}$) of the L3 vertebrae from mice after sham operation, OVX or OVX with SLIT3 injection. FIG. 27F-1 graphically illustrates osteoclast number/bone perimeter (No. Oc./B. Pm) in the endosteum of the L3 vertebrae from mice after sham operation, OVX or OVX with SLIT3 injection. FIG. 27F-2 graphically illustrates osteoblast surface/bone surface (Ob.S/BS, %) in the endosteum of

the L3 vertebrae from mice after sham operation, OVX or OVX with SLIT3 injection. Values represent mean ± s.e.m.; $*P < 0.05$ and $**P < 0.01$ by one-way ANOVA followed by a Tukey's posttest in all panels.

[0036] FIG. 28A-28C illustrate that SLIT3 has therapeutic effects in the ovariectomized (OVX) mouse model. FIG. 28A shows representative μCT images of the trabecular bone in the distal femur of mice after sham operation, OVX, or OVX with SLIT3 injection. Scale bar, 1mm. FIG. 28B-1 graphically illustrates bone volume/total volume in mice after sham operation, OVX, or OVX with SLIT3 injection. FIG. 28B-2 graphically illustrates cortical bone thickness in mice after sham operation, OVX, or OVX with SLIT3 injection. FIG. 28C shows representative flow cytometry dot plots and relative frequency of $CD31^{hi}Emcn^{hi}$ endothelial cells of the femur in mice after sham operation, OVX and OVX with SLIT3 injection. Expanded views of such representative flow cytometry dot plots are shown in U.S. Provisional Patent Application Ser. No. 62/630,557 filed February 14, 2018 (which is incorporated herein by reference in its entirety). Values represent mean ± s.e.m.; $*P < 0.05$, $***P < 0.01$, $***P < 0.001$ and $****P < 0.0001$ by one-way ANOVA followed by a Tukey's posttest in all panels.

[0037] FIG. 29A-29E illustrate SLIT2 expression and function in the skeletal system. FIG. 29A shows μCT images of bone present in a fracture callus of mice. Five-week-old mice underwent a midshaft osteotomy model of femoral fracture and were subsequently treated with recombinant SLIT2 delivered at 1mg/kg for each of 3-weekly IV injections or vehicle injections for a total period of 3 weeks. At the end of this period, effects on bone healing were determined by μCT of the fracture site. Shown are representative 3-dimensional reconstructions of μCT images. FIG. 29B graphically illustrates quantitation of the relative amount of bone present in the fracture callus for the bones described in FIG. 29A. FIG. 29C shows representative 3-dimensional reconstructions of μCT images of trabecular bone (B, BV/TV, bone volume/total volume). FIG. 29D graphically illustrates quantitation of the relative amount of bone present in trabecular bone (B, BV/TV, bone volume/total volume). For FIGs. 29B and 29C, 12-week old male mice with a conditional deletion of *Slit2* in osteoblast cells mediated by osxterix-cre ($Slit2^{osx}$ mice) were imaged and underwent analysis of bone mass by μCT. FIG. 29E-1 shows representative images of Alizarin red staining of human bone stromal cells infected with lentivirus expressing *Slit2* shRNA, *Slit3* shRNA, *Robo1* shRNA or a GFP-targeting control shRNA cultured under osteogenic conditions for 21 days. FIG. 29E-2 graphically illustrates quantitative relative mineralization capacity in human bone stromal cells infected with lentivirus expressing

Slit2 shRNA, *Slit3* shRNA, *Robo1* shRNA or a GFP-targeting control shRNA cultured under osteogenic conditions for 21 days.

[0038] FIG. 30A-30B illustrates SLIT3 functions in osteoblasts to regulate bone mass. FIG. 30A-1 shows representative images of trabecular bone from three-week old *Slit3*$^{f/f}$ and *Slit3*^{osx} mice. FIG. 30A-2 graphically illustrates trabecular bone mass (% BV/TV) of three-week old *Slit3*$^{f/f}$ and *Slit3*^{osx} mice. FIG. 30B-1 shows representative images of trabecular bone from twelve-week old *Slit3*$^{f/f}$ and *Slit3*^{osx} mice. FIG. 30B-2 graphically illustrates trabecular bone mass (% BV/TV) of twelve-week old *Slit3*$^{f/f}$ and *Slit3*^{osx} mice. Mice of the indicated genotypes were sacrificed at 3 and 12 weeks of age for FIGs. 30A and 30B, respectively. Trabecular bone mass was determined by μCT of the femur.

[0039] FIG. 31 shows that systemic treatment with SLIT3 induces vascular leakage in retinal vasculature. Five-week old mice were treated with recombinant SLIT3 delivered at 1mg/kg for each of 3 weekly IV injections or vehicle injections for a total period of 3 weeks. PE-tagged dextran (red) was infused prior to sacrifice to measure vascular permeability and retinal vessels were visualized by infusion of FITC tagged anti-CDH5 antibodies (green). Retinal vessel morphology (green) and permeability (red) were visualized by fluorescence microscopy of retinal mounts.

[0040] FIG. 32 schematically illustrates the strategy used for flow cytometry for analysis of osteoclast progenitor (OCPs).

[0041] FIG. 33A-33E illustrate that SLIT3 is dispensable for osteoclastogenesis *in vitro*. FIG. 33A graphically illustrates mRNA expression of *Slit3* in BMMs treated with RANKL for up to three days, as measured by quantitative real-time PCR analysis, where brain tissue was used as a positive control. (n=3). FIG. 33B shows an immunoblot illustrating SLIT3 protein expression in BMMs treated with RANKL for two days, where the whole brain lysate from *Slit3*$^{+/+}$ and *Slit3*$^{-/-}$ mice as the positive and negative control. FIG. 33C graphically illustrates mRNA expression of *Ntftac1, Itgb3, Dcstamp, Ctsk, Calcr* and *Trap* in BMMs treated with RANKL for three days as measured by quantitative real-time PCR analysis. FIG. 33D-1 shows osteoclast differentiation using WT BMMs stimulated with RANKL and recombinant SLIT3 for three days. TRAP staining was performed and the area of TRAP-positive multinucleated cells (MNCs) (≥3 nuclei/cell) per well relative to the WT control was calculated. FIG. 33D-2 graphically illustrates numbers of osteoclasts per well. FIG. 33E-1 shows representative images of osteoclasts cultured in the presence of various concentrations of SLIT3. FIG. 33E-2 graphically illustrates the numbers of osteoclasts per well in cultures described for FIG. 33E-1.

[0042] FIG. 34A-34E illustrate that deletion of SLIT3 results in normal bone volume and normal osteoclast numbers *in vivo*. FIG. 34A-1 illustrates flow cytometric analysis of *in vivo* osteoclast precursor populations of $Slit3^{+/+}$ and $Slit3^{-/-}$ mice. Representative flow cytometry plots for each experiment are shown. FIG. 34A-2 graphically illustrates the frequency of osteoclast precursors in $Slit3^{+/+}$and $Slit3^{-/-}$ mice. FIG. 34B-1 illustrates the amount of osteoclast precursors in $Slit3^{f/f}$ mice and in $Slit3^{f/f}$ mice bred to cre-deleter strains targeting osteoblasts via OSX-cre ($Slit3^{osx}$ mice). FIG. 34B-2 graphically illustrates the frequency of osteoclast precursors in $Slit3^{f/f}$ and $Slit3^{osx}$ mice. FIG. 34C-1 illustrates the amount of osteoclast precursors $Slit3^{f/f}$ mice and in $Slit3^{f/f}$ mice that were bred to a cre-deleter strain targeting mature osteoclasts, CTSK-cre ($Slit3^{ctsk}$). FIG. 34C-2 graphically illustrates the frequency of osteoclast precursors in $Slit3^{f/f}$ and $Slit3^{ctsk}$ mice. FIG. 34D-1 shows images of osteoclast differentiation utilizing osteoclast precursor cells isolated from $Slit3^{ctsk}$ mice and $Slit3^{f/f}$. FIG. 34D-2 graphically illustrates the numbers of osteoclasts per well generated from cultures of cells isolated from $Slit3^{ctsk}$ mice and $Slit3^{f/f}$. FIG. 34E-1 shows representative micro-CT images of the distal femurs isolated from 5-week-old male $Slit3^{ctsk}$ mice and $Slit3^{f/f}$ mice. FIG. 34E-2 graphically illustrates femoral bone volume over total volume (BV/TV) of trabecular bone of the distal femurs isolated from 5-week-old littermate male $Slit3^{ctsk}$ mice and $Slit3^{f/f}$ mice. FIG. 34E-3 graphically illustrates cortical bone thickness of the distal femurs isolated from 5-week-old littermate male $Slit3^{ctsk}$ mice and $Slit3^{f/f}$ mice. FIG. 34E-4 graphically illustrates bone morphometric analysis (trabecular number (Tb. N)) of trabecular bone of the distal femurs isolated from 5-week-old littermate male $Slit3^{ctsk}$ mice and $Slit3^{f/f}$ mice. FIG. 34E-5 graphically illustrates bone morphometric analysis (trabecular thickness (Tb. Th)) of trabecular bone of the distal femurs isolated from 5-week-old littermate male $Slit3^{ctsk}$ mice and $Slit3^{f/f}$ mice. FIG. 34E-6 graphically illustrates bone morphometric analysis (trabecular space (Tb. Sp)) of trabecular bone of the distal femurs isolated from 5-week-old littermate male $Slit3^{ctsk}$ mice and $Slit3^{f/f}$ mice.

[0043] FIG. 35A-35D show that chimeric mice lacking SLIT3 in BM cells exhibit normal bone phenotype and skeletal vasculature. FIG. 35A is a schematic diagram illustrating the protocol for a BM transplantation experiment. FIG. 35B shows representative micro-CT images of trabecular bone from the distal femurs isolated from WT mice with bone marrow transplantation derived from $Slit3^{+/+}$ and $Slit3^{-/-}$ mice. FIG. 35C-1 graphically illustrates BV/TV of trabecular bone of the distal femurs isolated from $Slit3^{+/+}$ and $Slit3^{-/-}$ mice. FIG. 35C-2 graphically illustrates cortical bone thickness of trabecular bone of the distal femurs isolated from $Slit3^{+/+}$ and $Slit3^{-/-}$ mice. FIG. 35C-3 graphically illustrates bone morphometric analysis (trabecular number (Tb. N)) of trabecular bone of the distal femurs isolated from $Slit3^{+/+}$ and $Slit3^{-/-}$ mice. FIG. 35C-4

graphically illustrates bone morphometric analysis (trabecular thickness (Tb. Th)) of trabecular bone of the distal femurs isolated from *Slit3*$^{+/+}$ and *Slit3*$^{-/-}$ mice. FIG. 35C-5 graphically illustrates bone morphometric analysis (trabecular space (Tb. Sp)) of trabecular bone of the distal femurs isolated from *Slit3*$^{+/+}$ and *Slit3*$^{-/-}$ mice. FIG. 35D shows histomorphometry and immunofluorescence staining of SLIT3 from osteoclast lineage cells illustrating that neither osteoclast numbers nor bone vasculature were altered by bone marrow transplantation and the absence of SLIT3 from osteoclast lineage cells.

Detailed Description

[0044] In the following description, reference is made to the accompanying drawings that form a part hereof, and in which is shown by way of illustration specific embodiments which may be practiced. These embodiments are described in detail to enable those skilled in the art to practice the invention, and it is to be understood that other embodiments may be utilized and that logical changes may be made without departing from the scope of the present invention. The following description of example embodiments is, therefore, not to be taken in a limited sense, and the scope of the present invention is defined by the appended claims.

[0045] The Abstract is provided to comply with 37 C.F.R. §1.72(b) to allow the reader to quickly ascertain the nature and gist of the technical disclosure. The Abstract is submitted with the understanding that it will not be used to interpret or limit the scope or meaning of the claims.

[0046] Recent studies have identified a specialized subset of CD31^{hi}EMCN^{hi} vascular endothelium that regulates bone formation. However, it remains unclear how CD31^{hi}EMCN^{hi} endothelium levels are coupled to anabolic bone formation. Analysis of a strain of mutant mice with elevated bone formation, *Shn3*$^{-/-}$ mice, demonstrated an increase in CD31^{hi}EMCN^{hi} endothelium that cell-specific genetic models mapped to osteoblasts.

[0047] Transcriptomic analysis identified SLIT3 as an osteoblast derived, SHN3-regulated proangiogenic factor, and absence of *Slit3* reduced skeletal CD31^{hi}EMCN^{hi} endothelium, resulted in low bone mass due to impaired bone formation, and partially reversed the high bone mass phenotype of *Shn3*$^{-/-}$ mice. This coupling between osteoblasts and CD31^{hi}EMCN^{hi} endothelium is essential for bone healing, as shown by defective fracture repair in SLIT3-mutant mice and enhanced fracture repair in SHN3-mutant mice. Drugs that target the SLIT3 pathway are a novel class of vascular-targeted osteoanabolic therapy as administration of recombinant SLIT3 both enhanced bone-fracture healing and counteracted bone loss in a mouse model of postmenopausal osteoporosis.

[0048] SLIT agonists are an entirely novel class of pro-anabolic agents distinct from all existing drugs, as SLITs do not act directly on osteoblasts but rather indirectly promote bone formation by enhancing the formation of type H endothelium in bone, a specialized subtype of blood vessels that promote bone formation. This means that SLITs will likely have a distinct set of advantages versus all existing agents. Due to the known importance of blood vessels in fracture healing, we propose that this indication and other related orthopedic bone repair applications potentially represent a unique application for SLITs. In this respect, they may also function as growth factors applied locally to a site where enhanced bone repair is desired in a manner similar to recombinant BMPs.

[0049] Impaired fracture healing is observed in elderly patients, patients with systemic vascular diseases such as diabetes, patients with inflammatory disorders or chronic infection, or in patients with large traumatic bone defects (Buza and Einhorn 2016). For these classes of patients, a single bone fracture often results in many years of pain, severely impaired mobility and numerous attempts at surgical management of their fracture. From this perspective, developing a means for medical therapy to promote fracture healing is urgently needed. Interestingly, the phenotypes observed with disruption of the SHN3/SLIT3 axis may extend beyond simply promoting more bone formation, as the fracture callus observed in SHN3-deficient mice was markedly more mature, including displaying overall more mature lamellar bone in addition to enhanced recruitment of hematopoietic elements to the callus. Conversely, SLIT3-deficient mice displayed an arrest at early stages of fracture callus maturation, displaying a lack of propagation of the mineralization sites on either side of the callus.

[0050] We have demonstrated that exogenous SLIT3 promotes bone fracture healing and prevents bone loss in a model of postmenopausal osteoporosis. Notably, these findings contrast with a prior in vitro study indicating that SLIT2 suppresses osteoblast differentiation *in vitro* (Sun et al. 2009). These results show that agents targeting bone vasculature represent a novel class of bone anabolics and that vascular-targeted anabolics may have a synergistic or complimentary effect when used in combination with an osteoblast targeted anabolic such as a PTH analogue or an anti-SOST antibody.

[0051] Development of new categories of bone anabolic agents is especially important given the current limitations on the maximum duration of therapy with PTH-based anabolic agents. Likewise, in light of increasing evidence establishing that osteoporosis drugs can be used in a sequential or combination manner to obtain superior clinical outcomes, having therapeutic access to a larger diversity of anabolic pathways is highly desirable (Leder et al. 2015). Further enhancement of the magnitude of SLIT3

effect is possible by optimization of dosing and delivery strategies. For instance, bone targeting strategies such as a bisphosphonate conjugation or $(AspSerSer)_6$-liposomes and Aptamer-functionalized lipid nanoparticles may enhance the potency or anabolic effects of SLIT3 by increasing the fractional distribution to bone (Zhang, Guo, et al. 2012, Liang et al. 2015, Guan et al. 2012, Yao et al. 2013).

Subjects

[0052] The subject may be any animal, including a human or non-human animal. Non-human animals include all vertebrates, e.g., mammals and non-mammals, such as non-human primates, sheep, dogs, cats, cows, horses, chickens, amphibians, and reptiles, although mammals are preferred, such as non-human primates, sheep, dogs, cats, cows and horses. The subject may also be livestock such as, cattle, swine, sheep, poultry, and horses, or pets, such as dogs and cats.

[0053] Preferred subjects include human subjects, for example, those in need of preventing bone loss or of promoting bone growth, strengthening, or healing, or in need of preventing bone growth. The subject can be diagnosed with such a condition by skilled artisans, such as a medical practitioner.

[0054] The methods described herein can be employed for subjects of any species, gender, age, ethnic population, or genotype. Accordingly, the term subject includes males and females, and it includes elderly, elderly-to-adult transition age adult subjects, adult-to-pre-adult transition age subjects, and pre-adults, including adolescents, children, and infants.

[0055] Examples of human ethnic populations include Caucasians, Asians, Hispanics, Africans, African Americans, Native Americans, Semites, and Pacific Islanders. The methods described herein may be more appropriate for some ethnic populations such as Caucasians, especially northern European populations, as well as Asian populations.

[0056] The term subject also includes subjects of any genotype or phenotype. For example, any subject in need of treatment as described herein can be provided with such treatment. In addition, the subject can have the genotype or phenotype for any hair color, eye color, skin color or any combination thereof.

[0057] The term subject includes a subject of any body height, body weight, or any organ or body part size or shape.

[0058] **A subject in need of prevention of bone loss or of promoting bone growth, bone strengthening, or bone healing** includes a subject who has experienced a bone defect, fracture or break, a tooth replacement, either replacement of a subjects' own tooth or a prosthetic tooth, or ameliorate symptoms of an ongoing condition, such as for example, bone loss associated with, for example peri-menopause or menopause.

The fracture or defect be congenital, a result of aging, of an accident, or a surgical procedure. It may for example the result of a bone or spine fusion procedure, or a tumor resection, or any procedure where bone may be resected or drilled, including the placements of implants or other medical hardware in or on any bone, including but not limited to spine, knee, and hips. The subject may have received a bone graft. The subject may have a critical size defect, or a persistent non- or partial-union following a fracture. The subject may have a disease or condition that causes bone loss or degradation, such as osteoarthritis or rheumatoid arthritis or osteoporosis, including idiopathic osteoporosis, secondary osteoporosis, transient osteoporosis of the hip, osteomalacia, skeletal changes of hyperparathyroidism, chronic renal failure (renal osteodystrophy), osteitis deformans (Paget's disease of bone), osteolytic metastases, and osteopenia in which there is progressive loss of bone density and thinning of bone tissue. Osteoporosis and osteopenia can result not only from aging and reproductive status but can also be secondary to numerous diseases and disorders, as well as due to prolonged use of numerous medications, e.g., anticonvulsants, corticosteroids, and/or immunosuppressive agents. Other diseases in which osteoporosis may be secondary include, but are not limited to, juvenile rheumatoid arthritis, diabetes, osteogenesis imperfecta, hyperthyroidism, hyperparathyroidism, Cushing's syndrome, malabsorption syndromes, anorexia nervosa and/or kidney disease. In addition, numerous behaviors have been associated with osteoporosis, such as, prolonged inactivity or immobility, inadequate nutrition (especially calcium, vitamin D), excessive exercise leading to amenorrhea (absence of periods), smoking, and/or alcohol abuse. The subject may have any disease or condition known in the art wherein bone growth, bone strengthening, or prevention of bone loss would be beneficial. This can also include applications to enhance the integration of orthopedic hardware, such as used in joint arthoplasty, spinal fusion, or internal or external fixation of bone with the surrounding bone to prevent hardware loosening. Similar applications include counteracting the osteolysis observed at the site of orthopedic implants due to implant wear particles, infection, inflammation or other causes.

[0059] **A subject in need of preventing bone growth** includes subjects with conditions in which there is premature fusing of two or more bones, or bone density is too high, such as for example, craniosynostosis (synostosis), osteopetrosis (including malignant infantile form, intermediate form, and adult form), heterotopic ossification secondary to burn, traumatic injury or other condition, fibrodysplasia ossificans progressiva, osteitis deformans (Paget's disease of bone), primary extra-skeletal bone formation, e.g., multiple miliary osteoma cutis of the face, and osteitis condensans, or other diseases or conditions known in the art.

SLIT3 or SLIT2 agents

[0060] For the purposes of this application, a SLIT3 or SLIT2 agent is a nucleic acid or protein construct, wherein the SLIT 3 or SLIT2 nucleic acid expresses a SLIT3 or SLIT3 protein construct or polypeptide.

[0061] One example of a *Homo sapiens* SLIT3 protein sequence (e.g., with NCBI accession number AAQ89243) is shown below as SEQ ID NO:1.

```
   1 MAPGWAGVGA AVRARLALAL ALASVLSGPP AVACPTKCTC
  41 SAASVDCHGL GLRAVPRGIP RNAERLDLDR NNITRITKMD
  81 FAGLKNLRVL HLEDNQVSVI ERGAFQDLKQ LERLRLNKNK
 121 LQVLPELLFQ STPKLTRLDL SENQIQGIPR KAFRGITDVK
 161 NLQLDNNHIS CIEDGAFRAL RDLEILTLNN NNISRILVTS
 181 FNHMPKIRTL RLHSNHLYCD CHLAWLSDWL RQRRTVGQFT
 241 LCMAPVHLRG FNVADVQKKE YVCPAPHSEP PSCNANSISC
 281 PSPCTCSNNI VDCRGKGLME IPANLPEGIV EIRLEQNSIK
 321 AIPAGAFTQY KKLKRIDISK NQISDIAPDA FQGLKSLTSL
 361 VLYGNKITEI AKGLFDGLVS LQLLLLNANK INCLRVNTFQ
 401 DLQNLNLLSL YDNKLQTISK GLFAPLQSIQ TLHLAQNPFV
 441 CDCHLKWLAD YLQDNPIETS GARCSSPRRL ANKRISQIKS
 481 KKFRCSGSED YRSRFSSECF MDLVCPEKCR CEGTIVDCSN
 521 QKLVRIPSHL PEYVTDLRLN DNEVSVLEAT GIFKKLPNLR
 561 KINLSNNKIK EVREGAFDGA ASVQELMLTG NQLETVHGRV
 601 FRGLSGLKTL MLRSNLISCV SNDTFAGLSS VRLLSLYDNR
 641 ITTITPGAFT TLVSLSTINL LSNPFNCNCH LAWLGKWLRK
 681 RRIVSGNPRC QKPFFLKEIP IQDVAIQDFT CDGNEESSCQ
 721 LSPRCPEQCT CMETVVRCSN KGLRALPRGM PKDVTELYLE
 761 GNHLTAVPRE LSALRHLTLI DLSNNSISML TNYTFSNMSH
 801 LSTLILSYNR LRCIPVHAFN GLRSLRVLTL HGNDISSVPE
 841 GSFNDLTSLS HLALGTNPLH CDCSLRWLSE WVKAGYKEPG
 881 IARCSSPEPM ADRLLLTTPT HRFQCKGPVD INIVAKCNAC
 921 LSSPCKNNGT CTQDPVELYR CACPYSYKGK DCTVPINTCI
 961 QNPCQHGGTC HLSDSHKDGF SCSCPLGFEG QRCEINPDDC
1001 EDNDCENNAT CVDGINNYVC ICPPNYTGEL CDEVIDHCVP
1041 ELNLCQHEAK CIPLDKGFSC ECVPGYSGKL CETDNDDCVA
1081 HKCRHGAQCV DTINGYTCTC PQGFSGPFCE HPPPMVLLQT
1121 SPCDQYECQN GAQCIVVQQE PTCRCPPGFA GPRCEKLITV
1161 NFVGKDSYVE LASAKVRPQA NISLQVATDK DNGILLYKGD
1201 NDPLALELYQ GHVRLVYDSL SSPPTTVYSV ETVNDGQFHS
1241 VELVTLNQTL NLVVDKGTPK SLGKLQKQPA VGINSPLYLG
1281 GIPTSTGLSA LRQGTDRPLG GFHGCIHEVR INNELQDFKA
1321 LPPQSLGVSP GCKSCTVCKH GLCRSVEKDS VVCECRPGWT
1361 GPLCDQEARD PCLGHRCHHG KCVATGTSYM CKCAEGYGGD
1401 LCDNKNDSAN ACSAFKCHHG QCHISDQGEP YCLCQPGFSG
1441 EHCQQENPCL GQVVREVIRR QKGYASCATA SKVPIMECRG
1481 GCGPQCCQPT RSKRRKYVFQ CTDGSSFVEE VERHLECGCL
1521 ACS
```

[0062] Amino acids at plus or minus one (±1) position of amino acid positions at any of 565, 566, 662, 761, 784, 832, 853, 855, or 869 (highlighted above) within SLIT3 proteins (e.g. having SEQ ID NO:1) can be involved in substrate binding. Amino acids at plus or minus one (±1) position of amino acid positions at any of 956-994, 998-1031,

1035-1072, 1074-1110, within SLIT3 proteins (e.g. having SEQ ID NO:1) can be at least part of a calcium-binding EGF-like domain. For example, amino acids at plus or minus one (±1) position of amino acid positions at any of 1074, 1077, or 1091 within SLIT3 proteins (e.g. having SEQ ID NO:1) can be at least part of a calcium-binding site (ion binding). Amino acids at plus or minus one (±1) position of amino acid positions at any of 1123-1153 or 1466-1521 within SLIT3 proteins (e.g. having SEQ ID NO:1) can be at least part of an EGF-like domain. Amino acids at plus or minus one (±1) position of amino acid positions at any of 1188-1314 within SLIT3 proteins (e.g. having SEQ ID NO:1) can be at least part of a Laminin G domain.

[0063] An example of a nucleic acid that encodes the SEQ ID NO:1 SLIT3 protein is shown (NCBI accession number AY358884; SEQ ID NO:2).

```
   1 CGCGCTCCCC GCGCGCCTCC TCGGGCTCCA CGCGTCTTGC
  41 CCCGCAGAGG CAGCCTCCTC CAGGAGCGGG GCCCTGCACA
  81 CCATGGCCCC CGGGTGGGCA GGGGTCGGCG CCGCCGTGCG
 121 CGCCCGCCTG GCGCTGGCCT TGGCGCTGGC GAGCGTCCTG
 161 AGTGGGCCTC CAGCCGTCGC CTGCCCCACC AAGTGTACCT
 201 GCTCCGCTGC CAGCGTGGAC TGCCACGGGC TGGGCCTCCG
 241 CGCGGTTCCT CGGGGCATCC CCCGCAACGC TGAGCGCCTT
 281 GACCTGGACA GAAATAATAT CACCAGGATC ACCAAGATGG
 321 ACTTCGCTGG GCTCAAGAAC CTCCGAGTCT TGCATCTGGA
 361 AGACAACCAG GTCAGCGTCA TCGAGAGAGG CGCCTTCCAG
 401 GACCTGAAGC AGCTAGAGCG ACTGCGCCTG AACAAGAATA
 441 AGCTGCAAGT CCTTCCAGAA TTGCTTTTCC AGAGCACGCC
 481 GAAGCTCACC AGACTAGATT TGAGTGAAAA CCAGATCCAG
 521 GGGATCCCGA GGAAGGCGTT CCGCGGCATC ACCGATGTGA
 561 AGAACCTGCA ACTGGACAAC AACCACATCA GCTGCATTGA
 601 AGATGGAGCC TTCCGAGCGC TGCGCGATTT GGAGATCCTT
 641 ACCCTCAACA ACAACAACAT CAGTCGCATC CTGGTCACCA
 681 GCTTCAACCA CATGCCGAAG ATCCGAACTC TGCGCCTCCA
 721 CTCCAACCAC CTCTACTGCG ACTGCCACCT GGCCTGGCTC
 761 TCGGATTGGC TGCGACAGCG ACGGACAGTT GGCCAGTTCA
 801 CACTCTGCAT GGCTCCTGTG CATTTGAGGG GCTTCAACGT
 841 GGCGGATGTG CAGAAGAAGG AGTACGTGTG CCCAGCCCCC
 881 CACTCGGAGC CCCCATCCTG CAATGCCAAC TCCATCTCCT
 921 GCCCTTCGCC CTGCACGTGC AGCAATAACA TCGTGGACTG
 961 TCGAGGAAAG GGCTTGATGG AGATTCCTGC CAACTTGCCG
1001 GAGGGCATCG TCGAAATACG CCTAGAACAG AACTCCATCA
1041 AAGCCATCCC TGCAGGAGCC TTCACCCAGT ACAAGAAACT
1081 GAAGCGAATA GACATCAGCA AGAATCAGAT ATCGGATATT
1121 GCTCCAGATG CCTTCCAGGG CCTGAAATCA CTCACATCGC
1161 TGGTCCTGTA TGGGAACAAG ATCACCGAGA TTGCCAAGGG
1201 ACTGTTTGAT GGGCTGGTGT CCCTACAGCT GCTCCTCCTC
1241 AATGCCAACA AGATCAACTG CCTGCGGGTG AACACGTTTC
1281 AGGACCTGCA GAACCTCAAC TTGCTCTCCC TGTATGACAA
1321 CAAGCTGCAG ACCATCAGCA AGGGGCTCTT CGCCCCTCTG
1361 CAGTCCATCC AGACACTCCA CTTAGCCCAA AACCCATTTG
1401 TGTGCGACTG CCACTTGAAG TGGCTGGCCG ACTACCTCCA
1441 GGACAACCCC ATCGAGACAA GCGGGGCCCG CTGCAGCAGC
1481 CCGCGCCGAC TCGCCAACAA GCGCATCAGC CAGATCAAGA
1521 GCAAGAAGTT CCGCTGCTCA GGCTCCGAGG ATTACCGCAG
```

1561 CAGGTTCAGC AGCGAGTGCT TCATGGACCT CGTGTGCCCC
1601 GAGAAGTGTC GCTGTGAGGG CACGATTGTG GACTGCTCCA
1641 ACCAGAAGCT GGTCCGCATC CCAAGCCACC TCCCTGAATA
1681 TGTCACCGAC CTGCGACTGA ATGACAATGA GGTATCTGTT
1721 CTGGAGGCCA CTGGCATCTT CAAGAAGTTG CCCAACCTGC
1761 GGAAAATAAA TCTGAGTAAC AATAAGATCA AGGAGGTGCG
1801 AGAGGGAGCT TTCGATGGAG CAGCCAGCGT GCAGGAGCTG
1841 ATGCTGACAG GGAACCAGCT GGAGACCGTG CACGGGCGCG
1881 TGTTCCGTGG CCTCAGTGGC CTCAAAACCT TGATGCTGAG
1921 GAGTAACTTG ATCAGCTGTG TGAGTAATGA CACCTTTGCC
1961 GGCCTGAGTT CGGTGAGACT GCTGTCCCTC TATGACAATC
2001 GGATCACCAC CATCACCCCT GGGGCCTTCA CCACGCTTGT
2041 CTCCCTGTCC ACCATAAACC TCCTGTCCAA CCCCTTCAAC
2081 TGCAACTGCC ACCTGGCCTG GCTCGGCAAG TGGTTGAGGA
2121 AGAGGCGGAT CGTCAGTGGG AACCCTAGGT GCCAGAAGCC
2161 ATTTTTCCTC AAGGAGATTC CCATCCAGGA TGTGGCCATC
2201 CAGGACTTCA CCTGTGATGG CAACGAGGAG AGTAGCTGCC
2241 AGCTGAGCCC GCGCTGCCCG GAGCAGTGCA CCTGTATGGA
2281 GACAGTGGTG CGATGCAGCA ACAAGGGGCT CCGCGCCCTC
2321 CCCAGAGGCA TGCCCAAGGA TGTGACCGAG CTGTACCTGG
2361 AAGGAAACCA CCTAACAGCC GTGCCCAGAG AGCTGTCCGC
2401 CCTCCGACAC CTGACGCTTA TTGACCTGAG CAACAACAGC
2441 ATCAGCATGC TGACCAATTA CACCTTCAGT AACATGTCTC
2481 ACCTCTCCAC TCTGATCCTG AGCTACAACC GGCTGAGGTG
2521 CATCCCCGTC CACGCCTTCA ACGGGCTGCG GTCCCTGCGA
2561 GTGCTAACCC TCCATGGCAA TGACATTTCC AGCGTTCCTG
2601 AAGGCTCCTT CAACGACCTC ACATCTCTTT CCCATCTGGC
2641 GCTGGGAACC AACCCACTCC ACTGTGACTG CAGTCTTCGG
2681 TGGCTGTCGG AGTGGGTGAA GGCGGGGTAC AAGGAGCCTG
2721 GCATCGCCCG CTGCAGTAGC CCTGAGCCCA TGGCTGACAG
2761 GCTCCTGCTC ACCACCCCAA CCCACCGCTT CCAGTGCAAA
2801 GGGCCAGTGG ACATCAACAT TGTGGCCAAA TGCAATGCCT
2841 GCCTCTCCAG CCCGTGCAAG AATAACGGGA CATGCACCCA
2881 GGACCCTGTG GAGCTGTACC GCTGTGCCTG CCCCTACAGC
2921 TACAAGGGCA AGGACTGCAC TGTGCCCATC AACACCTGCA
2961 TCCAGAACCC CTGTCAGCAT GGAGGCACCT GCCACCTGAG
3001 TGACAGCCAC AAGGATGGGT TCAGCTGCTC CTGCCCTCTG
3041 GGCTTTGAGG GGCAGCGGTG TGAGATCAAC CCAGATGACT
3081 GTGAGGACAA CGACTGCGAA AACAATGCCA CCTGCGTGGA
3121 CGGGATCAAC AACTACGTGT GTATCTGTCC GCCTAACTAC
3261 ACAGGTGAGC TATGCGACGA GGTGATTGAC CACTGTGTGC
3201 CTGAGCTGAA CCTCTGTCAG CATGAGGCCA AGTGCATCCC
3241 CCTGGACAAA GGATTCAGCT GCGAGTGTGT CCCTGGCTAC
3281 AGCGGGAAGC TCTGTGAGAC AGACAATGAT GACTGTGTGG
3321 CCCACAAGTG CCGCCACGGG GCCCAGTGCG TGGACACAAT
3361 CAATGGCTAC ACATGCACCT GCCCCCAGGG CTTCAGTGGA
3401 CCCTTCTGTG AACACCCCCC ACCCATGGTC CTACTGCAGA
3441 CCAGCCCATG CGACCAGTAC GAGTGCCAGA ACGGGGCCCA
3481 GTGCATCGTG GTGCAGCAGG AGCCCACCTG CCGCTGCCCA
3521 CCAGGCTTCG CCGGCCCCAG ATGCGAGAAG CTCATCACTG
3561 TCAACTTCGT GGGCAAAGAC TCCTACGTGG AACTGGCCTC
3601 CGCCAAGGTC CGACCCCAGG CCAACATCTC CCTGCAGGTG
3641 GCCACTGACA AGGACAACGG CATCCTTCTC TACAAAGGAG
3681 ACAATGACCC CCTGGCACTG GAGCTGTACC AGGGCCACGT
3721 GCGGCTGGTC TATGACAGCC TGAGTTCCCC TCCAACCACA
3761 GTGTACAGTG TGGAGACAGT GAATGATGGG CAGTTTCACA

```
3801 GTGTGGAGCT GGTGACGCTA AACCAGACCC TGAACCTAGT
3841 AGTGGACAAA GGAACTCCAA AGAGCCTGGG GAAGCTCCAG
3881 AAGCAGCCAG CAGTGGGCAT CAACAGCCCC CTCTACCTTG
3921 GAGGCATCCC CACCTCCACC GGCCTCTCCG CCTTGCGCCA
3961 GGGCACGGAC CGGCCTCTAG GCGGCTTCCA CGGATGCATC
4001 CATGAGGTGC GCATCAACAA CGAGCTGCAG GACTTCAAGG
4041 CCCTCCCACC ACAGTCCCTG GGGGTGTCAC CAGGCTGCAA
4081 GTCCTGCACC GTGTGCAAGC ACGGCCTGTG CCGCTCCGTG
4121 GAGAAGGACA GCGTGGTGTG CGAGTGCCGC CCAGGCTGGA
4161 CCGGCCCACT CTGCGACCAG GAGGCCCGGG ACCCCTGCCT
4201 CGGCCACAGA TGCCACCATG GAAAATGTGT GGCAACTGGG
4241 ACCTCATACA TGTGCAAGTG TGCCGAGGGC TATGGAGGGG
4281 ACTTGTGTGA CAACAAGAAT GACTCTGCCA ATGCCTGCTC
4321 AGCCTTCAAG TGTCACCATG GGCAGTGCCA CATCTCAGAC
4361 CAAGGGGAGC CCTACTGCCT GTGCCAGCCC GGCTTTAGCG
4441 GCGAGCACTG CCAACAAGAG AATCCGTGCC TGGGACAAGT
4441 AGTCCGAGAG GTGATCCGCC GCCAGAAAGG TTATGCATCA
4481 TGTGCCACAG CCTCCAAGGT GCCCATCATG GAATGTCGTG
4521 GGGGCTGTGG GCCCCAGTGC TGCCAGCCCA CCCGCAGCAA
4561 GCGGCGGAAA TACGTCTTCC AGTGCACGGA CGGCTCCTCG
4601 TTTGTAGAAG AGGTGGAGAG ACACTTAGAG TGCGGCTGCC
4641 TCGCGTGTTC CTAAGCCCCT GCCCGCCTGC CTGCCACCTC
4681 TCGGACTCCA GCTTGATGGA GTTGGGACAG CCATGTGGGA
4721 CCCCCTGGTG ATTCAGCATG AAGGAAATGA AGCTGGAGAG
4761 GAAGGTAAAG AAGAAGAGAA TATTAAGTAT ATTGTAAAAT
4801 AAACAAAAAA TAGAACTTAA AAAAAAAAAA AAAAAAAAAA
4841 AA
```

[0064] Another example of a *Homo sapiens* SLIT3 protein sequence (e.g., with NCBI accession number NP_003053) is shown below as SEQ ID NO:3.

```
   1 MAPGWAGVGA AVRARLALAL ALASVLSGPP AVACPTKCTC
  41 SAASVDCHGL GLRAVPRGIP RNAERLDLDR NNITRITKMD
  81 FAGLKNLRVL HLEDNQVSVI ERGAFQDLKQ LERLRLNKNK
 121 LQVLPELLFQ STPKLTRLDL SENQIQGIPR KAFRGITDVK
 161 NLQLDNNHIS CIEDGAFRAL RDLEILTLNN NNISRILVTS
 201 FNHMPKIRTL RLHSNHLYCD CHLAWLSDWL RQRRTVGQFT
 241 LCMAPVHLRG FNVADVQKKE YVCPAPHSEP PSCNANSISC
 281 PSPCTCSNNI VDCRGKGLME IPANLPEGIV EIRLEQNSIK
 321 AIPAGAFTQY KKLKRIDISK NQISDIAPDA FQGLKSLTSL
 361 VLYGNKITEI AKGLFDGLVS LQLLLLNANK INCLRVNTFQ
 401 DLQNLNLLSL YDNKLQTISK GLFAPLQSIQ TLHLAQNPFV
 441 CDCHLKWLAD YLQDNPIETS GARCSSPRRL ANKRISQIKS
 481 KKFRCSGSED YRSRFSSECF MDLVCPEKCR CEGTIVDCSN
 521 QKLVRIPSHL PEYVTDLRLN DNEVSVLEAT GIFKKLPNLR
 561 KINLSNNKIK EVREGAFDGA ASVQELMLTG NQLETVHGRV
 601 FRGLSGLKTL MLRSNLIGCV SNDTFAGLSS VRLLSLYDNR
 641 ITTITPGAFT TLVSLSTINL LSNPFNCNCH LAWLGKWLRK
 681 RRIVSGNPRC QKPFFLKEIP IQDVAIQDFT CDGNEESSCQ
 721 LSPRCPEQCT CMETVVRCSN KGLRALPRGM PKDVTELYLE
 761 GNHLTAVPRE LSALRHLTLI DLSNNSISML TNYTFSNMSH
 801 LSTLILSYNR LRCIPVHAFN GLRSLRVLTL HGNDISSVPE
 841 GSFNDLTSLS HLALGTNPLH CDCSLRWLSE WVKAGYKEPG
 881 IARCSSPEPM ADRLLLTTPT HRFQCKGPVD INIVAKCNAC
 921 LSSPCKNNGT CTQDPVELYR CACPYSYKGK DCTVPINTCI
```

```
 961 QNPCQHGGTC HLSDSHKDGF SCSCPLGFEG QRCEINPDDC
1001 EDNDCENNAT CVDGINNYVC ICPPNYTGEL CDEVIDHCVP
1041 ELNLCQHEAK CIPLDKGFSC ECVPGYSGKL CETDNDDCVA
1081 HKCRHGAQCV DTINGYTCTC PQGFSGPFCE HPPPMVLLQT
1121 SPCDQYECQN GAQCIVVQQE PTCRCPPGFA GPRCEKLITV
1161 NFVGKDSYVE LASAKVRPQA NISLQVATDK DNGILLYKGD
1201 NDPLALELYQ GHVRLVYDSL SSPPTTVYSV ETVNDGQFHS
1241 VELVTLNQTL NLVVDKGTPK SLGKLQKQPA VGINSPLYLG
1281 GIPTSTGLSA LRQGTDRPLG GFHGCIHEVR INNELQDFKA
1321 LPPQSLGVSP GCKSCTVCKH GLCRSVEKDS VVCECRPGWT
1361 GPLCDQEARD PCLGHRCHHG KCVATGTSYM CKCAEGYGGD
1401 LCDNKNDSAN ACSAFKCHHG QCHISDQGEP YCLCQPGFSG
1441 EHCQQENPCL GQVVREVIRR QKGYASCATA SKVPIMECRG
1481 GCGPQCCQPT RSKRRKYVFQ CTDGSSFVEE VERHLECGCL
1521 ACS
```

[0065] Another example of a *Homo sapiens* SLIT3 protein sequence (e.g., with NCBI accession number XP_016865268) is shown below as SEQ ID NO:4.

```
   1 MMGDLDRNNI TRITKMDFAG LKNLRVLHLE DNQVSVIERG
  41 AFQDLKQLER LRLNKNKLQV LPELLFQSTP KLTRLDLSEN
  81 QIQGIPRKAF RGITDVKNLQ LDNNHISCIE DGAFRALRDL
 121 EILTLNNNNI SRILVTSFNH MPKIRTLRLH SNHLYCDCHL
 161 AWLSDWLRQR RTVGQFTLCM APVHLRGFNV ADVQKKEYVC
 201 PAPHSEPPSC NANSISCPSP CTCSNNIVDC RGKGLMEIPA
 241 NLPEGIVEIR LEQNSIKAIP AGAFTQYKKL KRIDISKNQI
 281 SDIAPDAFQG LKSLTSLVLY GNKITEIVKG LFDGLVSLQL
 321 LLLNANKINC LRVNTFQDLQ NLNLLSLYDN KLQTISKGLF
 361 APLQSIQTLH LAQNPFVCDC HLKWLADYLQ DNPIETSGAR
 401 CSSPRRLANK RISQIKSKKF RCSGSEDYRS RFSSECFMDL
 441 VCPEKCRCEG TIVDCSNQKL VRIPSHLPEY VTDLRLNDNE
 481 VSVLEATGIF KKLPNLRKIN LSNNKIKEVR EGAFDGAASV
 521 QELMLTGNQL ETVHGRVFRG LSGLKTLMLR SNLIGCVSND
 561 TFAGLSSVRL LSLYDNRITT ITPGAFTTLV SLSTINLLSN
 601 PFNCNCHLAW LGKWLRKRRI VSGNPRCQKP FFLKEIPIQD
 641 VAIQDFTCDG NEESSCQLSP RCPEQCTCME TVVRCSNKGL
 681 RALPRGMPKD VTELYLEGNH LTAVPRELSA LRHLTLIDLS
 721 NNSISMLTNY TFSNMSHLST LILSYNRLRC IPVHAFNGLR
 761 SLRVLTLHGN DISSVPEGSF NDLTSLSHLA LGTNPLHCDC
 801 SLRWLSEWVK AGYKEPGIAR CSSPEPMADR LLLTTPTHRF
 841 QCKGPVDINI VAKCNACLSS PCKNNGTCTQ DPVELYRCAC
 881 PYSYKGKDCT VPINTCIQNP CQHGGTCHLS DSHKDGFSCS
 921 CPLGFEGQRC EINPDDCEDN DCENNATCVD GINNYVCICP
 961 PNYTGELCDE VIDHCVPELN LCQHEAKCIP LDKGFSCECV
1001 PGYSGKLCET DNDDCVAHKC RHGAQCVDTI NGYTCTCPQG
1041 FSGPFCEHPP PMVLLQTSPC DQYECQNGAQ CIVVQQEPTC
1081 RCPPGFAGPR CEKLITVNFV GKDSYVELAS AKVRPQANIS
1121 LQVATDKDNG ILLYKGDNDP LALELYQGHV RLVYDSLSSP
1161 PTTVYSVETV NDGQFHSVEL VTLNQTLNLV VDKGTPKSLG
1201 KLQKQPAVGI NSPLYLGGIP TSTGLSALRQ GTDRPLGGFH
1241 GCIHEVRINN ELQDFKALPP QSLGVSPGCK SCTVCKHGLC
1281 RSVEKDSVVC ECRPGWTGPL CDQEARDPCL GHRCHHGKCV
1321 ATGTSYMCKC AEGYGGDLCD NKNDSANACS AFKCHHGQCH
1361 ISDQGEPYCL CQPGFSGEHC QQENPCLGQV VREVIRRQKG
1401 YASCATASKV PIMECRGGCG PQCCQPTRSK RRKYVFQCTD
```

```
1441 GSSFVEEVER HLECGCLACS
```

[0066] A comparison of the SEQ ID NO:1 and SEQ ID NO:3 SLIT3 amino acid sequences is shown below.

```
99.9% identity in 1523 residues overlap; Score: 8255.0; Gap
frequency: 0.0%

Seq1    1
MAPGWAGVGAAVRARLALALALASVLSGPPAVACPTKCTCSAASVDCHGLGLRAVPRGIP
Seq3    1
MAPGWAGVGAAVRARLALALALASVLSGPPAVACPTKCTCSAASVDCHGLGLRAVPRGIP

************************************************************

Seq1 61
RNAERLDLDRNNITRITKMDFAGLKNLRVLHLEDNQVSVIERGAFQDLKQLERLRLNKNK
Seq3 61
RNAERLDLDRNNITRITKMDFAGLKNLRVLHLEDNQVSVIERGAFQDLKQLERLRLNKNK

************************************************************

Seq1 121
LQVLPELLFQSIPKLTRLDLSENQIQGIPRKAFRGITDVKNLQLDNNHISCIEDGAFRAL
Seq3 121
LQVLPELLFQSIPKLTRLDLSENQIQGIPRKAFRGITDVKNLQLDNNHISCIEDGAFRAL

************************************************************

Seq1 181
RDLEILTLNNNNISRILVTSFNHMPKIRTLRLHSNHLYCDCHLAWLSDWLRQRRTVGQFT
Seq3 181
RDLEILTLNNNNISRILVTSFNHMPKIRTLRLHSNHLYCDCHLAWLSDWLRQRRTVGQFT

************************************************************

Seq1 241
LCMAPVHLRGFNVADVQKKEYVCPAPHSEPPSCNANSISCPSPCTCSNNIVDCRGKGLME
Seq3 241
LCMAPVHLRGFNVADVQKKEYVCPAPHSEPPSCNANSISCPSPCTCSNNIVDCRGKGLME

************************************************************

Seq1 301
IPANLPEGIVEIRLEQNSIKAIPAGAFTQYKKLKRIDISKNQISDIAPDAFQGLKSLTSL
Seq3 301
IPANLPEGIVEIRLEQNSIKAIPAGAFTQYKKLKRIDISKNQISDIAPDAFQGLKSLTSL

************************************************************

Seq1 361
VLYGNKITEIAKGLFDGLVSLQLLLLNANKINCLRVNTFQDLQNLNLLSLYDNKLQTISK
Seq3 361
VLYGNKITEIAKGLFDGLVSLQLLLLNANKINCLRVNTFQDLQNLNLLSLYDNKLQTISK

************************************************************

Seq1 421
GLFAPLQSIQTLHLAQNPFVCDCHLKWLADYLQDNPIETSGARCSSPRRLANKRISQIKS
```

```
Seq3 421
GLFAPLQSIQTLHLAQNPFVCDCHLKWLADYLQDNPIETSGARCSSPRRLANKRISQIKS

************************************************************

Seq1 481
KKFRCSGSEDYRSRFSSECFMDLVCPEKCRCEGTIVDCSNQKLVRIPSHLPEYVTDLRLN
Seq3 481
KKFRCSGSEDYRSRFSSECFMDLVCPEKCRCEGTIVDCSNQKLVRIPSHLPEYVTDLRLN

************************************************************

Seq1 541
DNEVSVLEATGIFKKLPNLRKINLSNNKIKEVREGAFDGAASVQELMLTGNQLETVHGRV
Seq3 541
DNEVSVLEATGIFKKLPNLRKINLSNNKIKEVREGAFDGAASVQELMLTGNQLETVHGRV

************************************************************

Seq1 601
FRGLSGLKTLMLRSNLISCVSNDTFAGLSSVRLLSLYDNRITTITPGAFTTLVSLSTINL
Seq3 601
FRGLSGLKTLMLRSNLIGCVSNDTFAGLSSVRLLSLYDNRITTITPGAFTTLVSLSTINL
****************.*****************************************

Seq1 661
LSNPFNCNCHLAWLGKWLRKRRIVSGNPRCQKPFFLKEIPIQDVAIQDFTCDGNEESSCQ
Seq3 661
LSNPFNCNCHLAWLGKWLRKRRIVSGNPRCQKPFFLKEIPIQDVAIQDFTCDGNEESSCQ

************************************************************

Seq1 721
LSPRCPEQCTCMETVVRCSNKGLRALPRGMPKDVTELYLEGNHLTAVPRELSALRHLTLI
Seq3 721
LSPRCPEQCTCMETVVRCSNKGLRALPRGMPKDVTELYLEGNHLTAVPRELSALRHLTLI

************************************************************

Seq1 781
DLSNNSISMLTNYTFSNMSHLSTLILSYNRLRCIPVHAFNGLRSLRVLILHGNDISSVPE
Seq3 781
DLSNNSISMLTNYTFSNMSHLSTLILSYNRLRCIPVHAFNGLRSLRVLILHGNDISSVPE

************************************************************

Seq1 841
GSFNDLTSLSHLALGTNPLHCDCSLRWLSEWVKAGYKEPGIARCSSPEPMADRLLLTTPT
Seq3 841
GSFNDLTSLSHLALGTNPLHCDCSLRWLSEWVKAGYKEPGIARCSSPEPMADRLLLTTPT

************************************************************

Seq1 901
HRFQCKGPVDINIVAKCNACLSSPCKNNGTCTQDPVELYRCACPYSYKGKDCTVPINTCI
Seq3 901
HRFQCKGPVDINIVAKCNACLSSPCKNNGTCTQDPVELYRCACPYSYKGKDCTVPINTCI

************************************************************

Seq1 961
QNPCQHGGTCHLSDSHKDGFSCSCPLGFEGQRCEINPDDCEDNDCENNATCVDGINNYVC
```

```
Seq3 961
QNPCQHGGTCHLSDSHKDGFSCSCPLGFEGQRCEINPDDCEDNDCENNATCVDGINNYVC

************************************************************

Seq1 1021
ICPPNYTGELCDEVIDHCVPELNLCQHEAKCIPLDKGFSCECVPGYSGKLCETDNDDCVA
Seq3 1021
ICPPNYTGELCDEVIDHCVPELNLCQHEAKCIPLDKGFSCECVPGYSGKLCETDNDDCVA

************************************************************

Seq1 1081
HKCRHGAQCVDTINGYTCTCPQGFSGPFCEHPPPMVLLQTSPCDQYECQNGAQCIVVQQE
Seq3 1081
HKCRHGAQCVDTINGYTCTCPQGFSGPFCEHPPPMVLLQTSPCDQYECQNGAQCIVVQQE

************************************************************

Seq1 1141
PTCRCPPGFAGPRCEKLITVNFVGKDSYVELASAKVRPQANISLQVATDKDNGILLYKGD
Seq3 1141
PTCRCPPGFAGPRCEKLITVNFVGKDSYVELASAKVRPQANISLQVATDKDNGILLYKGD

************************************************************

Seq1 1201
NDPLALELYQGHVRLVYDSLSSPPTTVYSVETVNDGQFHSVELVTLNQTLNLVVDKGTPK
Seq3 1201
NDPLALELYQGHVRLVYDSLSSPPTTVYSVETVNDGQFHSVELVTLNQTLNLVVDKGTPK

************************************************************

Seq1 1261
SLGKLQKQPAVGINSPLYLGGIPTSTGLSALRQGTDRPLGGFHGCIHEVRINNELQDFKA
Seq3 1261
SLGKLQKQPAVGINSPLYLGGIPTSTGLSALRQGTDRPLGGFHGCIHEVRINNELQDFKA

************************************************************

Seq1 1321
LPPQSLGVSPGCKSCTVCKHGLCRSVEKDSVVCECRPGWTGPLCDQEARDPCLGHRCHHG
Seq3 1321
LPPQSLGVSPGCKSCTVCKHGLCRSVEKDSVVCECRPGWTGPLCDQEARDPCLGHRCHHG

************************************************************

Seq1 1381
KCVATGTSYMCKCAEGYGGDLCDNKNDSANACSAFKCHHGQCHISDQGEPYCLCQPGFSG
Seq3 1381
KCVATGTSYMCKCAEGYGGDLCDNKNDSANACSAFKCHHGQCHISDQGEPYCLCQPGFSG

************************************************************

Seq1 1441
EHCQQENPCLGQVVREVIRRQKGYASCATASKVPIMECRGGCGPQCCQPTRSKRRKYVFQ
Seq3 1441
EHCQQENPCLGQVVREVIRRQKGYASCATASKVPIMECRGGCGPQCCQPTRSKRRKYVFQ

************************************************************

Seq1 1501 CTDGSSFVEEVERHLECGCLACS
```

```
Seq3 1501 CIDGSSFVEEVERHLECGCLACS
          ************************
```

[0067] A comparison of the SEQ ID NO:1 and SEQ ID NO:4 SLIT3 amino acid sequences is shown below.

```
99.9% identity in 1457 residues overlap; Score: 7909.0; Gap
frequency: 0.0%

Seq1   67
DLDRNNITRITKMDFAGLKNLRVLHLEDNQVSVIERGAFQDLKQLERLRLNKNKLQVLPE
Seq4    4
DLDRNNITRITKMDFAGLKNLRVLHLEDNQVSVIERGAFQDLKQLERLRLNKNKLQVLPE

************************************************************

Seq1  127
LLFQSTPKLTRLDLSENQIQGIPRKAFRGITDVKNLQLDNNHISCIEDGAFRALRDLEIL
Seq4   64
LLFQSTPKLTRLDLSENQIQGIPRKAFRGITDVKNLQLDNNHISCIEDGAFRALRDLEIL

************************************************************

Seq1  187
TLNNNNISRILVTSFNHMPKIRTLRLHSNHLYCDCHLAWLSDWLRQRRTVGQFTLCMAPV
Seq4  124
TLNNNNISRILVTSFNHMPKIRTLRLHSNHLYCDCHLAWLSDWLRQRRTVGQFTLCMAPV

************************************************************

Seq1  247
HLRGFNVADVQKKEYVCPAPHSEPPSCNANSISCPSPCTCSNNIVDCRGKGLMEIPANLP
Seq4  184
HLRGFNVADVQKKEYVCPAPHSEPPSCNANSISCPSPCTCSNNIVDCRGKGLMEIPANLP

************************************************************

Seq1  307
EGIVEIRLEQNSIKAIPAGAFTQYKKLKRIDISKNQISDIAPDAFQGLKSLTSLVLYGNK
Seq4  244
EGIVEIRLEQNSIKAIPAGAFTQYKKLKRIDISKNQISDIAPDAFQGLKSLTSLVLYGNK

************************************************************

Seq1  367
ITEIAKGLFDGLVSLQLLLLNANKINCLRVNTFQDLQNLNLLSLYDNKLQTISKGLFAPL
Seq4  304
ITEIVKGLFDGLVSLQLLLLNANKINCLRVNTFQDLQNLNLLSLYDNKLQTISKGLFAPL
****  ********************************************************

Seq1  427
QSIQTLHLAQNPFVCDCHLKWLADYLQDNPIETSGARCSSPRRLANKRISQIKSKKFRCS
Seq4  364
QSIQTLHLAQNPFVCDCHLKWLADYLQDNPIETSGARCSSPRRLANKRISQIKSKKFRCS

************************************************************

Seq1  487
GSEDYRSRFSSECFMDLVCPEKCRCEGTIVDCSNQKLVRIPSHLPEYVTDLRLNDNEVSV
Seq4  424
GSEDYRSRFSSECFMDLVCPEKCRCEGTIVDCSNQKLVRIPSHLPEYVTDLRLNDNEVSV
```

```
************************************************************

Seq1  547
LEATGIFKKLPNLRKINLSNNKIKEVREGAFDGAASVQELMLTGNQLETVHGRVFRGLSG
Seq4  484
LEATGIFKKLPNLRKINLSNNKIKEVREGAFDGAASVQELMLTGNQLETVHGRVFRGLSG

************************************************************

Seq1  607
LKTLMLRSNLISCVSNDTFAGLSSVRLLSLYDNRITTITPGAFTTLVSLSTINLLSNPFN
Seq4  544
LKTLMLRSNLIGCVSNDTFAGLSSVRLLSLYDNRITTITPGAFTTLVSLSTINLLSNPFN
********** **************************************************

Seq1  667
CNCHLAWLGKWLRKRRIVSGNPRCQKPFFLKEIPIQDVAIQDFTCDGNEESSCQLSPRCP
Seq4  604
CNCHLAWLGKWLRKRRIVSGNPRCQKPFFLKEIPIQDVAIQDFTCDGNEESSCQLSPRCP

************************************************************

Seq1  727
EQCTCMETVVRCSNKGLRALPRGMPKDVTELYLEGNHLTAVPRELSALRHLTLIDLSNNS
Seq4  664
EQCTCMETVVRCSNKGLRALPRGMPKDVTELYLEGNHLTAVPRELSALRHLTLIDLSNNS

************************************************************

Seq1  787
ISMLTNYTFSNMSHLSTLILSYNRLRCIPVHAFNGLRSLRVLTLHGNDISSVPEGSFNDL
Seq4  724
ISMLTNYTFSNMSHLSTLILSYNRLRCIPVHAFNGLRSLRVLTLHGNDISSVPEGSFNDL

************************************************************

Seq1  847
TSLSHLALGTNPLHCDCSLRWLSEWVKAGYKEPGIARCSSPEPMADRLLLTTPTHRFQCK
Seq4  784
TSLSHLALGTNPLHCDCSLRWLSEWVKAGYKEPGIARCSSPEPMADRLLLTTPTHRFQCK

************************************************************

Seq1  907
GPVDINIVAKCNACLSSPCKNNGTCTQDPVELYRCACPYSYKGKDCTVPINTCIQNPCQH
Seq4  844
GPVDINIVAKCNACLSSPCKNNGTCTQDPVELYRCACPYSYKGKDCTVPINTCIQNPCQH

************************************************************

Seq1  967
GGTCHLSDSHKDGFSCSCPLGFEGQRCEINPDDCEDNDCENNATCVDGINNYVCICPPNY
Seq4  904
GGTCHLSDSHKDGFSCSCPLGFEGQRCEINPDDCEDNDCENNATCVDGINNYVCICPPNY

************************************************************

Seq1 1027
TGELCDEVIDHCVPELNLCQHEAKCIPLDKGFSCECVPGYSGKLCETDNDDCVAHKCRHG
Seq4  964
TGELCDEVIDHCVPELNLCQHEAKCIPLDKGFSCECVPGYSGKLCETDNDDCVAHKCRHG
```

```
************************************************************

Seq1 1087
AQCVDTINGYTCTCPQGFSGPFCEHPPPMVLLQTSPCDQYECQNGAQCIVVQQEPTCRCP
Seq4 1024
AQCVDTINGYTCTCPQGFSGPFCEHPPPMVLLQTSPCDQYECQNGAQCIVVQQEPTCRCP

************************************************************

Seq1 1147
PGFAGPRCEKLITVNFVGKDSYVELASAKVRPQANISLQVATDKDNGILLYKGDNDPLAL
Seq4 1084
PGFAGPRCEKLITVNFVGKDSYVELASAKVRPQANISLQVATDKDNGILLYKGDNDPLAL

************************************************************

Seq1 1207
ELYQGHVRLVYDSLSSPPTTVYSVETVNDGQFHSVELVTLNQTLNLVVDKGTPKSLGKLQ
Seq4 1144
ELYQGHVRLVYDSLSSPPTTVYSVETVNDGQFHSVELVTLNQTLNLVVDKGTPKSLGKLQ

************************************************************

Seq1 1267
KQPAVGINSPLYLGGIPTSTGLSALRQGTDRPLGGFHGCIHEVRINNELQDFKALPPQSL
Seq4 1204
KQPAVGINSPLYLGGIPTSTGLSALRQGTDRPLGGFHGCIHEVRINNELQDFKALPPQSL

************************************************************

Seq1 1327
GVSPGCKSCTVCKHGLCRSVEKDSVVCECRPGWTGPLCDQEARDPCLGHRCHHGKCVATG
Seq4 1264
GVSPGCKSCTVCKHGLCRSVEKDSVVCECRPGWTGPLCDQEARDPCLGHRCHHGKCVATG

************************************************************

Seq1 1387
TSYMCKCAEGYGGDLCDNKNDSANACSAFKCHHGQCHISDQGEPYCLCQPGFSGEHCQQE
Seq4 1324
TSYMCKCAEGYGGDLCDNKNDSANACSAFKCHHGQCHISDQGEPYCLCQPGFSGEHCQQE

************************************************************

Seq1 1447
NPCLGQVVREVIRRQKGYASCATASKVPIMECRGGCGPQCCQPTRSKRRKYVFQCTDGSS
Seq4 1384
NPCLGQVVREVIRRQKGYASCATASKVPIMECRGGCGPQCCQPTRSKRRKYVFQCTDGSS

************************************************************

Seq1 1507 FVEEVERHLECGCLACS
Seq4 1444 FVEEVERHLECGCLACS
          *****************
```

[0068] Such sequence comparisons illustrate portions of the SLIT3 protein that tend to be conserved, and portions of the SLIT3 protein that are not so conserved.

[0069] An example of a SLIT2 protein sequence is shown below (NCBI accession number AAD25539; SEQ ID NO:5).

```
   1 MRGVGWQMLS LSLGLVLAIL NKVAPQACPA QCSCSGSTVD
  41 CHGLALRSVP RNIPRNTERL DLNGNNITRI TKTDFAGLRH
  81 LRVLQLMENK ISTIERGAFQ DLKELERLRL NRNHLQLFPE
 121 LLFLGTAKLY RLDLSENQIQ AIPRKAFRGA VDIKNLQLDY
 161 NQISCIEDGA FRALRDLEVL TLNNNNITRL SVASFNHMPK
 201 LRTFRLHSNN LYCDCHLAWL SDWLRKRPRV GLYTQCMGPS
 241 HLRGHNVAEV QKREFVCSDE EEGHQSFMAP SCSVLHCPAA
 281 CTCSNNIVDC RGKGLTEIPT NLPETITEIR LEQNTIKVIP
 321 PGAFSPYKKL RRIDLSNNQI SELAPDAFQG LRSLNSLVLY
 361 GNKITELPKS LFEGLFSLQL LLLNANKINC LRVDAFQDLH
 401 NLNLLSLYDN KLQTIAKGTF SPLRAIQTMH LAQNPFICDC
 441 HLKWLADYLH TNPIETSGAR CTSPRRLANK RIGQIKSKKF
 481 RCSGTEDYRS KLSGDCFADL ACPEKCRCEG TTVDCSNQKL
 521 NKIPEHIPQY TAELRLNNNE FTVLEATGIF KKLPQLRKIN
 561 FSNNKITDIE EGAFEGASGV NEILLTSNRL ENVQHKMFKG
 601 LESLKTLMLR SNRITCVGND SFIGLSSVRL LSLYDNQITT
 641 VAPGAFDTLH SLSTLNLLAN PFNCNCYLAW LGEWLRKKRI
 681 VTGNPRCQKP YFLKEIPIQD VAIQDFTCDD GNDDNSCSPL
 721 SRCPTECTCL DTVVRCSNKG LKVLPKGIPR DVTELYLDGN
 761 QFTLVPKELS NYKHLTLIDL SNNRISTLSN QSFSNMTQLL
 801 TLILSYNRLR CIPPRTFDGL KSLRLLSLHG NDISVVPEGA
 841 FNDLSALSHL AIGANPLYCD CNMQWLSDWV KSEYKEPGIA
 881 RCAGPGEMAD KLLLTTPSKK FTCQGPVDVN ILAKCNPCLS
 921 NPCKNDGTCN SDPVDFYRCT CPYGFKGQDC DVPIHACISN
 961 PCKHGGTCHL KEGEEDGFWC ICADGFEGEN CEVNVDDCED
1001 NDCENNSTCV DGINNYTCLC PPEYTGELCE EKLDFCAQDL
1041 NPCQHDSKCI LTPKGFKCDC TPGYVGEHCD IDFDDCQDNK
1081 CKNGAHCTDA VNGYTCICPE GYSGLFCEFS PPMVLPRTSP
1121 CDNFDCQNGA QCIVRINEPI CQCLPGYQGE KCEKLVSVNF
1161 INKESYLQIP SAKVRPQTNI TLQIATDEDS GILLYKGDKD
1201 HIAVELYRGR VRASYDTGSH PASAIYSVET INDGNFHIVE
1241 LLALDQSLSL SVDGGNPKII TNLSKQSTLN FDSPLYVGGM
1281 PGKSNVASLR QAPGQNGTSF HGCIRNLYIN SELQDFQKVP
1321 MQTGILPGCE PCHKKVCAHG TCQPSSQAGF TCECQEGWMG
1361 PLCDQRTNDP CLGNKCVHGT CLPINAFSYS CKCLEGHGGV
1401 LCDEEEDLFN PCQAIKCKHG KCRLSGLGQP YCECSSGYTG
1441 DSCDREISCR GERIRDYYQK QQGYAACQTT KKVSRLECRG
1481 GCAGGQCCGP LRSKRRKYSF ECTDGSSFVD EVEKVVKCGC
1521 TRCVS
```

[0070] An example of a nucleic acid that encodes the SEQ ID NO:5 SLIT2 protein is shown (NCBI accession number AF133270; SEQ ID NO:6).

```
   1 ATGCGCGGCG TTGGCTGGCA GATGCTGTCC CTGTCGCTGG
  41 GGTTAGTGCT GGCGATCCTG AACAAGGTGG CACCGCAGGC
  81 GTGCCCGGCG CAGTGCTCTT GCTCGGGCAG CACAGTGGAC
 121 TGTCACGGGC TGGCGCTGCG CAGCGTGCCC AGGAATATCC
 161 CCCGCAACAC CGAGAGACTG GATTTAAATG GAAATAACAT
 201 CACAAGAATT ACGAAGACAG ATTTTGCTGG TCTTAGACAT
 241 CTAAGAGTTC TTCAGCTTAT GGAGAATAAG ATTAGCACCA
 281 TTGAAAGAGG AGCATTCCAG GATCTTAAAG AACTAGAGAG
 321 ACTGCGTTTA AACAGAAATC ACCTTCAGCT GTTTCCTGAG
```

```
 361 TTGCTGTTTC TTGGGACTGC GAAGCTATAC AGGCTTGATC
 401 TCAGTGAAAA CCAAATTCAG GCAATCCCAA GGAAAGCTTT
 441 CCGTGGGGCA GTTGACATAA AAAATTTGCA ACTGGATTAC
 481 AACCAGATCA GCTGTATTGA AGATGGGGCA TTCAGGGCTC
 521 TCCGGGACCT GGAAGTGCTC ACTCTCAACA ATAACAACAT
 561 TACTAGACTT TCTGTGGCAA GTTTCAACCA TATGCCTAAA
 601 CTTAGGACTT TTCGACTGCA TTCAAACAAC CTGTATTGTG
 641 ACTGCCACCT GGCCTGGCTC TCCGACTGGC TTCGCAAAAG
 681 GCCTCGGGTT GGTCTGTACA CTCAGTGTAT GGGCCCCTCC
 721 CACCTGAGAG GCCATAATGT AGCCGAGGTT CAAAAACGAG
 761 AATTTGTCTG CAGTGATGAG GAAGAAGGTC ACCAGTCATT
 801 TATGGCTCCT TCTTGTAGTG TTTTGCACTG CCCTGCCGCC
 841 TGTACCTGTA GCAACAATAT CGTAGACTGT CGTGGGAAAG
 881 GTCTCACTGA GATCCCCACA AATCTTCCAG AGACCATCAC
 921 AGAAATACGT TTGGAACAGA ACACAATCAA AGTCATCCCT
 961 CCTGGAGCTT TCTCACCATA TAAAAAGCTT AGACGAATTG
1001 ACCTGAGCAA TAATCAGATC TCTGAACTTG CACCAGATGC
1041 TTTCCAAGGA CTACGCTCTC TGAATTCACT TGTCCTCTAT
1081 GGAAATAAAA TCACAGAACT CCCCAAAAGT TTATTTGAAG
1121 GACTGTTTTC CTTACAGCTC CTATTATTGA ATGCCAACAA
1161 GATAAACTGC CTTCGGGTAG ATGCTTTTCA GGATCTCCAC
1201 AACTTGAACC TTCTCTCCCT ATATGACAAC AAGCTTCAGA
1241 CCATCGCCAA GGGGACCTTT TCACCTCTTC GGGCCATTCA
1281 AACTATGCAT TTGGCCCAGA ACCCCTTTAT TTGTGACTGC
1321 CATCTCAAGT GGCTAGCGGA TTATCTCCAT ACCAACCCGA
1361 TTGAGACCAG TGGTGCCCGT TGCACCAGCC CCCGCCGCCT
1401 GGCAAACAAA AGAATTGGAC AGATCAAAAG CAAGAAATTC
1441 CGTTGTTCAG GTACAGAAGA TTATCGATCA AAATTAAGTG
1481 GAGACTGCTT TGCGGATCTG GCTTGCCCTG AAAAGTGTCG
1521 CTGTGAAGGA ACCACAGTAG ATTGCTCTAA TCAAAAGCTC
1561 AACAAAATCC CGGAGCACAT TCCCCAGTAC ACTGCAGAGT
1601 TGCGTCTCAA TAATAATGAA TTTACCGTGT TGGAAGCCAC
1641 AGGAATCTTT AAGAAACTTC CTCAATTACG TAAAATAAAC
1681 TTTAGCAACA ATAAGATCAC AGATATTGAG GAGGGAGCAT
1721 TTGAAGGAGC ATCTGGTGTA AATGAAATAC TTCTTACGAG
1761 TAATCGTTTG GAAAATGTGC AGCATAAGAT GTTCAAGGGA
1801 TTGGAAAGCC TCAAAACTTT GATGTTGAGA AGCAATCGAA
1841 TAACCTGTGT GGGGAATGAC AGTTTCATAG GACTCAGTTC
1881 TGTGCGTTTG CTTTCTTTGT ATGATAATCA AATTACTACA
1921 GTTGCACCAG GGGCATTTGA TACTCTCCAT TCTTTATCTA
1961 CTCTAAACCT CTTGGCCAAT CCTTTTAACT GTAACTGCTA
2001 CCTGGCTTGG TTGGGAGAGT GGCTGAGAAA GAAGAGAATT
2041 GTCACGGGAA ATCCTAGATG TCAAAAACCA TACTTCCTGA
2081 AAGAAATACC CATCCAGGAT GTGGCCATTC AGGACTTCAC
2121 TTGTGATGAC GGAAATGATG ACAATAGTTG CTCCCCACTT
2161 TCTCGCTGTC CTACTGAATG TACTTGCTTG GATACAGTCG
2201 TCCGATGTAG CAACAAGGGT TTGAAGGTCT TGCCGAAAGG
2241 TATTCCAAGA GATGTCACAG AGTTGTATCT GGATGGAAAC
2281 CAATTTACAC TGGTTCCCAA GGAACTCTCC AACTACAAAC
2321 ATTTAACACT TATAGACTTA AGTAACAACA GAATAAGCAC
2361 GCTTTCTAAT CAGAGCTTCA GCAACATGAC CCAGCTCCTC
2401 ACCTTAATTC TTAGTTACAA CCGTCTGAGA TGTATTCCTC
2441 CTCGCACCTT TGATGGATTA AAGTCTCTTC GATTACTTTC
2481 TCTACATGGA AATGACATTT CTGTTGTGCC TGAAGGTGCT
2521 TTCAATGATC TTTCTGCATT ATCACATCTA GCAATTGGAG
2561 CCAACCCTCT TTACTGTGAT TGTAACATGC AGTGGTTATC
```

2601 CGACTGGGTG AAGTCGGAAT ATAAGGAGCC TGGAATTGCT
2641 CGTTGTGCTG GTCCTGGAGA AATGGCAGAT AAACTTTTAC
2681 TCACAACTCC CTCCAAAAAA TTTACCTGTC AAGGTCCTGT
2721 GGATGTCAAT ATTCTAGCTA AGTGTAACCC CTGCCTATCA
2761 AATCCGTGTA AAAATGATGG CACATGTAAT AGTGATCCAG
2801 TTGACTTTTA CCGATGCACC TGTCCATATG GTTTCAAGGG
2841 GCAGGACTGT GATGTCCCAA TTCATGCCTG CATCAGTAAC
2881 CCATGTAAAC ATGGAGGAAC TTGCCACTTA AAGGAAGGAG
2921 AAGAAGATGG ATTCTGGTGT ATTTGTGCTG ATGGATTTGA
2961 AGGAGAAAAT TGTGAAGTCA ACGTTGATGA TTGTGAAGAT
3001 AATGACTGTG AAAATAATTC TACATGTGTC GATGGCATTA
3041 ATAACTACAC ATGCCTTTGC CCACCTGAGT ATACAGGTGA
3081 GTTGTGTGAG GAGAAGCTGG ACTTCTGTGC CCAGGACCTG
3121 AACCCCTGCC AGCACGATTC AAAGTGCATC CTAACTCCAA
3161 AGGGATTCAA ATGTGACTGC ACACCAGGGT ACGTAGGTGA
3201 ACACTGCGAC ATCGATTTTG ACGACTGCCA AGACAACAAG
3241 TGTAAAAACG GAGCCCACTG CACAGATGCA GTGAACGGCT
3281 ATACGTGCAT ATGCCCCGAA GGTTACAGTG GCTTGTTCTG
3321 TGAGTTTTCT CCACCCATGG TCCTCCCTCG TACCAGCCCC
3361 TGTGATAATT TTGATTGTCA GAATGGAGCT CAGTGTATCG
3401 TCAGAATAAA TGAGCCAATA TGTCAGTGTT TGCCTGGCTA
3441 TCAGGGAGAA AAGTGTGAAA AATTGGTTAG TGTGAATTTT
3481 ATAAACAAAG AGTCTTATCT TCAGATTCCT TCAGCCAAGG
3521 TTCGGCCTCA GACGAACATA ACACTTCAGA TTGCCACAGA
3561 TGAAGACAGC GGAATCCTCC TGTATAAGGG TGACAAAGAC
3601 CATATCGCGG TAGAACTCTA TCGGGGGCGT GTTCGTGCCA
3641 GCTATGACAC CGGCTCTCAT CCAGCTTCTG CCATTTACAG
3681 TGTGGAGACA ATCAATGATG GAAACTTCCA CATTGTGGAA
3721 CTACTTGCCT TGGATCAGAG TCTCTCTTTG TCCGTGGATG
3761 GTGGGAACCC CAAAATCATC ACTAACTTGT CAAAGCAGTC
3801 CACTCTGAAT TTTGACTCTC CACTCTATGT AGGAGGCATG
3841 CCAGGGAAGA GTAACGTGGC ATCTCTGCGC CAGGCCCCTG
3881 GGCAGAACGG AACCAGCTTC CACGGCTGCA TCCGGAACCT
3921 TTACATCAAC AGTGAGCTGC AGGACTTCCA GAAGGTGCCG
3961 ATGCAAACAG GCATTTTGCC TGGCTGTGAG CCATGCCACA
4001 AGAAGGTGTG TGCCCATGGC ACATGCCAGC CCAGCAGCCA
4041 GGCAGGCTTC ACCTGCGAGT GCCAGGAAGG ATGGATGGGG
4081 CCCCTCTGTG ACCAACGGAC CAATGACCCT TGCCTTGGAA
4121 ATAAATGCGT ACATGGCACC TGCTTGCCCA TCAATGCGTT
4161 CTCCTACAGC TGTAAGTGCT TGGAGGGCCA TGGAGGTGTC
4201 CTCTGTGATG AAGAGGAGGA TCTGTTTAAC CCATGCCAGG
4241 CGATCAAGTG CAAGCATGGG AAGTGCAGGC TTTCAGGTCT
4281 GGGGCAGCCC TACTGTGAAT GCAGCAGTGG ATACACGGGG
4321 GACAGCTGTG ATCGAGAAAT CTCTTGTCGA GGGGAAAGGA
4361 TAAGAGATTA TTACCAAAAG CAGCAGGGCT ATGCTGCTTG
4441 CCAAACAACC AAGAAGGTGT CCCGATTAGA GTGCAGAGGT
4441 GGGTGTGCAG GAGGGCAGTG CTGTGGACCG CTGAGGAGCA
4481 AGCGGCGGAA ATACTCTTTC GAATGCACTG ACGGCTCCTC
4521 CTTTGTGGAC GAGGTTGAGA AAGTGGTGAA GTGCGGCTGT
4561 ACGAGGTGTG TGTCCTAAAC ACACTCCCGG CAGCTCTGTC
4601 TTTGGAAAAG GTTGTATACT TCTTGACCAT GTGGGACTAA
4641 TGAATGCTTC ATAGTGGAAA TATTTGAAAT ATATTGTAAA
4681 ATACAGAACA GACTTATTTT TATTATGAGA ATAAAGACTT
4721 TTTTTCTGCA TTTGGAAAAA AAAAAAAAAA AAACTCGA

[0071] A comparison of the SLIT3 with SEQ ID NO:1, and the SLIT2 with SEQ ID NO:5 amino acid sequences is shown below.

```
67.0% identity in 1515 residues overlap; Score: 5664.0; Gap
frequency: 0.7%

Seq1   16
LALALALASVLSGPPAVACPTKCTCSAASVDCHGLGLRAVPRGIPRNAERLDLDRNNITR
Seq5   11
LSLGLVLA-ILNKVAPQACPAQCSCSGSTVDCHGLALRSVPRNIPRNTERLDLNGNNITR
* * * **  *      ***  * **   ****** ** *** **** *****  *****

Seq1   76
ITKMDFAGLKNLRVLHLEDNQVSVIERGAFQDLKQLERLRLNKNKLQVLPELLFQSTPKL
Seq5   70
ITKTDFAGLRHLRVLQLMENKISTIERGAFQDLKELERLRLNRNHLQLFPELLFLGTAKL
*** *****  **** *  *  * ********** ******* * **  *****  * **

Seq1  136
TRLDLSENQIQGIPRKAFRGITDVKNLQLDNNHISCIEDGAFRALRDLEILTLNNNNISR
Seq5  130
YRLDLSENQIQAIPRKAFRGAVDIKNLQLDYNQISCIEDGAFRALRDLEVLTLNNNNITR
 ********** ********  * ****** * *************** ******** *

Seq1  196
ILVTSFNHMPKIRTLRLHSNHLYCDCHLAWLSDWLRQRRIVGQFTLCMAPVHLRGFNVAD
Seq5  190
LSVASFNHMPKLRTFRLHSNNLYCDCHLAWLSDWLRKRPRVGLYTQCMGPSHLRGHNVAE
  * ******* ** ***** *************** *  **  * ** * **** ***

Seq1  256
VQKKEYVCPAPHSEPPSCNANSIS---CPSPCTCSNNIVDCRGKGLMEIPANLPEGIVEI
Seq5  250
VQKREFVCSDEEEGHQSFMAPSCSVLHCPAACTCSNNIVDCRGKGLTEIPTNLPETITEI
*** * **        *  * * *   **  *************** *** **** * **

Seq1  313
RLEQNSIKAIPAGAFTQYKKLKRIDISKNQISDIAPDAFQGLKSLTSLVLYGNKITEIAK
Seq5  310
RLEQNTIKVIPPGAFSPYKKLRRIDLSNNQISELAPDAFQGLRSLNSLVLYGNKITELPK
***** ** ** ***  **** *** * ****  ******** ** ***********  *

Seq1  373
GLFDGLVSLQLLLLNANKINCLRVNTFQDLQNLNLLSLYDNKLQTISKGLFAPLQSIQTL
Seq5  370
SLFEGLFSLQLLLLNANKINCLRVDAFQDLHNLNLLSLYDNKLQTIAKGTFSPLRAIQTM
 ** ** ****************  **** ************** ** * **  ***

Seq1  433
HLAQNPFVCDCHLKWLADYLQDNPIETSGARCSSPRRLANKRISQIKSKKFRCSGSEDYR
Seq5  430
HLAQNPFICDCHLKWLADYLHTNPIETSGARCTSPRRLANKRIGQIKSKKFRCSGTEDYR
******* ************  ********** ********** *********** ****

Seq1  493
SRFSSECFMDLVCPEKCRCEGTIVDCSNQKLVRIPSHLPEYVTDLRLNDNEVSVLEATGI
Seq5  490
SKLSGDCFADLACPEKCRCEGTTVDCSNQKLNKIPEHIPQYTAELRLNNNEFTVLEATGI
*  *  ** ** ********** ********  ** * * *   **** **  *******
```

```
Seq1  553
FKKLPNLRKINLSNNKIKEVREGAFDGAASVQELMLTGNQLETVHGRVFRGLSGLKTLML
Seq5  550
FKKLPQLRKINFSNNKITDIEEGAFEGASGVNEILLTSNRLENVQHKMFKGLESLKTLML
***** ***** *****    **** **  * *  ** * ** *    * **  ******

Seq1  613
RSNLISCVSNDTFAGLSSVRLLSLYDNRITTITPGAFTTLVSLSTINLLSNPFNCNCHLA
Seq5  610
RSNRITCVGNDSFIGLSSVRLLSLYDNQITTVAPGAFDTLHSLSTLNLLANPFNCNCYLA
*** * ** ** * ************* ***  **** ** **** *** ******* **

Seq1  673
WLGKWLRKRRIVSGNPRCQKPFFLKEIPIQDVAIQDFTCD-GNEESSCQLSPRCPEQCTC
Seq5  670
WLGEWLRKKRIVTGNPRCQKPYFLKEIPIQDVAIQDFTCDDGNDDNSCSPLSRCPTECTC
*** **** *** ******** ****************** **   **    ***  ***

Seq1  732
METVVRCSNKGLRALPRGMPKDVTELYLEGNHLTAVPRELSALRHLTLIDLSNNSISMLT
Seq5  730
LDTVVRCSNKGLKVLPKGIPRDVTELYLDGNQFTLVPKELSNYKHLTLIDLSNNRISTLS
  **********  ** * * ******* **  * ** ***   ********** ** *

Seq1  792
NYTFSNMSHLSTLILSYNRLRCIPVHAFNGLRSLRVLTLHGNDISSVPEGSFNDLTSLSH
Seq5  790
NQSFSNMTQLLTLILSYNRLRCIPPRTFDGLKSLRLLSLHGNDISVVPEGAFNDLSALSH
*  ****  * *************   * ** *** * ******* **** ****  ***

Seq1  852
LALGTNPLHCDCSLRWLSEWVKAGYKEPGIARCSSPEPMADRLLLITPTHRFQCKGPVDI
Seq5  850
LAIGANPLYCDCNMQWLSDWVKSEYKEPGIARCAGPGEMADKLLLTTPSKKFTCQGPVDV
** * *** ***   *** ***  *********  *  *** ******   * * ****

Seq1  912
NIVAKCNACLSSPCKNNGTCTQDPVELYRCACPYSYKGKDCTVPINTCIQNPCQHGGTCH
Seq5  910
NILAKCNPCLSNPCKNDGTCNSDPVDFYRCTCPYGFKGQDCDVPIHACISNPCKHGGTCH
** **** *** **** ***  ***  *** ***  ** ** ***  ** *** ******

Seq1  972
LSDSHKDGFSCSCPLGFEGQRCEINPDDCEDNDCENNATCVDGINNYVCICPPNYTGELC
Seq5  970
LKEGEEDGFWCICADGFEGENCEVNVDDCEDNDCENNSTCVDGINNYTCLCPPEYTGELC
*     *** * *  ****  ** * ********** ********* * *** ******

Seq1 1032
DEVIDHCVPELNLCQHEAKCIPLDKGFSCECVPGYSGKLCETDNDDCVAHKCRHGAQCVD
Seq5 1030
EEKLDFCAQDLNPCQHDSKCILTPKGFKCDCTPGYVGEHCDIDFDDCQDNKCKNGAHCTD
 *  * *   ** ***  ***   *** * * *** *  *  * ***   **  ** * *

Seq1 1092
TINGYTCTCPQGFSGPFCEHPPPMVLLQTSPCDQYECQNGAQCIVVQQEPTCRCPPGFAG
Seq5 1090
AVNGYTCICPEGYSGLFCEFSPPMVLPRTSPCDNFDCQNGAQCIVRINEPICQCLPGYQG
  ***** ** * ** ***  *****  *****   *********   ** * * **  *

Seq1 1152
PRCEKLITVNFVGKDSYVELASAKVRPQANISLQVATDKDNGILLYKGDNDPLALELYQG
```

```
Seq5 1150
EKCEKLVSVNFINKESYLQIPSAKVRPQTNITLQIATDEDSGILLYKGDKDHIAVELYRG
  ****  ***  * **    ******* ** ** *** * ******** *  * *** *

Seq1 1212
HVRLVYDSLSSPPTTVYSVETVNDGQFHSVELVTLNQTLNLVVDKGIPKSLGKLQKQPAV
Seq5 1210
RVRASYDTGSHPASAIYSVETINDGNFHIVELLALDQSLSLSVDGGNPKIITNLSKQSTL
 **  **  * *    ***** *** ** ***  * * * * ** * **    * **

Seq1 1272
GINSPLYLGGIPTSTGLSALRQGTDRPLGGFHGCIHEVRINNELQDFKALPPQSLGVSPG
Seq5 1270
NFDSPLYVGGMPGKSNVASLRQAPGQNGTSFHGCIRNLYINSELQDFQKVPMQT-GILPG
   **** ** *       ***        *****    ** *****   * *  *  **

Seq1 1332
CKSC----TVCKHGLCRSVEKDSVVCECRPGWTGPLCDQEARDPCLGHRCHHGKCVATGT-S
Seq5 1329
CEPCHKKVCAHGTCQPSSQAGFTCECQEGWMGPLCDQRTNDPCLGNKCVHGTCLPINAFS
*  *   ** ** *          ***  ** ******   *****  * ** *      *

Seq1 1389
YMCKCAEGYGGDLCDNKNDSANACSAFKCHHGQCHISDQGEPYCLCQPGFSGEHCQQENP
Seq5 1389
YSCKCLEGHGGVLCDEEEDLFNPCQAIKCKHGKCRLSGLGQPYCECSSGYTGDSCDREIS
* *** ** ** ***   *  * * * ** ** *  *  * *** *  *  *  *  *

Seq1 1449
CLGQVVREVIRRQKGYASCATASKVPIMECRGGC-GPQCCQPTRSKRRKYVFQCTDGSSF
Seq5 1449
CRGERIRDYYQKQQGYAACQTTKKVSRLECRGGCAGGQCCGPLRSKRRKYSFECTDGSSF
* *   *     * *** * *  **   ****** * *** * ******* * *******

Seq1 1508 VEEVERHLECGCLAC
Seq5 1509 VDEVEKVVKCGCTRC
          * ***    ***  *
```

[0072] As illustrated, the SLIT# and SLIT2 proteins with SEQ ID NOs:1 and5, respectively, share about 67% sequence identity but as described herein SLIT2 andSLIT3 proteins are both useful in the described methods. Hence, SLIT proteins can have sequence variations without loss of function.

[0073] Another example of a SLIT2 protein sequence is shown below (NCBI accession number AAI43979; SEQ ID NO:7).

```
  1 MRGVGWQMLS LSLGLVLAIL NKVAPQACPA QCSCSGSTVD
 41 CHGLALRSVP RNIPRNTERL DLNGNNITRI TKTDFAGLRH
 81 LRVLQLMENK ISTIERGAFQ DLKELERLRL NRNHLQLFPE
121 LLFLGTAKLY RLDLSENQIQ AIPRKAFRGA VDIKNLQLDY
161 NQISCIEDGA FRALRDLEVL TLNNNNITRL SVASFNHMPK
201 LRTFRLHSNN LYCDCHLAWL SDWLRQRPRV GLYTQCMGPS
241 HLRGHNVAEV QKREFVCSGH QSFMAPSCSV LHCPAACTCS
281 NNIVDCRGKG LTEIPTNLPE TITEIRLEQN TIKVIPPGAF
321 SPYKKLRRID LSNNQISELA PDAFQGLRSL NSLVLYGNKI
361 TELPKSLFEG LFSLQLLLLN ANKINCLRVD AFQDLHNLNL
401 LSLYDNKLQT IAKGTFSPLR AIQTMHLAQN PFICDCHLKW
441 LADYLHTNPI ETSGARCTSP RRLANKRIGQ IKSKKFRCSG
```

```
 481 TEDYRSKLSG DCFADLACPE KCRCEGTTVD CSNQKLNKIP
 521 EHIPQYTAEL RLNNNEFTVL EATGIFKKLP QLRKINFSNN
 561 KITDIEEGAF EGASGVNEIL LTSNRLENVQ HKMFKGLESL
 601 KTLMLRSNRI TCVGNDSFIG LSSVRLLSLY DNQITTVAPG
 641 AFDTLHSLST LNLLANPFNC NCYLAWLGEW LRKKRIVTGN
 681 PRCQKPYFLK EIPIQDVAIQ DFTCDDGNDD NSCSPLSRCP
 721 TECTCLDTVV RCSNKGLKVL PKGIPRDVTE LYLDGNQFTL
 761 VPKELSNYKH LTLIDLSNNR ISTLSNQSFS NMTQLLTLIL
 801 SYNRLRCIPP RTFDGLKSLR LLSLHGNDIS VVPEGAFNDL
 841 SALSHLAIGA NPLYCDCNMQ WLSDWVKSEY KEPGIARCAG
 881 PGEMADKLLL TTPSKKFTCQ GPVDVNILAK CNPCLSNPCK
 921 NDGTCNSDPV DFYRCTCPYG FKGQDCDVPI HACISNPCKH
 961 GGTCHLKEGE EDGFWCICAD GFEGENCEVN VDDCEDNDCE
1001 NNSTCVDGIN NYTCLCPPEY TGELCEEKLD FCAQDLNPCQ
1041 HDSKCILTPK GFKCDCTPGY VGEHCDIDFD DCQDNKCKNG
1081 AHCTDAVNGY TCICPEGYSG LFCEFSPPMV LPRTSPCDNF
1121 DCQNGAQCIV RINEPICQCL PGYQGEKCEK LVSVNFINKE
1161 SYLQIPSAKV RPQTNITLQI ATDEDSGILL YKGDKDHIAV
1201 ELYRGRVRAS YDTGSHPASA IYSVETINDG NFHIVELLAL
1241 DQSLSLSVDG GNPKIITNLS KQSTLNFDSP LYVGGMPGKS
1281 NVASLRQAPG QNGTSFHGCI RNLYINSELQ DFQKVPMQTG
1321 ILPGCEPCHK KVCAHGTCQP SSQAGFTCEC QEGWMGPLCD
1361 QRTNDPCLGN KCVHGTCLPI NAFSYSCKCL EGHGGVLCDE
1401 EEDLFNPCQA IKCKHGKCRL SGLGQPYCEC SSGYTGDSCD
1441 REISCRGERI RDYYQKQQGY AACQTTKKVS RLECRGGCAG
1481 GQCCGPLRSK RRKYSFECTD GSSFVDEVEK VVKCGCTRCV
1521 S
```

[0074] Another example of a SLIT2 protein sequence is shown below (NCBI accession number NP_001276065 XP_005248270; SEQ ID NO:8).

```
   1 MRGVGWQMLS LSLGLVLAIL NKVAPQACPA QCSCSGSTVD
  41 CHGLALRSVP RNIPRNTERL DLNGNNITRI TKTDFAGLRH
  81 LRVLQLMENK ISTIERGAFQ DLKELERLRL NRNHLQLFPE
 121 LLFLGTAKLY RLDLSENQIQ AIPRKAFRGA VDIKNLQLDY
 161 NQISCIEDGA FRALRDLEVL TLNNNNITRL SVASFNHMPK
 201 LRTFRLHSNN LYCDCHLAWL SDWLRQRPRV GLYTQCMGPS
 241 HLRGHNVAEV QKREFVCSGH QSFMAPSCSV LHCPAACTCS
 281 NNIVDCRGKG LTEIPTNLPE TITEIRLEQN TIKVIPPGAF
 321 SPYKKLRRID LSNNQISELA PDAFQGLRSL NSLVLYGNKI
 361 TELPKSLFEG LFSLQLLLLN ANKINCLRVD AFQDLHNLNL
 401 LSLYDNKLQT IAKGTFSPLR AIQTMHLAQN PFICDCHLKW
 441 LADYLHTNPI ETSGARCTSP RRLANKRIGQ IKSKKFRCSG
 481 TEDYRSKLSG DCFADLACPE KCRCEGTTVD CSNQKLNKIP
 521 EHIPQYTAEL RLNNNEFTVL EATGIFKKLP QLRKINFSNN
 561 KITDIEEGAF EGASGVNEIL LTSNRLENVQ HKMFKGLESL
 601 KTLMLRSNRI TCVGNDSFIG LSSVRLLSLY DNQITTVAPG
 641 AFDTLHSLST LNLLANPFNC NCYLAWLGEW LRKKRIVTGN
 681 PRCQKPYFLK EIPIQDVAIQ DFTCDDGNDD NSCSPLSRCP
 721 TECTCLDTVV RCSNKGLKVL PKGIPRDVTE LYLDGNQFTL
 761 VPKELSNYKH LTLIDLSNNR ISTLSNQSFS NMTQLLTLIL
 801 SYNRLRCIPP RTFDGLKSLR LLSLHGNDIS VVPEGAFNDL
 841 SALSHLAIGA NPLYCDCNMQ WLSDWVKSEY KEPGIARCAG
 881 PGEMADKLLL TTPSKKFTCQ GPVDVNILAK CNPCLSNPCK
 921 NDGTCNSDPV DFYRCTCPYG FKGQDCDVPI HACISNPCKH
```

```
 961 GGTCHLKEGE EDGFWCICAD GFEGENCEVN VDDCEDNDCE
1001 NNSTCVDGIN NYTCLCPPEY TGELCEEKLD FCAQDLNPCQ
1041 HDSKCILTPK GFKCDCTPGY VGEHCDIDFD DCQDNKCKNG
1081 AHCTDAVNGY TCICPEGYSG LFCEFSPPMV LPRTSPCDNF
1121 DCQNGAQCIV RINEPICQCL PGYQGEKCEK LVSVNFINKE
1161 SYLQIPSAKV RPQTNITLQI ATDEDSGILL YKGDKDHIAV
1201 ELYRGRVRAS YDTGSHPASA IYSVETINDG NFHIVELLAL
1241 DQSLSLSVDG GNPKIITNLS KQSTLNFDSP LYVGGMPGKS
1281 NVASLRQAPG QNGTSFHGCI RNLYINSELQ DFQKVPMQTG
1321 ILPGCEPCHK KVCAHGTCQP SSQAGFTCEC QEGWMGPLCD
1361 QRTNDPCLGN KCVHGTCLPI NAFSYSCKCL EGHGGVLCDE
1401 EEDLFNPCQA IKCKHGKCRL SGLGQPYCEC SSGYTGDSCD
1441 REISCRGERI RDYYQKQQGY AACQTTKKVS RLECRGGCAG
1481 GQCCGPLRSK RRKYSFECTD GSSFVDEVEK VVKCGCTRCV
1521 S
```

[0075] SLIT3 or SLIT2 is the designation for a human gene and its associated protein, referred to in databases for example, as Entrez Gene: 6586, Ensembl: ENSG00000184347, OMIM: 60374, and5 UniProtKB: O75094. For example, the sequence of the UniProtKB: O75094 SLIT3 protein is shown below as SEQ ID NO:9.

```
        10         20         30         40         50
MAPGWAGVGA AVRARLALAL ALASVLSGPP AVACPTKCTC SAASVDCHGL
        60         70         80         90        100
GLRAVPRGIP RNAERLDLDR NNITRITKMD FAGLKNLRVL HLEDNQVSVI
       110        120        130        140        150
ERGAFQDLKQ LERLRLNKNK LQVLPELLFQ STPKLTRLDL SENQIQGIPR
       160        170        180        190        200
KAFRGITDVK NLQLDNNHIS CIEDGAFRAL RDLEILTLNN NNISRILVTS
       210        220        230        240        250
FNHMPKIRTL RLHSNHLYCD CHLAWLSDWL RQRRTVGQFT LCMAPVHLRG
       260        270        280        290        300
FNVADVQKKE YVCPAPHSEP PSCNANSISC PSPCTCSNNI VDCRGKGLME
       310        320        330        340        350
IPANLPEGIV EIRLEQNSIK AIPAGAFTQY KKLKRIDISK NQISDIAPDA
       360        370        380        390        400
FQGLKSLTSL VLYGNKITEI VKGLFDGLVS LQLLLLNANK INCLRVNTFQ
       410        420        430        440        450
DLQNLNLLSL YDNKLQTISK GLFAPLQSIQ TLHLAQNPFV CDCHLKWLAD
       460        470        480        490        500
YLQDNPIETS GARCSSPRRL ANKRISQIKS KKFRCSGSED YRSRFSSECF
       510        520        530        540        550
MDLVCPEKCR CEGTIVDCSN QKLVRIPSHL PEYVTDLRLN DNEVSVLEAT
       560        570        580        590        600
GIFKKLPNLR KINLSNNKIK EVREGAFDGA ASVQELMLTG NQLETVHGRV
       610        620        630        640        650
FRGLSGLKTL MLRSNLIGCV SNDTFAGLSS VRLLSLYDNR ITTITPGAFT
       660        670        680        690        700
TLVSLSTINL LSNPFNCNCH LAWLGKWLRK RRIVSGNPRC QKPFFLKEIP
       710        720        730        740        750
IQDVAIQDFT CDGNEESSCQ LSPRCPEQCT CMETVVRCSN KGLRALPRGM
       760        770        780        790        800
PKDVTELYLE GNHLTAVPRE LSALRHLTLI DLSNNSISML TNYTFSNMSH
       810        820        830        840        850
LSTLILSYNR LRCIPVHAFN GLRSLRVLTL HGNDISSVPE GSFNDLTSLS
       860        870        880        890        900
```

```
HLALGINPLH CDCSLRWLSE WVKAGYKEPG IARCSSPEPM ADRLLLTTPT
       910        920        930        940        950
HRFQCKGPVD INIVAKCNAC LSSPCKNNGT CTQDPVELYR CACPYSYKGK
       960        970        980        990       1000
DCTVPINTCI QNPCQHGGTC HLSDSHKDGF SCSCPLGFEG QRCEINPDDC
      1010       1020       1030       1040       1050
EDNDCENNAT CVDGINNYVC ICPPNYTGEL CDEVIDHCVP ELNLCQHEAK
      1060       1070       1080       1090       1100
CIPLDKGFSC ECVPGYSGKL CETDNDDCVA HKCRHGAQCV DTINGYTCTC
      1110       1120       1130       1140       1150
PQGFSGPFCE HPPPMVLLQT SPCDQYECQN GAQCIVVQQE PTCRCPPGFA
      1160       1170       1180       1190       1200
GPRCEKLITV NFVGKDSYVE LASAKVRPQA NISLQVATDK DNGILLYKGD
      1210       1220       1230       1240       1250
NDPLALELYQ GHVRLVYDSL SSPPTTVYSV ETVNDGQFHS VELVTLNQTL
      1260       1270       1280       1290       1300
NLVVDKGTPK SLGKLQKQPA VGINSPLYLG GIPTSTGLSA LRQGTDRPLG
      1310       1320       1330       1340       1350
GFHGCIHEVR INNELQDFKA LPPQSLGVSP GCKSCTVCKH GLCRSVEKDS
      1360       1370       1380       1390       1400
VVCECRPGWT GPLCDQEARD PCLGHRCHHG KCVATGTSYM CKCAEGYGGD
      1410       1420       1430       1440       1450
LCDNKNDSAN ACSAFKCHHG QCHISDQGEP YCLCQPGFSG EHCQQENPCL
      1460       1470       1480       1490       1500
GQVVREVIRR QKGYASCATA SKVPIMECRG GCGPQCCQPT RSKRRKYVFQ
      1510       1520
CTDGSSFVEE VERHLECGCL ACS
```

[0076] SLIT2 and SLIT3 are conserved genes, with orthologs in around 160 organisms other than humans, including chimpanzee, Rhesus monkey, dog, cow, mouse, rat, chicken, zebrafish, and frog. Other sequences of the *SLIT2* and *SLIT3* genes, cDNAs, mRNAs, and proteins are available.

[0077] As a composition, the SLIT3 or SLIT2 agent may be delivered as cDNA in a vector, for example a viral vector, as an mRNA construct, or as a protein. The DNA, RNA, or amino acid may be the same as the human reference sequences or may have a sequence in one or more monomers (e.g., nucleotides or amino acids) has been substituted with other, chemically, sterically and/or electronically similar one, without substantially altering the biological activity.

[0078] As employed herein, the term "substantially the same sequence" refers to sequences having at least about 60% sequence homology or identity with respect to any of the sequences described herein ("reference sequences") and retaining comparable functional and biological activity characteristic of the protein, DNA, or mRNA defined by the reference sequences described. In some cases, molecules having "substantially the same sequence" will have at least about 80%, or about 90% identity with respect to a reference sequence; or with greater than about 95%, or 96%, or 97%, or 98%, or 99% sequence identity. It is recognized, however, that a sequence containing less than the described levels of sequence identity arising as splice variants or that are modified by conservative substitutions are also encompassed within the scope of the present

invention. The degree of sequence homology is determined by conducting an amino acid sequence similarity search of a protein data base, such as the database of the National Center for Biotechnology Information (NCBI; see website at ncbi.nlm.nih.gov/BLAST/), using a computerized algorithm, such as PowerBLAST, QBLAST, PSI-BLAST, PHI-BLAST, gapped or ungapped BLAST.

[0079] Also encompassed within "SLIT3 or SLIT2 agent" are biologically functional or active analogs of SLIT3 or SLIT2. The term "analog" includes any polypeptide or polynucleotide having a sequence substantially identical to a sequence specifically referenced herein in which one or more residues have been conservatively substituted with a functionally similar residue and which displays the ability to mimic the biological activity of SLIT3 or SLIT2. Examples of conservative substitutions for amino acids include the substitution of one non-polar (hydrophobic) residue such as isoleucine, valine, leucine or methionine for another, the substitution of one polar (hydrophilic) residue for another such as between arginine and lysine, between glutamine and asparagine, between glycine and serine, the substitution of one basic residue such as lysine, arginine or histidine for another, or the substitution of one acidic residue, such as aspartic acid or glutamic acid for another.

[0080] The phrase "conservative substitution" also includes the use of a chemically derivatized residue in place of a non-derivatized residue, provided that the polypeptide or expressed polypeptide displays the requisite biological activity.

[0081] "Chemical derivative" refers to a subject polypeptide or polynucleotide having one or more residues chemically derivatized by reaction of a functional side group.

[0082] Such derivatized molecules include with respect to polypeptides, for example, those molecules in which free amino groups have been derivatized to form amine hydrochlorides, p-toluene sulfonyl groups, carbobenzoxy groups, t-butyloxycarbonyl groups, chloroacetyl groups or formyl groups. Free carboxyl groups may be derivatized to form salts, methyl and ethyl esters or other types of esters or hydrazides. Free hydroxyl groups may be derivatized to form O-acyl or O-alkyl derivatives. The imidazole nitrogen of histidine may be derivatized to form N-im-benzylhistidine. Also included as chemical derivatives are those peptides which contain one or more naturally occurring amino acid derivatives of the twenty standard amino acids. For example, 4-hydroxyproline may be substituted for proline; 5-hydroxylysine may be substituted for lysine; 3-methylhistidine may be substituted for histidine; homoserine may be substituted for serine; and ornithine may be substituted for lysine. The useful polypeptide can also include any polypeptide having one or more additions and/or deletions of residues, relative to the sequence of a polypeptide whose sequence is

shown herein. For example, useful polypeptides can include one or more amino acid substitution, deletion, insertion, or other modification so long as the at least some SLIT3 or SLIT2 biological activity is maintained.

[0083] For example, useful SLIT2 and/or SLIT3 variant polypeptides with sequence variations compared to the sequences described herein can have at least 20%, or at least 30%, or at least 40%, or at least 50%, or at least 60%, or at least 70%, or at least 75%, or at least 80%, or at least 85%, or at least 90%, or at least 95% of the activity of an unmodified SLIT2 and/or SLIT3 protein (e.g., a wild type protein or a SLIT2 or SLIT3 protein with a sequence described herein).

SLIT3, SLIT2 or SHN3-interfering agents

[0084] Described herein are also SLIT3, SLIT2 or SHN3-interfering agents, which include antibodies and small interfering RNA (siRNA) molecules against *SLIT3 or SLIT2,* and methods of using same to prevent bone growth. Anti-SLIT3, SLIT2 or SHN3antibodies and siRNA molecules targeted to the *SLIT3, or SLIT2* gene ("*SLIT3, or SLIT2* siRNA") have been found to prevent bone growth. However, reduction of *SHN3* expression can enhance bone growth.

Small interfering RNA as SLIT3, SLIT2 or SHN3-interfering agents

[0085] The *SLIT3, SLIT2* or *SHN3* siRNA are targeted to a mammalian *SLIT3, SLIT2* or *SHN3* genes and can inhibit the expression of such target genes, respectively. The *SLIT3, SLIT2* or *SHN3* siRNA include a specific antisense sequence that is complementary to a portion of the mRNA transcribed from the target gene (i.e. the target mRNA) and can be double stranded (i.e. composed of an antisense strand, comprising the specific antisense sequence, and a complementary sense strand) or single-stranded (i.e. composed of an antisense strand, comprising the specific antisense sequence, only) as described in more detail below. Short-hairpin siRNA (shRNA) against *SLIT3, SLIT2* or *SHN3* are also described herein.

[0086] As is known in the art, the specificity of siRNA molecules is determined by the binding of the antisense strand of the molecule to its target mRNA. Effective siRNA molecules are generally less than 30 to 35 base pairs in length to prevent them triggering non-specific RNA interference pathways in the cell via the interferon response, although longer siRNA can also be effective

[0087] Design and construction of siRNA molecules is known in the art [see, for example, Elbashir, et al., Nature, 411:494-498 (2001); Bitko and Barik, BMC Microbiol., 1:34 (2001)]; Elbashir, S. M., et al. (2001) EMBO J. 20, 6877- 6888; and Zamore, P.D., et al. (2000) Cell 101, 25-33). Use of *SLIT3, SLIT2, or SHN3* siRNA is also disclosed in the Examples herein.

[0088] In one embodiment, the target mRNA sequence for the *SLIT3, SLIT2, or SHN3* siRNA is selected from the entire *SLIT3, SLIT2, or SHN3* mRNA sequence. In another embodiment, the target mRNA sequence for the *SLIT3, SLIT2, or SHN3* siRNA is selected from the 5' untranslated region of the *SLIT3, SLIT2, or SHN3* mRNA. In still another embodiment, the target mRNA sequence for the *SLIT3, SLIT2, or SHN3* siRNA is selected from the 3' untranslated region of the *SLIT3, SLIT2, or SHN3* mRNA. In one embodiment, the mRNA target sequence for the *SLIT3, SLIT2, or SHN3* siRNA is within the coding region of the target mRNA. In another embodiment, the target sequence for the *SLIT3, SLIT2, or SHN3* siRNA is selected from the region of the target mRNA beginning 50 to 100 nucleotides downstream of the start codon and ending at the stop codon. In an additional embodiment, the target sequence for the *SLIT3, SLIT2, or SHN3* siRNA is selected from the 3' end of the coding region, for example, the region of the target mRNA beginning 500 to 600 nucleotides downstream of the start codon and ending at the stop codon. In a further embodiment, the target mRNA sequence for the *SLIT3, SLIT2, or SHN3* siRNA is within an individual exon. In another embodiment, the target mRNA sequence for the *SLIT3, SLIT2, or SHN3* siRNA is selected from a region of the target mRNA which spans an exon-exon junction.

[0089] In another embodiment, a target mRNA sequence is selected that comprises the sequence 5'-AA(N_x)-3' or 5'-NA(N_x)-3', where N is any nucleotide and "x" is an integer between 10 and 50. In another embodiment, "x" is between 15 and 30. In yet another embodiment, "x" is between 19 and 23. In a further embodiment, "x" is 19 or 20.

[0090] In another embodiment, a target mRNA sequence is selected that comprises between about 30% and about 70% G/C content. In another embodiment, a target sequence is selected that comprises between about 30% and about 60% G/C content. In another embodiment, a target sequence is selected that comprises between about 35% and about 55% G/C content.

[0091] Double-stranded siRNA molecules can also be assembled from a single oligonucleotide in a stem-loop structure, wherein self-complementary sense and antisense regions of the siRNA molecule are linked by means of a nucleic acid based or non-nucleic acid-based linker(s), as well as circular single-stranded RNA having two or more loop structures and a stem comprising self-complementary sense and antisense strands, wherein the circular RNA can be processed either in vivo or in vitro to generate an active siRNA molecule capable of mediating RNAi.

[0092] Small hairpin RNA (shRNA) molecules thus are also contemplated herein. These molecules comprise a specific antisense sequence in addition to the reverse complement (sense) sequence, typically separated by a spacer or loop sequence.

Cleavage of the spacer or loop provides a single-stranded RNA molecule and its reverse complement, such that they may anneal to form a dsRNA molecule (optionally with additional processing steps that may result in addition or removal of one, two, three or more nucleotides from the 3' end and/or the 5' end of either or both strands). The spacer can be of a sufficient length to permit the antisense and sense sequences to anneal and form a double-stranded structure (or stem) prior to cleavage of the spacer (and, optionally, subsequent processing steps that may result in addition or removal of one, two, three, four, or more nucleotides from the 3' end and/or the 5' end of either or both strands). The spacer sequence is typically an unrelated nucleotide sequence that is situated between two complementary nucleotide sequence regions which, when annealed into a double-stranded nucleic acid, comprise a shRNA (see, for example, Brummelkamp et al., 2002 Science 296:550; Paddison et al., 2002 Genes Develop. 16:948; Paul et al., Nat. Biotechnol. 20:505-508 (2002); Grabarek et al., BioTechniques 34:734-44 (2003)). The spacer sequence generally comprises between about 3 and about 100 nucleotides.

[0093] In one embodiment, the siRNA molecule is a double- or single-stranded siRNA between about 15 and about 40 nucleotides in length. In another embodiment, the siRNA molecule is a double- or single-stranded siRNA between about 15 and about 35 nucleotides in length. In another embodiment, the siRNA molecule is a double- or single-stranded siRNA between about 17 and about 30 nucleotides in length. In another embodiment, the siRNA molecule is a double- or single-stranded siRNA between about 19 and about 25 nucleotides in length. In another embodiment, the siRNA molecule is a double- or single-stranded siRNA between about 21 to about 23 nucleotides in length.

[0094] In an alternative embodiment, the siRNA molecule is a shRNA molecule or circular siRNA molecule between about 50 and about 100 nucleotides in length. In a further embodiment, the siRNA molecule is a shRNA molecule between about 50 to about 60 nucleotides in length.

[0095] The specific antisense sequence comprised by the siRNA molecule can be identical or substantially identical to the complement of the target sequence. In one embodiment, the specific antisense sequence comprised by the siRNA molecule is at least about 75% identical to the complement of the target mRNA sequence. In another embodiment, the specific antisense sequence comprised by the siRNA molecule is at least about 90% identical to the complement of the target mRNA sequence. In a further embodiment, the specific antisense sequence comprised by the siRNA molecule is at least about 95% identical to the complement of the target mRNA sequence. In another embodiment, the specific antisense sequence comprised by the siRNA molecule is at least about 97% or 98% identical to the complement of the target mRNA sequence.

Methods of determining sequence identity are known in the art and can be determined, for example, by using the BLASTN program of the University of Wisconsin Computer Group (GCG) software or provided on the NCBI website.

[0096] The specific antisense sequence of the siRNA molecules described herein may exhibit variability by differing (e.g. by nucleotide substitution, including transition or transversion) at one, two, three, four or more nucleotides from the sequence of the target mRNA. When such nucleotide substitutions are present in the antisense strand of a dsRNA molecule, the complementary nucleotide in the sense strand with which the substitute nucleotide would typically form hydrogen bond base-pairing may or may not be correspondingly substituted. dsRNA molecules in which one or more nucleotide substitution occurs in the sense sequence, but not in the antisense strand, are also contemplated. When the antisense sequence of a siRNA molecule comprises one or more mismatches between the nucleotide sequence of the siRNA and the target nucleotide sequence, as described above, the mismatches may be found at the 3' terminus, the 5' terminus or in the central portion of the antisense sequence.

[0097] A modified siRNA molecule can comprise one or more modified nucleotides, for example, a siRNA molecule comprising modified ribonucleotide(s) can comprise about 5% to about 100% modified nucleotides (for example, 5%, 10%, 15%, 20%, 25%, 30%, 35%, 40%, 45%, 50%, 55%, 60%, 65%, 70%, 75%, 80%, 85%, 90%, 95% or 100% modified nucleotides). The actual percentage of modified nucleotides present in a given siRNA molecule will depend on the total number of nucleotides present in the siRNA. If the siRNA molecule is a single-stranded RNA (ssRNA) molecule, the percent modification will be based upon the total number of nucleotides present in the ssRNA molecule. When the siRNA molecule is a dsRNA molecule, the percent modification can be based upon the total number of nucleotides present in the sense strand, antisense strand, or both the sense and antisense strands of the molecule. In accordance with the present invention, a siRNA molecule that comprises one or more modified nucleotides or linkages maintains the ability to inhibit expression of the target gene.

[0098] A nucleoside is a base-sugar combination and a nucleotide is a nucleoside that further includes a phosphate group covalently linked to the sugar portion of the nucleoside. In forming RNA molecules, the phosphate groups covalently link adjacent nucleosides to one another to form a linear polymeric compound, with the normal linkage or backbone of RNA being a 3' to 5' phosphodiester linkage. Specific examples of siRNA molecules useful in this invention include siRNA molecules containing modified backbones or non-natural internucleoside linkages. siRNA molecules having

modified backbones include both those that retain a phosphorus atom in the backbone and those that lack a phosphorus atom in the backbone.

[0100] The siRNA molecules can comprise one or more 5' and/or 3'-cap structures. The siRNA molecule can comprise a cap structure at the 3 '-end of the sense strand, the antisense strand, or both the sense and antisense strands; or at the 5 '-end of the sense strand, the antisense strand, or both the sense and antisense strands of the siRNA molecule. Alternatively, the siRNA molecule can comprise a cap structure at both the 3 '-end and 5'-end of the siRNA molecule. The term "cap structure" refers to a chemical modification incorporated at either terminus of an oligonucleotide, which protects the molecule from exonuclease degradation, and may also facilitate delivery and/or localization within a cell.

[0101] The present invention also contemplates siRNA comprising ribonucleotide mimetics in which both the sugar and the internucleoside linkage of the nucleotide units are replaced with novel groups. Modified siRNA molecules may also contain one or more substituted sugar moieties and may also include modifications or substitutions to the nucleobase. As used herein, "unmodified" or "natural" nucleobases include the purine bases adenine (A) and guanine (G), and the pyrimidine bases thymine (T), cytosine (C) and uracil (U). Modified nucleobases include other synthetic and natural nucleobases known in the art.

[0102] Another modification applicable to the siRNA molecules is the chemical linkage to the siRNA molecule of one or more moieties or conjugates which enhance the activity, cellular distribution, cellular uptake, bioavailability, pharmacokinetic properties and/or stability of the siRNA molecule. The conjugate molecule can be linked to the siRNA molecule by way of a linker, for example, via a biodegradable linker. The conjugate molecule can be attached at the 3'-end of the sense strand, the antisense strand, or both the sense and antisense strands of the siRNA molecule. Alternatively, the conjugate molecule can be attached at the 5'-end of the sense strand, the antisense strand, or both the sense and antisense strands of the siRNA molecule. It is also contemplated that a conjugate molecule can be attached at both the 3'-end and 5'-end of the siRNA molecule. When more than one conjugate molecule is attached to the siRNA molecule, the conjugate molecules can be the same or different.

[0103] One skilled in the art will recognize that it is not necessary for all positions in a given siRNA molecule to be uniformly modified. The present invention, therefore, contemplates the incorporation of more than one of the aforementioned modifications into single siRNA molecules.

Antibodies as SLIT3, SLIT2, or SHN3-interfering agents

[0104] In one aspect, the present disclosure relates to use of isolated antibodies, which may monoclonal antibodies, which may be humanized or fully human monoclonal antibodies that bind specifically to SLIT3, SLIT2 or SHN3. In certain embodiments, the antibodies of the invention exhibit one or more desirable functional properties, such as high affinity binding to SLIT3, SLIT2, or SHN3, or the ability to inhibit binding of SLIT2 or SLIT3 to a ROBO receptor.

[0105] In another aspect, the disclosure pertains to methods of preventing bone growth in a subject using anti-SLIT2 or SLIT3 antibodies. In another aspect, the disclosure pertains to methods of increasing bone growth in a subject using anti-SHN3 antibodies.

[0106] The term "antibody" as referred to herein includes whole antibodies and any antigen binding fragment (i.e., "antigen-binding portion") or single chains thereof. An "antibody" refers to a glycoprotein comprising at least two heavy (H) chains and two light (L) chains inter-connected by disulfide bonds, or an antigen binding portion thereof. Each heavy chain is comprised of a heavy chain variable region (abbreviated herein as V_H) and a heavy chain constant region. The heavy chain constant region is comprised of three domains, C_{H1}, C_{H2} and C_{H3}. Each light chain is comprised of a light chain variable region (abbreviated herein as V_L) and a light chain constant region. The light chain constant region is comprised of one domain, C_L. The V_H and V_L regions can be further subdivided into regions of hypervariability, termed complementarity determining regions (CDR), interspersed with regions that are more conserved, termed framework regions (FR). Each V_H and V_L is composed of three CDRs and four FRs, arranged from amino-terminus to carboxy-terminus in the following order: FR1, CDR1, FR2, CDR2, FR3, CDR3, FR4. The variable regions of the heavy and light chains contain a binding domain that interacts with an antigen. The constant regions of the antibodies may mediate the binding of the immunoglobulin to host tissues or factors, including various cells of the immune system (e.g., effector cells) and the first component (C1q) of the classical complement system.

[0107] The term "antigen-binding portion" of an antibody (or simply "antibody portion"), as used herein, refers to one or more fragments of an antibody that retain the ability to specifically bind to an antigen (e.g. a ROBO-binding domain of SLIT2 or SLIT3). It has been shown that the antigen-binding function of an antibody can be performed by fragments of a full-length antibody. Examples of binding fragments encompassed within the term "antigen-binding portion" of an antibody include (i) a Fab fragment, a monovalent fragment consisting of the V_L, V_H, C_L and C_{H1} domains; (ii) a $F(ab')_2$ fragment, a bivalent fragment comprising two Fab fragments linked by a disulfide bridge at the hinge region; (iii) a Fd fragment consisting of the V_H and C_{H1}

domains; (iv) a Fv fragment consisting of the V_L and V_H domains of a single arm of an antibody, (v) a dAb fragment (Ward et al., (1989) Nature 341:544-546), which consists of a V_H domain; and (vi) an isolated complementarity determining region (CDR). Furthermore, although the two domains of the Fv fragment, V_L and V_H, are coded for by separate genes, they can be joined, using recombinant methods, by a synthetic linker that enables them to be made as a single protein chain in which the V_L and V_H regions pair to form monovalent molecules (known as single chain Fv (scFv); see e.g., Bird et al. (1988) Science 242:423-426; and Huston et al. (1988) Proc. Natl. Acad. Sci. USA 85:5879-5883). Such single chain antibodies are also intended to be encompassed within the term "antigen-binding portion" of an antibody. These antibody fragments are obtained using conventional techniques known to those with skill in the art, and the fragments are screened for utility in the same manner as are intact antibodies.

[0108] An "isolated antibody," as used herein, is intended to refer to an antibody that is substantially free of other antibodies having different antigenic specificities (e.g., an isolated antibody that specifically binds SLIT3, SLIT2 or SHN3 is substantially free of antibodies that specifically bind antigens other than SLIT3, SLIT2 or SHN3). An isolated antibody that specifically binds SLIT3, SLIT2, or SHN3 may, however, have cross-reactivity to other antigens, such as SLIT1 or SLIT-family molecules from other species. Moreover, an isolated antibody may be substantially free of other cellular material and/or chemicals.

[0109] The terms "monoclonal antibody" or "monoclonal antibody composition" as used herein refer to a preparation of antibody molecules of single molecular composition. A monoclonal antibody composition displays a single binding specificity and affinity for a particular epitope.

[0110] The term "human antibody," as used herein, is intended to include antibodies having variable regions in which both the framework and CDR regions are derived from human germline immunoglobulin sequences. Furthermore, if the antibody contains a constant region, the constant region also is derived from human germline immunoglobulin sequences. The human antibodies of the invention may include amino acid residues not encoded by human germline immunoglobulin sequences (e.g., mutations introduced by random or site-specific mutagenesis in vitro or by somatic mutation in vivo). However, the term "human antibody," as used herein, is not intended to include antibodies in which CDR sequences derived from the germline of another mammalian species, such as a mouse, have been grafted onto human framework sequences.

[0111] The term "human monoclonal antibody" refers to antibodies displaying a single binding specificity which have variable regions in which both the framework

and CDR regions are derived from human germline immunoglobulin sequences. In one embodiment, the human monoclonal antibodies are produced by a hybridoma which includes a B cell obtained from a transgenic nonhuman animal, e.g., a transgenic mouse, having a genome comprising a human heavy chain transgene and a light chain transgene fused to an immortalized cell.

[0112] The term "recombinant human antibody," as used herein, includes all human antibodies that are prepared, expressed, created or isolated by recombinant means, such as (a) antibodies isolated from an animal (e.g., a mouse) that is transgenic or transchromosomal for human immunoglobulin genes or a hybridoma prepared therefrom (described further below), (b) antibodies isolated from a host cell transformed to express the human antibody, e.g., from a transfectoma, (c) antibodies isolated from a recombinant, combinatorial human antibody library, and (d) antibodies prepared, expressed, created or isolated by any other means that involve splicing of human immunoglobulin gene sequences to other DNA sequences. Such recombinant human antibodies have variable regions in which the framework and CDR regions are derived from human germline immunoglobulin sequences. In certain embodiments, however, such recombinant human antibodies can be subjected to in vitro mutagenesis (or, when an animal transgenic for human Ig sequences is used, in vivo somatic mutagenesis) and thus the amino acid sequences of the V_L and V_H regions of the recombinant antibodies are sequences that, while derived from and related to human germline V_L and V_H sequences, may not naturally exist within the human antibody germline *repertoire in vivo*.

[0113] As used herein, "isotype" refers to the antibody class (e.g., IgM or IgG1) that is encoded by the heavy chain constant region genes.

[0114] The phrases "an antibody recognizing an antigen" and "an antibody specific for an antigen" are used interchangeably herein with the term "an antibody which binds specifically to an antigen."

[0115] The term "human antibody derivatives" refers to any modified form of the human antibody, e.g., a conjugate of the antibody and another agent or antibody.

[0116] The term "humanized antibody" is intended to refer to antibodies in which CDR sequences derived from the germline of another mammalian species, such as a mouse, have been grafted onto human framework sequences. Additional framework region modifications may be made within the human framework sequences.

[0117] The term "chimeric antibody" is intended to refer to antibodies in which the variable region sequences are derived from one species and the constant region sequences are derived from another species, such as an antibody in which the variable

region sequences are derived from a mouse antibody and the constant region sequences are derived from a human antibody.

[0118] As used herein, an antibody that "specifically binds to human SLIT3, SLIT2, or SHN3" is intended to refer to an antibody that binds to human SLIT2 or SLIT2 with a K_D of $1x10^{-7}$ M or less, more preferably $5x10^{-8}$ M or less, more preferably $1x10^{-8}$ M or less, more preferably $5x10^{-9}$ M or less, even more preferably between $1x10^{-8}$ M and $1x10^{-10}$ M or less.

[0119] The term "K_{assoc}" or "K_a," as used herein, is intended to refer to the association rate of a particular antibody-antigen interaction, whereas the term "K_{dis}" or "K_d," as used herein, is intended to refer to the dissociation rate of a particular antibody-antigen interaction. The term "K_D," as used herein, is intended to refer to the dissociation constant, which is obtained from the ratio of K_d to K_a (i.e., K_d/K_a) and is expressed as a molar concentration (M). K_D values for antibodies can be determined using methods well established in the art. A preferred method for determining the K_D of an antibody is by using surface plasmon resonance, preferably using a biosensor system such as a Biacore™ system.

[0120] The antibodies of the invention are characterized by particular functional features or properties of the antibodies. For example, the antibodies bind specifically to human SLIT3, SLIT2, or SHN3. Preferably, an antibody of the invention binds to SLIT3, SLIT2, or SHN3 with high affinity, for example with a K_D of $1x10^{-7}$ M or less. The anti-SLIT2, anti-SLIT3, or anti-SHN3 antibodies preferably exhibit one or more of the following characteristics:

(a) binds to human SLIT3, SLIT2, or SHN3 with a K_D of $1x10^{-7}$ M or less;

(b) anti-SLIT2 or anti-SLIT3 prevents bone growth; or

(c) anti-SHN3 increases bone growth.

[0121] Preferably, the antibody binds to human SLIT3, SLIT2, or SHN3 with a K_D of $5x10^{-8}$ M or less, binds to human SLIT3, SLIT2, or SHN3 with a K_D of $1x10^{-8}$ M or less, binds to human SLIT3, SLIT2, or SHN3 with a K_D of $5x10^{-9}$ M or less, binds to human SLIT3, SLIT2, or SHN3 with a K_D of $4x10^{-9}$ M or less, binds to human SLIT3, SLIT2, or SHN3 with a K_D of $2x10^{-9}$ M or less, or binds to human SLIT3, SLIT2, or SHN3 with a K_D of between $1x10^{-9}$ M and $1x10^{-10}$ M or less.

[0122] Standard assays to evaluate the binding ability of the antibodies toward SLIT3, SLIT2, or SHN3 are available, including for example, ELISAs, Western blots and RIAs. Suitable assays are described in detail in the Examples. The binding kinetics (e.g., binding affinity) of the antibodies also can be assessed by standard assays known in the art, such as by Biacore™. analysis.

[0123] Given that each of the subject antibodies can bind to SLIT3, SLIT2, or SHN3, the V_L and V_H sequences can be "mixed and matched" to create other anti-SHN3, anti-SLIT2 or anti-SLIT3 binding molecules of the invention. SLIT3, SLIT2, or SHN3 binding of such "mixed and matched" antibodies can be tested using the binding assays described above and in the examples (e.g., ELISAs). Preferably, when V_L and V_H chains are mixed and matched, a V_H sequence from a particular V_H / V_L pairing is replaced with a structurally similar V_H sequence. Likewise, preferably a V_L sequence from a particular V_H / V_L pairing is replaced with a structurally similar V_L sequence.

[0124] Accordingly, in one aspect, the invention provides an isolated monoclonal antibody, or antigen binding portion thereof comprising:

(a) a heavy chain variable region comprising an amino acid sequence; and

(b) a light chain variable region comprising an amino acid sequence;

wherein the antibody specifically binds SLIT3, SLIT2, or SHN3, preferably human SLIT3, SLIT2, or SHN3.

[0125] Given that each of these antibodies can bind to SLIT3, SLIT2, or SHN3 and that antigen-binding specificity is provided primarily by the CDR1, CDR2, and CDR3 regions, the V_H CDR1, CDR2, and CDR3 sequences and V_k CDR1, CDR2, and CDR3 sequences can be "mixed and matched" (i.e., CDRs from different antibodies can be mixed and match, although each antibody must contain a V_H CDR1, CDR1, and CDR3 and a V_k CDR1, CDR2, and CDR3) to create other anti-SLIT2 or anti-SLIT3 binding molecules of the invention. SLIT3, SLIT2, or SHN3 binding of such "mixed and matched" antibodies can be tested using the binding assays described above and in the Examples (e.g., ELISAs, Biacore analysis). Preferably, when V_H CDR sequences are mixed and matched, the CDR1, CDR2 and/or CDR3 sequence from a particular V_H sequence is replaced with a structurally similar CDR sequence(s). Likewise, when V_k CDR sequences are mixed and matched, the CDR1, CDR2 and/or CDR3 sequence from a particular V_k sequence preferably is replaced with a structurally similar CDR sequence(s). Novel V_H and V_L sequences can be created by substituting one or more V_H and/or V_L CDR region sequences with structurally similar sequences from the CDR sequences of the antibodies disclosed herein.

[0126] It is well known in the art that the CDR3 domain, independently from the CDR1 and/or CDR2 domain(s), alone can determine the binding specificity of an antibody for a cognate antigen and that multiple antibodies can predictably be generated having the same binding specificity based on a common CDR3 sequence. See, for example, Klimka et al., British J. of Cancer 83(2):252-260 (2000) (describing the production of a humanized anti-CD30 antibody using only the heavy chain variable domain CDR3 of murine anti-CD30 antibody Ki-4); Beiboer et al., J. Mol. Biol.

296:833-849 (2000) (describing recombinant epithelial glycoprotein-2 (EGP-2) antibodies using only the heavy chain CDR3 sequence of the parental murine MOC-31 anti-EGP-2 antibody); Rader et al., Proc. Natl. Acad. Sci. U.S.A. 95:8910-8915 (1998) (describing a panel of humanized anti-integrin .alpha..sub.v.beta..sub.3 antibodies using a heavy and light chain variable CDR3 domain

Bispecific Molecules

[0127] In another aspect, the present invention features bispecific molecules comprising an anti-SLIT3, SLIT2 or SHN3 antibody, or a fragment thereof, of the invention. An antibody of the invention, or antigen-binding portions thereof, can be derivatized or linked to another functional molecule, e.g., another peptide or protein (e.g., another antibody or ligand for a receptor) to generate a bispecific molecule that binds to at least two different binding sites or target molecules. The antibody of the invention may in fact be derivatized or linked to more than one other functional molecule to generate multispecific molecules that bind to more than two different binding sites and/or target molecules; such multispecific molecules are also intended to be encompassed by the term "bispecific molecule" as used herein. To create a bispecific molecule of the invention, an antibody of the invention can be functionally linked (e.g., by chemical coupling, genetic fusion, noncovalent association or otherwise) to one or more other binding molecules, such as another antibody, antibody fragment, peptide or binding mimetic, such that a bispecific molecule results.

[0128] Accordingly, the present invention includes bispecific molecules comprising at least one first binding specificity for SLIT3, SLIT2, or SHN3 and a second binding specificity for a second target epitope. In some cases, the second target epitope is an Fc receptor, e.g., human FcγRI (CD64) or a human

Gene transfer vectors

[0129] SLIT3 or SLIT2 nucleic acid constructs, be they intended to generate SLIT3 or SLIT2, or to interfere with SLIT3 or SLIT2 function, may be delivered via gene transfer vectors. Similarly, SHN2 interfering nucleic acids (that can reduce SHN3 expression) may be delivered via gene transfer vectors.

[0130] The invention also provides a gene transfer vector comprising a nucleic acid sequence which encodes a SLIT3 or SLIT2 polypeptide or an interfering RNA molecule against SLIT3, SHN3, or SLIT2. The invention further provides a method of promoting or preventing bone growth, which method comprises administering to the mammal the above-described gene transfer vector. Various aspects of the inventive gene transfer vector and method are discussed below. Although each parameter is discussed separately, the inventive gene transfer vector and method comprise combinations of the parameters set forth below to treat a subject in need thereof.

Accordingly, any combination of parameters can be used according to the inventive gene transfer vector and the inventive method.

[0131] For example, administration of a SLIT3 or SLIT2 polypeptide, or a gene transfer vector comprising a nucleic acid sequence which encodes a SLIT3 or SLIT2 polypeptide, can increase bone volume or the maximal load tolerated by a bone by at least 5%, or at least 10%, or at least 20%, or at least 25%, %, or at least 30%, or at least 40%, or at least 50%, or at least 60%, or at least 70%, or at least 75%, or at least 80%, or at least 90%, or at least 95%, compared to administration of a placebo (or no administration of SLIT3 or SLIT2 polypeptide or vector). In some cases, administration of a SLIT3 or SLIT2 polypeptide, or a gene transfer vector comprising a nucleic acid sequence which encodes a SLIT3 or SLIT2 polypeptide, can increase bone volume or the maximal load tolerated by a bone by at least 1.5-fold, or by at least 2-fold.

[0132] A "gene transfer vector" is any molecule or composition that can carry a heterologous nucleic acid sequence into a suitable host cell where synthesis of the encoded protein takes place. Typically, a gene transfer vector is a nucleic acid molecule that has been engineered, using recombinant DNA techniques that available to those of ordinary skill in the art, to incorporate the heterologous nucleic acid sequence. Desirably, the gene transfer vector is comprised of DNA. Examples of suitable DNA-based gene transfer vectors include plasmids and viral vectors. However, gene transfer vectors that are not based on nucleic acids, such as liposomes, are also known and used in the art. The inventive gene transfer vector can be based on a single type of nucleic acid (e.g., a plasmid) or non-nucleic acid molecule (e.g., a lipid or a polymer). The gene transfer vector can be integrated into the host cell genome or can be present in the host cell in the form of an episome.

[0133] In one embodiment, the gene transfer vector is a viral vector. Suitable viral vectors include, for example, lentiviral vectors, retroviral vectors, herpes simplex virus (HSV)-based vectors, parvovirus-based vectors, e.g., adeno-associated virus (AAV)-based vectors, AAV-adenoviral chimeric vectors, and adenovirus-based vectors. These viral vectors can be prepared using standard recombinant DNA techniques described in, for example, Sambrook et al., *Molecular Cloning, a Laboratory Manual*, 3rd edition, Cold Spring Harbor Press, Cold Spring Harbor, N.Y. (2001), and Ausubel et al., *Current Protocols in Molecular Biology*, Greene Publishing Associates and John Wiley & Sons, New York, N.Y. (1994).

[0134] In an embodiment, the invention provides an adeno-associated virus (AAV) vector which comprises, consists essentially of, or consists of a nucleic acid sequence encoding a SLIT3 or SLIT2 polypeptide or an interfering RNA molecule against SLIT3 or SLIT2 or SHN3. When the inventive AAV vector consists essentially

of a nucleic acid sequence encoding a SLIT3 or SLIT2 polypeptide or an interfering RNA molecule against SLIT3 or SLIT2 or SHN3, additional components can be included that do not materially affect the AAV vector (e.g., genetic elements such as poly(A) sequences or restriction enzyme sites that facilitate manipulation of the vector *in vitro*).

[0135] Adeno-associated virus is a member of the Parvoviridae family and comprises a linear, single-stranded DNA genome of less than about 5,000 nucleotides. AAV requires co-infection with a helper virus (i.e., an adenovirus or a herpes virus), or expression of helper genes, for efficient replication. AAV vectors used for administration of therapeutic nucleic acids typically have approximately 96% of the parental genome deleted, such that only the terminal repeats (ITRs), which contain recognition signals for DNA replication and packaging, remain. This eliminates immunologic or toxic side effects due to expression of viral genes. In addition, delivering specific AAV proteins to producing cells enables integration of the AAV vector comprising AAV ITRs into a specific region of the cellular genome, if desired (see, e.g., U.S. Patents 6,342,390 and 6,821,511). Host cells comprising an integrated AAV genome show no change in cell growth or morphology (see, for example, U.S. Patent 4,797,368).

[0136] The AAV ITRs flank the unique coding nucleotide sequences for the non-structural replication (Rep) proteins and the structural capsid (Cap) proteins (also known as virion proteins (VPs)). The terminal 145 nucleotides are self-complementary and are organized so that an energetically stable intramolecular duplex forming a T-shaped hairpin may be formed. These hairpin structures function as an origin for viral DNA replication by serving as primers for the cellular DNA polymerase complex. The Rep genes encode the Rep proteins Rep78, Rep68, Rep52, and Rep40. Rep78 and Rep68 are transcribed from the p5 promoter, and Rep 52 and Rep40 are transcribed from the p19 promoter. The Rep78 and Rep68 proteins are multifunctional DNA binding proteins that perform helicase and nickase functions during productive replication to allow for the resolution of AAV termini (see, e.g., Im et al., Cell, 61:447 (1990)). These proteins also regulate transcription from endogenous AAV promoters and promoters within helper viruses (see, e.g., Pereira et al., J. Virol., 71:1079 (1997)). The other Rep proteins modify the function of Rep78 and Rep68. The cap genes encode the capsid proteins VP1, VP2, and VP3. The cap genes are transcribed from the p40 promoter.

[0137] The AAV vector may be generated using any AAV serotype known in the art. Several AAV serotypes and over 100 AAV variants have been isolated from adenovirus stocks or from human or nonhuman primate tissues (reviewed in, e.g., Wu et

al., Molecular Therapy, 14(3): 316 (2006)). Generally, the AAV serotypes have genomic sequences of significant homology at the nucleic acid sequence and amino acid sequence levels, such that different serotypes have an identical set of genetic functions, produce virions which are essentially physically and functionally equivalent, and replicate and assemble by practically identical mechanisms. AAV serotypes 1-6 and 7-9 are defined as "true" serotypes, in that they do not efficiently cross-react with neutralizing sera specific for all other existing and characterized serotypes. In contrast, AAV serotypes 6, 10 (also referred to as Rh10), and 11 are considered "variant" serotypes as they do not adhere to the definition of a "true" serotype. AAV serotype 2 (AAV2) has been used extensively for gene therapy applications due to its lack of pathogenicity, wide range of infectivity, and ability to establish long-term transgene expression (see, e.g., Carter, Hum. Gene Ther., 16:541 (2005); and Wu et al., *supra*). Genome sequences of various AAV serotypes and comparisons thereof are disclosed in, for example, GenBank Accession numbers U89790, J01901, AF043303, and AF085716; Chiorini et al., J. Virol., 71:6823 (1997); Srivastava et al., J. Virol., 45:555 (1983); Chiorini et al., J. Virol., 73:1309 (1999); Rutledge et al., J. Virol., 72:309 (1998); and Wu et al., J. Virol., 74:8635 (2000)).

[0138] AAV rep and ITR sequences are particularly conserved across most AAV serotypes. For example, the Rep78 proteins of AAV2, AAV3A, AAV3B, AAV4, and AAV6 are reportedly about 89-93% identical (see Bantel-Schaal et al., J. Virol., 73(2):939 (1999)). It has been reported that AAV serotypes 2, 3A, 3B, and 6 share about 82% total nucleotide sequence identity at the genome level (Bantel-Schaal et al., *supra*). Moreover, the rep sequences and ITRs of many AAV serotypes are known to efficiently cross-complement (e.g., functionally substitute) corresponding sequences from other serotypes during production of AAV particles in mammalian cells.

[0139] Generally, the cap proteins, which determine the cellular tropicity of the AAV particle, and related cap protein-encoding sequences, are significantly less conserved than Rep genes across different AAV serotypes. In view of the ability Rep and ITR sequences to cross-complement corresponding sequences of other serotypes, the AAV vector can comprise a mixture of serotypes and thereby be a "chimeric" or "pseudotyped" AAV vector. A chimeric AAV vector typically comprises AAV capsid proteins derived from two or more (e.g., 2, 3, 4, etc.) different AAV serotypes. In contrast, a pseudotyped AAV vector comprises one or more ITRs of one AAV serotype packaged into a capsid of another AAV serotype. Chimeric and pseudotyped AAV vectors are further described in, for example, U.S. Patent No. 6,723,551; Flotte, Mol. Ther., 13(1):1 (2006); Gao et al., J. Virol., 78:6381 (2004); Gao et al., Proc. Natl. Acad.

Sci. USA, 99:11854 (2002); De et al., Mol. Ther., 13:67 (2006); and Gao et al., Mol. Ther., 13:77 (2006).

[0140] In one embodiment, the AAV vector is generated using an AAV that infects humans (e.g., AAV2). Alternatively, the AAV vector is generated using an AAV that infects non-human primates, such as, for example, the great apes (e.g., chimpanzees), Old World monkeys (e.g., macaques), and New World monkeys (e.g., marmosets). In one embodiment, the AAV vector is generated using an AAV that infects a non-human primate pseudotyped with an AAV that infects humans. Examples of such pseudotyped AAV vectors are disclosed in, e.g., Cearley et al., Molecular Therapy, 13:528 (2006). In one embodiment, an AAV vector can be generated which comprises a capsid protein from an AAV that infects rhesus macaques pseudotyped with AAV2 inverted terminal repeats (ITRs). In some cases, the inventive AAV vector comprises a capsid protein from AAV10 (also referred to as "AAVrh.10"), which infects rhesus macaques pseudotyped with AAV2 ITRs (see, e.g., Watanabe et al., Gene Ther., 17(8):1042 (2010); and Mao et al., Hum. Gene Therapy, 22:1525 (2011)).

[0141] In addition to the nucleic acid sequence encoding a SLIT3 or SLIT2 polypeptide or an interfering RNA molecule against SLIT3 or SLIT2, the AAV vector may comprise expression control sequences, such as promoters, enhancers, polyadenylation signals, transcription terminators, internal ribosome entry sites (IRES), and the like, that provide for the expression of the nucleic acid sequence in a host cell. Exemplary expression control sequences are known in the art and described in, for example, Goeddel, Gene Expression Technology: Methods in Enzymology, Vol. 185, Academic Press, San Diego, CA. (1990).

[0142] A variety of promoters, including constitutive, inducible, and repressible promoters, from a variety of different sources can be used in the vectors. Representative sources of promoters include for example, virus, mammal, insect, plant, yeast, and bacteria, and suitable promoters from these sources are readily available, or can be made synthetically, based on sequences publicly available, for example, from depositories such as the ATCC as well as other commercial or individual sources. Promoters can be unidirectional (i.e., initiate transcription in one direction) or bi-directional (i.e., initiate transcription in either a 3' or 5' direction). Non-limiting examples of promoters include, for example, the T7 bacterial expression system, pBAD (araA) bacterial expression system, the cytomegalovirus (CMV) promoter, the SV40 promoter, and the RSV promoter. Inducible promoters include, for example, the Tet system (U.S. Patent Nos. 5,464,758 and 5,814,618), the Ecdysone inducible system (No et al., Proc. Natl. Acad. Sci., 93:3346 (1996)), the T-REXTM system (Invitrogen, Carlsbad, CA), LACSWITCH™ System (Stratagene, San Diego, CA), and the Cre-ERT

tamoxifen inducible recombinase system (Indra et al., Nuc. Acid. Res., 27:4324 (1999); Nuc. Acid. Res., 28:e99 (2000); U.S. Patent No. 7,112,715; and Kramer & Fussenegger, Methods Mol. Biol., 308:123 (2005)).

[0143] The term "enhancer" as used herein, refers to a DNA sequence that increases transcription of, for example, a nucleic acid sequence to which it is operably linked. Enhancers can be located many kilobases away from the coding region of the nucleic acid sequence and can mediate the binding of regulatory factors, patterns of DNA methylation, or changes in DNA structure. A variety of enhancers from a variety of different sources are available or can be obtained within cloned polynucleotides (from, e.g., depositories such as the ATCC as well as other commercial or individual sources). A number of polynucleotides comprising promoters (such as the CMV promoter) also comprise enhancer sequences. Enhancers can be located upstream, within, or downstream of coding sequences. In some cases, the nucleic acid sequence encoding a SLIT3 or SLIT2 polypeptide or an interfering RNA molecule against SLIT3 or SLIT2, is operably linked to a CMV enhancer/chicken beta-actin promoter (also referred to as a "CAG promoter") (see, e.g., Niwa et al., Gene, 108:193 (1991); Daly et al., Proc. Natl. Acad. Sci. U.S.A., 96:2296 (1999); and Sondhi et al., Mol. Ther., 15:481 (2007)).

[0144] Typically, AAV vectors are produced using well characterized plasmids. For example, human embryonic kidney 293T cells are transfected with one of the transgene specific plasmids and another plasmid containing the adenovirus helper and AAV rep and cap genes (specific to AAVrh.10, 8 or 9 as required). After 72 hours, the cells are harvested, and the vector is released from the cells by five freeze/thaw cycles. Subsequent centrifugation and benzonase treatment removes cellular debris and unencapsidated DNA. Iodixanol gradients and ion exchange columns may be used to further purify each AAV vector. Next, the purified vector is concentrated by a size exclusion centrifuge spin column to the required concentration. Finally, the buffer is exchanged to create the final vector products formulated (for example) in 1x phosphate buffered saline. The viral titers may be measured by TaqMan® real-time PCR and the viral purity may be assessed by SDS-PAGE.

Formulations and delivery

[0145] The present invention also provides a method to prevent bone loss, or promote bone growth, strengthening, or healing in a subject in need thereof, by administering to said subject a SLIT3 or SLIT2 agent and it provides a method to prevent bone growth in a subject in need thereof, by administering to said subject a SLIT3 or SLIT2-interfering agent, in each case with a pharmaceutically acceptable

excipient. In cases wherein the SLIT3 or SLIT2 agent or SLIT3 or SLIT2-interfering agent is a nucleic acid, including interfering RNA, it may be carried in a vector.

[0146] In another aspect, the present invention provides pharmaceutically acceptable compositions which comprise a therapeutically-effective amount of one or more of a SLIT3 or SLIT2 agent or a SLIT3 or SLIT2-interfering agent, including vectors carrying them, as described above, formulated together with one or more pharmaceutically acceptable excipients. In another aspect, the present invention provides pharmaceutically acceptable compositions which comprise a therapeutically-effective amount of one or more of a SLIT3 or SLIT2 agent or a SLIT3 or SLIT2-interfering agent, as described above, formulated together with one or more pharmaceutically acceptable excipients and other therapeutically effective medications known in the art allowing for but not limited to combination therapies to improve overall efficacy of each individual therapeutic or to limit the concentration of either therapeutic to avoid side effects and maintain efficacy. The active ingredient and excipient(s) may be formulated into compositions and dosage forms. The active ingredient or compositions thereof can be administered with an orthopedic implant. For example, the active ingredient or compositions thereof can coat or be bound (covalently or non-covalently) to an orthopedic implant.

[0147] As described in detail below, the pharmaceutical compositions of the present invention may be specially formulated for administration in solid or liquid form, including those adapted for the following: (1) oral administration, for example, tablets, capsules, powders, granules, pastes for application to the tongue, aqueous or non-aqueous solutions or suspensions, drenches, or syrups; (2) parenteral administration, for example, by subcutaneous, intramuscular or intravenous injection as, for example, a sterile solution or suspension; (3) topical application, for example, as a cream, ointment or spray applied to bone,. or provided in a depot formulation, for example embedded or coating a medical device, (4) intravaginally or intrarectally, for example, as a pessary, cream or foam; (5) sublingually or buccally; (6) ocularly; (7) transdermally; (8) nasally; or (9) locally. In some cases, administration is locally, for example, to a bone or site close to a bone.

[0148] A therapeutically effective amount of the pharmaceutical composition of the present invention is sufficient to treat or prevent a disease characterized by symptoms comprising loss of bone, weakened, damaged, degraded, or broken bones, or by excessive bone growth, or the risk of these things. The dosage of active ingredient(s) may vary, depending on the reason for use and the individual subject. The dosage may be adjusted based on the subject's weight, the age and health of the subject, and tolerance for the compound or composition.

[0149] For example, the proteins, nucleic acids encoding such proteins, inhibitors, nucleic acids encoding such peptide inhibitors, and combinations thereof, may be administered as single or divided dosages. For example, proteins, nucleic acids encoding such proteins, or inhibitors, nucleic acids encoding such peptide inhibitors, can be administered in dosages of at least about 0.01 mg/kg to about 500 to 750 mg/kg, of at least about 0.01 mg/kg to about 300 to 500 mg/kg, at least about 0.1 mg/kg to about 100 to 300 mg/kg, at least about 1 mg/kg to about 100 mg/kg, or at least about 0.1 mg/kg to about 50 to 100 mg/kg of body weight, although other dosages may provide beneficial results. The amount administered will vary depending on various factors including, but not limited to, the proteins, nucleic acids encoding such proteins, inhibitors, or nucleic acids encoding such peptide inhibitors chosen for administration, the disease, the weight, the physical condition, the health, and the age of the mammal. Such factors can be determined using the information provided herein.

[0150] The phrase "pharmaceutically acceptable" is employed herein to refer to those compounds, materials, compositions, and/or dosage forms which are, within the scope of sound medical judgment, suitable for use in contact with the tissues of the subject with toxicity, irritation, allergic response, or other problems or complications, commensurate with a reasonable benefit/risk ratio.

[0151] The phrase "pharmaceutically-acceptable excipient" as used herein refers to a pharmaceutically-acceptable material, composition or vehicle, such as a liquid or solid filler, diluent, carrier, manufacturing aid (e.g., lubricant, talc magnesium, calcium or zinc stearate, or steric acid), solvent or encapsulating material, involved in carrying or transporting the therapeutic compound for administration to the subject. Each excipient should be "acceptable" in the sense of being compatible with the other ingredients of the formulation and not injurious to the subject. Some examples of materials which can serve as pharmaceutically-acceptable excipients include: sugars, such as lactose, glucose and sucrose; starches, such as corn starch and potato starch; cellulose and its derivatives, such as sodium carboxymethyl cellulose, ethyl cellulose and cellulose acetate; gelatin; talc; waxes; oils, such as peanut oil, cottonseed oil, safflower oil, sesame oil, olive oil, corn oil and soybean oil; glycols, such as ethylene glycol and propylene glycol; polyols, such as glycerin, sorbitol, mannitol and polyethylene glycol; esters, such as ethyl oleate and ethyl laurate; agar; buffering agents; water; isotonic saline; pH buffered solutions; and other non-toxic compatible substances employed in pharmaceutical formulations. If desired, certain sweetening and/or flavoring and/or coloring agents may be added. Other suitable excipients can be found in standard pharmaceutical texts, e.g. in "Remington's Pharmaceutical Sciences",

The Science and Practice of Pharmacy, 19th Ed. Mack Publishing Company, Easton, Pa., (1995).

[0152] Excipients are added to the composition for a variety of purposes. Diluents increase the bulk of a solid pharmaceutical composition and may make a pharmaceutical dosage form containing the composition easier for the patient and caregiver to handle. Diluents for solid compositions include, for example, microcrystalline cellulose (e.g. Avicel®), microfine cellulose, lactose, starch, pregelatinized starch, calcium carbonate, calcium sulfate, sugar, dextrates, dextrin, dextrose, dibasic calcium phosphate dihydrate, tribasic calcium phosphate, kaolin, magnesium carbonate, magnesium oxide, maltodextrin, mannitol, polymethacrylates (e.g. Eudragit®), potassium chloride, powdered cellulose, sodium chloride, sorbitol and talc.

[0153] Solid pharmaceutical compositions that are compacted into a dosage form, such as a tablet, may include excipients whose functions include helping to bind the active ingredient and other excipients together after compression. Binders for solid pharmaceutical compositions include acacia, alginic acid, carbomer (e.g. carbopol), carboxymethylcellulose sodium, dextrin, ethyl cellulose, gelatin, guar gum, hydrogenated vegetable oil, hydroxyethyl cellulose, hydroxypropyl cellulose (e.g. Klucel®), hydroxypropyl methyl cellulose (e.g. Methocel®), liquid glucose, magnesium aluminum silicate, maltodextrin, methylcellulose, polymethacrylates, povidone (e.g. Kollidon®, Plasdone®), pregelatinized starch, sodium alginate and starch.

[0154] Glidants can be added to improve the flowability of a non-compacted solid composition and to improve the accuracy of dosing. Excipients that may function as glidants include colloidal silicon dioxide, magnesium trisilicate, powdered cellulose, starch, talc and tribasic calcium phosphate.

[0155] In liquid pharmaceutical compositions of the present invention, the SLIT3 or SLIT2 agent, or SLIT3 or SLIT2-interfering agent, as described above, and any other solid excipients are dissolved or suspended in a liquid carrier such as water, water-for-injection, vegetable oil, alcohol, polyethylene glycol, propylene glycol or glycerin.

[0156] Liquid pharmaceutical compositions may contain emulsifying agents to disperse uniformly throughout the composition an active ingredient or other excipient that is not soluble in the liquid carrier. Emulsifying agents that may be useful in liquid compositions of the present invention include, for example, gelatin, egg yolk, casein, cholesterol, acacia, tragacanth, chondrus, pectin, methyl cellulose, carbomer, cetostearyl alcohol and cetyl alcohol.

[0157] Liquid pharmaceutical compositions of the present invention may also contain a viscosity enhancing agent to improve the mouth feel of the product and/or coat the lining of the gastrointestinal tract. Such agents include acacia, alginic acid bentonite, carbomer, carboxymethylcellulose calcium or sodium, cetostearyl alcohol, methyl cellulose, ethylcellulose, gelatin guar gum, hydroxyethyl cellulose, hydroxypropyl cellulose, hydroxypropyl methyl cellulose, maltodextrin, polyvinyl alcohol, povidone, propylene carbonate, propylene glycol alginate, sodium alginate, sodium starch glycolate, starch tragacanth and xanthan gum.

[0158] Preservatives and chelating agents such as alcohol, sodium benzoate, butylated hydroxy toluene, butylated hydroxyanisole and ethylenediamine tetraacetic acid may be added at levels safe for ingestion to improve storage stability.

[0159] According to the present invention, a liquid composition may also contain a buffer such as gluconic acid, lactic acid, citric acid or acetic acid, sodium gluconate, sodium lactate, sodium citrate or sodium acetate. Selection of excipients and the amounts used may be readily determined by the formulation scientist based upon experience and consideration of standard procedures and reference works in the field.

[0160] Suitable formulations for the composition include aqueous and non-aqueous solutions, isotonic sterile solutions, which can contain anti-oxidants, buffers, and bacteriostats, and aqueous and non-aqueous sterile suspensions that can include suspending agents, solubilizers, thickening agents, stabilizers, and preservatives. The formulations can be presented in unit-dose or multi-dose sealed containers, such as ampules and vials, and can be stored in a freeze-dried (lyophilized) condition requiring only the addition of the sterile liquid carrier, for example, water, immediately prior to use. Extemporaneous solutions and suspensions can be prepared from sterile powders, granules, and tablets of the kind previously described. In one embodiment, the carrier is a buffered saline solution. In one embodiment, the inventive gene transfer vector is administered in a composition formulated to protect the gene transfer vector from damage prior to administration. For example, the composition can be formulated to reduce loss of the gene transfer vector on devices used to prepare, store, or administer the gene transfer vector, such as glassware, syringes, or needles. The composition can be formulated to decrease the light sensitivity and/or temperature sensitivity of the gene transfer vector. To this end, the composition may comprise a pharmaceutically acceptable liquid carrier, such as, for example, those described above, and a stabilizing agent selected from the group consisting of polysorbate 80, L-arginine, polyvinylpyrrolidone, trehalose, and combinations thereof. Use of such a composition will extend the shelf life of the gene transfer vector, facilitate administration, and increase the efficiency of the inventive method. Formulations for gene transfer vector -

containing compositions are further described in, for example, Wright et al., *Curr. Opin. Drug Discov. Devel.*, *6*(2): 174-178 (2003) and Wright et al., *Molecular Therapy*, *12*: 171-178 (2005)).

[0161] Solid and liquid compositions may also be dyed using any pharmaceutically acceptable colorant to improve their appearance and/or facilitate patient identification of the product and unit dosage level.

[0162] The dosage form of the present invention may be a capsule containing the composition, for example, a powdered or granulated solid composition of the invention, within either a hard or soft shell. The shell may be made from gelatin and optionally contain a plasticizer such as glycerin and sorbitol, and an opacifying agent or colorant.

[0163] A composition for tableting or capsule filling may be prepared by wet granulation. In wet granulation, some or all of the active ingredients and excipients in powder form are blended and then further mixed in the presence of a liquid, typically water, that causes the powders to clump into granules. The granulate is screened and/or milled, dried and then screened and/or milled to the desired particle size. The granulate may then be tableted, or other excipients may be added prior to tableting, such as a glidant and/or a lubricant.

[0164] Suitable formulations for the composition include solid and semi-solid compositions. For example, vectors and/or proteins can be mixed with or complexed to a carrier to render it resistant to dispersion from the site of delivery, to inhibit acidic and enzymatic hydrolysis, or a combination thereof. In some cases, the vectors and/or proteins can be packaged in a carrier that includes one or more types of crystalline materials, amorphous materials, liposomes, lipids, charged lipids (e.g., cytofectins), DNA-protein complexes, and biopolymers. The compositions can be encapsulated, e.g., in liposomes or bioploymerws, or in a formulation that provides for slow or reduced release of the active ingredient. Liposomes can be used for encapsulation and transfection of nucleic acids and proteins *in vitro*. Synthetic cationic lipids can limit problems encountered with liposome-mediated transfection and can be used to prepare liposomes for in vivo transfection of a nucleic acids (Feigner et al, Proc. Natl. Acad. Sci. USA. 84:1413 (1987); Mackey et al, Proc. Natl Acad Sci. USA £5:8027 (1988); and Ulmer et al, Science 259:1145 (1993)). The use of cationic lipids may promote encapsulation of negatively charged nucleic acids and can promote fusion with negatively charged cell membranes (Feigner et al., Science 337:387 (1989)). Useful lipid compounds and compositions for transfer of nucleic acids are described in WO95/18863, WO96/17823 and U.S. 5,459,127. Lipofection can be used to introduce exogenous genes into the specific sites in vivo. Lipids may be chemically coupled to

other molecules for targeting the complex to specific sites (e.g., to bone-related sites). Targeted peptides, e.g., hormones or neurotransmitters, and proteins such as antibodies, or non-peptide molecules (e.g., ligands) can be coupled to liposomes or to other carriers.

[0165] In some cases, the effect of a drug or active agent can be prolonged, for example, by slowing the absorption of the drug from local administration, subcutaneous injection, or intramuscular injection. This may be accomplished using a liquid suspension of crystalline or amorphous material having poor water solubility. The rate of absorption of the drug then depends upon its rate of dissolution which, in turn, may depend upon crystal size and crystalline form. Alternatively, delayed absorption of a locally-administered drug form is accomplished by dissolving or suspending the drug in an oil vehicle. Injectable depot forms can be made by forming microencapsulated matrices of the subject compounds in biodegradable polymers such as collagen, gelatin, or polylactide-polyglycolide. Depending on the ratio of active ingredient to polymer, and the nature of the particular polymer employed, the rate of active ingredient release can be controlled. Examples of other biodegradable polymers include poly(orthoesters) and poly(anhydrides). Depot injectable formulations are also prepared by entrapping the drug in liposomes or microemulsions which are compatible with body tissue.

[0166] With respect to delivering SLIT3 or SLIT2 agents, or SLIT3 or SLIT2 interfering agents to bone, methods can include delivery the active ingredient with bone morphogenic protein, platelet-derived growth factor, or a combination thereof to bone in the contexts of oral, periodontic, ortheopedic, spine, and other surgeries and procedures. *See* each of Shah et al. (2012) and Friedlaender, GE et al. (2013), each of which is incorporated herein by reference in its entirety. This includes versions of SLIT3 or SLIT2 protein or antibodies against SLIT3 or SLIT2, with additions of anionic amino acids such as glutamic and aspartic acid, intended to provide electrostatic targeting of SLIT3 or SLIT2 to bone surface.

Liposomes and nanoparticles

[0167] In an embodiment of the present invention, the pharmaceutical composition or formulation containing a SLIT3 or SLIT2 agent, or a SLIT3 or SLIT2 interfering agent can be encapsulated in a lipid formulation, for example as described in Semple et al., "Rational Design of Cationic Lipids for siRNA Delivery," *Nature Biotech.* 28:172-176 (2010), WO2011/034798 to Bumcrot et al., WO2009/111658 to Bumcrot et al., and WO2010/105209 to Bumcrot et al., which are hereby incorporated by reference in their entirety.

[0168] In another embodiment of the present invention, the delivery vehicle is a nanoparticle. A variety of nanoparticle delivery vehicles are known in the art and are suitable for delivery of a SLIT3 or SLIT2 agent, or SLIT3 or SLIT2 interfering agent, of

the invention (see *e.g.*, van Vlerken et al., "Multi-functional Polymeric Nanoparticles for Tumour-Targeted Drug Delivery," *Expert Opin. Drug Deliv.* 3(2):205-216 (2006), which is hereby incorporated by reference in its entirety). Suitable nanoparticles include, without limitation, poly(beta-amino esters) (Sawicki et al., "Nanoparticle Delivery of Suicide DNA for Epithelial Ovarian Cancer Cell Therapy," *Adv. Exp. Med. Biol.* 622:209-219 (2008), which is hereby incorporated by reference in its entirety), polyethylenimine-alt-poly(ethylene glycol) copolymers (Park et al., "Degradable Polyethylenimine-alt-Poly(ethylene glycol) Copolymers As Novel Gene Carriers," *J. Control Release* 105(3):367-80 (2005) and Park et al., "Intratumoral Administration of Anti-KITENIN shRNA-Loaded PEI-alt-PEG Nanoparticles Suppressed Colon Carcinoma Established Subcutaneously in Mice," *J Nanosci. Nanotechnology* 10(5):3280-3 (2010), which are hereby incorporated by reference in their entirety), and liposome-entrapped siRNA nanoparticles (Kenny et al., "Novel Multifunctional Nanoparticle Mediates siRNA Tumor Delivery, Visualization and Therapeutic Tumor Reduction *In Vivo*," *J. Control Release* 149(2): 111-116 (2011), which is hereby incorporated by reference in its entirety). Other nanoparticle delivery vehicles suitable for use in the present invention include microcapsule nanotube devices disclosed in U.S. Patent Publication No. 2010/0215724 to Prakash et al., which is hereby incorporated by reference in its entirety.

[0169] SLIT3 or SLIT2 agents, or SLIT3 or SLIT2 interfering agents, including liposomes or nanoparticles carrying them or into which they are incorporated, may be targeted to bone using strategies such as a bisphosphonate conjugation or (AspSerSer)6-liposomes and Aptamer-functionalized lipid nanoparticles to increase the fractional distribution to bone (Zhang, Guo, et al. 2012, Liang et al. 2015, Guan et al. 2012, Yao et al. 2013).

Polymers

[0170] Hydrophilic polymers suitable for use in the present invention can be those which are readily water-soluble. Hydrophilic polymers can also be covalently attached to a vesicle-forming lipid. The polymers employed can include those which are tolerated in vivo without toxic effects (i.e., are biocompatible). Suitable polymers include collagen, polyethylene glycol (PEG), polylactic (also termed polylactide), polyglycolic acid (also termed polyglycolide), a polylactic-polyglycolic acid copolymer, and polyvinyl alcohol. Polymers include those having a molecular weight of from about 100 or 120 daltons up to about 5,000 or 10,000 daltons, and for example those having a molecular weight of from about 300 daltons to about 5,000 daltons. In some cases, the polymer can be polyethylene glycol having a molecular weight of from about 100 to about 5,000 daltons or having a molecular weight of from about 300 to about 5,000

daltons. In some cases, the polymer is polyethylene glycol of 750 daltons (PEG(750)). Polymers may also be defined by the number of monomers therein; in some cases, polymers of at least about three monomers, such PEG polymers consisting of three monomers (approximately 150 daltons) can be used.

[0171] Other hydrophilic polymers which may be suitable for use in the present invention include polyvinylpyrrolidone, polymethoxazoline, polyethyloxazoline, polyhydroxypropyl methacrylamide, polymethacrylamide, polydimethylacrylamide, and derivatized celluloses such as hydroxymethylcellulose or hydroxyethylcellulose.

[0172] In certain embodiments, a formulation of the present invention comprises a biocompatible polymer selected from the group consisting of polyamides, polycarbonates, polyalkylenes, polymers of acrylic and methacrylic esters, polyvinyl polymers, polyglycolides, polysiloxanes, polyurethanes and co-polymers thereof, celluloses, polypropylene, polyethylenes, polystyrene, polymers of lactic acid and glycolic acid, polyanhydrides, poly(ortho)esters, poly(butic acid), poly(valeric acid), poly(lactide-co-caprolactone), polysaccharides, proteins, polyhyaluronic acids, polycyanoacrylates, and blends, mixtures, or copolymers thereof.

Cyclodextrins

[0173] Cyclodextrins are cyclic oligosaccharides, consisting of 6, 7 or 8 glucose units, designated by the Greek letter alpha, beta, or gamma, respectively. Cyclodextrins with fewer than six glucose units are not known to exist. The glucose units are linked by alpha-1,4-glucosidic bonds. As a consequence of the chair conformation of the sugar units, all secondary hydroxyl groups (at C-2, C-3) are located on one side of the ring, while all the primary hydroxyl groups at C-6 are situated on the other side. As a result, the external faces are hydrophilic, making the cyclodextrins water-soluble. In contrast, the cavities of the cyclodextrins are hydrophobic, since they are lined by the hydrogen of atoms C-3 and C-5, and by ether-like oxygens. These matrices allow complexation with a variety of relatively hydrophobic compounds, including, for instance, steroid compounds such as 17-beta-estradiol (see, e.g., van Uden et al. Plant Cell Tiss. Org. Cult. 38:1-3-113 (1994)). The complexation takes place by Van der Waals interactions and by hydrogen bond formation. For a general review of the chemistry of cyclodextrins, see, Wenz, Agnew. Chem. Int. Ed. Engl., 33:803-822 (1994).

[0174] The physico-chemical properties of the cyclodextrin derivatives depend strongly on the kind and the degree of substitution. For example, their solubility in water ranges from insoluble (e.g., triacetyl-beta-cyclodextrin) to 147% soluble (w/v) (G-2-beta-cyclodextrin). In addition, they are soluble in many organic solvents. The properties of the cyclodextrins enable the control over solubility of various formulation

components by increasing or decreasing their solubility. Numerous cyclodextrins and methods for their preparation have been described.

Examples

[0175] The present description is further illustrated by the following examples, which should not be construed as limiting in any way. The contents of all cited references (including literature references, issued patents, published patent applications as cited throughout this application) are hereby expressly incorporated by reference.

Example 1: SHN3/SLIT3 are Important for Bone Regeneration

Methods

Genetically modified mice

[0176] *Shn3*$^{-/-}$ (BALB/c), *Shn3*$^{KI/KI}$ (C57BL/6j), *Shn3* floxed allele (C57BL/6j), *Slit3*$^{-/-}$ (BALB/c), *Robo1*$^{-/-}$ (ICR) and *Robo4*$^{-/-}$ (C57BL/6j) mice were all previously reported, with *Robo1*$^{-/-}$ mice being a generous gift from Dr. Marc Tessier-Lavigne (Jaworski and Tessier-Lavigne 2012, Shim et al. 2013, Wein et al. 2012, Zhang et al. 2009, Jones et al. 2008, Yuan et al. 2003). To generate *Slit3* floxed mice, the SLIT3-F08 mouse embryonic stem (ES) cell line in which exon 8 is flanked by *loxP* sites was obtained from International Mouse Phenotyping Consortium (IMPC). After validation, F08 EC cells were injected into C57BL/6J blastocysts, and the derived chimeras displaying germline transmissions were selected for further breeding. The LacZ and neo cassettes were removed by intercrossing with transgenic mice expressing Flp recombinase. *Slit3* floxed mice were backcrossed with C57BL/6j mice for 8 generations.

[0177] Transgenic mice expressing Cre recombinase under control of the cdh5 promoter (cdh5-Cre) (Chen et al. 2009), osterix promoter (osx-Cre) (Rodda and McMahon 2006), dmp1 promoter (dmp1-Cre) (Lu et al. 2007) and Osteocalcin-CreERT mice (Park et al. 2012) were mated with *Shn3* floxed mice or *Slit3* floxed mice to obtain various *Shn3 or Slit3* conditional KO mouse. For postnatal activation of CreERT, 100mg/kg tamoxifen (Sigma) in corn oil (Sigma) was intraperitoneally injected to one-month-old mice once a day for five consecutive days. Littermate controls were utilized for all experiments.

[0178] All animals were maintained in accordance with the National Institutes of Health Guide for the Care and Use of Laboratory Animals and were handled according to protocols approved by the Weill Cornell Medical College subcommittee on animal care (IACUC).

µCT Analysis

[0179] Micro-CT (µCT) analysis was conducted on a Scanco Medical µCT 35 system at the Citigroup Biomedical Imaging Core using the previously described

parameters. (Shim et al. 2013). μCT analysis was performed by an investigator blinded to the genotypes of the animals under analysis.

Immunofluorescence, histology and histomorphometry

[0180] For immunofluorescence, fresh bone dissected and soft tissues from wild-type mice and mutant mice were collected and immediately fixed in ice-cold 4% paraformaldehyde solution for overnight. Decalcification was specially carried out with 0.5 M EDTA at 4℃ with constant shaking for bone samples from mice (age ≥ 1W). All samples were embedded in OCT compound (Sakura) and cut into 25-um-thick sagittal sections using a cryostat (Leica). Immunofluorescence staining, and analysis was performed as described by Fukuda et al. (2013) and Xu et al. (2017a, b). Briefly, after treatment with 0.2% Triton X-100 for 10 min, sections were blocked with 5% donkey serum at room temperature for 30 min and incubated overnight at 4℃ with antibodies: CD31 (553370, BD Pharmigen, 1:100), CD31 conjugated to Alexa Fluor 488 (FAB3628G, R&D Systems, 1:50), Endomucin (sc-65495, Santa Cruz, 1:100) or Beta Galactosidase antibody (GTX77365, Gene Tex, 1:100). Primary antibodies were visualized with species appropriate Alexa Fluor-coupled secondary antibodies (1:400, Molecular Probes). Nuclei were counterstained with DAPI. An Olympus IX81 confocal microscope or Zeiss LSM-880 confocal microscope was used to image samples. Quantification of skeletal vasculature was performed as previously described (Fukuda et al. 2013). Briefly, the CD31-postive or Endomucin-positive (red) area relative to the total bone marrow area (visualized in blue) was calculated using Image J software (see website at rsbweb,nih,gov/ij/).

[0181] For whole-mount immunostaining, retinas were collected from adult mice after systemic or local SLIT3 administration in bone fracture models.

[0182] For histological analysis, hindlimbs were dissected from the mice or human callus, fixed in 10% neutral buffered formalin for 24-48 hours, and decalcified by daily changes of 15% tetrasodium EDTA for 2 weeks. Tissues were dehydrated by passage through an ethanol series, cleared twice in xylene, embedded in paraffin, and sectioned at 7μm thickness. Decalcified sections were stained with hematoxylin and eosin (H&E). We incubated the slides with primary antibody to mouse EMCN (sc-65495, Santa Cruz, 1:200) and human Slit3 (ab198726, Abcam 1:50) at 37 °C for 2 h and subsequently used a horseradish peroxidase–streptavidin detection system (Dako) to detect the immunoreactivity. The number and volume of positively stained vessels was measured in four random visual fields of callus in 3 sequential sections per mouse in each group.

[0183] For histomorphometry, mice were injected with calcein (25mg/kg, Sigma), and undecalcified sections of the lumbar vertebrae were stained using von

Kossa and TRAP as described by Fukuda et al. (2013). Static and dynamic histomorphometric analysis was performed with using the Osteomeasure Analysis System (Osteometrics) following standard nomenclature as described (Dempster et al. 2013). Bone volume/total volume (BV/TV), bone formation rate/bone surface (BFR/BS, $\mu m^3\ \mu m^{-1}\ yr^{-1}$), mineral apposition rate (MM, um Day^{-1}), osteoblast surface/bone surface (Ob.S/BS, %) and osteoclast number/bone perimeter (No. OC/Bpm) were analyzed.

Flow cytometry and Cell Sorting

[0184] Femur and tibia were dissected from mutant mice and control groups after removing surrounding connective tissues. The metaphysis region and diaphysis regions of bone was crushed in Hanks Balanced Salt Solution (Life Technologies) containing 10 mM HEPES (pH 7.2) (CellGro) and enzymatically digested with 2.5 mg/mL Collagenase A (Roche) and 1 unit/mL Dispase II (Roche) for 15 minutes at 37°C under gentle agitation. The resulting cell suspensions were filtered (40 μm), washed using PBS (pH 7.2) containing 0.5% BSA (Fraction V) and 2 mM EDTA. After washing, equal numbers of cells per mouse were blocked with Purified Rat Anti-Mouse CD16/CD32 (BD Biosciences) for 30 min on ice, then stained with APC-conjugated EMCN antibody (ebioscience 50-5851-80), PE-conjugated CD31 (ebioscience 12-0311-81), FITC-conjugated CD45 (Tonbo 35-0451), APC/Cy7-conjugated Ter119 (Biolegend 116223) and PerCP-Cy5.5-conjugated CD146 (BD Biosciences 562231) for 45 min on ice. After washing, cells were resuspended in PBS (pH 7.2) with 2 mM EDTA and 1μg/mL 4-6,Diamidino-2-Phenylindole (DAPI) (live/dead exclusion) for analysis on an LSRII flow cytometer system (BD Biosciences) cytometer and analyzed using FlowJo software (TreeStar). Cell sorting was performed with a FACS Aria II SORP cell sorter (Becton Dickinson) at Weill Cornell Medical College, with exclusion of $DAPI^+$ cells and doublets. The strategy to sort $CD31^{hi}EMCN^{hi}$ endothelial cells is diagrammed in extended FIG. 7C.

Osteoblast Culture and Differentiation Assays.

[0185] Primary calvarial osteoblasts were isolated from five-day-old mice by triple collagenase/dispase II digestion. Cells were cultured in α-MEM medium (Gibco) containing 10% FBS, 2 mM L-glutamine, 1% penicillin/streptomycin, 1% Hepes, and 1% nonessential amino acids and differentiated with ascorbic acid and β-glycerophosphate. Conditioned medium was collected from culture of primary osteoblasts and stocked at -80 °C. hMSCs were cultured and differentiated into osteoblasts using a commercial kit (Cyagen). All cells were routinely tested to be mycoplasma negative.

[0186] For staining of extracellular matrix mineralization, cells were fixed with 10% neutral buffered formalin and stained with alizarin red. Mineralization activity was measured by colorimetric analysis. For alkaline phosphatase (ALP) activity, osteoblasts were fixed with 10% neutral formalin buffer and stained with the solution containing Fast Blue and Naphthol (Sigma-Aldrich). Alternatively, osteoblasts were incubated with 10-fold diluted Alamar Blue solution, washed, and incubated with a solution containing 6.5 mM Na_2CO_3, 18.5 mM $NaHCO_3$, 2 mM $MgCl_2$, and phosphatase substrate (Sigma-Aldrich). ALP activity was measured by a spectrophotometer (Thermo).

Osteoclast Culture and Differentiation.

[0187] Murine bone marrow cells were flushed from the femur and tibia of mice and cultured in petri dishes in α-MEM medium with 10% FBS and 20ng/ml of rM-CSF. Nonadherent cells were replated into tissue culture dishes and cultured in the same medium for 3 d to obtain osteoclast precursors. The osteoclast precursors then differentiated into osteoclasts in the presence of human RAMKL (50 ng/ml; PeproTech) and M-CSF for 3 days. Peripheral blood mononuclear cells from the whole blood of healthy volunteers were isolated by density gradient centrifugation using Ficoll (Invitrogen, Carlsbad, CA). CD14-positive cells were purified from fresh PBMCs using anti-CD14 magnetic beads (Miltenyi Biotec, Auburn, CA), as recommended by the manufacturer. Human monocytes were cultured in a-MEM with 10% FBS in the presence of M-CSF (20 ng/ml; PeproTech, Rocky Hill, NJ) for 2 d to obtain monocyte-derived macrophages. Experiments with human cells were approved by the Hospital for Special Surgery Institutional Review Board.

Endothelial cell culture and functional assays.

[0188] Mouse bone marrow derived late-stage endothelial progenitor outgrowth cells (EPOCs) were obtained from BioChain (7030031) and cultured in growth medium (BioChain Z7030035) as described previously (Xie et al. 2014). Endothelial cell migration assay was set up in Transwell-24 well plates with 8-um pore filters. Briefly, $1x10^5$ cells/well after 1-hour serum starvation were seeded in the upper chamber, then incubated with conditioned medium from osteoblasts and control in the lower chambers for a further 3h. The cells in the upper surface of each filter were removed with cotton swabs. The cells that migrated into the lower surface were fixed with 4% PFA for 30 min and then stained with crystal violet. The cell numbers were quantified by counting a centered microscope field per each filter (5 wells for each condition). Endothelial cell wound healing assays were conducted in 12-well plates precoated with gelatin (Stemcell Technologies). $3x10^5$ cells/well were plated overnight and stimulated with a wound in the form of a single linear scratch made with a yellow pipette tip. After gently washing the well twice, cells were cultured in medium with

SLIT3 or vehicle. At 6 and 12 hours after injury, cells were stained by 0.5% crystal violet and photographed. The width of the wound area was quantitatively evaluated using ImageJ (see website at rsb.info.nih.gov/ij/download.html). Endothelial cell proliferation assays were conducted in 96-well plates pre-coated with gelatin (Stemcell Technologies). EPOCs ($3x10^4$ cells/well) were seeded in the medium with a serial dilution of SLIT3 protein or vehicle in plates. At 0, 24, 48 hours after seeding, cells were incubated with 10-fold diluted Alamar Blue solution (Thermo Fisher) and the supernatant was evaluated with a spectrophotometer (Thermo) (5 wells for each condition). Endothelial cell tube formation assay was conducted in 96-well plates pre-coated with Matrigel (BD). After 1h serum starvation, EPOCs ($3x10^4$ cells/well) were seeded in conditioned medium dilution or control medium on polymerized Matrigel in plates. After 5 hours incubation at 37 ℃, the number of tube branches each well was observed and quantified by counting four random fields per well with microscopy (5 wells for each condition).

Quantitative real-time PCR analysis

[0189] Total RNA was extracted using TRIzol reagent (Invitrogen) or RNeasy Mini Kit (Qiagen), and reverse transcription was performed with the High-Capacity cDNA Reverse Transcription Kit from Applied Biosystems according to the manufacturer's instructions. We performed quantitative analysis of gene expression using SYBR® Green PCR Master Mix (Applied Biosystems) with the Mx3000P real-time PCR system (Agilent Technologies). *Hprt* expression was used as an internal control.

RNA sequencing and analysis.

[0190] Reads were aligned to the mm9 mouse transcripts using STAR (version 2.3.0e) (Dobin et al. 2013) using default parameters and resulting bam files were sorted and indexed using samtools. Gene counts were obtained by applying feature counts (version 1.4.3) (Liao, Smyth, and Shi 2014) to sorted bam files, and only unique-mapping reads were used. Genes without any expression counts in any sample were discarded. The DESeq2 (version 1.4.5) R package (Love, Huber, and Anders 2014) was employed to normalize gene count data, and then detect differentially expressed genes (DEG) between mutant mice and control groups with (FDR<0.1 and absolute log2 fold-change>0.5). Mosaic version 1.1 was used to retrieve gene ontology (GO) information for all genes of the mouse genome (Zhang, Hanspers, et al. 2012). Functional analysis was performed on DEG with DAVID (Huang da, Sherman, and Lempicki 2009) (version 6.7) and biological process GO terms with enrichment $p<0.05$ were selected as overrepresented functions

Western blot analysis.

[0191] Western blot analysis was performed according to a previously described standard protocol. (Greenblatt et al. 2016) Primary antibodies were specific for SLIT3 (1:500; R&D Systems, AF3629), ROBO1 (1:500; Abcam, ab7279), ROBO2 (1:1000; Abcam, ab75014), YAP (1:1,000; Cell Signaling, 4912), p-YAP (1:1,000; Cell signaling, 4911), AKT (1:1,000; Cell Signaling, 4691), p-AKT (1:1,000; Cell Signaling, 4060), ERK (1:1,000; Cell Signaling, 9102), p-ERK (1:1,000; Cell Signaling, 9101) and beta-actin (1:5,000; sc-47778, Santa Cruz) or Hsp90 (1:1000; sc-13119, Santa Cruz). Secondary anti-mouse/rabbit HRP-conjugated antibodies were subsequently applied.

ELISA analysis.

[0192] SLIT3 ELISA (Lifespan LS-F7173) and CTX ELISA (Lifespan LS-F21349) analysis was performed by using a kit. All ELISA assays were run according to the manufacturer's instructions.

Bone fracture model

[0193] All surgical procedures were performed under isoflurane (1-4%) anesthesia via nosecone. Surgical sites were sterilized using a betadine/iodide/isopropanol prep after hair removal by a clipper with a #40 blade and depilatory cream (Nair). After surgery, the visceral lining or muscle was sutured with absorbable Ethicon vicryl sutures (VWR, Cat #95057-014) prior to closing the skin with wound clips that were then removed 2 weeks post-operatively. Animals received intraperitoneal Buprenex (0.5 mg/kg) and oral Meloxicam (2.0 mg/kg) as analgesia prior to surgery and once every 24 hours post-surgery for 3 days. All surgical procedures are approved by the IACUC of Weill Cornell Medical College (Protocol #2012-0005).

[0194] Bone fracture was done following previously described protocols with modifications (Bradaschia-Correa et al. 2017). In brief, after anesthesia and surgical site sterilization, an incision above the right anterolateral femur was made. The femur and patella were then exposed, and a 27-gauge syringe needle was inserted parallel with the long axis of the femur through the patellar groove into the marrow cavity. The needle was then removed, and a single cut was made in the middle of the femoral diaphysis using a dremel saw with a diamond thin cutting wheel (VWR, Cat#100230-724). A blunt 25-gauge needle was then inserted into the marrow space through the hole made in the patella to stabilize the fracture. The needle was then trimmed to avoid it from projecting into the patella-femoral joint space. Muscle was then placed over the osteotomy site and stitched with absorbable sutures prior to closing the skin with wound clips.

[0195] When assessing the therapeutic effects of SLIT3, 1mg/kg body weight of SLIT3 recombinant protein (R&D) or vehicle was intravenous injected to the mice twice per week for 3 weeks after the surgery. Alternatively, the gelatin sponge was

manually soaked with SLIT3 (300ug/ml in PBS) or vehicle for 1 hour on ice and immediately placed to the surgical fracture area. All animals were euthanized by CO2 at time points indicated.

Ovariectomy-induced bone loss

[0196] For the prophylactic model, 12-week-old female mice (JAX) were anesthetized and bilaterally ovariectomized or sham operated. Ovariectomized mice were given twice weekly intravenous injections of 1mg per kg body weight of SLIT3 or vehicle or daily subcutaneous (sc) injections of 80ug/kg PTH (1-34) for 6 weeks starting 2 weeks after ovariectomy. For the model where SLIT3 was delivered in a therapeutic manner after osteopenia onset, OVX was performed in 12-week old mice, mice were observed for 8 weeks post-OVX to allow for onset of osteopenia, and then mice were treated with SLIT3 (1mg/kg) or vehicle for 6 further weeks. All mice were then randomly assigned to one of four groups: Sham, OVX +vehicle, OVX + SLIT3 and OVX + PTH. Three days after the last injection, all of the mice were euthanized and subjected to bone analysis as described earlier.

Biomechanical Analysis

[0197] All bones were tested to failure using four-point bending on a precision electromagnetic-based load frame (EnduraTEC ELF 3200, Bose Corporation, Minnetonka, MC). Femurs were placed with the posterior surface on the lower supports, spaced 9.9 mm apart. The upper supports were spaced 3.3 mm. Load was applied at a rate of 0.1 mm/s until failure occurred. The failure load (N) and bending stiffness (N/mm^2) within the elastic range were calculated from the force-displacement curves and the four-point dimensions.

Human bone callus collection

[0198] The project was approved by the Ethics Committee of Shaoxing People's Hospital (No. 080) and the protocol was carried out in accordance with approved guidelines. Preoperative informed consent was obtained from each patient. From January 2010 to June 2014, bone callus samples were obtained from patients undergoing surgical treatment in the Department of Orthopedics of Shaoxing People's Hospital. Callus was collected from patients who required surgical treatment for failure of skeletal traction.

[0199] Inclusion criteria were as follows: (1) surgeries after failure of conservative treatment or external fixation were applied temporarily before open reduction and plate fixation for long bone fractures; (2) secondary surgeries after failure of internal fixation, including loosened or broken plates or screws, bent or broken intramedullary nails, and fracture angulation and aversion abnormalities; and (3) secondary surgeries for hypertrophic nonunion. Exclusion criteria were as follows: (1)

fracture complicated with microbial infection; (2) fracture complicated with brain injury; (3) bone tumors; (4) systemic bone-related diseases; and (5) patients treated with hormones, steroids, vitamin D, or calcium.

Statistical Methods

[0200] All data were presented as the mean ± s.e.m. Sample sizes were calculated on the assumption that a 30% difference in the parameters measured would be considered biologically significant with an estimate of sigma of 10-20% of the expected mean. Alpha and Beta were set to the standard values of .05 and 0.8, respectively. No animals or samples were excluded from analysis, and, where applicable, animals were randomized to treatment versus control groups. For data analysis, where relevant, we first performed the Shapiro-Wilk normality test for checking normal distributions of the groups. If normality tests passed, two-tailed, unpaired Student's *t*-test and if normality tests failed, and Mann-Whitney tests were used for the comparisons between two groups. For the comparisons of three or four groups, we used one-way ANOVA if normality tests passed, followed by Tukey`s multiple comparison test for all pairs of groups. If normality tests failed, Kruskal-Wallis test was performed and was followed by Dunn`s multiple comparison test. The GraphPad PRISM software (v6.0a, La Jolla, CA) was used for statistical analysis. $P <$ 0.05 was considered statistically significant. $*P<0.05$, $**P<0.01$, $***P<0.001$, $****$ $P<0.0001$.

Results

***Shn3*$^{-/-}$ mice exhibit increases in CD31^{hi}EMCN^{hi} endothelium**

[0201] To address our hypothesis that osteoblasts are able to coordinate levels of osteogenic CD31^{hi}EMCN^{hi} endothelium to maintain bone formation capacity, CD31^{hi}EMCN^{hi} endothelium levels were assessed in a mouse strain displaying augmented postnatal bone formation, *Shn3*$^{-/-}$ mice. CD31, EMCN-double positive endothelium was present in the marrow immediately beneath the growth plate and was significantly increased in *Shn3*$^{-/-}$ mice (**FIG. 1A-1D**). This increase was bone-specific as *Shn3*$^{-/-}$ mice displayed normal levels of EMCN-positive vessels in other organs including heart, brain, lung and kidney (**FIG. 7A**). This vessel phenotype was present in neonatal *Shn3*$^{-/-}$ mice and thus preceded the appearance of the high bone mass phenotype (Jones et al. 2006) (**FIG. 7B**). Flow cytometry also confirmed an increase in CD31^{hi}EMCN^{hi} vascular endothelium in the bones of *Shn3*$^{-/-}$ mice (**FIG. 1E-1F** and **FIG. 7C**). Taken together, these observations indicate that SHN3 regulates levels of skeletal CD31^{hi}EMCN^{hi} endothelium in addition to its role in regulating osteoblast activity.

Osteoblasts regulate levels of CD31^{hi}EMCN^{hi} endothelium

[0202] As SHN3 acts in a cell intrinsic manner to regulate bone formation by osteoblasts, we reasoned that SHN3 also acts in osteoblasts to control levels of $CD31^{hi}EMCN^{hi}$ endothelium. To test this directly, mice harboring a *Shn3* allele in which exon 4 is flanked by loxP sites (called $Shn3^{f/f}$ mice) were bred to a cre-deleter strain targeting osteoblast progenitors, OSX-cre, and to a cre-deleter strain targeting mature osteoblasts, DMP1-cre. Both $Shn3^{osx}$ and $Shn3^{dmp1}$ mice exhibited a similar degree of increased bone mass, including increased cortical bone thickness, largely recapitulating the characteristic bone phenotype of $Shn3^{-/-}$ mice (**FIG. 2A-2B** and **FIG. 8A-8C**). Based on this, the $Shn3^{dmp1}$ strain was selected for further study as it implicates a more restricted subpopulation in any phenotypes observed (Zhang and Link 2016, Chen et al. 2014). Histomorphometric analysis confirmed that the high bone mass phenotype of $Shn3^{dmp1}$ mice was due to increased osteoblast-mediated bone formation predominantly on the endosteal surface (**FIG. 2C-2D** and **FIG. 8D-8E**). Analysis of skeletal $CD31^{hi}EMCN^{hi}$ endothelium by both immunostaining and flow cytometry demonstrated that $Shn3^{dmp1}$ mice displayed a similar increase in this subset of endothelial cells as that observed in $Shn3^{-/-}$ mice (**FIG. 2E-2G** and **FIG. 8F-8H**).

[0203] To further confirm that the function of SHN3 to regulate skeletal $CD31^{hi}EMCN^{hi}$ vascular endothelium maps to osteoblasts, endothelial cell-specific Shn3-deficient mice ($Shn3^{cdh5}$ mice) were generated using the Cdh5 (VE-cadherin)-Cre. Despite observing efficient deletion of *Shn3* in bone marrow endothelial cells (**FIG. 9A**), levels of $CD31^{hi}EMCN^{hi}$ endothelial cells were unchanged in $Shn3^{cdh5}$ mice (**FIG. 9B-9E**). Accordingly, $Shn3^{cdh5}$ mice also displayed normal bone mass (**FIG. 9F-9G**). Taken together with the $Shn3^{-/-}$ and $Shn3^{dmp1}$ phenotype, we conclude that osteoblasts regulate skeletal $CD31^{hi}EMCN^{hi}$ vascular endothelium in a SHN3-dependent manner, and that SHN3 does not act directly in endothelial cells to regulate skeletal phenotypes.

[0204] To determine if osteoblasts continuously participate in this regulation or if this process is limited to embryonic development, $Shn3^{f/f}$ mice were intercrossed with osteocalcin-CreERT mice expressing a tamoxifen-activated Cre recombinase in mature osteoblasts under the control of the osteocalcin promoter ($Shn3^{ocn\text{-}ert}$ mice). Cre-mediated deletion was induced with tamoxifen, generating tamoxifen-inducible inhibition of *Shn3* ($Shn3^{ocn\text{-}ert}$) in these mice, and the resulting skeletal and vascular phenotypes exhibited by the mice were analyzed. Tamoxifen treatment increased $CD31^{hi}EMCN^{hi}$ endothelial levels and both trabecular bone mass and cortical bone thickness, with the increase in $CD31^{hi}EMCN^{hi}$ endothelium preceding the increase in bone mass (**FIG. 2H-2L** and **FIG. 10**). Thus, mature osteoblasts continuously participate in tuning the levels of $CD31^{hi}EMCN^{hi}$ endothelium in bone, and this coupling is not solely a developmental phenomenon.

SHN3 regulates *Slit3* expression in osteoblasts

[0205] To investigate if the regulation of marrow angiogenesis by SHN3 is a direct effect of osteoblasts on endothelial cells, conditioned medium was harvested from WT and *Shn3*$^{-/-}$ primary osteoblasts and introduced to cultures of primary bone-marrow derived endothelial cells. Conditioned medium from *Shn3*$^{-/-}$ primary osteoblasts displayed an enhanced ability to induce endothelial migration and capillary tube formation, indicating that the osteoblasts secrete a soluble mediator that can induce endothelial migration and capillary tube formation (**FIG. 3A-3D**). To identify potential proangiogenic factors regulated by SHN3 in osteoblasts, RNA sequencing and transcriptional profiling was performed. Gene ontology (GO) analysis demonstrated that the set of differentially expressed genes in *Shn3*$^{-/-}$ versus WT osteoblasts is enriched for genes mediating angiogenesis in addition to the expected enrichment for genes involved with bone development and mineralization (**FIG. 3E**). Examination of the expression of a number of proangiogenic factors revealed that only SLIT3, a soluble axonal chemorepellent recently shown to have angiogenic functions, showed a substantial increase in *Shn3*$^{-/-}$ osteoblasts (**FIG. 3F**) (Zhang et al. 2009, Xie et al. 2014). Further expression analysis confirmed robust *Slit3* expression in osteoblasts and demonstrated negligible *Slit3* expression in osteoclasts (**FIG. 11A-11B**)(Su et al. 2004). Similarly, immunofluorescence for beta-galactosidase in *Slit3*$^{+/-}$ mice (Yuan et al. 2003) bearing a targeted insertion of a LacZ cassette into the *Slit3* locus identified SLIT3 expression in cells adjacent to the bone surface consistent with osteoblasts (**FIG. 12**). *Slit3* was also found to be expressed in human mesenchymal stromal cell-derived osteoblasts (**FIG. 11C**). To verify that *Slit3* expression is increased in *Shn3*$^{-/-}$ osteoblasts, three complimentary approaches were utilized. First, real-time PCR was used to validate the increase in *Slit3* observed in *Shn3*$^{-/-}$ osteoblasts by RNA sequencing (**FIG. 3G**). Second, overexpression or knockdown of *Shn3* in human mesenchymal stem cell (hMSC)-derived osteoblasts demonstrated, respectively, a suppression or an enhancement of both mRNA and protein levels of *Slit3* (**FIG. 3H-3I**). Moreover, overexpression of *Shn3* in murine primary osteoblasts also dramatically reduced SLIT3 expression (**FIG. 11D**). Lastly, ELISA demonstrated a 3-fold increase in SLIT3 secretion in conditioned medium from *Shn3*$^{-/-}$ osteoblasts relative to controls (**FIG. 3J**). Thus, SHN3 is a negative regulator of SLIT3 expression in osteoblasts.

[0206] Recent studies have shown that preosteoclast-derived PDGF-BB is able to induce CD31^{hi}EMCN^{hi} endothelium in bone (Xie et al. 2014). PDGF-BB secretion by osteoblasts was not detected, and negligible *Pdgfb* mRNA was observed in both WT and *Shn3*$^{-/-}$ osteoblasts (**FIG. 3F** and **FIG. 11E**). In addition, serum PDGF-BB levels are

unaltered in *Shn3*$^{-/-}$ mice (**FIG. 11E**). Thus, we do not observe evidence of regulation of PDGF-BB by SHN3.

[0207] SHN3 acts predominantly by regulating ERK activity, as mice bearing a knock-in of a mutation in 3 amino acids within the ERK interacting motif (*Shn3*$^{KI/KI}$ mice) in SHN3 largely recapitulate the high bone mass phenotype of *Shn3*$^{-/-}$ mice. *Slit3* levels demonstrated a similar increase in primary *Shn3*$^{KI/KI}$ osteoblasts as that seen in *Shn3*$^{-/-}$ osteoblasts (**FIG. 3K**). Similarly, treatment with the ERK pathway inhibitor trametinib (TTNB) reduced *Slit3* expression in both hMSC-derived osteoblasts and murine primary calvarial osteoblasts (**FIG. 3L** and **FIG. 11F**). Consistent with these observations, *Shn3*$^{KI/KI}$ mice displayed an increase in CD31^{hi}EMCN^{hi} skeletal endothelium similar to that seen in *Shn3*$^{-/-}$ mice (**FIG. 3M**). Thus, SHN3 regulates SLIT3 expression and CD31^{hi}EMCN^{hi} endothelium levels via its ability to bind and regulate ERK.

SLIT3 promotes CD31^{hi}EMCN^{hi} endothelium formation and bone formation *in vivo*

[0208] To determine if SLIT3 contributes to the regulation of bone marrow endothelium by osteoblasts *in vitro*, a dose response curve for SLIT3 treatment was conducted as described in prior studies (Zhang et al. 2009, Geutskens, Hordijk, and van Hennik 2010, Naska et al. 2010). Bone marrow endothelial progenitor outgrowth cells (EPOCs) treated with recombinant SLIT3 displayed enhanced migration and tube formation (**FIG. 4A-4B** and **FIG. 13A**). Additionally, SLIT3 modestly increased the proliferation of bone marrow derived EPOCs, consistent with the activity of SLIT3 observed in non-skeletal vascular endothelium (Zhang et al. 2009) (**FIG. 13B**). SLIT1 and SLIT2 displayed a similar ability to promote tube formation, consistent with observations that each of the SLITs displays a similar capacity for ROBO binding and activation (Howitt, Clout, and Hohenester 2004, Liu et al. 2004, Rama et al. 2015) (**FIG. 14A-14B**). Next, conditioned medium was collected from WT and *Shn3*$^{-/-}$ osteoblasts and placed on bone marrow derived endothelial cells together with an anti-SLIT3 blocking antibody or an isotype control. Enhanced tube formation was seen with conditioned medium from SHN3-deficient osteoblasts, and treatment with an anti-SLIT3 blocking antibody abrogated this effect (**FIG. 4C-4D**). Investigation of the signaling pathways downstream of SLIT3 in bone marrow endothelial cells demonstrated activation of ERK MAPK and Hippo signaling, pathways known to participate in angiogenesis (**FIG. 15**) (Shin et al. 2016, Choi et al. 2015). Interestingly, we also noted that treatment of bone marrow-derived endothelial cells with SLIT3 enhanced the acquisition of a CD31^{hi}EMCN^{hi} surface immunophenotype in culture (**FIG. 16A**).

SLIT2 and SLIT3 unexpectedly display divergent functions in the skeletal system

[0209] Current biochemical evidence shows that the ROBO receptors are largely unable to discriminate among SLIT ligands. Thus, based on current theories, one would expect that SLIT2 would show a similar ability as SLIT3 to promote fracture healing.

[0210] Systemic administration of SLIT3 increased levels of skeletal $CD31^{hi}EMCN^{hi}$ endothelium production *in vivo* (**FIG. 16B**). In addition, SLIT2 increased formation of $CD31^{hi}EMCN^{hi}$ endothelium *in vivo*. (**FIG. 14C**).

[0211] To assess if SLIT3 regulates $CD31^{hi}EMCN^{hi}$ endothelium under physiologic conditions, immunofluorescence and flow cytometry were performed on *Slit3*$^{-/-}$ mice, with both approaches revealing a reduction in $CD31^{hi}EMCN^{hi}$ skeletal endothelium (**FIG. 4E-14G** and **FIG. 5A-5B**). Concurrent with this reduction in $CD31^{hi}EMCN^{hi}$ endothelium, total bone mass and cortical bone thickness were also substantially reduced in *Slit3*$^{-/-}$ mice (**FIG. 4H-4I; FIG. 5C**). Consistent with prior reports (Yuan et al. 2003), *Slit3*$^{-/-}$ mice displayed a decrease in body weight at 1 month of age, with body weight normalization occurring by 3 months of age (**FIG. 17A**). Thus, osetopenia could be observed even at ages where the weight of *Slit3*$^{-/-}$ mice was indistinguishable from that of littermate controls. Such osteopenia was due to reduced osteoblast activity, as bone formation was reduced without significant alterations in osteoclast numbers or serum CTX, a marker of osteoclast activity (**FIG. 5D-5F** and **FIG. 17B**). To evaluate if this decrease in bone formation was due to cell intrinsic defects in osteoblast activity, the differentiation of SLIT3-deficient osteoblasts was examined. Mineralization activity, ALP induction, and induction of characteristic osteoblast transcripts were all intact or even slightly enhanced in the absence of SLIT3 (**FIG. 17C-17E**). Furthermore, treatment of osteoblasts with recombinant SLIT3 did not enhance osteoblast activation, nor did treatment with a ROBO1-Fc fusion that blocks SLIT signaling impair osteoblast differentiation (**FIG. 17F-17G**). Thus, the ability of SLIT3 to enhance bone formation *in vivo* is not attributable to the direct effects of SLIT3 on osteoblasts, consistent with the model that SLIT3 directly increases levels of $CD31^{hi}EMCN^{hi}$ endothelium to augment bone formation. To confirm if osteoblasts represent the key cellular source of SLIT3 controlling levels of skeletal $CD31^{hi}EMCN^{hi}$ endothelium and bone mass accrual *in vivo*, mice bearing a conditional *Slit3* floxed allele (*Slit3*$^{f/f}$ mice) were generated, and their deletion capacity was validated (**FIG. 18A**). *Slit3*$^{f/f}$ mice were bred to cre-deleter strains targeting either osteoblast progenitors, OSX-cre, or mature osteoblasts, DMP1-cre. Osteoblast-specific deletion of *Slit3 in vivo* recapitulated both the impaired $CD31^{hi}EMCN^{hi}$ endothelium levels and the osteopenia phenotypes observed in *Slit3*$^{-/-}$ mice (**FIG. 4J-4L** and **FIG.**

18B-18E). Furthermore, neither neuron-specific deletion of *Slit3* by using Synapsin-cre nor specific deletion of *Slit3* in endothelial cells by using Cdh5-cre *in vivo* led to detectable bone loss (**FIG. 19A-19B**). Thus, osteoblasts are the key functional source of SLIT3 influencing skeletal biology.

ROBO1 is a key receptor for SLIT3 on marrow endothelial cells.

[0212] As SLITs are known to signal through the Roundabout family (ROBO1-4) of receptors, we next explored which ROBO receptors might be acting in endothelial cells to mediate the response to SLIT3 (Blockus and Chedotal 2016). $CD31^{hi}EMCN^{hi}$ skeletal endothelial cells isolated by FACS and subjected to RNA-seq transcriptome analysis, revealed that *Robo1* and *Robo4* are the predominant ROBO family receptors expressed (**FIG. 20A**). Immunofluorescence for beta-galactosidase in the bones of $Robo1^{+/-}$ mice bearing a knock-in of a LacZ cassette into the *Robo1* locus confirmed that *Robo1* expression is present in endothelium near the growth plate, consistent with $CD31^{hi}EMCN^{hi}$ endothelial cells (**FIG. 12**). ROBO expression was also characterized in other skeletal cell types, indicating that osteoblasts express *Robo1* and *Robo2* whereas osteoclasts show negligible expression of ROBO family members. (**FIG. 20B-20C**). Given the expression of *Robo1* and *Robo4* in $CD31^{hi}EMCN^{hi}$ endothelial cells, the skeletal phenotype of $Robo1^{-/-}$ and $Robo4^{-/-}$ mice was examined. $Robo1^{-/-}$ but not $Robo4^{-/-}$ mice display low trabecular bone mass in long bones (**FIG. 5G** and **FIG. 18D-18E**), and $Robo1^{-/-}$ mice also showed decreased levels of $CD31^{hi}EMCN^{hi}$ skeletal endothelium **(FIG. 5H).** *Robo2* expression was not detected in either sorted $CD31^{hi}EMCN^{hi}$ skeletal endothelial cells or cultured bone marrow derived endothelial cells, and *Robo2* expression was not induced by either germline *Robo1*-deficiency or shRNA-mediated *Robo1* knockdown. (**FIG. 20F-20H**). Thus, no evidence of ROBO2-mediated compensation for ROBO1 loss-of-function was observed.

[0213] Next, the mechanism of SLIT3 mediated effects on bone marrow endothelial cells was investigated. Knockdown of *Robo1* in bone marrow derived endothelial cells impaired their response to SLIT3 as determined by both their tube formation capacity and phosphorylation of the hippo pathway signaling intermediate YAP (**FIG. 21A-21B**). YAP has been reported to play a crucial role endothelial cell migration and tube formation (Choi et al. 2015, Sakabe et al. 2017). Consistent with this, shRNA-mediated knockdown of YAP significantly reduced the ability of SLIT3 but not FGF2 to induce tube formation in bone marrow-derived endothelial cells, indicating that YAP acts downstream of the SLIT3/ROBO1 pathway to control tube formation (**FIG. 21C-21D**). Taken together, ROBO1 is a key receptor controlling both endothelial cell responses to SLIT3 and overall bone mass accrual.

Slit3* contributes to the ability of *Shn3* to control osteogenesis and skeletal endothelium *in vivo

[0214] We next questioned whether the enhanced production of SLIT3 by SHN3-deficient osteoblasts contributes to the high bone mass phenotype of SHN3-deficient mice. To address this, a genetic interaction study was performed by intercrossing *Shn3*$^{-/-}$ and *Slit3*$^{-/-}$ mice. As shown in **FIG. 5**, an epistatic genetic interaction was observed between *Shn3*- and *Slit3*-null alleles, as the increases in bone formation, trabecular bone mass, and CD31^{hi}EMCN^{hi} endothelial cell levels in *Shn3*$^{-/-}$ mice were partially reversed in *Shn3*$^{-/-}$*Slit3*$^{-/-}$ mice. Thus, SLIT3 contributes to both the high bone mass phenotype and enhanced CD31^{hi}EMCN^{hi} endothelium phenotype of SHN3-deficient mice *in vivo*. In addition, a genetic interaction similar to that observed with the *Shn3* and *Slit3* germline null alleles was recapitulated using conditional deletion of *Shn3* and *Slit3* alleles in osteoblasts using Osx-cre (**FIG. 22A-22B**). Thus, the interaction between *Shn3* and *Slit3* alleles to regulate bone mass is intrinsic to osteoblasts. Taken together, these results imply that SLIT3 production is utilized by osteoblasts to condition their environment through angiogenesis to be conducive for bone formation.

A SHN3/SLIT3 osteoblast:endothelium coupling pathway plays an essential role in fracture healing

[0215] Given that bone repair is accompanied by extensive elaboration of new blood vessels, we hypothesized that SHN3/SLIT3 pathway mediated communication between osteoblasts and endothelial cells may be vital for bone fracture healing. In support of this hypothesis, immunohistochemical analysis of human fracture callus tissue demonstrated robust expression of SLIT3 in osteoblasts and the presence of CD31^{+} endothelium in physical proximity to osteoblasts (**FIG. 23A-23B**). An open femoral midshaft fracture model was established and used to study bone healing in *Shn3*$^{-/-}$, *Slit3*$^{-/-}$, *Shn3*$^{-/-}$*Slit3*$^{-/-}$ and WT control mice. 21 days after fracture, μCT and histology analysis showed that fracture healing was enhanced in *Shn3*$^{-/-}$ mice. The fracture site in *Shn3*$^{-/-}$ mice displayed extensive bridging with mature lamellar bone that had already remodeled to contain marrow elements within the newly formed callus tissue. In contrast, deletion of *Slit3* led to complete non-union and arrest of fracture healing with only trace amounts of cartilaginous callus present (**FIG. 6A-6C**). Consistent with the results of the bone mass genetic interaction studies, SLIT3 deficiency largely reversed the enhanced healing phenotype of SHN3-deficient mice. These observations of enhanced and impaired healing in SHN3-deficient and SLIT3-deficient mice, respectively, translated into improved or impaired biomechanical properties of the callus, as shown by the load to failure or maximum load sustained

across the fracture site. Consistent with observations in basal bone mass phenotypes, *Shn3*$^{-/-}$ mice displayed enhanced angiogenesis throughout the callus, and this phenotype was reversed by SLIT3 deficiency (**FIG. 6D-6E and FIG. 24A-24B**). Thus, the coupling between osteoblasts and vascular endothelium mediated by the SHN3/SLIT3 pathway is essential for fracture healing.

SLIT3 has therapeutic effects in models of fracture healing and postmenopausal osteoporosis

[0216] Due to evidence that SLIT3 mediated crosstalk between osteoblasts and CD31^{hi}EMCN^{hi} endothelium is an important regulator of bone mass accrual and bone-fracture healing, we hypothesized that administration of exogenous SLIT3 may have therapeutic effects to promote bone formation and regeneration. To examine this, recombinant SLIT3 was administered twice weekly via IV injection in 5-week-old male mice concurrent with performing an open femoral midshaft fracture. After 21 days of treatment, μCT and histological analysis showed an enhancement of bone fracture healing in SLIT3-treated mice (**FIG. 6F-6G**). The bone volume in the callus area was increased almost 2-fold relative to controls (**FIG. 6H**). Furthermore, vascularization of fracture area including CD31^{hi}EMCN^{hi} endothelium was also increased by SLIT3 administration (**FIG. 6I** and **FIG. 24C**). Finally, biomechanical testing demonstrated that SLIT3 treatment significantly enhanced the maximum load sustained and stiffness of the fracture callus, demonstrating improvements in clinically meaningful endpoints (**FIG. 6J**).

[0217] However, it is currently unclear if systemic treatment with SLITs will result in systemic toxicity (Kruszka et al. 2017; Morin-Poulard et al. 2016; Jaworski and Tessier-Lavigne 2012; Kidd T et al. 1998). To investigate this, mice underwent systemic IV treatment with SLIT3 and were examined for unexpected toxicity. Notably, examination of vascular morphology did not detect alterations in lung, heart, kidney or retina, and no changes in brain ultrastructure were present after SLIT3 administration (**FIG. 25A-25D**). Thus, under this dosing strategy and with regards to these endpoints, the effects of SLIT3 were specific to bone. However, while SLIT3 did not alter retinal vascular morphogenesis, some mice treated with SLIT3 unexpectedly displayed increased retinal vascular permeability (**FIG. 31**, arrowheads). As increased retinal vascular permeability is known to result in vision loss as seen in conditions such as diabetic retinopathy or exudative macular degeneration, this toxicity may preclude systemic therapeutic administration of SLIT3.

Local delivery

[0218] Based on these observations, local delivery of SLIT3 would avoid the risk of an undesired effect of SLIT3 to promote retinal vascular permeability. As a

proof-of-principle strategy to avoid the potential extra-skeletal toxicities that were identified as described herein, local delivery of SLIT3 into a fracture site was achieved with a SLIT3-loaded collagen sponge. A hydrogel containing SLIT3 has also been implanted. These approaches recapitulated the effects of systemic SLIT3 delivery in promoting fracture healing as judged by improved mineralization and biomechanical properties of the fracture callus and increased formation of $CD31^{hi}EMCN^{hi}$ endothelium (**FIG. 6K-6L** and **FIG. 26**). Local delivery of SLIT3 also did not impact non-skeletal vascular abundance or morphology or brain ultrastructure (**FIG. 26B-26D**).

[0219] Thus, local delivery of SLIT3 using a SLIT3-containing construct is effective in preclinical models to enhance skeletal healing. This approach is expected to be broadly applicable for the treatment of skeletal diseases and conditions, including the treatment of osteoporosis.

[0220] Given the therapeutic effects of SLIT3 in a fracture model, we next examined whether systemic SLIT3 administration can protect from bone loss in the murine ovariectomy (OVX) model of postmenopausal osteoporosis (Bouxsein et al. 2005). Successful OVX was confirmed two months after OVX by the presence of both osteopenia and uterine atrophy (**FIG. 6M** and **FIG. 27A-27B**). First, the ability of SLIT3 to prevent bone loss was examined in this model. Mice were treated with IV injection of SLIT3 or vehicle twice weekly initiated two weeks after OVX. Micro-CT analysis showed that SLIT3 administration significantly countered OVX-induced bone loss as shown by increased trabecular BV/TV and cortical thickness (**FIG. 6M** and **FIG. 27C**). As the effects of SLIT3 were comparable to the effects of PTH treatment, this indicates that the magnitude of SLIT3 effect is clinically significant. Moreover, both SLIT3 and PTH administration reversed the attenuation of endosteal $CD31^{hi}EMCN^{hi}$ endothelium occurring after OVX and similarly rescued endosteal bone formation (**FIG. 27D-27F**). To further investigate the therapeutic activity of SLIT3, the ability of SLIT3 to promote bone formation after the onset of OVX-induced osteopenia was examined. Mice were treated with IV injection of SLIT3 or vehicle twice weekly initiated eight weeks after OVX surgery. SLIT3 administration significantly reversed bone loss as shown by increased trabecular BV/TV and cortical thickness (**FIG. 28A-28B**). Furthermore, SLIT3 administration significantly increased $CD31^{hi}EMCN^{hi}$ endothelial cells in this context (**FIG. 28C**). Taken together, these results provide proof-of-principle that SLIT3 may have clinical utility to enhance fracture healing and to treat disorders of low bone mass such as postmenopausal osteoporosis.

Discussion

[0221] Though bone formation is mediated solely by osteoblasts, it is likely that many other tissue types present in bone, such as vascular endothelium or autonomic

and sensory nerves, contribute to creating a conducive milieu for bone formation (Fukuda et al. 2013, Kusumbe, Ramasamy, and Adams 2014, Ramasamy et al. 2014, Zhang et al. 2016, Xu 2014). To the degree that the creation of a local osteogenic milieu should be coordinated with the cell intrinsic matrix production capacity of osteoblasts, it would be mechanistically attractive for osteoblasts to regulate their own matrix production alongside the activities of these supporting cell types. However, this remains a poorly understood facet of bone physiology. Here, the inventors hypothesized that mice with extreme increases in bone formation represent an opportunity to identify how osteoblasts regulate supporting tissue types in bone to create a pro-osteogenic milieu. In particular, the greatly enhanced bone formation phenotype of mice lacking the adaptor protein SHN3 was utilized to identify that osteoblast-derived SLIT3 enhances levels of an osteogenic subtype of vascular endothelium in bone, $CD31^{hi}EMCN^{hi}$ endothelium. Accordingly, mice lacking SLIT3 or the known SLIT receptor ROBO1 display reduction in both the levels of marrow $CD31^{hi}EMCN^{hi}$ endothelium and basal bone mass.

[0222] Support for osteoblasts being a key source of SLIT3 in bone include the observation of robust and specific SLIT3 expression in osteoblasts, without appreciable SLIT3 expression in osteoclasts or $CD31^{hi}EMCN^{hi}$ endothelium (**FIG. 11A-11B** and **FIG. 20A**). Conditional deletion of *Shn3* in late-stage osteoblasts enhanced SLIT3 expression and $CD31^{hi}EMCN^{hi}$ endothelium levels, and osteoblast derived conditioned medium enhanced bone marrow endothelial tube formation in a SLIT3-dependent manner. Moreover, genetic interaction studies demonstrated that the $CD31^{hi}EMCN^{hi}$ endothelium-promoting and enhanced bone formation effects of SHN3 deficiency are partially SLIT3 dependent. This rescue of the SHN3 phenotype is not a generic property of crossing SHN3 to a mouse with low bone mass, as crossing the $Shn3^{-/-}$ mouse strain to the osteopenic $Rsk2^{-/-}$ strain did not significantly alter the $Shn3^{-/-}$ phenotype (Shim, J. H., et al. 2013). Thus, the epistatic interaction between *Shn3* and *Slit3* alleles in both regulation of bone mass and $CD31^{hi}EMCN^{hi}$ endothelium levels provides in vivo genetic evidence that SLIT3 is a critical effector downstream of SHN3, though it does not preclude the existence of additional effectors.

[0223] Additionally, ROBO1-deficient but not ROBO4-deficient mice show an osteopenic phenotype, and accordingly ROBO1 knockdown partially blocks bone marrow endothelial responses to SLIT3. Though the phenotype of ROBO1-deficient mice and the in vitro studies indicate that it is a key receptor of SLIT signals in the regulation of bone mass accrual, it cannot be excluded that other SLIT/ROBO members similarly contribute in either an independent or redundant manner (Blockus and Chedotal 2016).

[0224] Flow cytometry analysis of $CD31^{hi}EMCN^{hi}$ endothelium indicates that this is a relatively rare population of cells, with only very limited numbers of cells present relative to other hematopoietic or mesenchymal lineages. This raises the question of how such a small population can exert such a large effect on organ physiology. One possible explanation is that the highest density of $CD31^{hi}EMCN^{hi}$ endothelium is observed at very active sites of bone formation, such as the primary spongiosum immediately adjacent to the growth plate of an actively growing long bone, and within this site $CD31^{hi}EMCN^{hi}$ endothelium is observed to be in close physical proximity with osteoblast-lineage cells. This physical proximity between $CD31^{hi}EMCN^{hi}$ endothelium and the osteoblast lineage cells they support may act to amplify each other's physiologic effects. Further work is needed to clarify the nature and mediators of these interactions beyond SLIT3. Additionally, much remains to be learned about properties that define $CD31^{hi}EMCN^{hi}$ endothelium, including how this population relates to other endothelial cell types present in bone (Ramalingam, Poulos, and Butler 2017).

[0225] Given the evidence that fracture healing is accompanied by extensive elaboration of new blood vessels, the role of SHN3/SLIT3 mediated coupling between osteogenesis and $CD31^{hi}EMCN^{hi}$ endothelium was explored in bone regeneration and found to be critically important.

Example 2: Osteoclasts Are Not a Source of Physiologically Relevant SLIT3

[0226] As described herein SLIT3 is of fundamental importance as an osteo-anabolic reagent. This Example describes further studies clarifying the cellular sources and targets of SLIT3.

Materials and Methods

[0227] **Animals.** *Slit3*$^{-/-}$ and CTSK-Cre mice were described previously. *Slit3*$^{fl/fl}$ were generated by homologous recombination insertion of a floxed allele into the *Slit3* locus. All experiments were performed according to protocols approved by the institutional animal care and use committee of Weill Cornell Medical College. All mice were maintained under specific pathogen free conditions, fed ad libitum chow and housed up to 4 animals per cage on a standard day-night cycle lighting.

[0228] **Osteoclast culture, differentiation assays, Western blotting and qPCR.** *In vitro* primary osteoclast cultures, quantitative PCR, Western blotting, and TRAP staining were performed as previously described. Primary antibodies were specific for SLIT3, (1:1,000; Cell Signaling) and HSP90 (1:2,000; Sigma).

[0229] **Micro-CT Analysis, histology, immunohistochemistry, and histomorphometry.** Micro-CT analysis was conducted on a Scanco Medical Micro-CT

35 system by an investigator blinded to the genotypes of the animals under analysis. Paraffin embedding, sectioning and TRAP staining were performed as previously described. Static and dynamic histomorphometric analyses were performed using the Osteomeasure Analysis System (Osteometrics) as previously described, also by an investigator blinded to the genotypes of the animals being analyzed. Immunofluorescence staining was performed according to a previously published protocol.

[0230] **Flow cytometry analysis and cell sorting.** Bone marrow cells collected from *Slit3*$^{fl/fl}$ and *Slit3*^{ctsk} mice were filtered through a cell strainer (70 μm; BD Falcon) to remove debris. After washing, equal numbers of cells per mouse were blocked with Purified Rat Anti-Mouse CD16/CD32 (BD Biosciences) for 30 min on ice, then stained with BUV395-conjugated B220 antibody (BD), Percp-Cy5.5-conjugated CD11b (Biolegend), FITC-conjugated CD115 (Biolegnd) and PE/Cy7-conjugated CD117 (BioLegend) for 45 min on ice. After washing, cells were resuspended in PBS (pH 7.2) with 2 mM EDTA and 1 μ g mL−1 DAPI (live/dead exclusion) for analysis on an LSRII flow cytometer system (BD Biosciences) cytometer and analyzed using FlowJo software (Tree Star). Cell sorting was performed with a FACSAria II SORP cell sorter (Becton Dickinson), with exclusion of DAPI+ cells and doublets. The strategy to sort osteoclast progenitor cells (OCPs) is diagrammed in FIG. 32.

[0231] **Bone marrow transplantation.** We followed a published protocol for bone marrow transplantation (Zhao B, et al. Nature Medicine 2009). Briefly, Bone marrow cells from wild-type or KO littermate mice were harvested and 5 million of total bone marrow cells from each donor were transplanted by intravenous tail vein injection into each of the irradiated wild-type recipients. Recipient mice (6-week-old BALB/c mice) were lethally irradiated with a single dose of 875 rads 1 day prior to transplantation. Bone marrow-chimeric mice were sacrificed 16 weeks after bone marrow transplantation. The experiments using chimeric mice were approved by the Hospital for Special Surgery Institutional Animal Care and Use Committee.

[0232] **Statistical methods.** All data were presented as the mean ± s.e.m. Sample sizes were calculated on the assumption that a 30% difference in the parameters measured would be considered biologically significant with an estimate of sigma of 10–20% of the expected mean. Alpha and Beta were set to the standard values of 0.05 and 0.8, respectively. No animals or samples were excluded from analysis, and where applicable, animals were randomized to treatment versus control groups. Statistical methods are indicated in the figure legends. The GraphPad PRISM software (v6.0a; GraphPad, La Jolla, CA, USA) was used for statistical analysis. A P value < 0.05 was considered statistically significant.

Results

[0233] To measure SLIT3 expression during osteoclastogenesis, an *in vitro* osteoclast formation assay was first performed using wild type bone marrow macrophages (BMMs). Interestingly, compared with the robust SLIT3 expression seen in brain, SLIT3 expression was not detected during osteoclastogenesis at either the mRNA or protein level (**FIG. 33A-33B**). This finding is consistent with a previous Gene-Chip analysis of axon guidance cues in osteoclast and osteoblast differentiation and another independent expression study in mouse macrophages. In addition, these data indicate that osteoblasts but not osteoclasts are a major source of SLIT3 production in bone compartments, consistent with findings described above on severe osteopenia in *Slit3*^{dmp1} and *Slit3*^{osx} mice.

[0234] To assess the effects of exogenous SLIT3 on osteoclastogenesis, BMMs were treated with recombinant SLIT3 at levels showing bioactivity in multiple other cellular assays, including tube formation assays in endothelial cells. Although SLIT3 treatment modestly inhibited expression of osteoclast marker genes, no significant changes were observed in the number of tartrate-resistant acid phosphatase (TRAP) positive osteoclasts compared with controls (**FIG. 33C-33D**). Similar negative results were obtained during a dose-titration of SLIT3 during osteoclast differentiation (**FIG. 33E**). Consistent with these *in vitro* findings, treatment for six weeks with recombinant SLIT3 *in vivo* was only able to increase amounts of CD31^{hi}EMCN^{hi} vasculature but not osteoclast formation, indicating that SLIT3 has *in vivo* angiogenic but not anti-osteoclastogenic activity *in vivo*.

[0235] To further assess the role of SLIT3 in osteoclastogenesis *in vivo*, CD117^{+}CD11b^{dim}CD115^{+} osteoclast precursors were first analyzed in *Slit3*$^{-/-}$ mice using flow cytometry. No significant difference was observed in the overall abundance of osteoclast cells in *Slit3*$^{-/-}$ mice, indicating that global deletion of SLIT3 is not able to disrupt osteoclast precursors (**FIG. 34A**). Next, as osteoblast-derived SLIT3 is crucial for bone mass accrual, the inventors designed tests to evaluate whether osteoblast derived SLIT3 would specifically affect osteoclast precursors. *Slit3*$^{f/f}$ mice were bred to cre-deleter strains targeting osteoblasts via OSX-cre (*Slit3*^{osx}). Like the observation using animals with global deletion of SLIT3, numbers of osteoclast precursors were unaltered in *Slit3*^{osx} mice (**FIG. 34B**). Lastly, to confirm the role of SLIT3 in osteoclasts, *Slit3*$^{f/f}$ mice were bred to a cre-deleter strain targeting mature osteoclasts, CTSK-cre (*Slit3*^{ctsk}). No apparent difference was observed in the overall abundance of osteoclast precursors in *Slit3*^{ctsk} mice, indicating that ablation of SLIT3 production by CTSK positive osteoclasts is not able to disrupt osteoclast precursors (**FIG. 34C**). Furthermore, osteoclast precursors derived from *Slit3*^{ctsk} mice and *Slit3*$^{f/f}$ mice were

sorted and an osteoclast formation assay was conducted. No differences in osteoclast production were detected (**FIG. 34D**). Consistent with this, *Slit3*^{ctsk} mice developed normally without any gross abnormality and display a normal bone mass relative to control mice at both 5 weeks (**FIG. 34E**). Consistent with this, histomorphometric analysis showed that mineralization rate, bone formation rate, osteoblast number and osteoclast number were not affected in *Slit3*^{ctsk} mice. Moreover, the skeletal vasculature was not altered in *Slit3*^{ctsk} mice relative to *Slit3*$^{f/f}$ mice as well.

[0236] As CathepsinK-cre deletes relatively late during osteoclast differentiation, bone marrow chimeras from *Slit3*$^{-/-}$ donors were created to assess the importance of SLIT3 production by early stage osteoclast-lineage cells. Bone marrow was collected from 8-week old *Slit3*$^{+/+}$ mice and *Slit3*$^{-/-}$ mice and then injected into lethally irradiated 8-week-old WT mice. The resulting chimeras were maintained for 12 weeks before analysis (the protocol is outlined in **FIG. 35A**). Micro-CT analysis showed that the mice reconstituted with bone marrow cells isolated from *Slit3*$^{-/-}$ mice had normal bone mass compared with those reconstituted with WT bone marrow cells, as illustrated by the analysis of the trabecular bone volume/total volume and cortical bone thickness (**FIG. 35B-35C**). Further histomorphometry and immunofluorescence staining showed that neither osteoclast numbers nor bone vasculature were altered by bone marrow transplantation and the absence of SLIT3 from osteoclast lineage cells (**FIG. 35D**). In summary, both by using conditional deletion of *Slit3* in mature osteoclasts and by creating bone marrow chimeras incapable of SLIT3 production in osteoclast-lineage cells, evidence for osteoclasts as a physiologically relevant source of SLIT3 was not observed.

[0237] The following statements are potential claims that may be converted to claims in a future application. No modifications of the following statements should be allowed to affect the interpretation of claims which may be drafted when this provisional application is converted into a regular utility application.

STATEMENTS

1) A method for prevention of bone loss or for promoting bone growth, bone-strengthening, or bone-healing in a subject in need thereof, comprising administering a SLIT3 or SLIT2 agent to said subject.

2) The method of statement 1, wherein the SLIT3 or SLIT2 agent is a protein.

3) The method of statement 1, wherein the SLIT3 or SLIT2 agent is a gene transfer vector comprising a promoter operably linked to nucleic segment encoding a SLIT3 or SLIT2 protein.

4) The method of statement 1, 2 or 3, wherein the SLIT3 or SLIT2 is targeted to bone.

5) The method of statement 1-3 or 4, wherein the SLIT3 or SLIT2 is delivered locally.

6) The method of statement 5, wherein said local administration is by injection or via a combination with a medical device.

7) The method of statement 1-5 or 6, wherein bone formation comprises promoting the formation or growth of $CD31^{hi}EMCN^{hi}$ endothelium.

8) The method of statement 1-6 or 7, further comprises administering an agent that inhibits *Shn3* expression or SHN3 activity.

9) The method of statement 1-7 or 8, wherein administering is daily, thrice weekly, twice weekly, once weekly, twice monthly, or once monthly.

10) The method of statement 1-7 or 8, wherein administering is every 2 months, every three months, every four months, every five months, every six months, or once per year.

11) The method of statement 1-9 or 10, wherein the SLIT3 or SLIT2 agent is a gene transfer vector comprising a promoter operably linked to nucleic segment encoding a SLIT3 or SLIT2 protein, and administering is once.

12) A method of preventing bone growth in a subject in need thereof, comprising administering a SLIT3 or SLIT2 inhibiting agent to said subject.

13) The method of statement 12, wherein the SLIT3 or SLIT2 inhibiting agent is targeted to bone or delivered locally.

14) The method of statement 12 or 13, wherein the SLIT3 or SLIT2 inhibiting agent is a small interfering RNA.

15) The method of statement 12, 13 or 14 wherein the SLIT3 or SLIT2 inhibiting agent is an antibody.

16) A method comprising locally administering a composition comprising one or more types of SLIT2 or SLIT3 protein, or one or more types of gene transfer vector encoding a SLIT2 or SLIT3 protein to a site where enhanced bone growth or repair is desired in a subject.

17) The method of statement 16, wherein the subject is a mammal or bird.

18) The method of statement 16 or 17, wherein the subject is a human.

19) The method of statement 16, 17, or 18, wherein the subject has substantially no vascular leakage in retinal vasculature from locally administering the SLIT2 or SLIT3 protein, or the *SLIT2* or *SLIT3* gene transfer vector.

20) The method of statement 16-18 or 19, wherein the composition comprises a carrier or excipient.

21) The method of statement 16-19 or 20, wherein the composition comprises one or more crystalline materials, amorphous materials, liposomes, lipids, charged lipids, DNA-protein complexes, polymers, or a combination thereof.

22) The method of statement 16-20 or 21, wherein the composition comprises gelatin or collagen.

23) The method of statement 16-21 or 22, wherein the composition comprises a sponge.

24) The method of statement 16-22 or 23, wherein the composition coats or is covalently bound to an orthopedic implant.

25) The method of statement 16-23 or 24, wherein the composition is formulated for slow or reduced release.

26) The method of statement 16-24 or 25, which promotes bone growth, strengthens bone, or heals bone the site in the subject.

27) The method of statement 16-25 or 26, which promotes bone growth or strengthens bone at the site in the subject, where the bone growth or bone strength is increased by at least 20% compared to animal that was not administered the SLIT2 or SLIT3 protein, or the *SLIT2* or *SLIT3* gene transfer vector to a subject.

28) The method of statement 16-26 or 27, which heals bone by increasing maximal load tolerated by a bone in the animal by at least 20% compared to animal that was not administered the SLIT2 or SLIT3 protein, or the *SLIT2* or *SLIT3* gene transfer vector to a subject.

29) The method of statement 16-27 or 28, wherein the composition comprises about 0.01 mg/kg to about 500 to 750 mg/kg of each SLIT2 protein, SLIT3 protein, gene transfer vector encoding a SLIT2, or gene transfer vector encoding a SLIT3 protein.

30) A method of preventing bone growth in a subject in need thereof, comprising administering a SLIT3 or SLIT2 inhibiting agent to said subject.

31) The method of statement 30, wherein the SLIT3 or SLIT2 inhibiting agent is targeted to bone or delivered locally.

32) The method of statement 30 or 31, wherein the SLIT3 or SLIT2 inhibiting agent is a small interfering RNA that binds to an endogenous SLIT3 or SLIT2 nucleic acid under physiological conditions.

33) The method of statement 30, 31 or 32, wherein the SLIT3 or SLIT2 inhibiting agent is an antibody that binds to SLIT3 protein or SLIT2 protein.

34) The method of statement 30-32 or 33, wherein the SLIT3 or SLIT2 inhibiting agent is trametinib (TTNB).

35) A composition comprising at least one SLIT2 protein, SLIT3 protein, *SLIT2* gene transfer vector or *SLIT3* gene transfer vector and a carrier or excipient that reduces release or diffusion of the SLIT2 protein, SLIT3 protein, *SLIT2* gene transfer vector, or *SLIT3* gene transfer vector.

36) The composition of statement 35, wherein the carrier or excipient comprises one or more crystalline materials, amorphous materials, liposomes, lipids, charged lipids, DNA-protein complexes, polymers, or a combination thereof.

37) The composition of statement 35 or 36, wherein the carrier or excipient comprises

gelatin or collagen.

38) The composition of statement 35, 36 or 37, wherein the carrier or excipient comprises a sponge.

39) An implant comprising at least one SLIT2 protein, SLIT3 protein, *SLIT2* gene transfer vector or *SLIT3* gene transfer.

40) The implant of statement 39 which is an orthopedic implant.

41) The implant of statement 39 or 40, wherein the at least one SLIT2 protein, SLIT3 protein, *SLIT2* gene transfer vector or *SLIT3* gene transfer coats the implant.

42) The implant of statement 39, 40, or 41, wherein the at least one SLIT2 protein, SLIT3 protein, *SLIT2* gene transfer vector or *SLIT3* gene transfer is covalently bond to the implant.

REFERENCES

Blockus, H., and A. Chedotal. 2016. "Slit-Robo signaling." Development 143 (17):3037-44. doi: 10.1242/dev.132829.

Bouxsein, M. L., K. S. Myers, K. L. Shultz, L. R. Donahue, C. J. Rosen, and W. G. Beamer. 2005. "Ovariectomy-induced bone loss varies among inbred strains of mice." J Bone Miner Res 20 (7):1085-92. doi: 10.1359/JBMR.050307.

Bradaschia-Correa, V., A. M. Josephson, D. Mehta, M. Mizrahi, S. S. Neibart, C. Liu, O. D. Kennedy, A. B. Castillo, K. A. Egol, and P. Leucht. 2017. "The Selective Serotonin Reuptake Inhibitor Fluoxetine Directly Inhibits Osteoblast Differentiation and Mineralization During Fracture Healing in Mice." J Bone Miner Res 32 (4):821-833. doi: 10.1002/jbmr.3045.

Buza, J. A., 3rd, and T. Einhorn. 2016. "Bone healing in 2016." Clin Cases Miner Bone Metab 13 (2):101-105. doi: 10.11138/ccmbm/2016.13.2.101.

Chen, J., Y. Shi, J. Regan, K. Karuppaiah, D. M. Ornitz, and F. Long. 2014. "Osx-Cre targets multiple cell types besides osteoblast lineage in postnatal mice." PLoS One 9 (1):e85161. doi: 10.1371/journal.pone.0085161.

Chen, M. J., T. Yokomizo, B. M. Zeigler, E. Dzierzak, and N. A. Speck. 2009. "Runx1 is required for the endothelial to haematopoietic cell transition but not thereafter." Nature 457 (7231):887-91. doi: 10.1038/nature07619.

Choi, H. J., H. Zhang, H. Park, K. S. Choi, H. W. Lee, V. Agrawal, Y. M. Kim, and Y. G. Kwon. 2015. "Yes-associated protein regulates endothelial cell contact-mediated expression of angiopoietin-2." Nat Commun 6:6943. doi: 10.1038/ncomms7943.

Dempster, D. W., J. E. Compston, M. K. Drezner, F. H. Glorieux, J. A. Kanis, H. Malluche, P. J. Meunier, S. M. Ott, R. R. Recker, and A. M. Parfitt. 2013. "Standardized nomenclature, symbols, and units for bone histomorphometry: a

2012 update of the report of the ASBMR Histomorphometry Nomenclature Committee." J Bone Miner Res 28 (1):2-17. doi: 10.1002/jbmr.1805.

Dobin, A., C. A. Davis, F. Schlesinger, J. Drenkow, C. Zaleski, S. Jha, P. Batut, M. Chaisson, and T. R. Gingeras. 2013. "STAR: ultrafast universal RNA-seq aligner." Bioinformatics 29 (1):15-21. doi: 10.1093/bioinformatics/bts635.

Friedlaender, GE; Lin, S; Solchaga, LA; Snel, LB; Lynch, SE (2013). "The role of recombinant human platelet-derived growth factor-BB (rhPDGF-BB) in orthopaedic bone repair and regeneration". Current pharmaceutical design. 19 (19): 3384–90. PMID 23432673.

Fukuda, T., S. Takeda, R. Xu, H. Ochi, S. Sunamura, T. Sato, S. Shibata, Y. Yoshida, Z. Gu, A. Kimura, C. Ma, C. Xu, W. Bando, K. Fujita, K. Shinomiya, T. Hirai, Y. Asou, M. Enomoto, H. Okano, A. Okawa, and H. Itoh. 2013. "Sema3A regulates bone-mass accrual through sensory innervations." Nature 497 (7450):490-3. doi: 10.1038/nature12115.

Geutskens, S. B., W. D. Andrews, A. M. van Stalborch, K. Brussen, S. E. Holtrop-de Haan, J. G. Parnavelas, P. L. Hordijk, and P. B. van Hennik. 2012. "Control of human hematopoietic stem/progenitor cell migration by the extracellular matrix protein Slit3." Lab Invest 92 (8):1129-39. doi: 10.1038/labinvest.2012.81.

Geutskens, S. B., P. L. Hordijk, and P. B. van Hennik. 2010. "The chemorepellent Slit3 promotes monocyte migration." J Immunol 185 (12):7691-8. doi: 10.4049/jimmunol.0903898.

Greenblatt, M. B., D. Y. Shin, H. Oh, K. Y. Lee, B. Zhai, S. P. Gygi, S. Lotinun, R. Baron, D. Liu, B. Su, L. H. Glimcher, and J. H. Shim. 2016. "MEKK2 mediates an alternative beta-catenin pathway that promotes bone formation." Proc Natl Acad Sci U S A 113 (9):E1226-35. doi: 10.1073/pnas.1600813113.

Guan, M., W. Yao, R. Liu, K. S. Lam, J. Nolta, J. Jia, B. Panganiban, L. Meng, P. Zhou, M. Shahnazari, R. O. Ritchie, and N. E. Lane. 2012. "Directing mesenchymal stem cells to bone to augment bone formation and increase bone mass." Nat Med 18 (3):456-62. doi: 10.1038/nm.2665.

Howitt, J. A., N. J. Clout, and E. Hohenester. 2004. "Binding site for Robo receptors revealed by dissection of the leucine-rich repeat region of Slit." EMBO J 23 (22):4406-12. doi: 10.1038/sj.emboj.7600446.

Huang da, W., B. T. Sherman, and R. A. Lempicki. 2009. "Systematic and integrative analysis of large gene lists using DAVID bioinformatics resources." Nat Protoc 4 (1):44-57. doi: 10.1038/nprot.2008.211.

Jaworski, A., and M. Tessier-Lavigne. 2012. "Autocrine/juxtaparacrine regulation of axon fasciculation by Slit-Robo signaling." Nat Neurosci 15 (3):367-9. doi: 10.1038/nn.3037.

Jones, C. A., N. R. London, H. Chen, K. W. Park, D. Sauvaget, R. A. Stockton, J. D. Wythe, W. Suh, F. Larrieu-Lahargue, Y. S. Mukouyama, P. Lindblom, P. Seth, A. Frias, N. Nishiya, M. H. Ginsberg, H. Gerhardt, K. Zhang, and D. Y. Li. 2008. "Robo4 stabilizes the vascular network by inhibiting pathologic angiogenesis and endothelial hyperpermeability." Nat Med 14 (4):448-53. doi: 10.1038/nm1742.

Jones, D. C., M. N. Wein, M. Oukka, J. G. Hofstaetter, M. J. Glimcher, and L. H. Glimcher. 2006. "Regulation of adult bone mass by the zinc finger adapter protein Schnurri-3." Science 312 (5777):1223-7. doi: 10.1126/science.1126313.

Kusumbe, A. P., S. K. Ramasamy, and R. H. Adams. 2014. "Coupling of angiogenesis and osteogenesis by a specific vessel subtype in bone." Nature 507 (7492):323-8. doi: 10.1038/nature13145.

Leder, B. Z., J. N. Tsai, A. V. Uihlein, P. M. Wallace, H. Lee, R. M. Neer, and S. A. Burnett-Bowie. 2015. "Denosumab and teriparatide transitions in postmenopausal osteoporosis (the DATA-Switch study): extension of a randomised controlled trial." Lancet 386 (9999):1147-55. doi: 10.1016/S0140-6736(15)61120-5.

Liang, C., B. Guo, H. Wu, N. Shao, D. Li, J. Liu, L. Dang, C. Wang, H. Li, S. Li, W. K. Lau, Y. Cao, Z. Yang, C. Lu, X. He, D. W. Au, X. Pan, B. T. Zhang, C. Lu, H. Zhang, K. Yue, A. Qian, P. Shang, J. Xu, L. Xiao, Z. Bian, W. Tan, Z. Liang, F. He, L. Zhang, A. Lu, and G. Zhang. 2015. "Aptamer-functionalized lipid nanoparticles targeting osteoblasts as a novel RNA interference-based bone anabolic strategy." Nat Med 21 (3):288-94. doi: 10.1038/nm.3791.

Liao, Y., G. K. Smyth, and W. Shi. 2014. "featureCounts: an efficient general purpose program for assigning sequence reads to genomic features." Bioinformatics 30 (7):923-30. doi: 10.1093/bioinformatics/btt656.

Liu, Z., K. Patel, H. Schmidt, W. Andrews, A. Pini, and V. Sundaresan. 2004. "Extracellular Ig domains 1 and 2 of Robo are important for ligand (Slit) binding." Mol Cell Neurosci 26 (2):232-40. doi: 10.1016/j.mcn.2004.01.002.

Love, M. I., W. Huber, and S. Anders. 2014. "Moderated estimation of fold change and dispersion for RNA-seq data with DESeq2." Genome Biol 15 (12):550. doi: 10.1186/s13059-014-0550-8.

Lu, Y., Y. Xie, S. Zhang, V. Dusevich, L. F. Bonewald, and J. Q. Feng. 2007. "DMP1-targeted Cre expression in odontoblasts and osteocytes." J Dent Res 86 (4):320-5. doi: 10.1177/154405910708600404.

Mehlen, P., C. Delloye-Bourgeois, and A. Chedotal. 2011. "Novel roles for Slits and netrins: axon guidance cues as anticancer targets?" Nat Rev Cancer 11 (3):188-97. doi: 10.1038/nrc3005.

Naska, S., D. C. Lin, F. D. Miller, and D. R. Kaplan. 2010. "p75NTR is an obligate signaling receptor required for cues that cause sympathetic neuron growth cone collapse." Mol Cell Neurosci 45 (2):108-20. doi: 10.1016/j.mcn.2010.05.015.

Nguyen Ba-Charvet, K. T., K. Brose, V. Marillat, T. Kidd, C. S. Goodman, M. Tessier-Lavigne, C. Sotelo, and A. Chedotal. 1999. "Slit2-Mediated chemorepulsion and collapse of developing forebrain axons." Neuron 22 (3):463-73.

Park, D., J. A. Spencer, B. I. Koh, T. Kobayashi, J. Fujisaki, T. L. Clemens, C. P. Lin, H. M. Kronenberg, and D. T. Scadden. 2012. "Endogenous bone marrow MSCs are dynamic, fate-restricted participants in bone maintenance and regeneration." Cell Stem Cell 10 (3):259-72. doi: 10.1016/j.stem.2012.02.003.

Paul, J. D., K. L. K. Coulombe, P. T. Toth, Y. Zhang, G. Marsboom, V. P. Bindokas, D. W. Smith, C. E. Murry, and J. Rehman. 2013. "SLIT3-ROBO4 activation promotes vascular network formation in human engineered tissue and angiogenesis in vivo." J Mol Cell Cardiol 64:124-31. doi: 10.1016/j.yjmcc.2013.09.005.

Rama, N., A. Dubrac, T. Mathivet, R. A. Ni Charthaigh, G. Genet, B. Cristofaro, L. Pibouin-Fragner, L. Ma, A. Eichmann, and A. Chedotal. 2015. "Slit2 signaling through Robo1 and Robo2 is required for retinal neovascularization." Nat Med 21 (5):483-91. doi: 10.1038/nm.3849.

Ramalingam, P., M. G. Poulos, and J. M. Butler. 2017. "Regulation of the hematopoietic stem cell lifecycle by the endothelial niche." Curr Opin Hematol 24 (4):289-299. doi: 10.1097/MOH.0000000000000350.

Ramasamy, S. K., A. P. Kusumbe, L. Wang, and R. H. Adams. 2014. "Endothelial Notch activity promotes angiogenesis and osteogenesis in bone." Nature 507 (7492):376-80. doi: 10.1038/nature13146.

Rodda, S. J., and A. P. McMahon. 2006. "Distinct roles for Hedgehog and canonical Wnt signaling in specification, differentiation and maintenance of osteoblast progenitors." Development 133 (16):3231-44. doi: 10.1242/dev.02480.

Sakabe, M., J. Fan, Y. Odaka, N. Liu, A. Hassan, X. Duan, P. Stump, L. Byerly, M. Donaldson, J. Hao, M. Fruttiger, Q. R. Lu, Y. Zheng, R. A. Lang, and M. Xin.

2017. "YAP/TAZ-CDC42 signaling regulates vascular tip cell migration." Proc Natl Acad Sci U S A 114 (41):10918-10923. doi: 10.1073/pnas.1704030114.

Shah, P; Keppler, L; Rutkowski, J (December 2012). "Bone morphogenic protein: an elixir for bone grafting--a review". The Journal of oral implantology. 38 (6): 767--78. doi:10.1563/AAID-JOI-D-10-00196. PMID 21574851.

Shim, J. H., M. B. Greenblatt, W. Zou, Z. Huang, M. N. Wein, N. Brady, D. Hu, J. Charron, H. R. Brodkin, G. A. Petsko, D. Zaller, B. Zhai, S. Gygi, L. H. Glimcher, and D. C. Jones. 2013. "Schnurri-3 regulates ERK downstream of WNT signaling in osteoblasts." J Clin Invest 123 (9):4010-22. doi: 10.1172/JCI69443.

Shin, M., T. J. Beane, A. Quillien, I. Male, L. J. Zhu, and N. D. Lawson. 2016. "Vegfa signals through ERK to promote angiogenesis, but not artery differentiation." Development 143 (20):3796-3805. doi: 10.1242/dev.137919.

Su, A. I., T. Wiltshire, S. Batalov, H. Lapp, K. A. Ching, D. Block, J. Zhang, R. Soden, M. Hayakawa, G. Kreiman, M. P. Cooke, J. R. Walker, and J. B. Hogenesch. 2004. "A gene atlas of the mouse and human protein-encoding transcriptomes." Proc Natl Acad Sci U S A 101 (16):6062-7. doi: 10.1073/pnas.0400782101.

Sun, H., K. Dai, T. Tang, and X. Zhang. 2009. "Regulation of osteoblast differentiation by slit2 in osteoblastic cells." Cells Tissues Organs 190 (2):69-80. doi: 10.1159/000178020.

Vasam, G., S. Joshi, S. E. Thatcher, S. H. Bartelmez, L. A. Cassis, and Y. P. Jarajapu. 2017. "Reversal of Bone Marrow Mobilopathy and Enhanced Vascular Repair by Angiotensin-(1-7) in Diabetes." Diabetes 66 (2):505-518. doi: 10.2337/db16-1039.

Wein, M. N., D. C. Jones, J. H. Shim, A. O. Aliprantis, R. Sulyanto, V. Lazarevic, S. L. Poliachik, T. S. Gross, and L. H. Glimcher. 2012. "Control of bone resorption in mice by Schnurri-3." Proc Natl Acad Sci U S A 109 (21):8173-8. doi: 10.1073/pnas.1205848109.

Xie, H., Z. Cui, L. Wang, Z. Xia, Y. Hu, L. Xian, C. Li, L. Xie, J. Crane, M. Wan, G. Zhen, Q. Bian, B. Yu, W. Chang, T. Qiu, M. Pickarski, L. T. Duong, J. J. Windle, X. Luo, E. Liao, and X. Cao. 2014. "PDGF-BB secreted by preosteoclasts induces angiogenesis during coupling with osteogenesis." Nat Med 20 (11):1270-8. doi: 10.1038/nm.3668.

Xu, R. 2014. "Semaphorin 3A: A new player in bone remodeling." Cell Adh Migr 8 (1):5-10. doi: 10.4161/cam.27752.

Xu, R., C. Zhang, D. Y. Shin, J. M. Kim, S. Lalani, N. Li, Y. S. Yang, Y. Liu, M. Eiseman, R. J. Davis, J. H. Shim, and M. B. Greenblatt. 2017a. "c-Jun N-

Terminal Kinases (JNKs) Are Critical Mediators of Osteoblast Activity In Vivo." J Bone Miner Res 32 (9):1811-1815. doi: 10.1002/jbmr.3184.

Xu, R., C. Zhang, D. Y. Shin, J. M. Kim, S. Lalani, N. Li, Y. S. Yang, Y. Liu, M. Eiseman, R. J. Davis, J. H. Shim, and M. B. Greenblatt. 2017b. "c-Jun N-terminal kinases (JNKs) are critical mediators of osteoblast activity in vivo." J Bone Miner Res. doi: 10.1002/jbmr.3184.

Yao, W., M. Guan, J. Jia, W. Dai, Y. A. Lay, S. Amugongo, R. Liu, D. Olivos, M. Saunders, K. S. Lam, J. Nolta, D. Olvera, R. O. Ritchie, and N. E. Lane. 2013. "Reversing bone loss by directing mesenchymal stem cells to bone." Stem Cells 31 (9):2003-14. doi: 10.1002/stem.1461.

Yuan, W., Y. Rao, R. P. Babiuk, J. J. Greer, J. Y. Wu, and D. M. Ornitz. 2003. "A genetic model for a central (septum transversum) congenital diaphragmatic hernia in mice lacking Slit3." Proc Natl Acad Sci U S A 100 (9):5217-22. doi: 10.1073/pnas.0730709100.

Zhang, B., U. M. Dietrich, J. G. Geng, R. Bicknell, J. D. Esko, and L. Wang. 2009. "Repulsive axon guidance molecule Slit3 is a novel angiogenic factor." Blood 114 (19):4300-9. doi: 10.1182/blood-2008-12-193326.

Zhang, C., K. Hanspers, A. Kuchinsky, N. Salomonis, D. Xu, and A. R. Pico. 2012. "Mosaic: making biological sense of complex networks." Bioinformatics 28 (14):1943-4. doi: 10.1093/bioinformatics/bts278.

Zhang, G., B. Guo, H. Wu, T. Tang, B. T. Zhang, L. Zheng, Y. He, Z. Yang, X. Pan, H. Chow, K. To, Y. Li, D. Li, X. Wang, Y. Wang, K. Lee, Z. Hou, N. Dong, G. Li, K. Leung, L. Hung, F. He, L. Zhang, and L. Qin. 2012. "A delivery system targeting bone formation surfaces to facilitate RNAi-based anabolic therapy." Nat Med 18 (2):307-14. doi: 10.1038/nm.2617.

Zhang, J., and D. C. Link. 2016. "Targeting of Mesenchymal Stromal Cells by Cre-Recombinase Transgenes Commonly Used to Target Osteoblast Lineage Cells." J Bone Miner Res 31 (11):2001-2007. doi: 10.1002/jbmr.2877.

Zhang, Y., J. Xu, Y. C. Ruan, M. K. Yu, M. O'Laughlin, H. Wise, D. Chen, L. Tian, D. Shi, J. Wang, S. Chen, J. Q. Feng, D. H. Chow, X. Xie, L. Zheng, L. Huang, S. Huang, K. Leung, N. Lu, L. Zhao, H. Li, D. Zhao, X. Guo, K. Chan, F. Witte, H. C. Chan, Y. Zheng, and L. Qin. 2016. "Implant-derived magnesium induces local neuronal production of CGRP to improve bone-fracture healing in rats." Nat Med 22 (10):1160-1169. doi: 10.1038/nm.4162.

Zhou, W. J., Z. H. Geng, J. R. Spence, and J. G. Geng. 2013. "Induction of intestinal stem cells by R-spondin 1 and Slit2 augments chemoradioprotection." Nature 501 (7465):107-11. doi: 10.1038/nature12416.

Kruszka P, Tanpaiboon P, Neas K, Crosby K, Berger SI, Martinez AF, et al. Loss of function in ROBO1 is associated with tetralogy of Fallot and septal defects. J Med Genet. 2017;

Morin-Poulard I, Sharma A, Louradour I, Vanzo N, Vincent A, Crozatier M. Vascular control of the Drosophila haematopoietic microenvironment by Slit/Robo signalling. Nat Commun. 2016;7:11634.

Jaworski A, Tessier-Lavigne M. Autocrine/juxtaparacrine regulation of axon fasciculation by Slit-Robo signaling. Nat Neurosci [Internet]. 2012;15:367–9. Available from: http://www.ncbi.nlm.nih.gov/pubmed/22306607

Kidd T, Brose K, Mitchell KJ, Fetter RD, Tessier-Lavigne M, Goodman CS, et al. Roundabout controls axon crossing of the CNS midline and defines a novel subfamily of evolutionarily conserved guidance receptors. Cell. 1998;92:205–15.

[0238] All patents and publications referenced or mentioned herein are indicative of the levels of skill of those skilled in the art to which the invention pertains, and each such referenced patent or publication is hereby specifically incorporated by reference to the same extent as if it had been incorporated by reference in its entirety individually or set forth herein in its entirety. Applicants reserve the right to physically incorporate into this specification any and all materials and information from any such cited patents or publications.

[0239] The specific proteins, nucleic acids, methods and compositions described herein are representative of preferred embodiments and are exemplary and not intended as limitations on the scope of the invention. Other objects, aspects, and embodiments will occur to those skilled in the art upon consideration of this specification and are encompassed within the spirit of the invention as defined by the scope of the claims. It will be readily apparent to one skilled in the art that varying substitutions and modifications may be made to the invention disclosed herein without departing from the scope and spirit of the invention. The invention illustratively described herein suitably may be practiced in the absence of any element or elements, or limitation or limitations, which is not specifically disclosed herein as essential.

[0240] The specific proteins, nucleic acids, methods and compositions illustratively described herein suitably may be practiced in differing orders of steps, and the methods and processes are not necessarily restricted to the orders of steps indicated herein or in the claims. As used herein and in the appended claims, the singular forms "a," "an," and "the" include plural reference unless the context clearly dictates otherwise. Thus, for example, a reference to "a protein," "a nucleic acid," "a

composition," "a vector" or "a promoter" includes a plurality of such proteins, nucleic acids, compositions, vectors or promoters (for example, a solution of proteins, nucleic acids, compositions, vectors, or a series of promoters), and so forth.

[0241] The term "about", as used herein, can allow for a degree of variability in a value or range, for example, within 10%, within 5%, or within 1% of a stated value or of a stated limit of a range.

[0242] Under no circumstances may the patent be interpreted to be limited to the specific examples or embodiments or methods specifically disclosed herein. Under no circumstances may the patent be interpreted to be limited by any statement made by any Examiner or any other official or employee of the Patent and Trademark Office unless such statement is specifically and without qualification or reservation expressly adopted in a responsive writing by Applicants.

[0243] The terms and expressions that have been employed are used as terms of description and not of limitation, and there is no intent in the use of such terms and expressions to exclude any equivalent of the features shown and described or portions thereof, but it is recognized that various modifications are possible within the scope of the invention as claimed. Thus, it will be understood that although the present invention has been specifically disclosed by preferred embodiments and optional features, modification and variation of the concepts herein disclosed may be resorted to by those skilled in the art, and that such modifications and variations are considered to be within the scope of this invention as defined by the appended claims and statements of the invention.

What is claimed:

1. A method comprising locally administering a composition comprising one or more types of SLIT2 or SLIT3 protein, or one or more types of gene transfer vector encoding a SLIT2 or SLIT3 protein to a site where enhanced bone growth or repair is desired in a subject.

2. The method of claim 1, wherein the subject is a mammal or bird.

3. The method of claim 1, wherein the subject is a human.

4. The method of claim 1, wherein the subject has substantially no vascular leakage in retinal vasculature from locally administering the SLIT2 or SLIT3 protein, or the *SLIT2* or *SLIT3* gene transfer vector.

5. The method of claim 1, wherein the composition comprises a carrier or excipient.

6. The method of claim 1, wherein the gene transfer vector comprises a viral vector.

7. The method of claim 1, wherein the composition comprises one or more crystalline materials, amorphous materials, liposomes, lipids, charged lipids, DNA-protein complexes, polymers, or a combination thereof.

8. The method of claim 1, wherein the composition comprises gelatin or collagen.

9. The method of claim 1, wherein the composition comprises a sponge.

10. The method of claim 1, wherein the composition coats or is covalently bound to an orthopedic implant.

11. The method of claim 1, wherein the composition is formulated for slow or reduced release.

12. The method of claim 1, which promotes bone growth, strengthens bone, or heals bone the site in the subject.

13. The method of claim 1, which promotes bone growth or strengthens bone at the site in the subject, where the bone growth or bone strength is increased by at least 20% compared to animal that was not administered the SLIT2 or SLIT3 protein, or the *SLIT2* or *SLIT3* gene transfer vector to a subject.

14. The method of claim 1, which heals bone by increasing maximal load tolerated by a bone in the animal by at least 20% compared to animal that was not administered the SLIT2 or SLIT3 protein, or the *SLIT2* or *SLIT3* gene transfer vector to a subject.

15. The method of claim 1, wherein the composition comprises about 0.01 mg/kg to about 500 to 750 mg/kg of each SLIT2 protein, SLIT3 protein, gene transfer vector encoding a SLIT2, or gene transfer vector encoding a SLIT3 protein.

16. A method of preventing bone growth in a subject in need thereof, comprising administering a SLIT3 or SLIT2 inhibiting agent to said subject.

17. The method of claim 16, wherein the SLIT3 or SLIT2 inhibiting agent is targeted to bone or delivered locally.

18. The method of claim 16, wherein the SLIT3 or SLIT2 inhibiting agent is a small interfering RNA that binds to an endogenous SLIT3 or SLIT2 nucleic acid under physiological conditions.

19. The method of claim 16, wherein the SLIT3 or SLIT2 inhibiting agent is an antibody that binds to SLIT3 protein or SLIT2 protein.

20. The method of claim 16, wherein the SLIT3 or SLIT2 inhibiting agent is trametinib (TTNB).

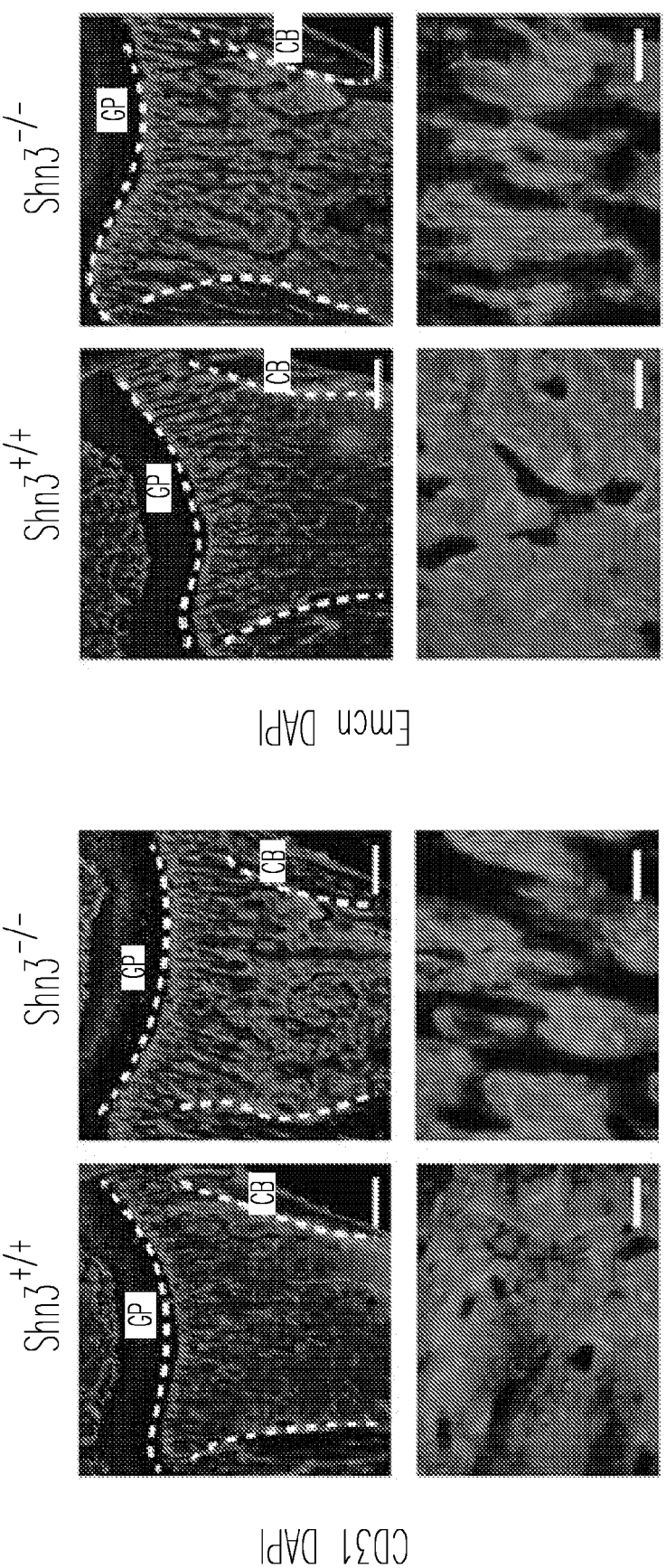

Fig. 1A

Fig. 1B

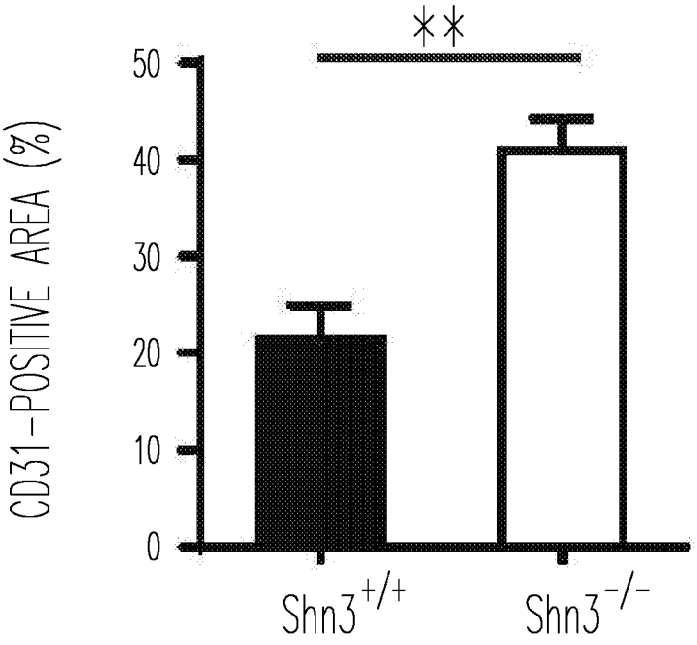

Fig. 1C-1

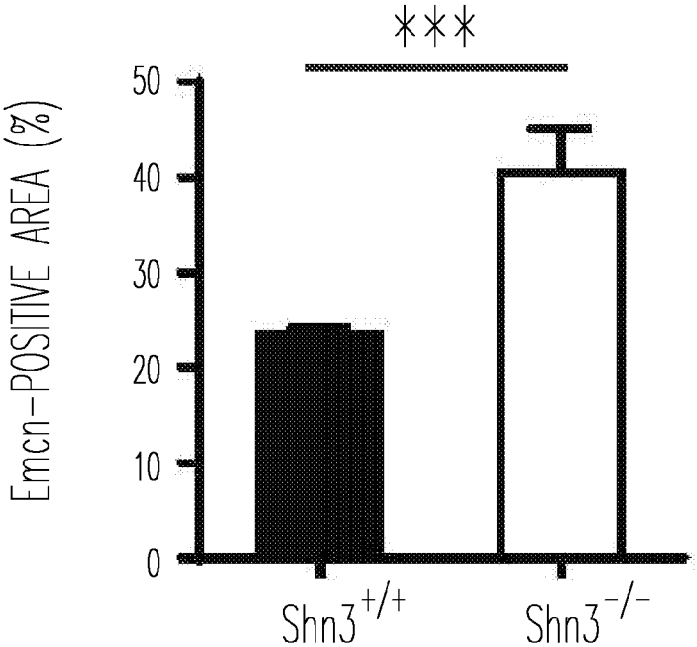

Fig. 1C-2

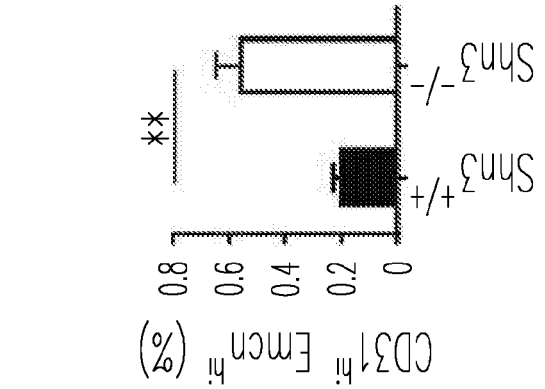

Fig. 1F

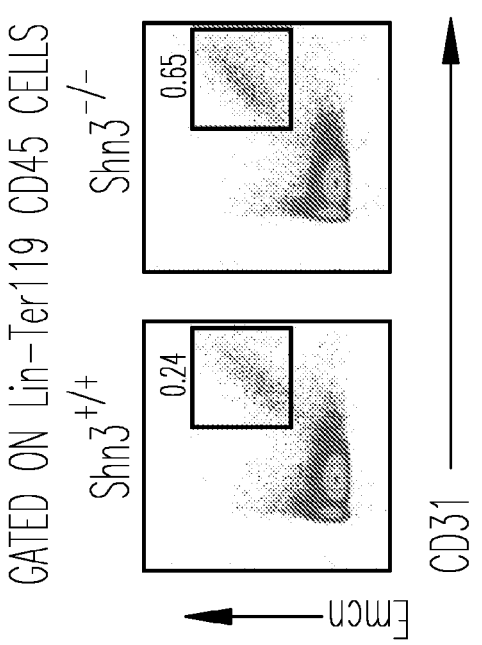

Fig. 1E

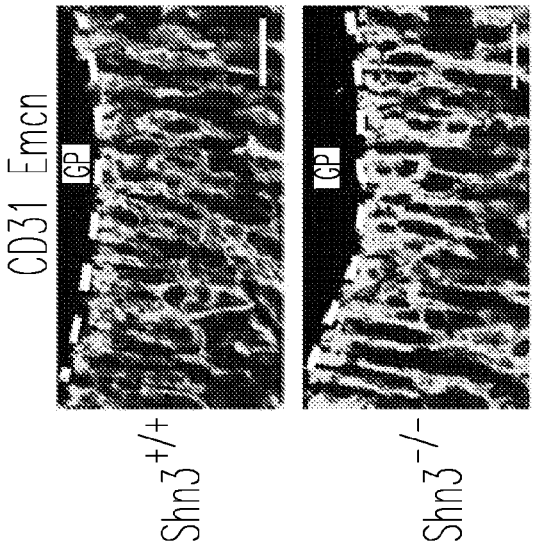

Fig. 1D

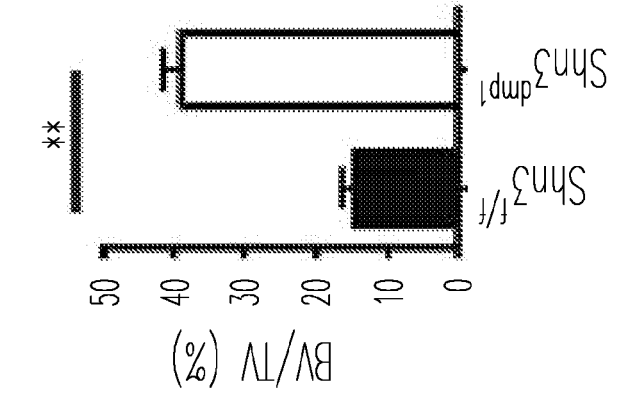

Fig.2A-2

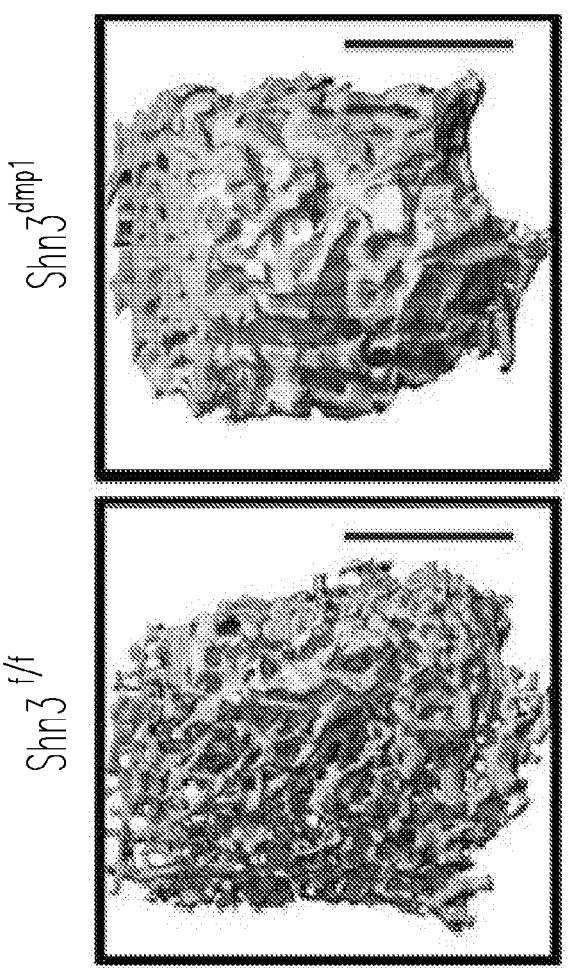

Fig.2A-1

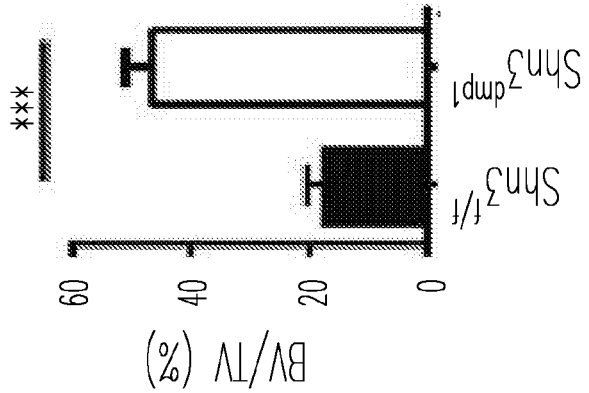

Fig.2B-2

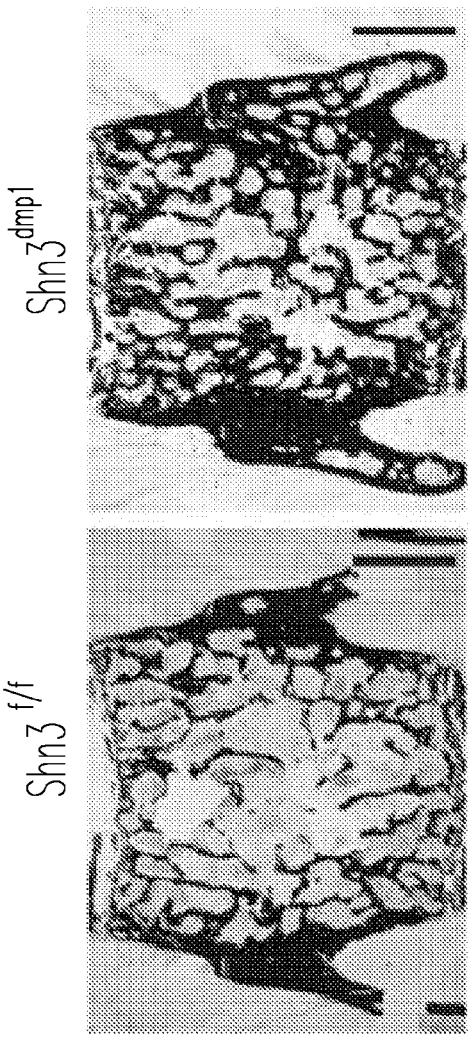

Fig.2B-1

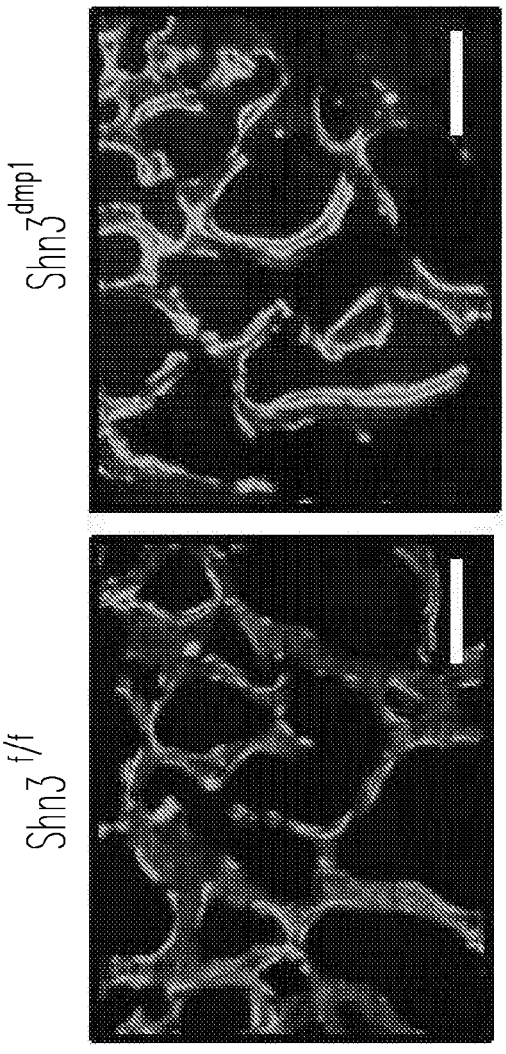
Shn3 f/f
Shn3 dmp1

Fig.2C

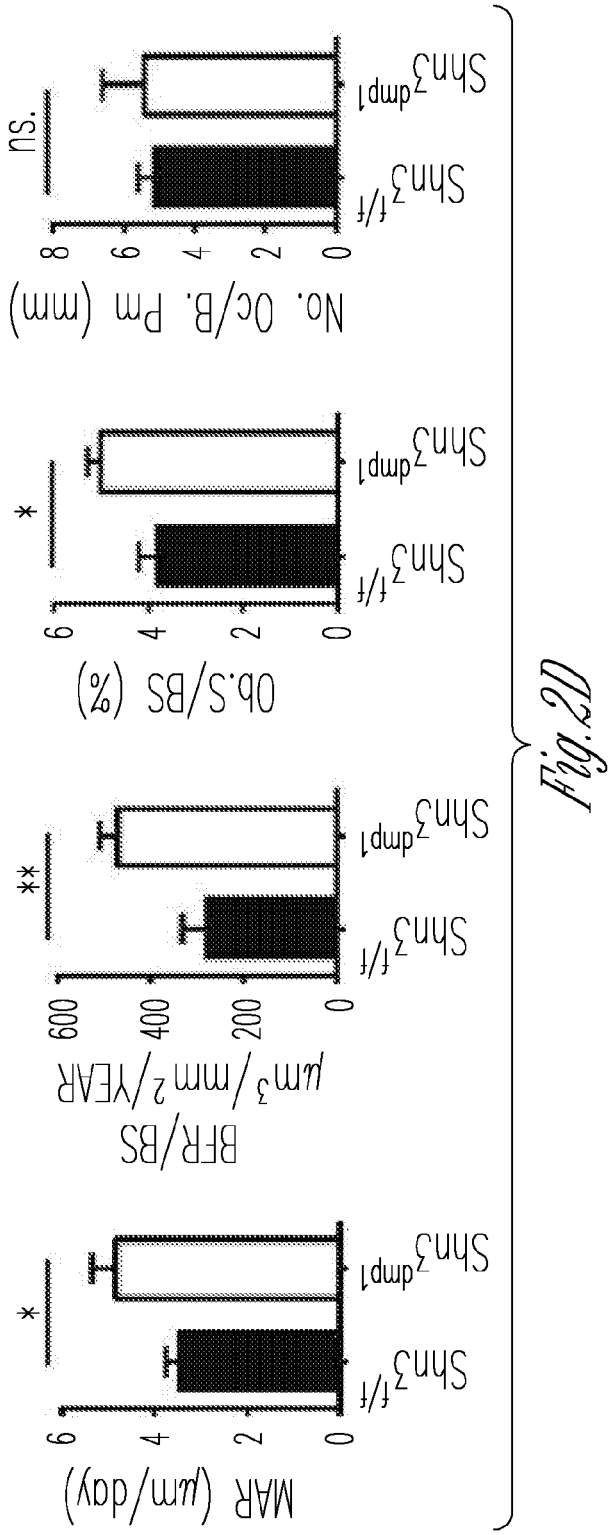
MAR (μm/day)
Shn3 f/f
Shn3 dmp1
*
0
2
4
6
BFR/BS
μm³/mm²/YEAR
**
0
200
400
600
Ob.S/BS (%)
*
0
2
4
6
No. Oc/B. Pm (mm)
ns.
0
2
4
6
8

Fig.2D

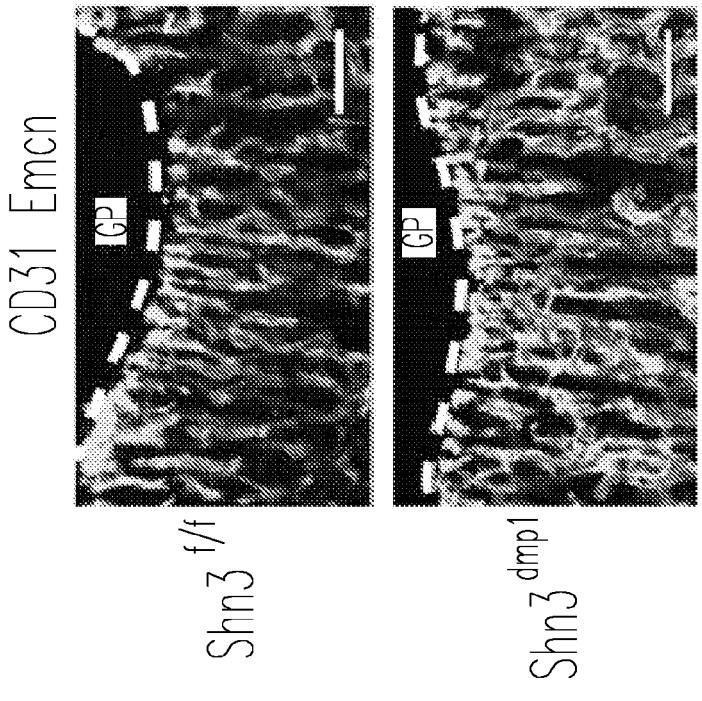
CD31 Emcn
GP
GP
Shn3 f/f
Shn3 dmp1

Fig.2E

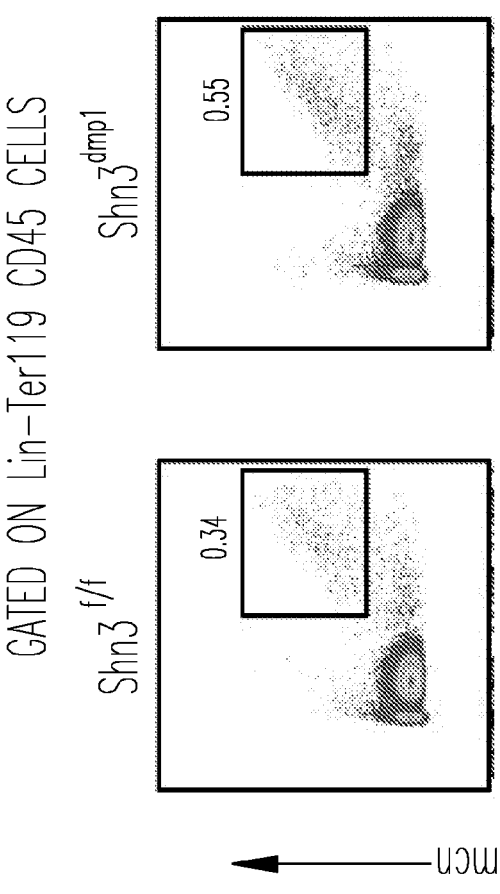
GATED ON Lin−Ter119 CD45 CELLS
Shn3 f/f
0.34
Shn3 dmp1
0.55
Emcn
CD31

Fig.2F

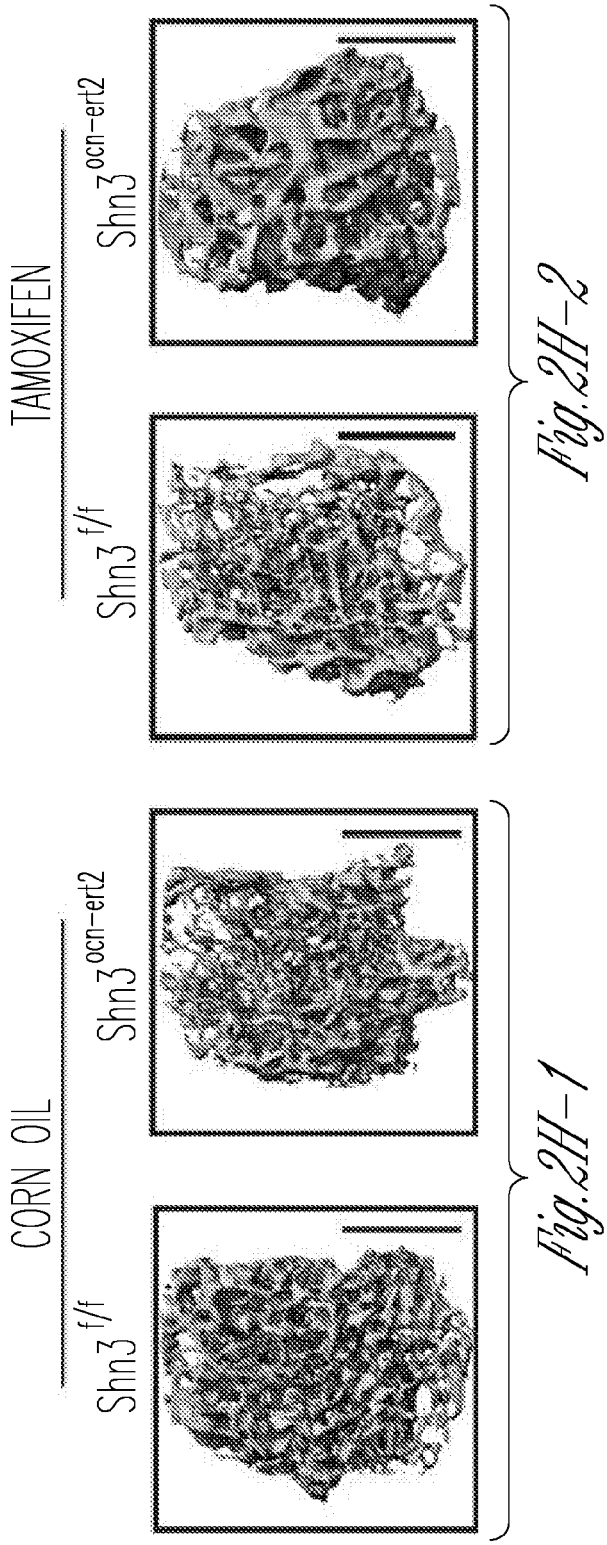

Fig.2H-1

Fig.2H-2

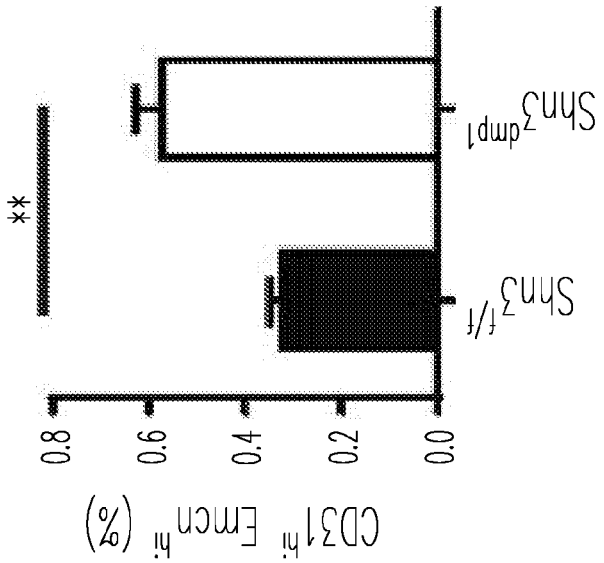

Fig.2G

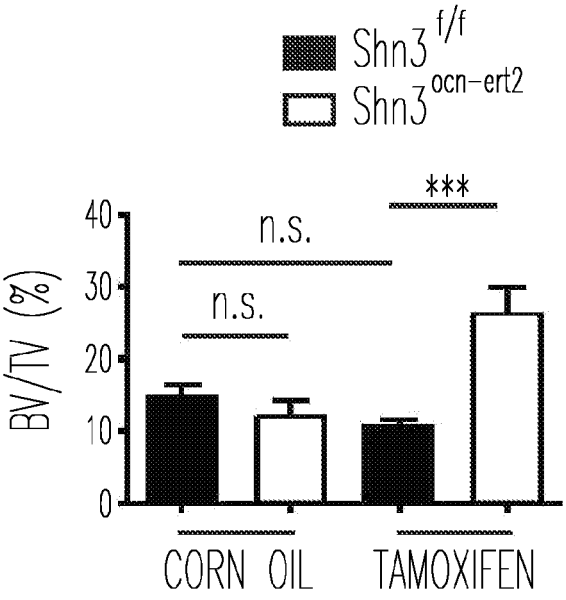
Shn3 f/f
Shn3 ocn-ert2
***
n.s.
n.s.
40
30
20
10
0
BV/TV (%)
CORN OIL
TAMOXIFEN

Fig.2I

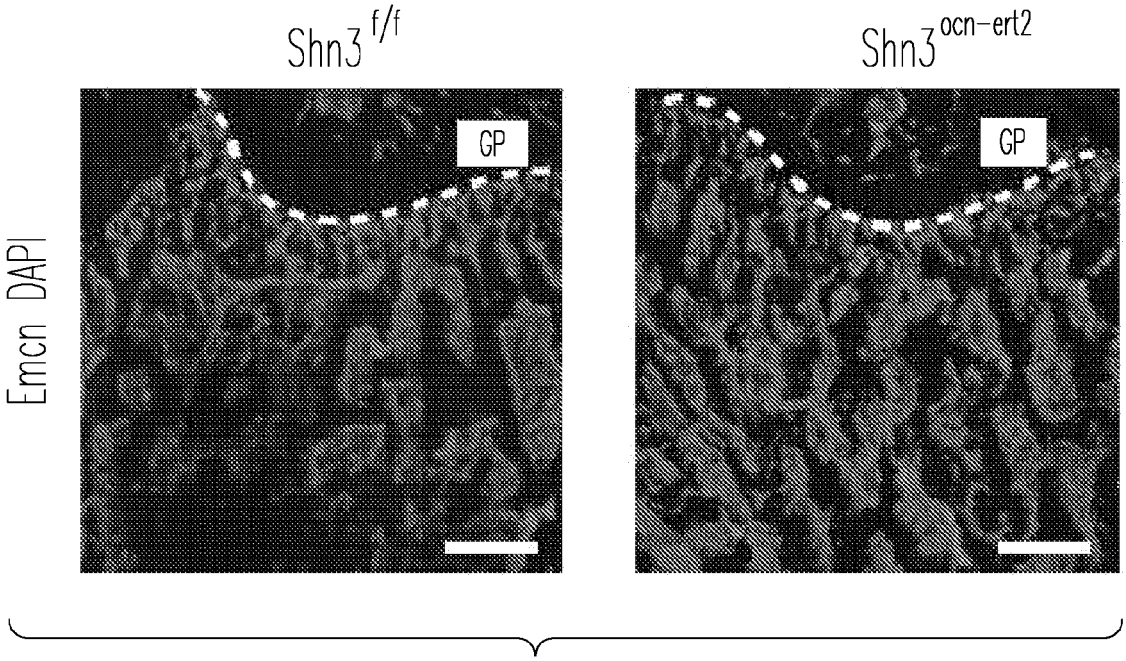
Shn3 f/f
Shn3 ocn-ert2
GP
GP
Emcn DAPI

Fig.2J

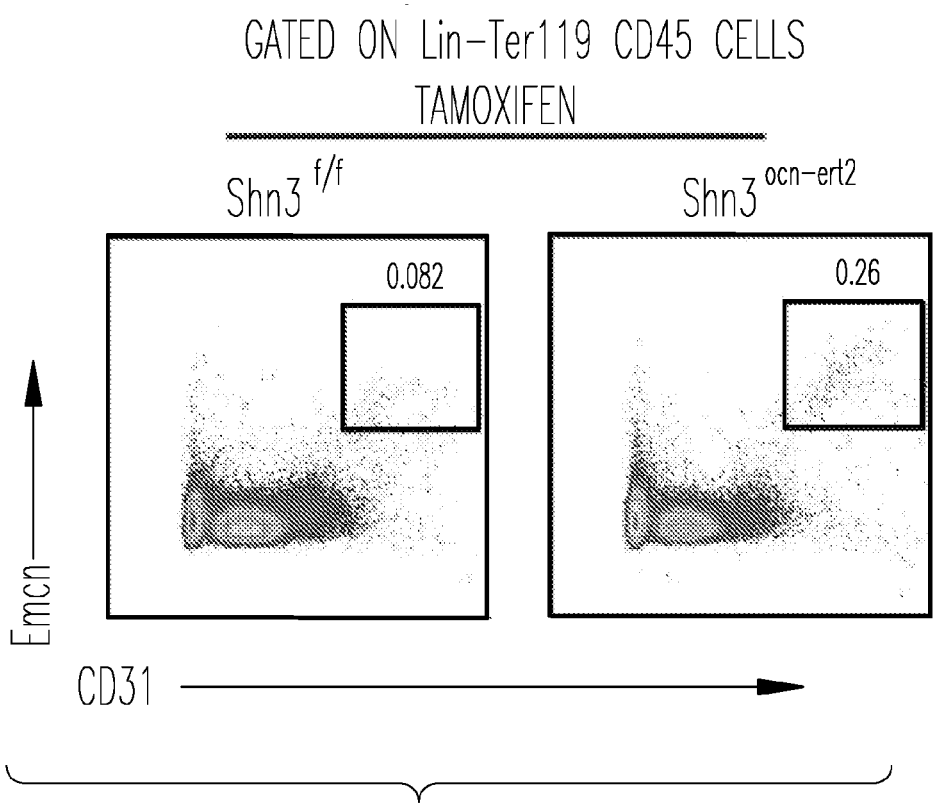
GATED ON Lin-Ter119 CD45 CELLS
TAMOXIFEN
Shn3 f/f
Shn3 ocn-ert2
0.082
0.26
Emcn
CD31

Fig.2K

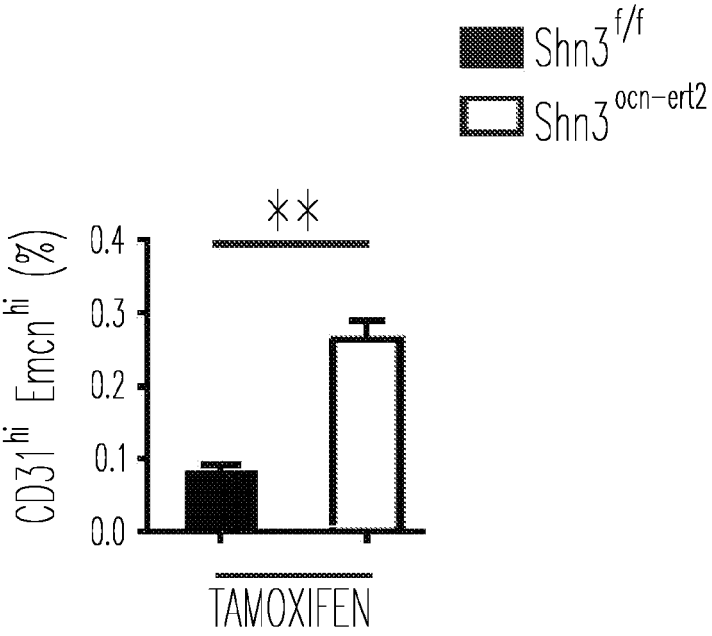
Shn3 f/f
Shn3 ocn-ert2
**
CD31hi Emcnhi (%)
0.4
0.3
0.2
0.1
0.0
TAMOXIFEN

Fig.2L

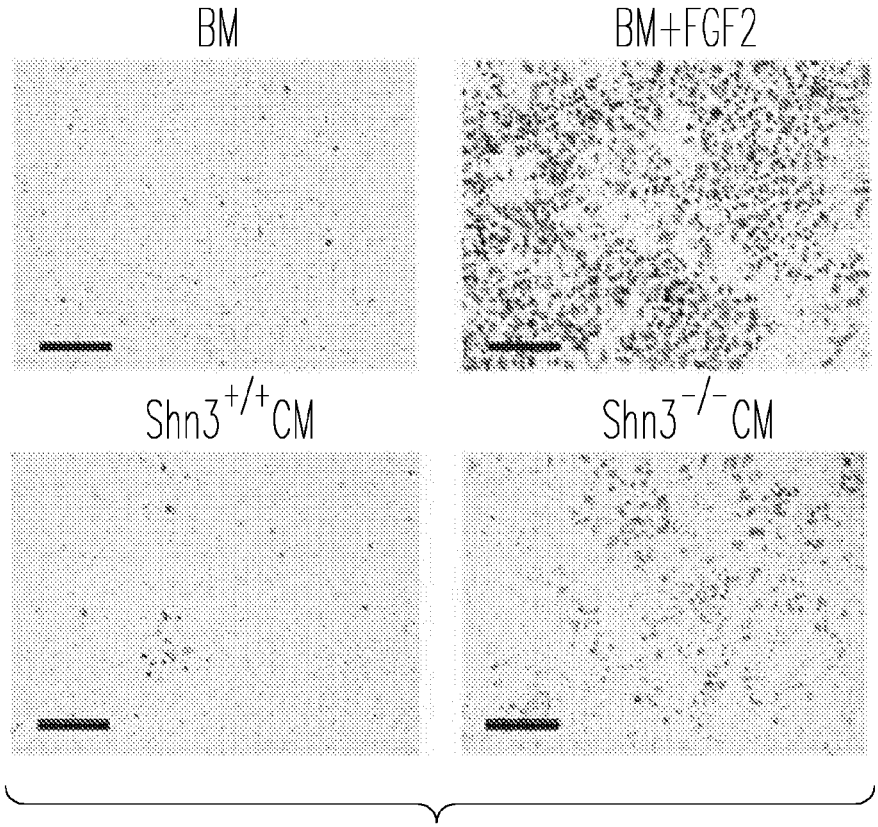
BM
BM+FGF2
Shn3+/+CM
Shn3−/−CM

Fig. 3A

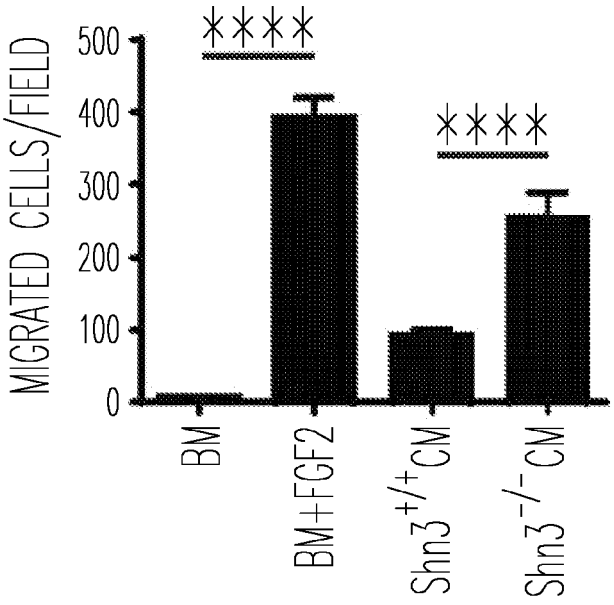
MIGRATED CELLS/FIELD
500
400
300
200
100
0
****
****
BM
BM+FGF2
Shn3+/+CM
Shn3−/−CM

Fig. 3B

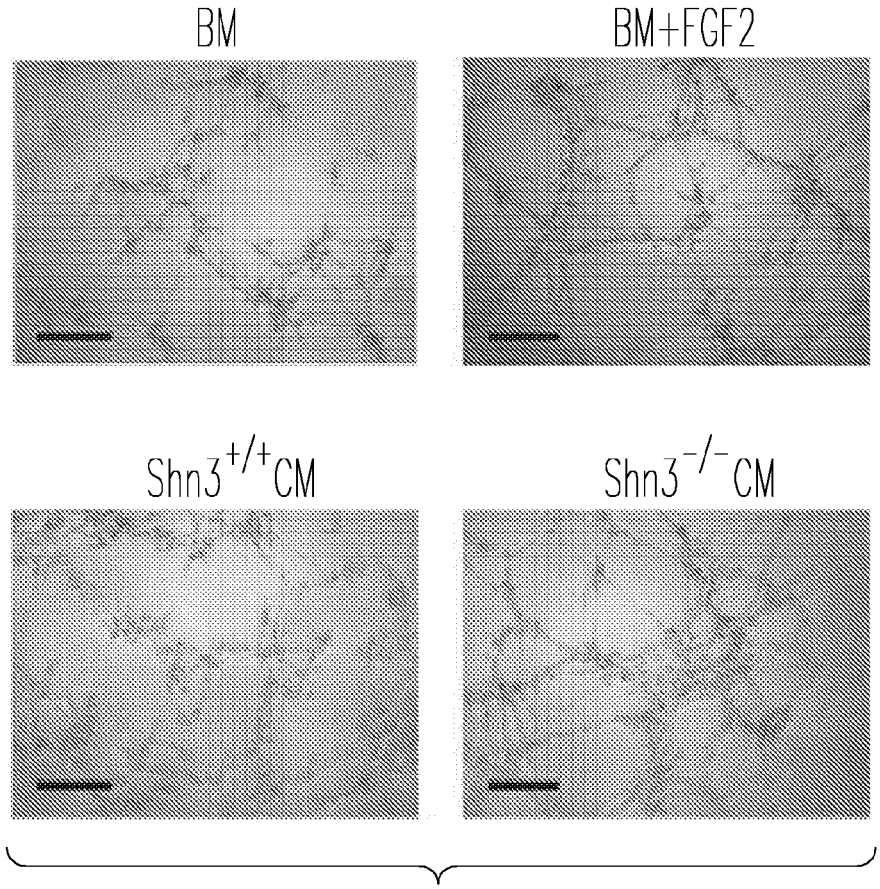
BM
BM+FGF2
Shn3+/+CM
Shn3-/-CM

Fig. 3C

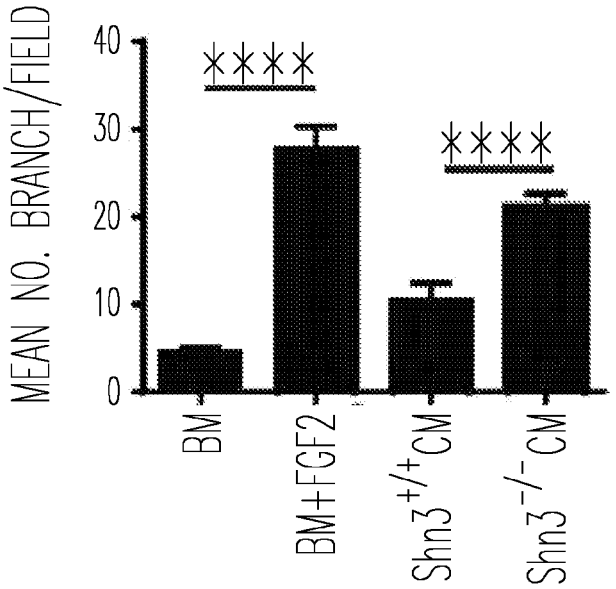
MEAN NO. BRANCH/FIELD
40
30
20
10
0
****
****
BM
BM+FGF2
Shn3+/+CM
Shn3-/-CM

Fig. 3D

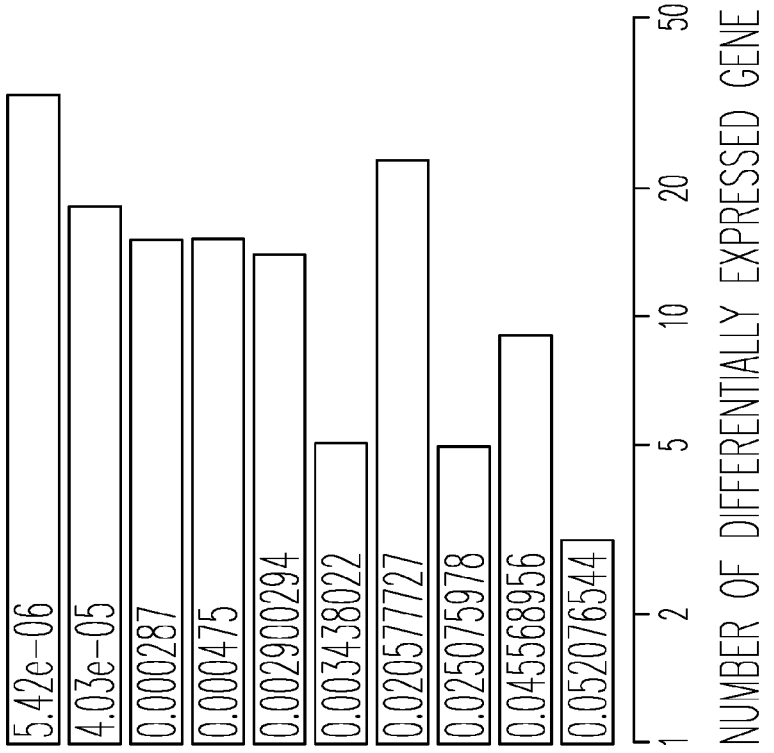
SKELETAL SYSTEM DEVELOPMENT
BONE DEVELOPMENT
EXTRACELLULAR MATRIX ORGANIZATION
OSSIFICATION
PROTEIN AMINO ACID DEPHOSPHORYLATION
BONE MINERALIZATION
REGULATION OF PHOSPHORYLATION
PATTERNING OF BLOOD VESSELS
REGULATION OF MAP KINASE ACTIVITY
NEGATIVE REGULATION OF AXON EXTENSION
5.42e-06
4.03e-05
0.000287
0.000475
0.002900294
0.003438022
0.020577727
0.025075978
0.045568956
0.052076544
1
2
5
10
20
50
NUMBER OF DIFFERENTIALLY EXPRESSED GENE

Fig. 3F

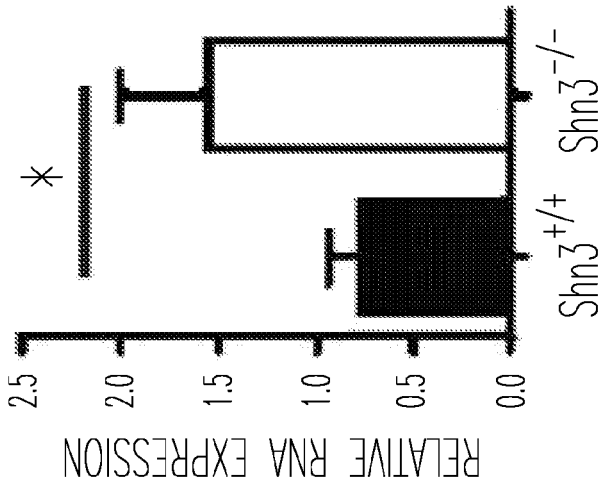
RELATIVE RNA EXPRESSION
2.5
2.0
1.5
1.0
0.5
0.0
Slit3
*
Shn3+/+
Shn3-/-

Fig. 3C

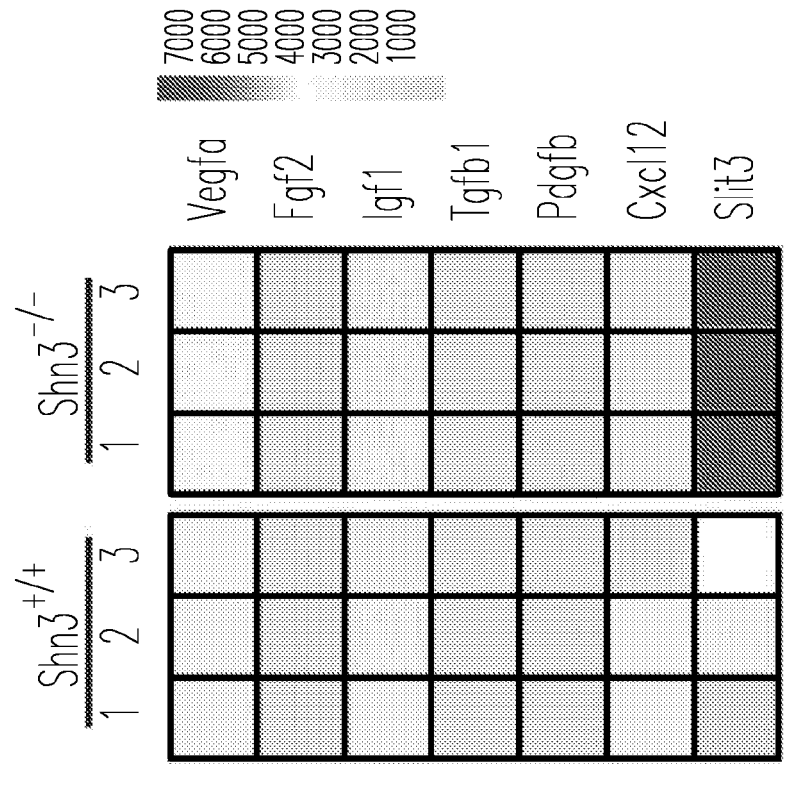
7000
6000
5000
4000
3000
2000
1000
Vegfa
Fgf2
Igf1
Tgfb1
Pdgfb
Cxcl12
Slit3
Shn3-/-
1 2 3
Shn3+/+
1 2 3

Fig. 3F

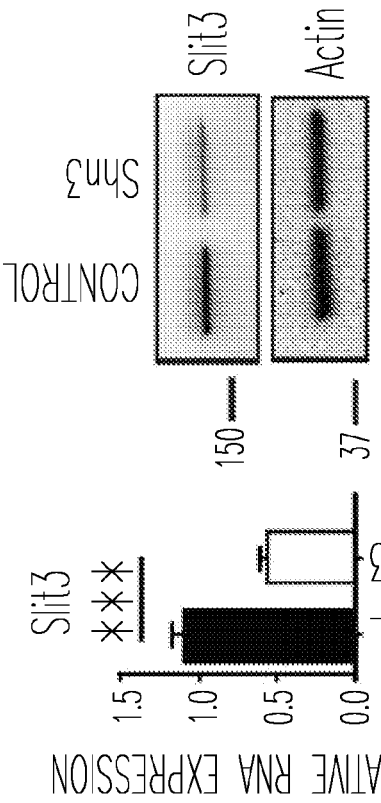

Fig. 3I-2

Fig. 3I-1

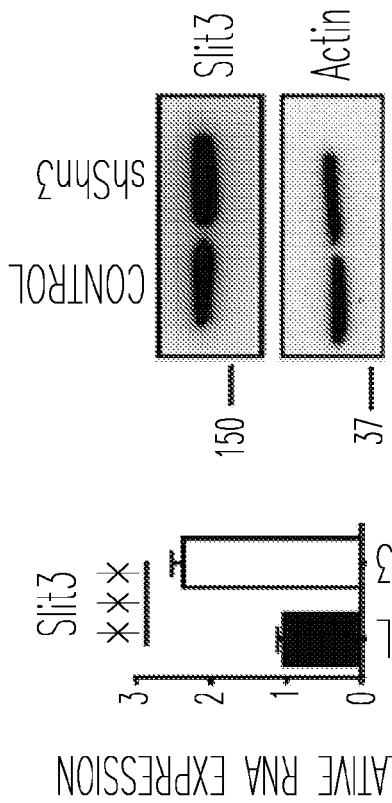

Fig. 3H-2

Fig. 3H-1

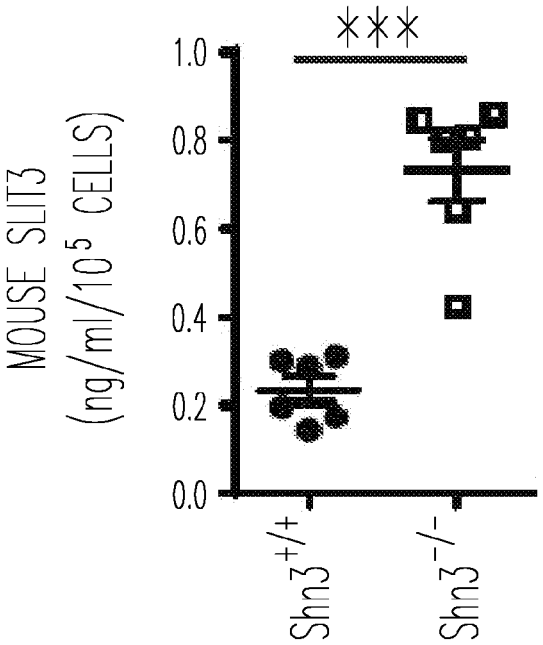

Fig. 3J

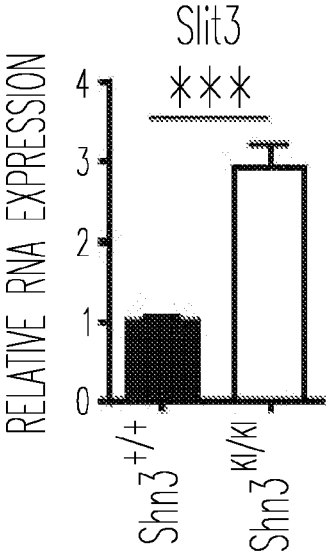

Fig. 3K

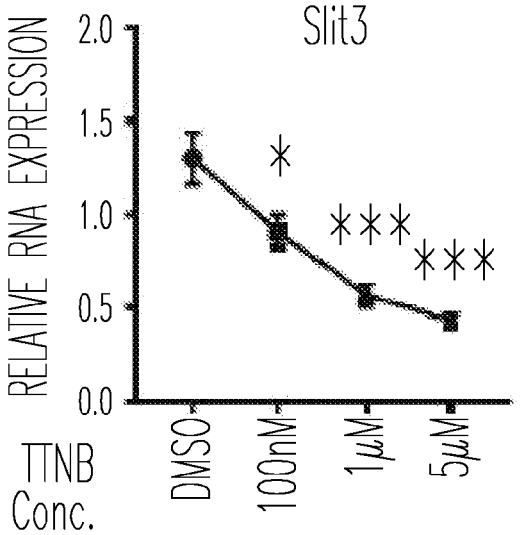

Fig. 3L

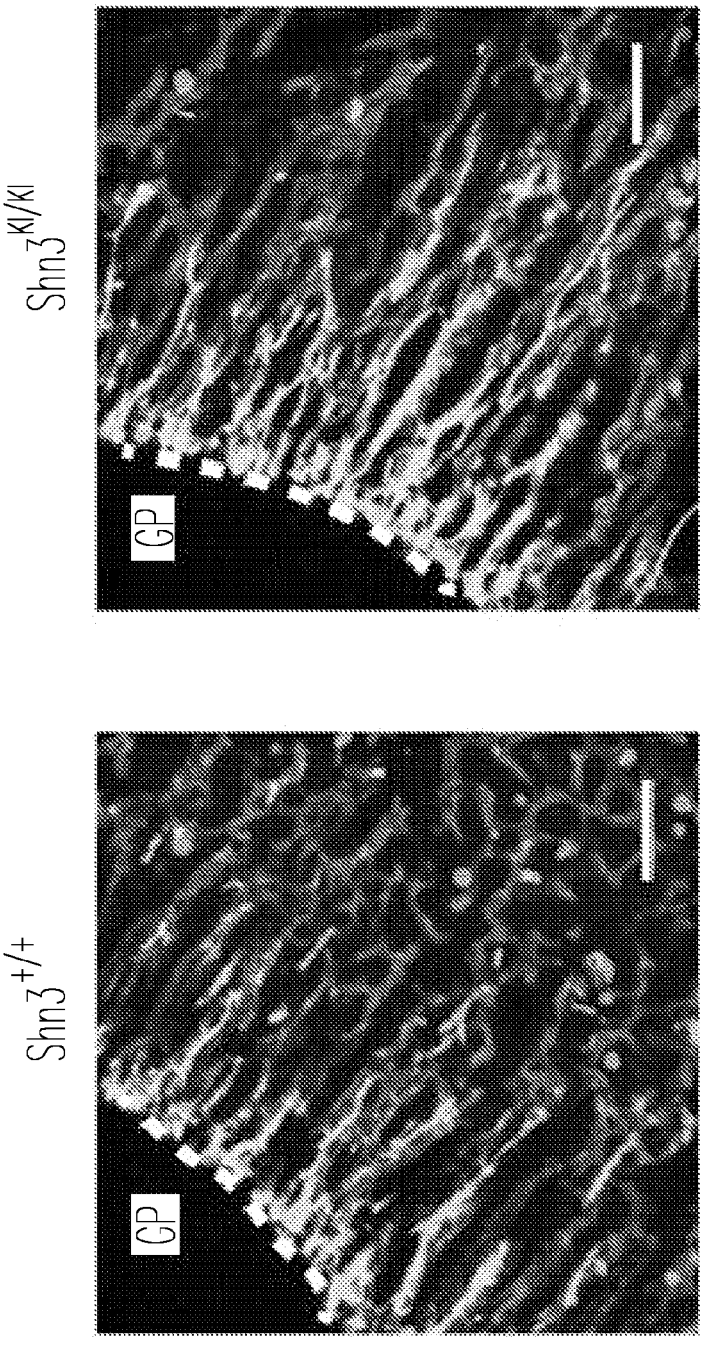

Fig. 3M

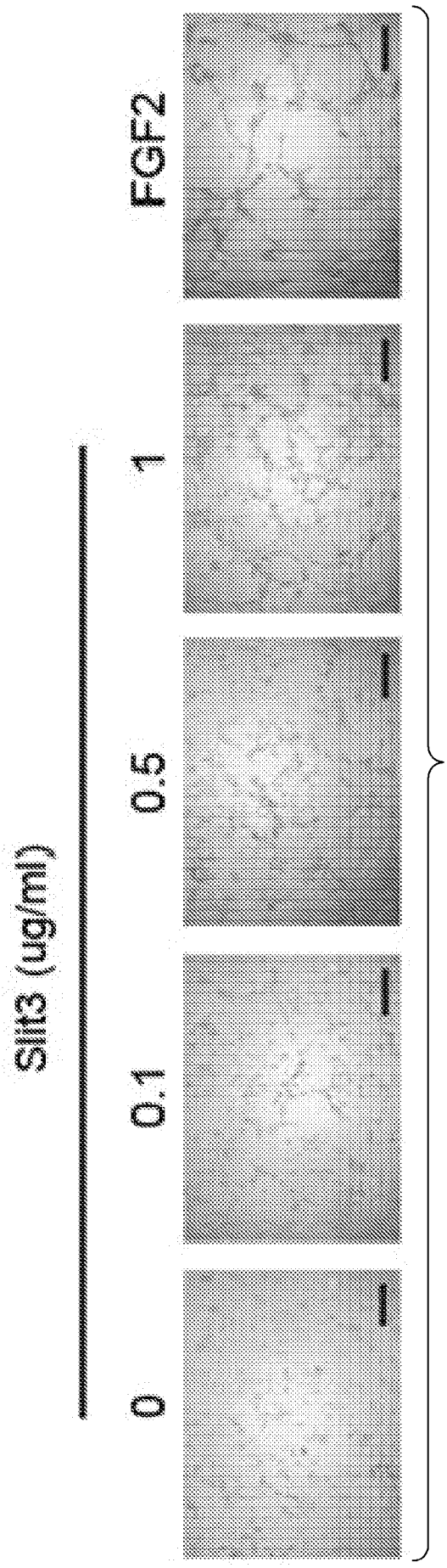
Slit3 (ug/ml)
0
0.1
0.5
1
FGF2

Fig. 4A

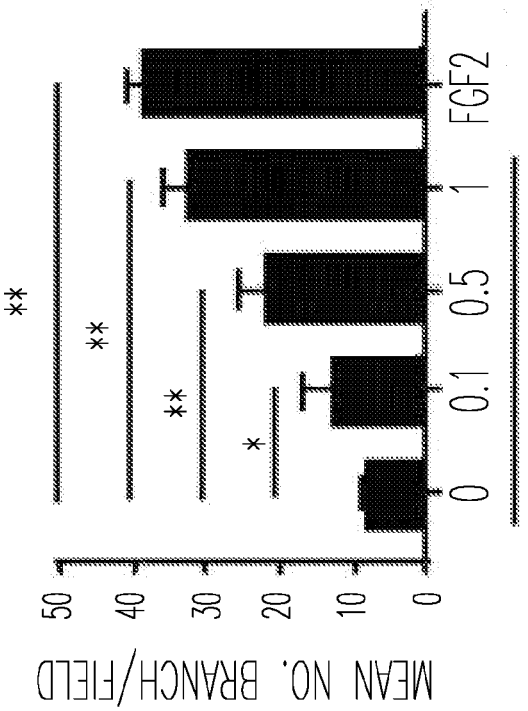
MEAN NO. BRANCH/FIELD
50
40
30
20
10
0
0
0.1
0.5
1
FGF2
*
**
**
**

Fig. 4B

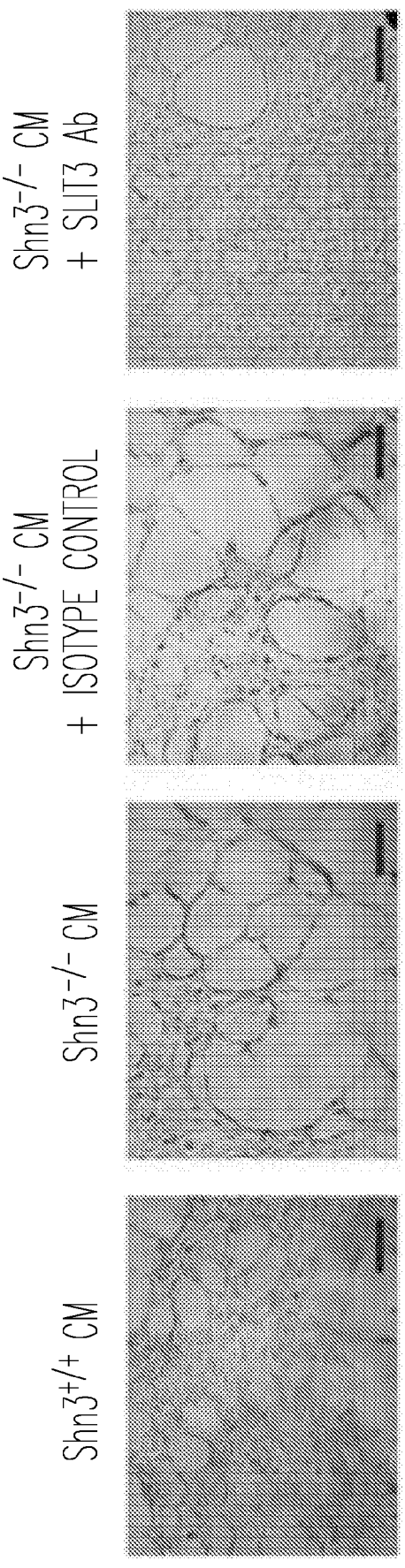

Fig. 4C

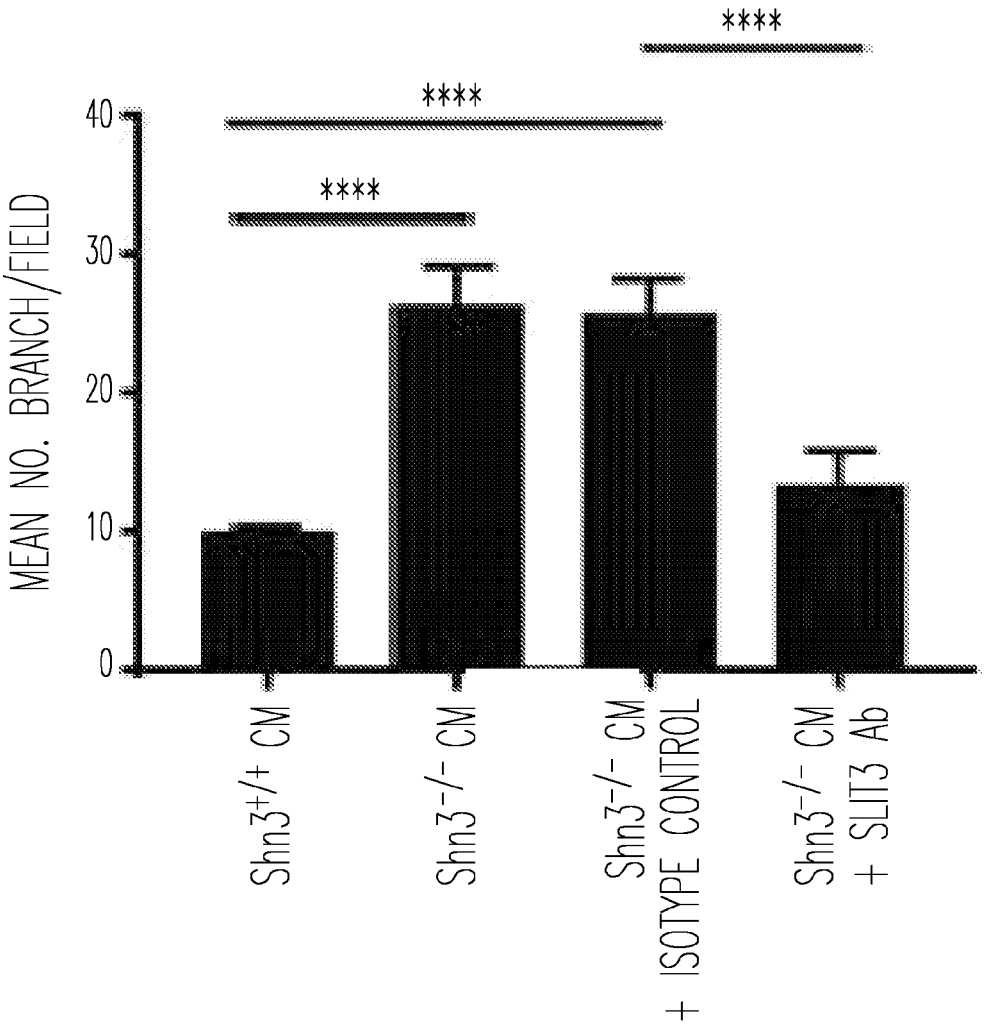
****
****
****
40
30
20
10
0
MEAN NO. BRANCH/FIELD
Shn3+/+ CM
Shn3-/- CM
Shn3-/- CM + ISOTYPE CONTROL
Shn3-/- CM + SLIT3 Ab

Fig. 4D

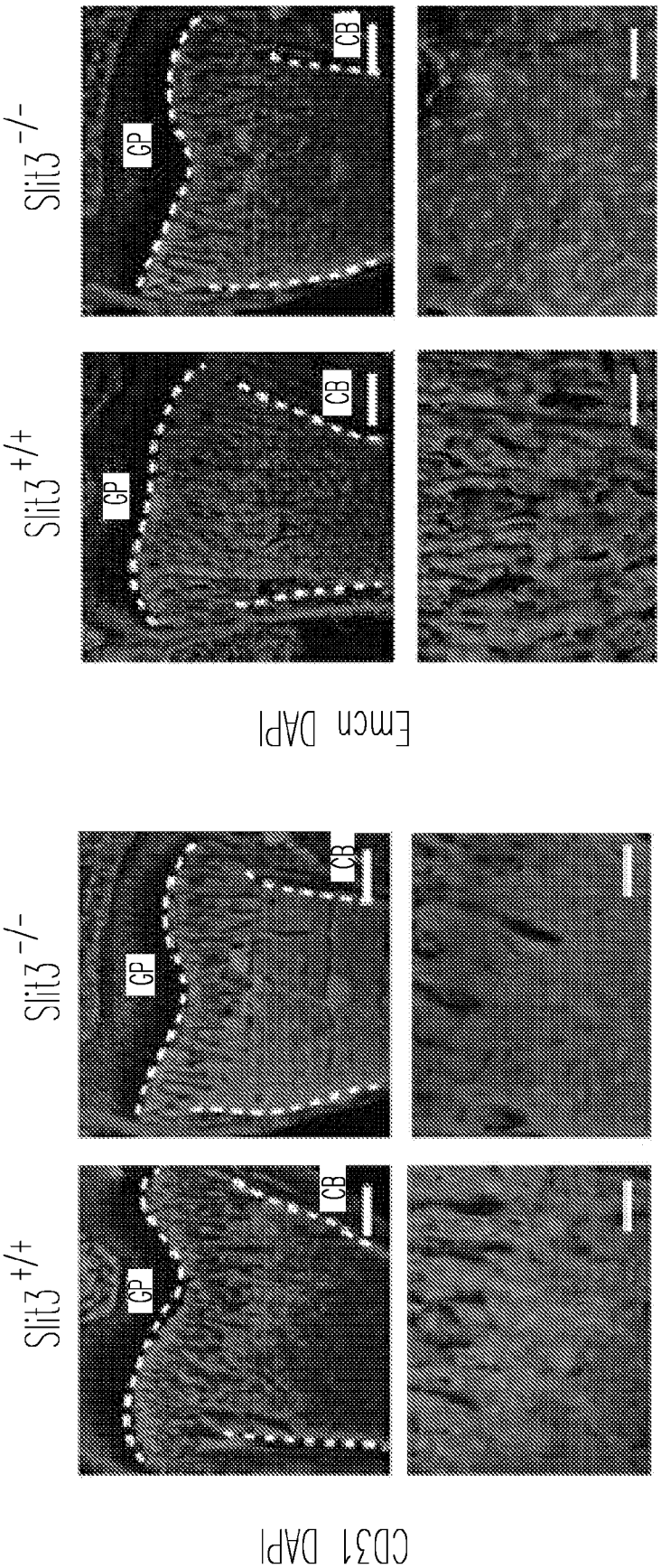

Fig. 4E

Fig. 4F

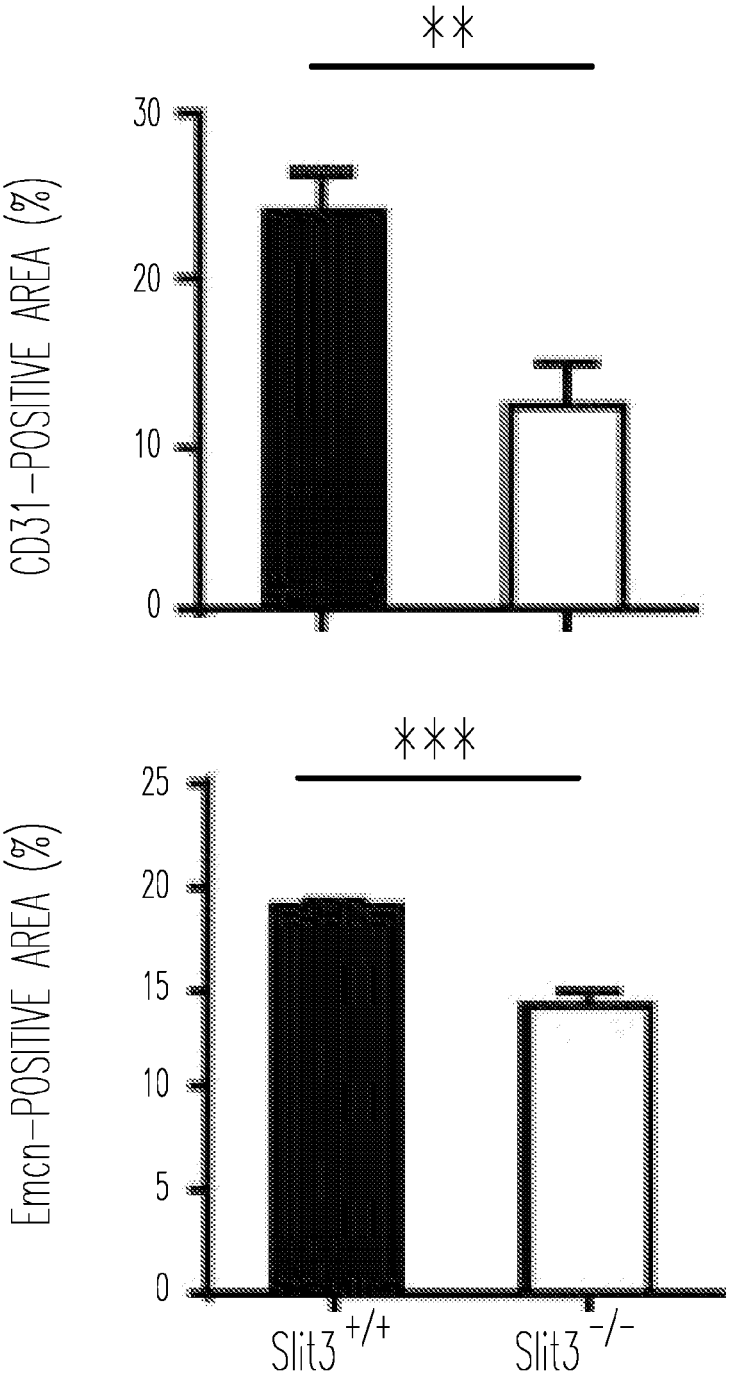
**
CD31-POSITIVE AREA (%)
30
20
10
0
***
Emcn-POSITIVE AREA (%)
25
20
15
10
5
0
Slit3 +/+
Slit3 -/-

Fig. 4C

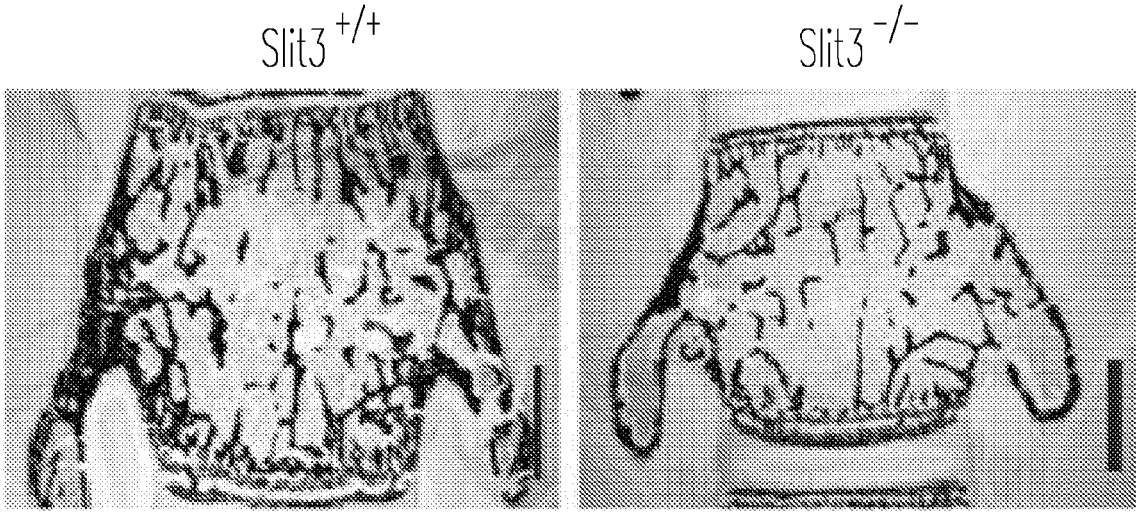

Fig. 4H-1

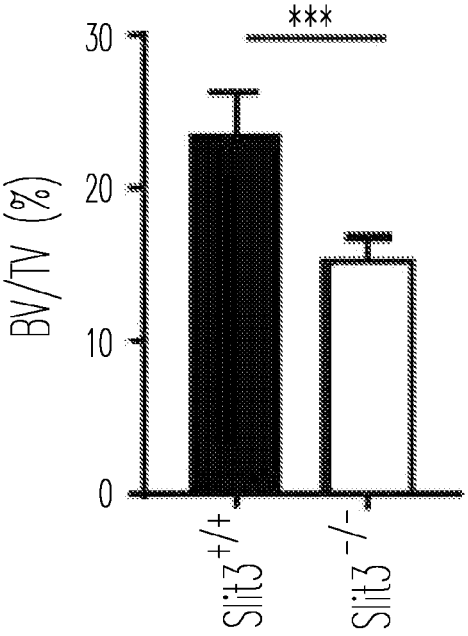

Fig. 4H-2

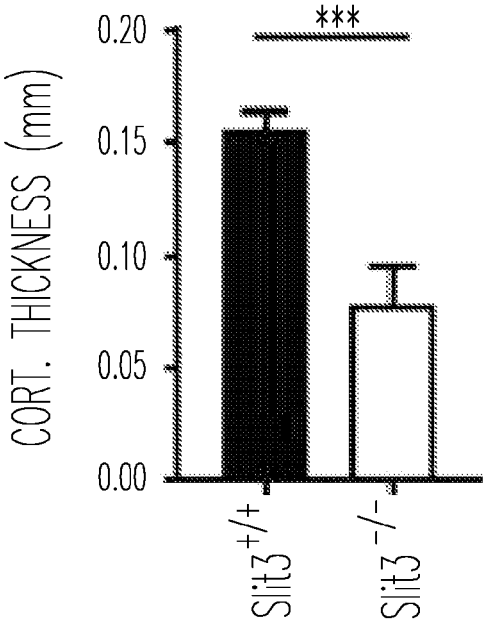

Fig. 4H-3

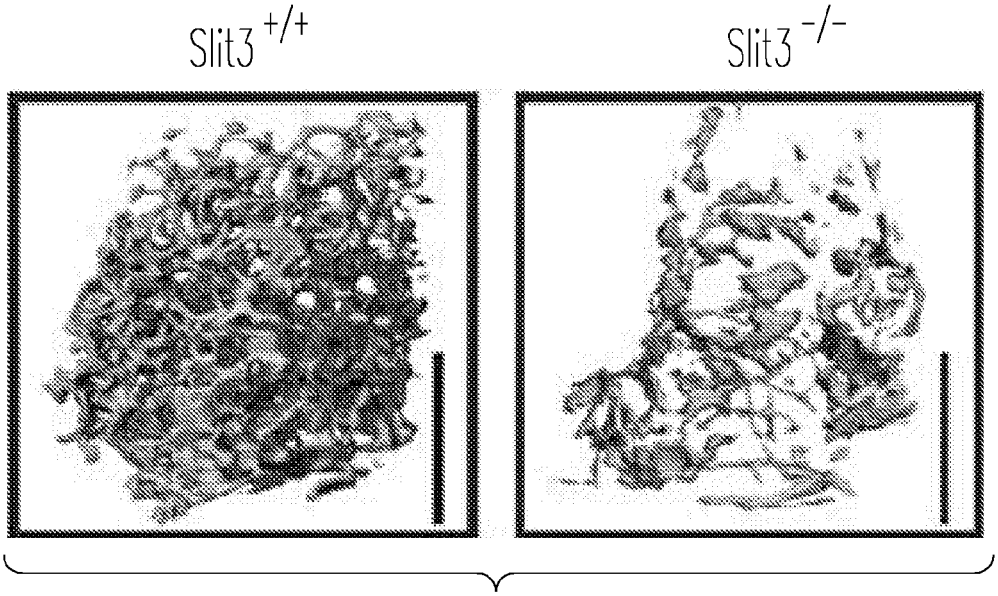

Fig. 4I-1

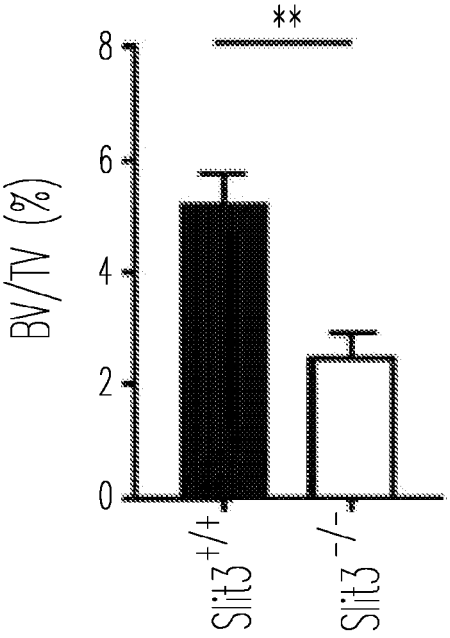

Fig. 4I-2

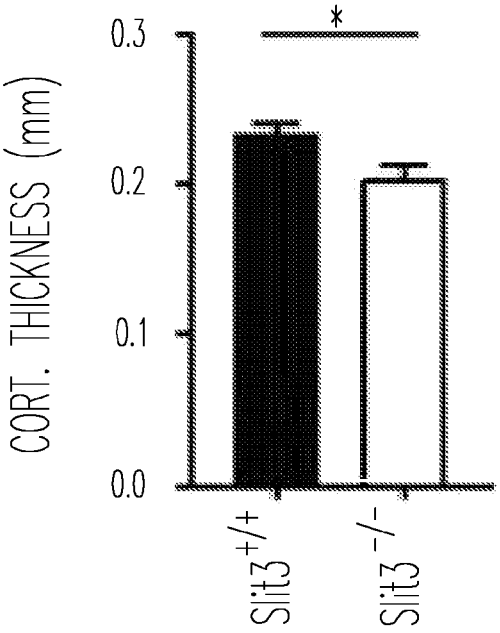

Fig. 4I-3

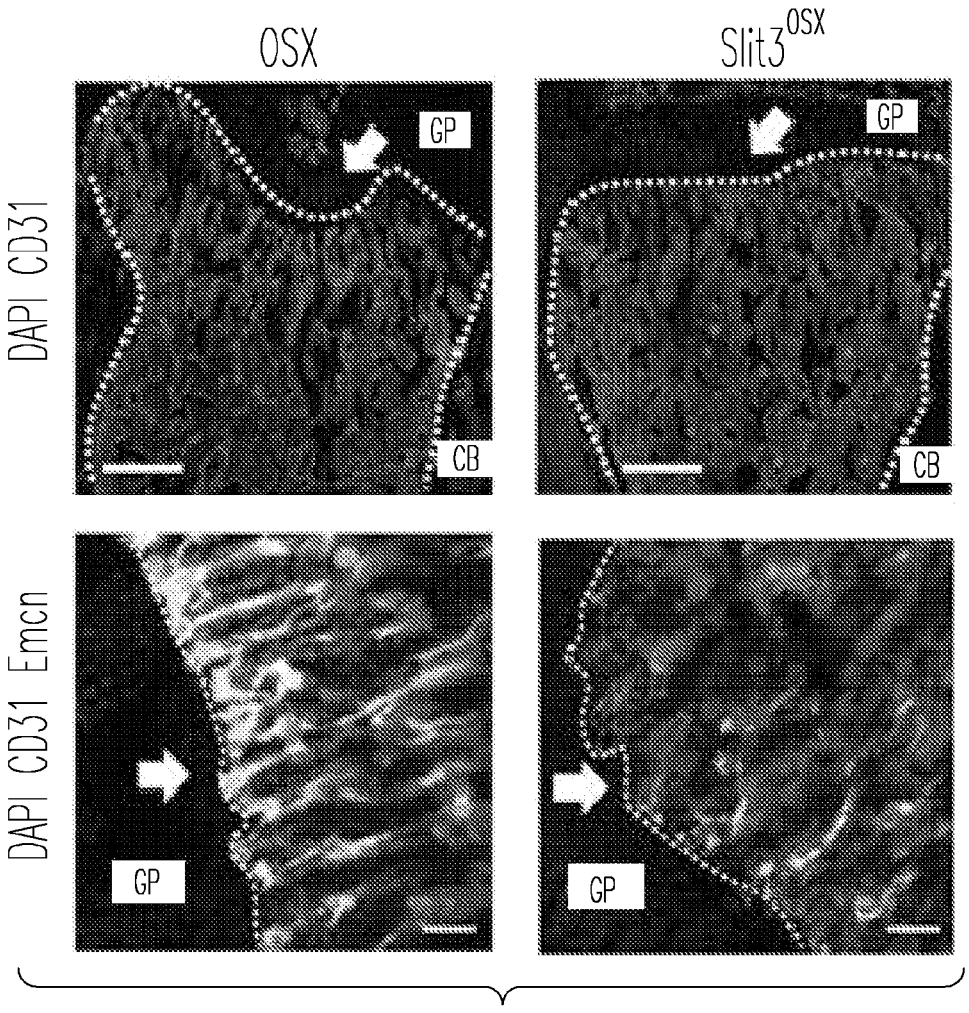

Fig. 4J

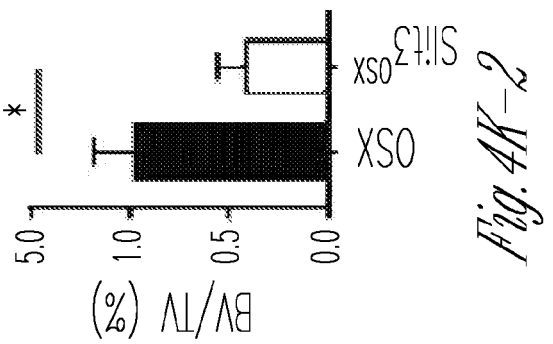

Fig. 4K-2

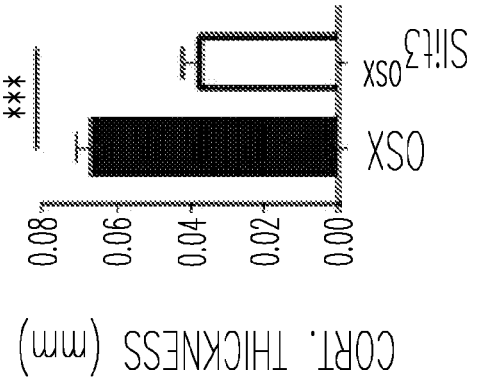

Fig. 4L-2

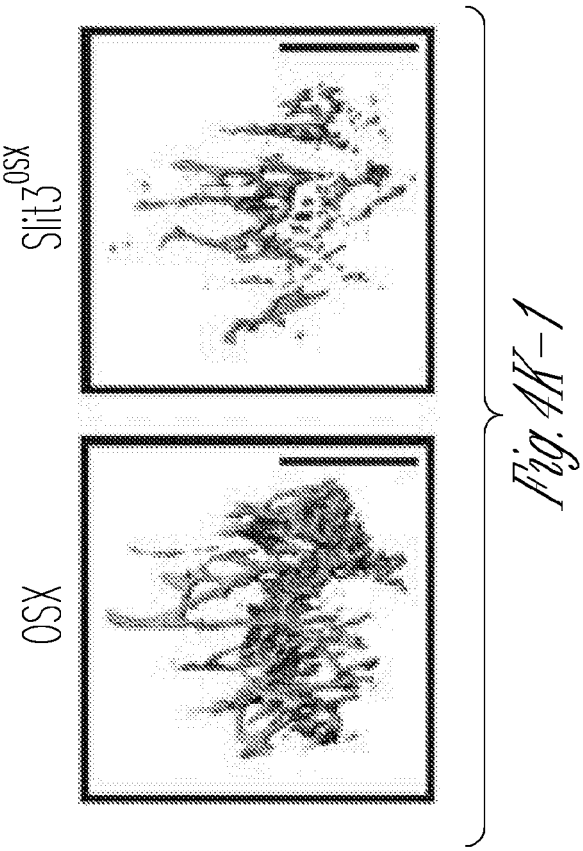

Fig. 4K-1

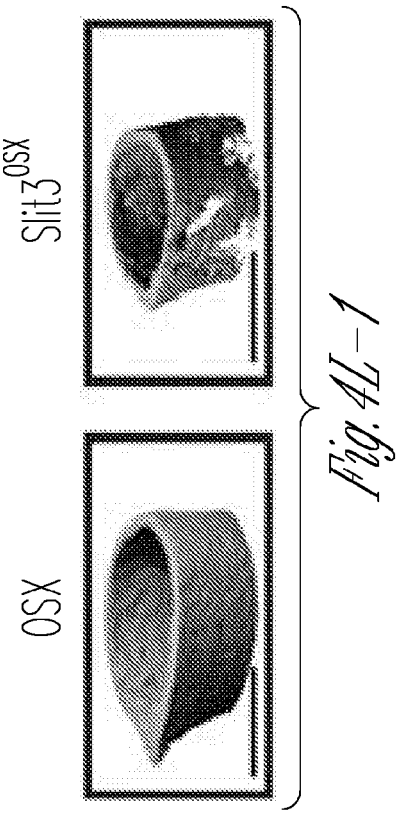

Fig. 4L-1

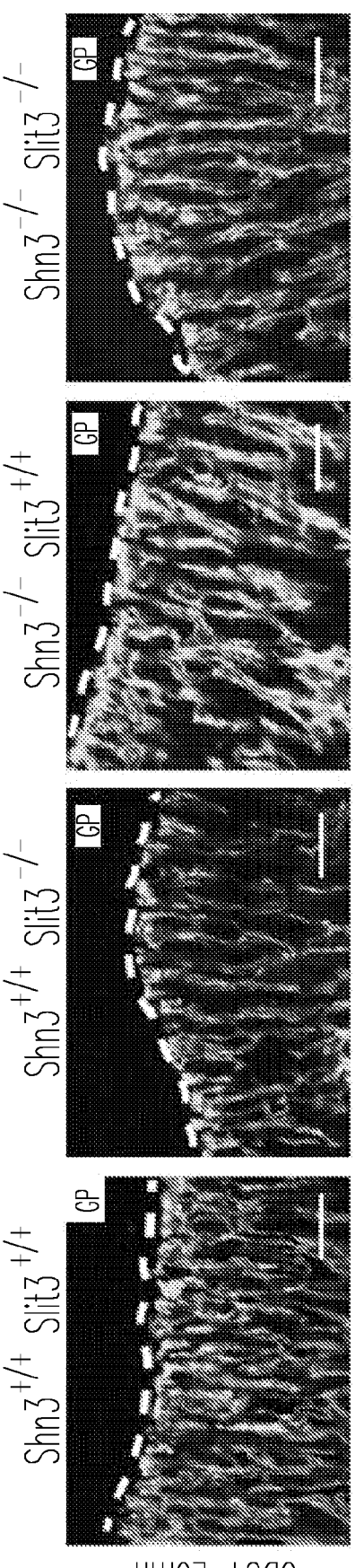
CD31 Ecmn
Shn3+/+ Slit3+/+
GP
Shn3+/+ Slit3-/-
GP
Shn3-/- Slit3+/+
GP
Shn3-/- Slit3-/-
GP

Fig. 5A

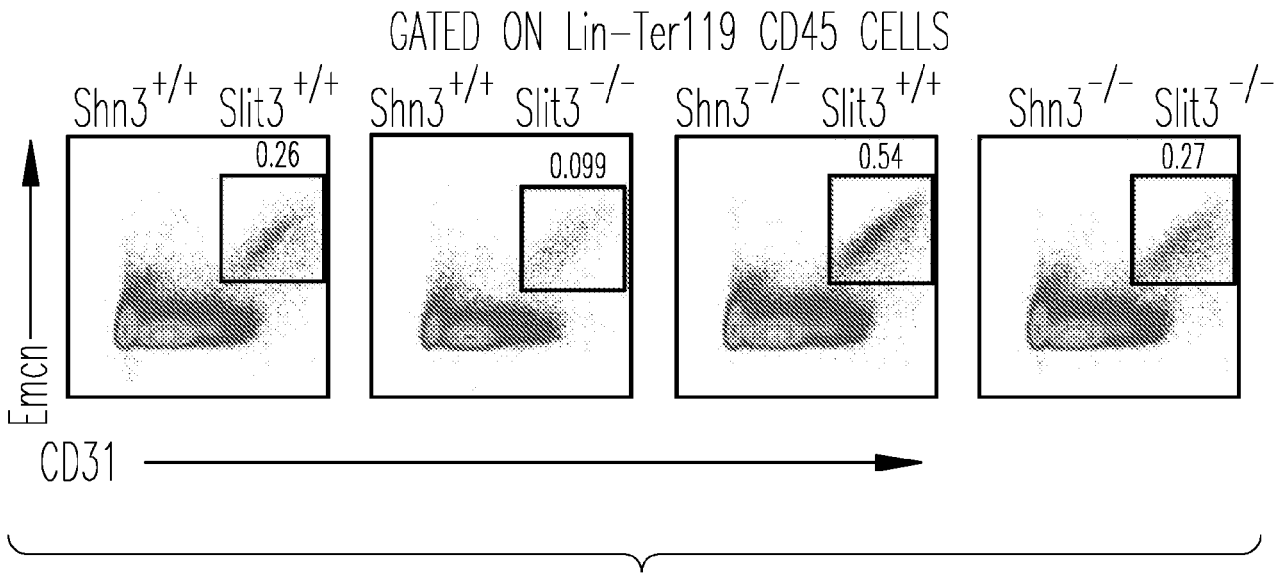

Fig. 5B-1

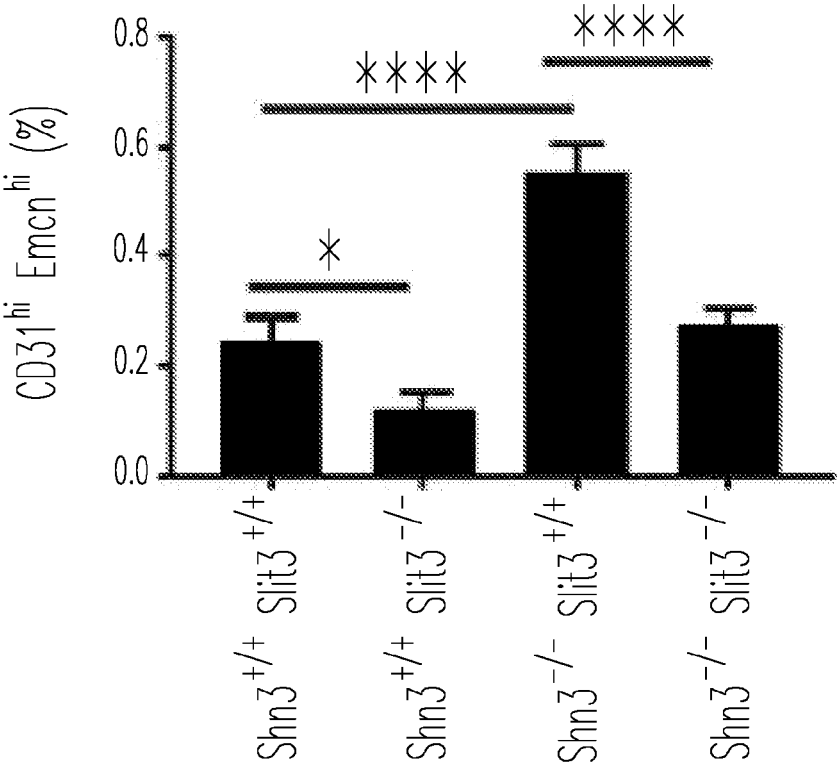

Fig. 5B-2

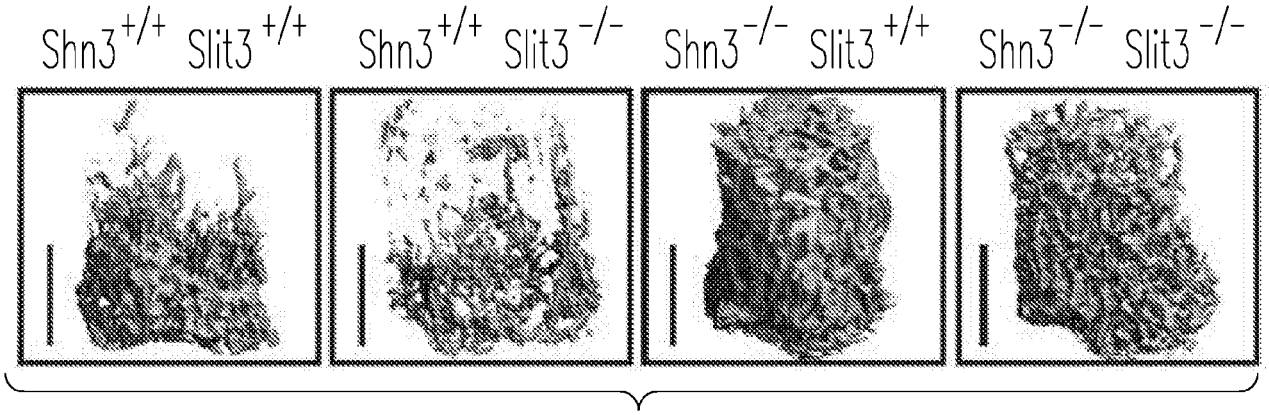
Shn3+/+ Slit3+/+
Shn3+/+ Slit3-/-
Shn3-/- Slit3+/+
Shn3-/- Slit3-/-

Fig. 5C

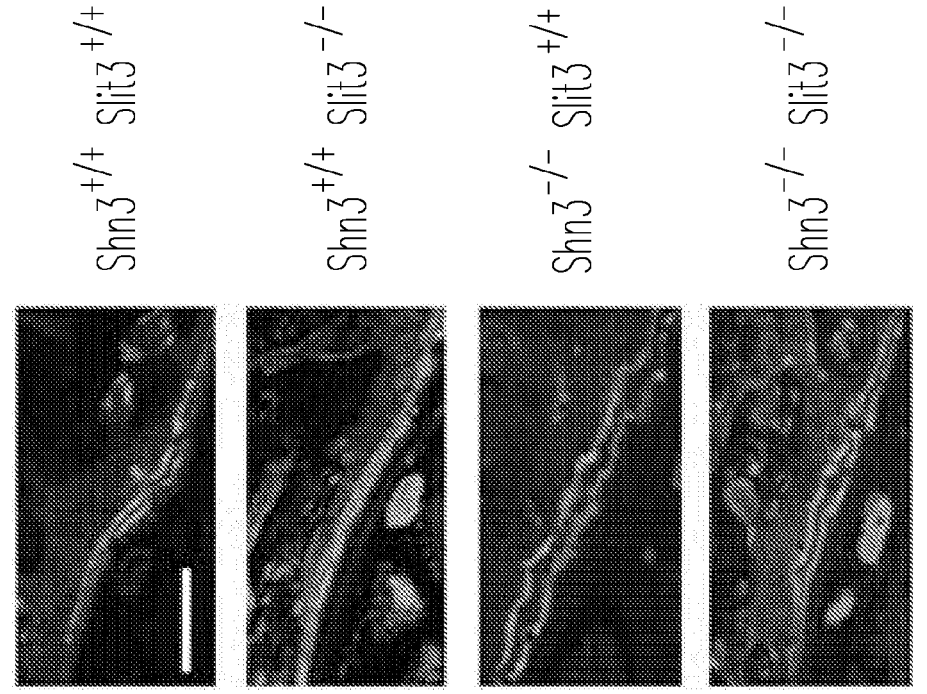
Shn3+/+ Slit3+/+
Shn3+/+ Slit3-/-
Shn3-/- Slit3+/+
Shn3-/- Slit3-/-

Fig. 5D

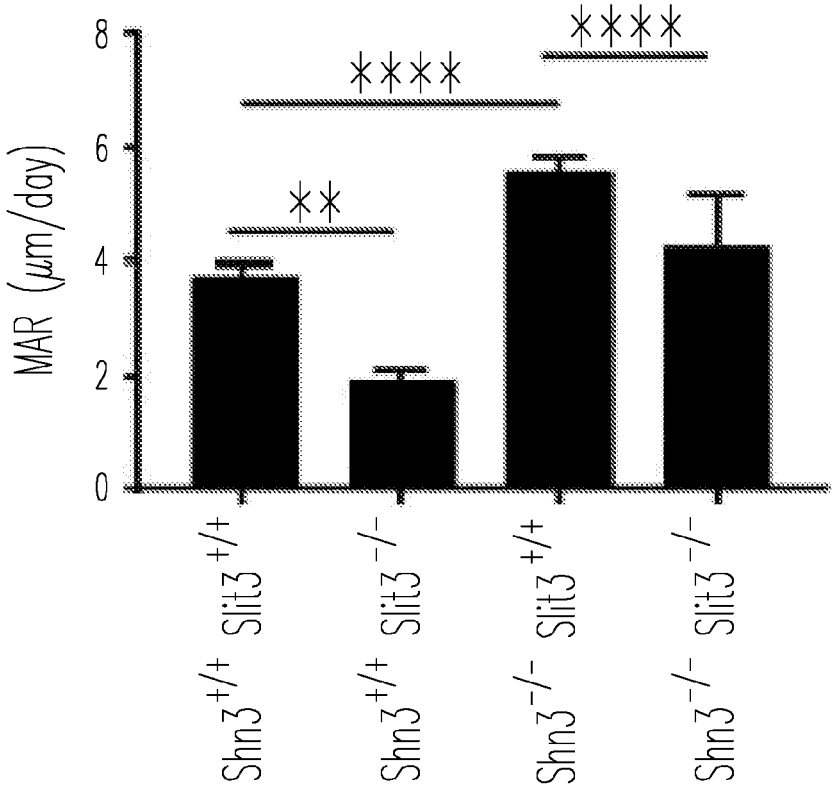

Fig. 5E

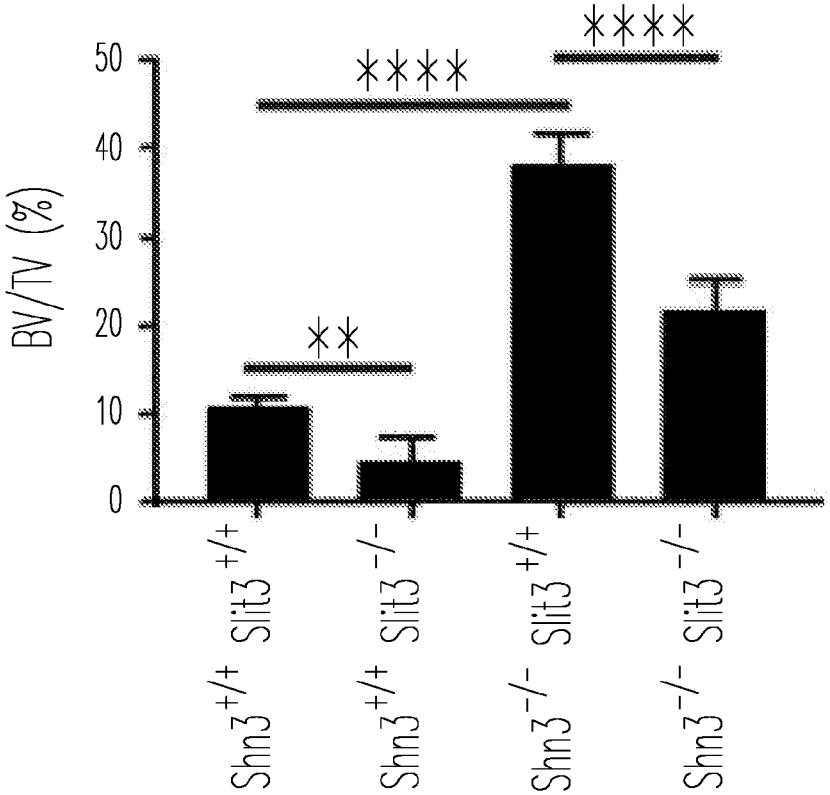

Fig. 5F-1

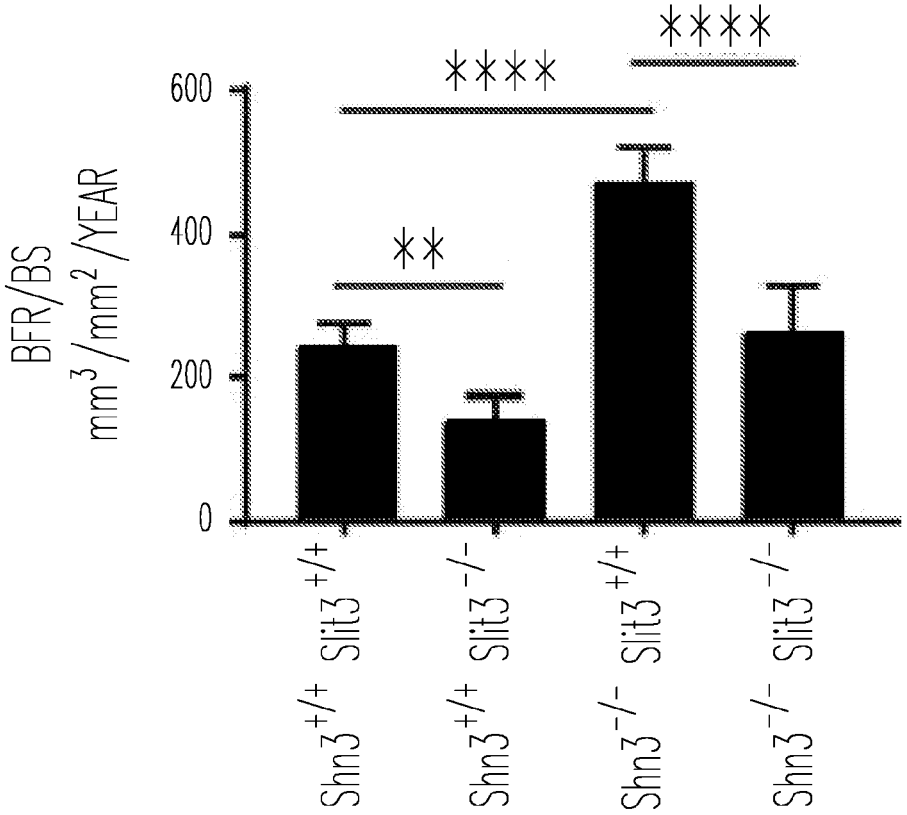
BFR/BS
mm3/mm2/YEAR
600
400
200
0
****
****
**
Shn3+/+ Slit3+/+
Shn3+/+ Slit3-/-
Shn3-/- Slit3+/+
Shn3-/- Slit3-/-

Fig. 5F-2

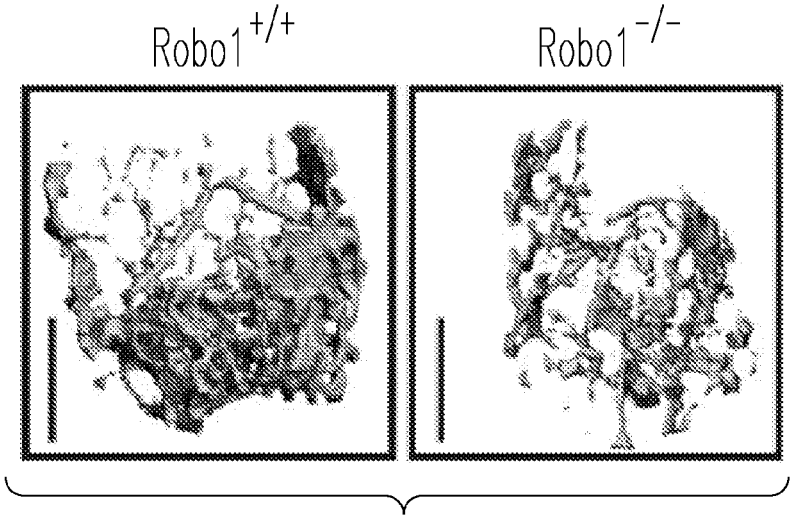

Fig. 5G-1

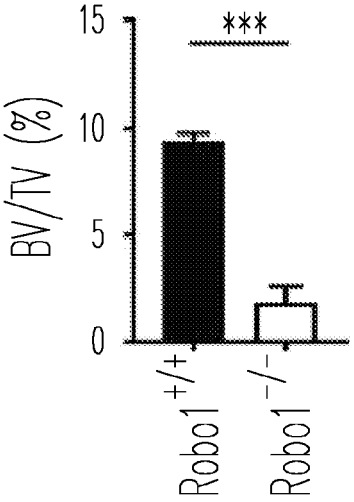

Fig. 5G-2

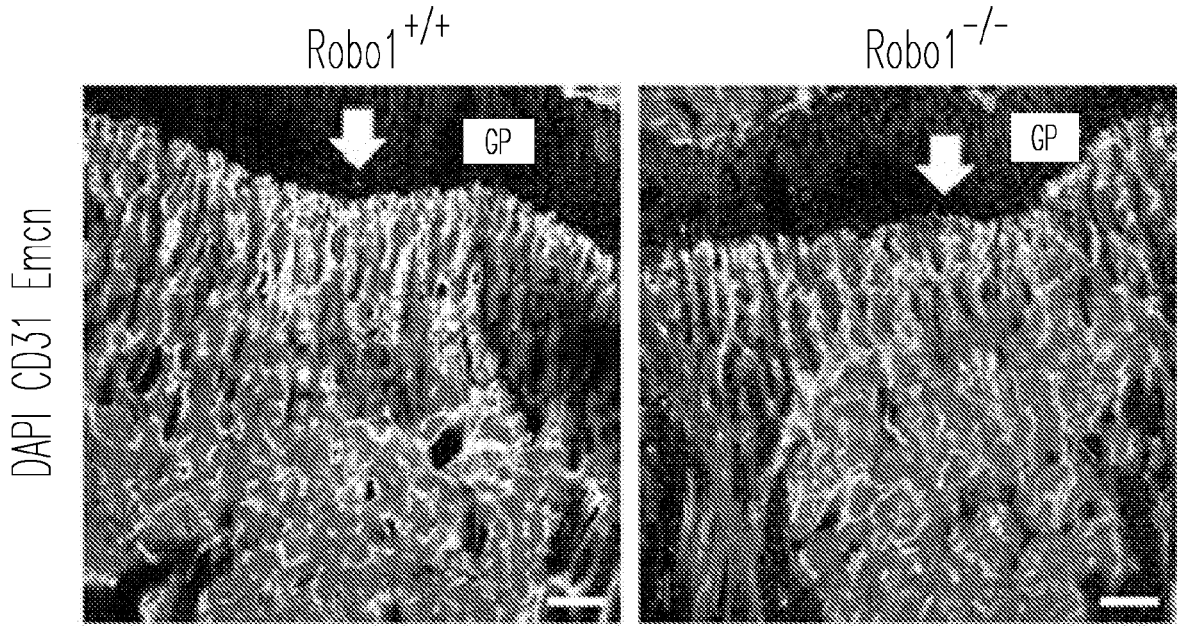

Fig. 5H

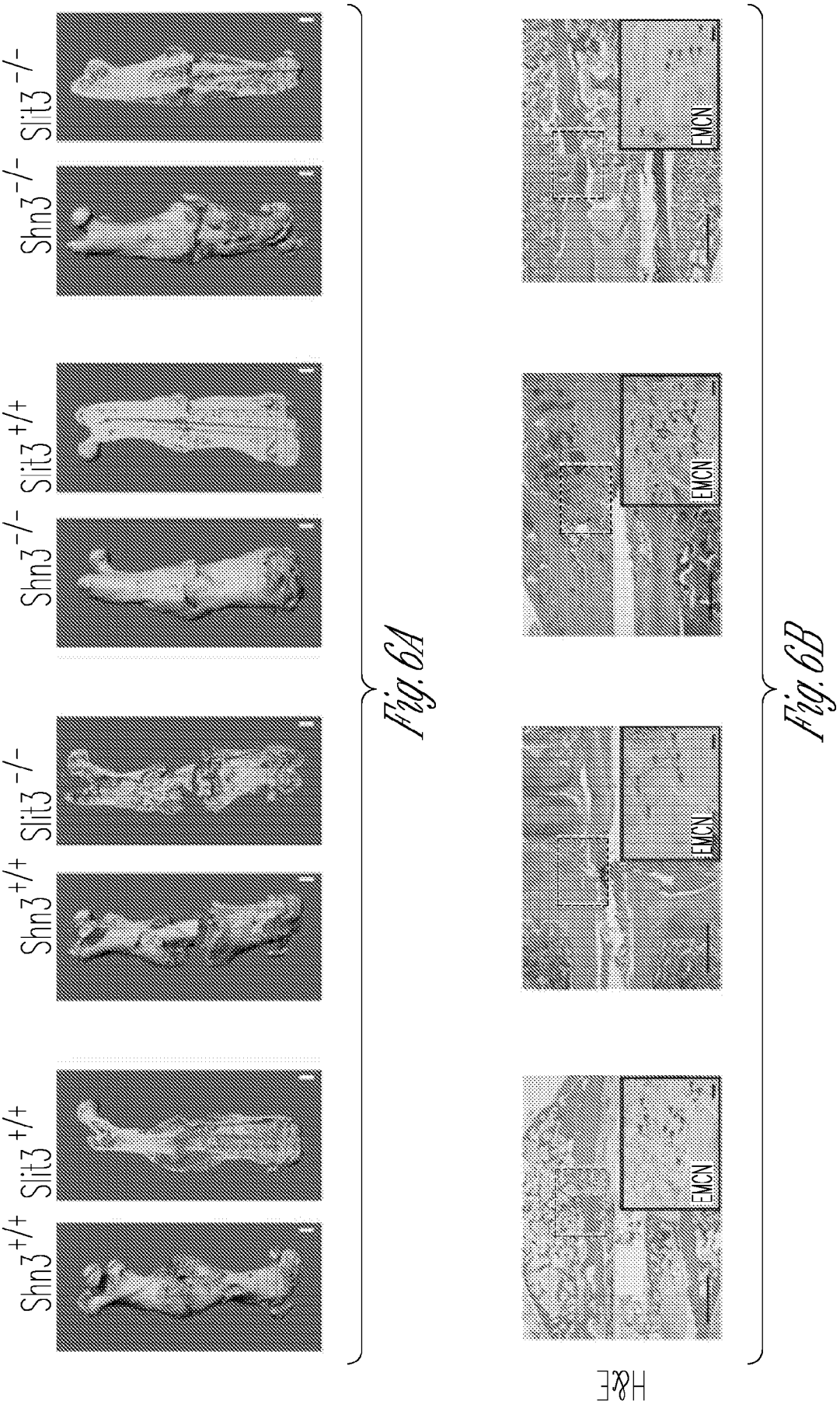
Shn3 +/+
Slit3 +/+
Shn3 +/+
Slit3 -/-
Shn3 -/-
Slit3 +/+
Shn3 -/-
Slit3 -/-
EMCN
EMCN
EMCN
EMCN
H&E

Fig. 6A

Fig. 6B

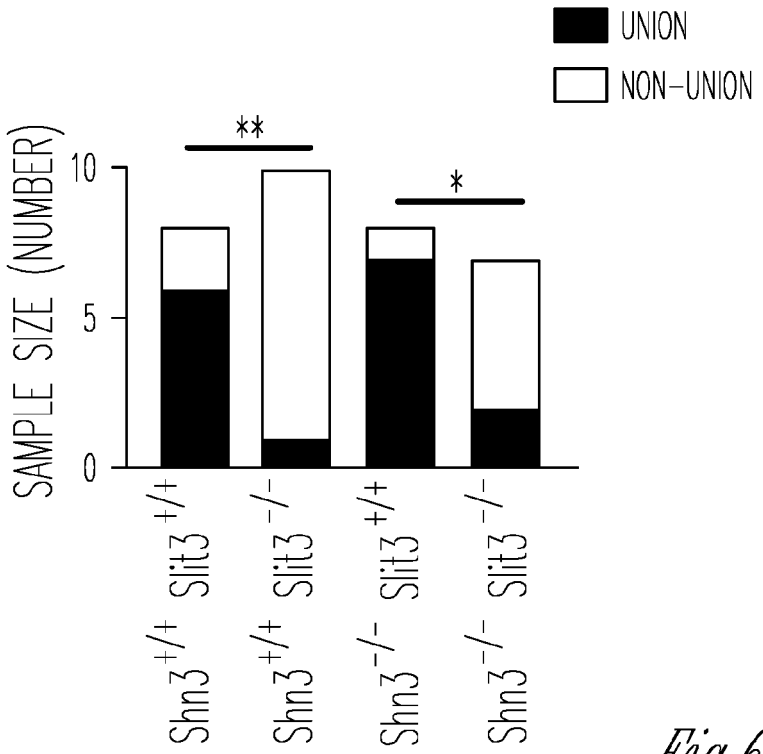
UNION
NON-UNION
SAMPLE SIZE (NUMBER)
10
5
0
**
*
Shn3+/+ Slit3+/+
Shn3+/+ Slit3-/-
Shn3-/- Slit3+/+
Shn3-/- Slit3-/-

Fig. 6C

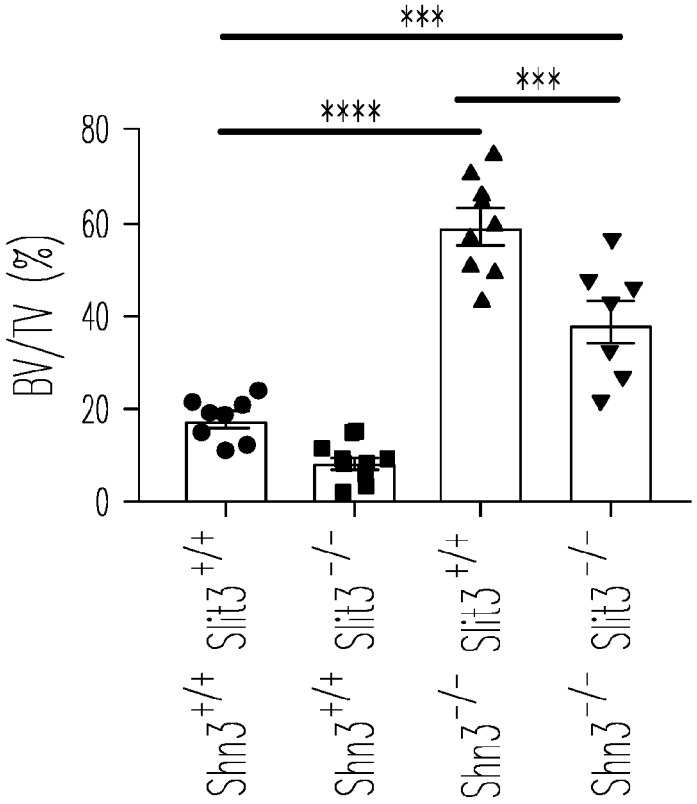
***
***
****
BV/TV (%)
80
60
40
20
0
Shn3+/+ Slit3+/+
Shn3+/+ Slit3-/-
Shn3-/- Slit3+/+
Shn3-/- Slit3-/-

Fig. 6D

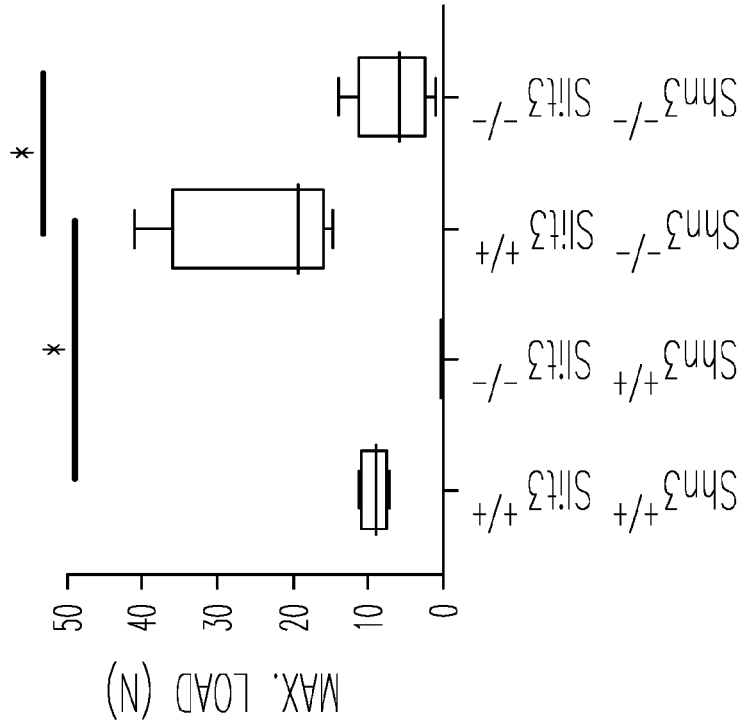

Fig. 6E-2

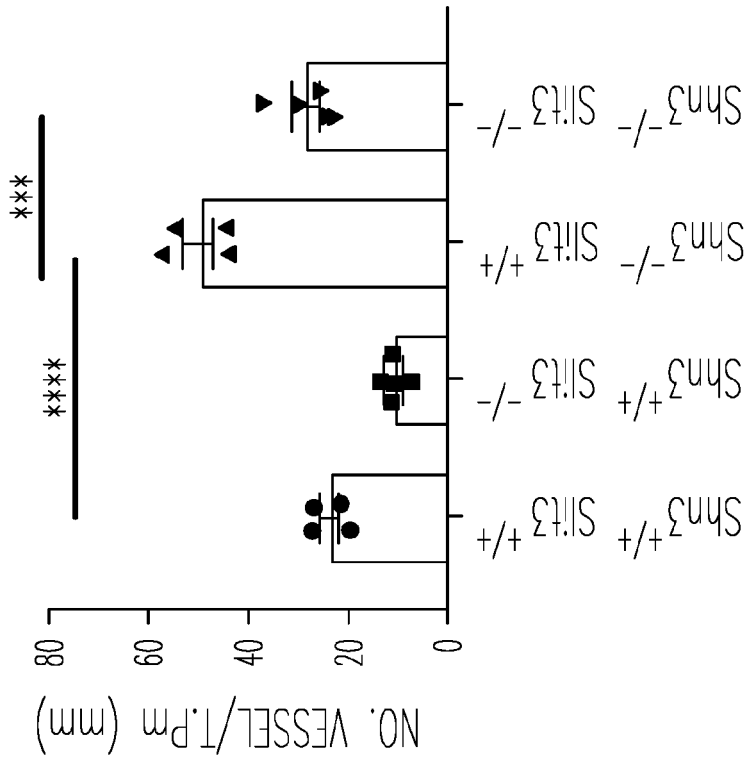

Fig. 6E-1

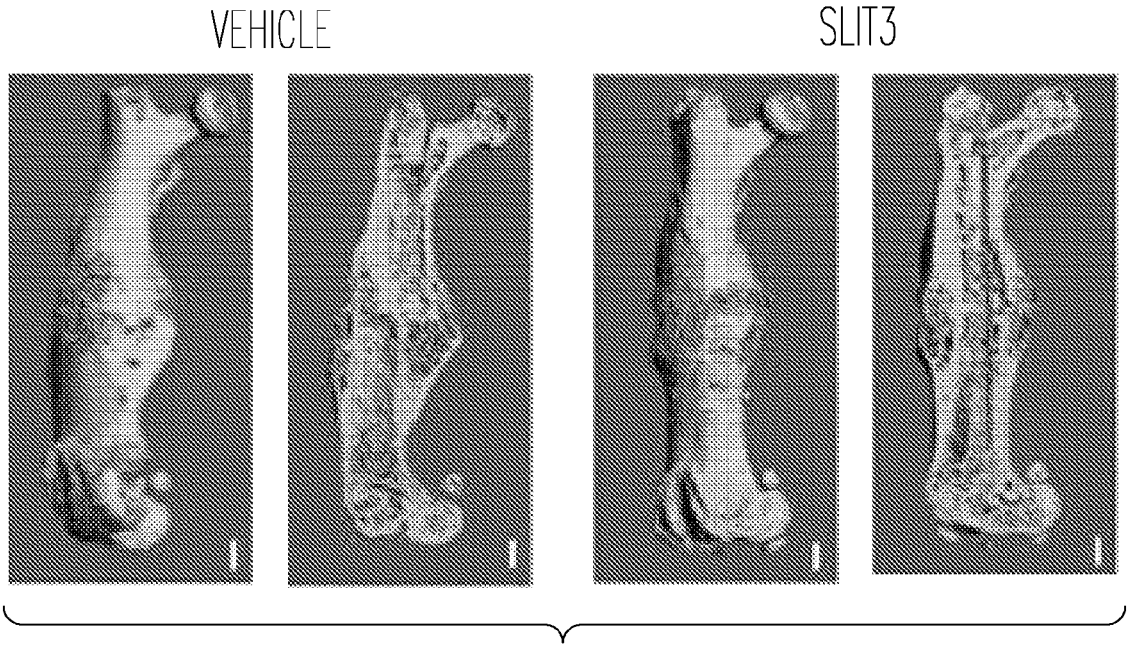

Fig. 6F

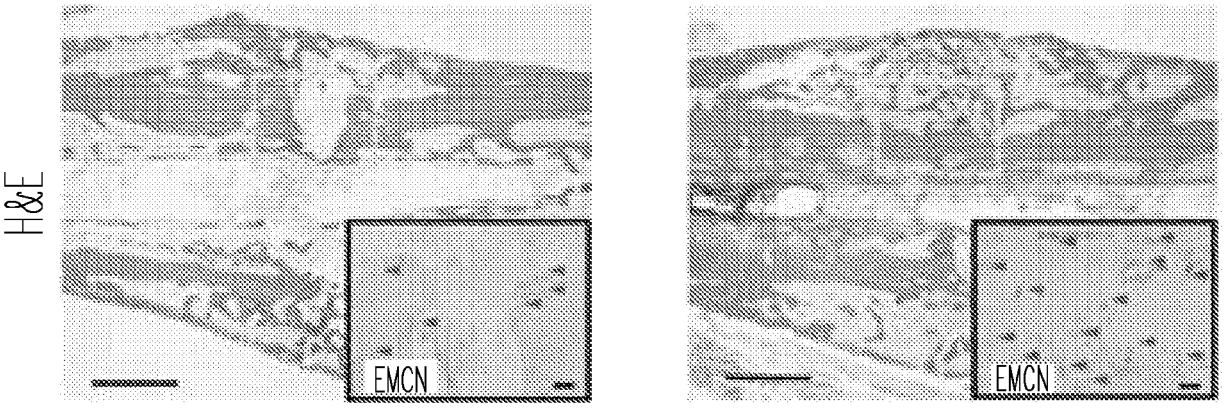

Fig. 6G

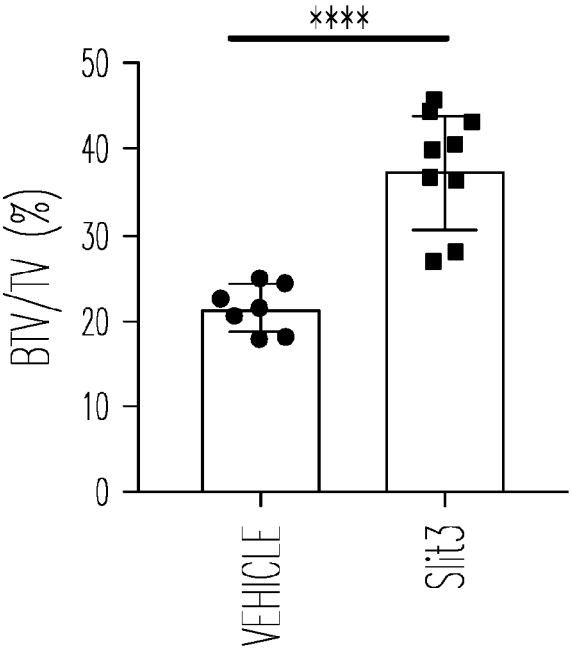

Fig. 6H

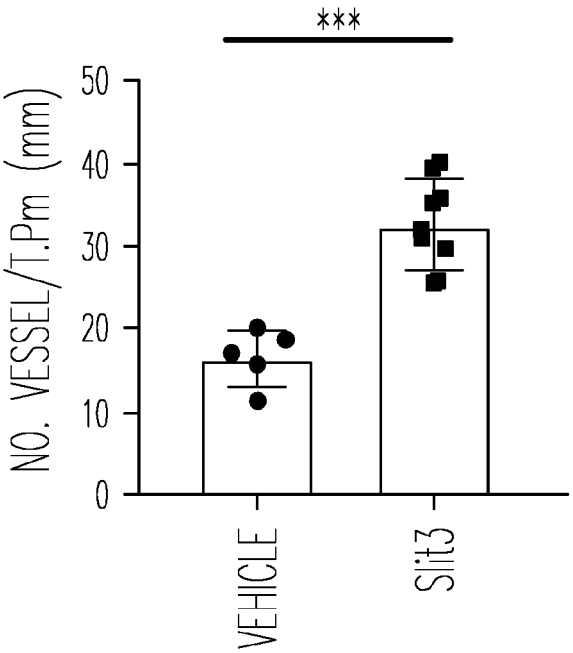

Fig. 6I-1

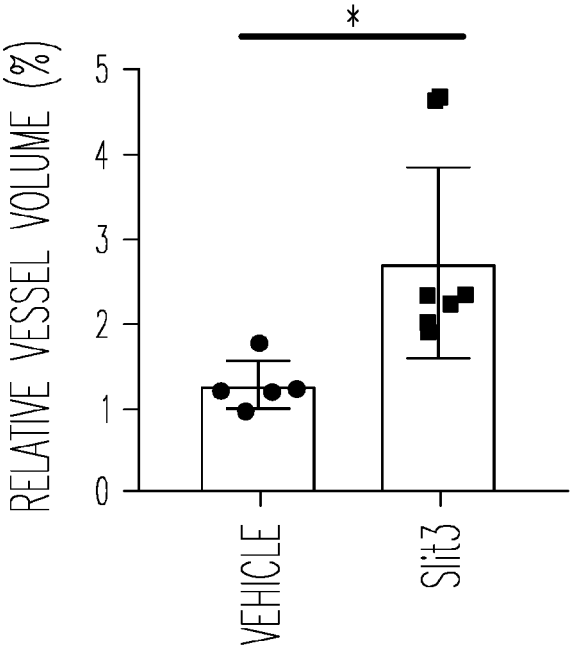

Fig. 6I-2

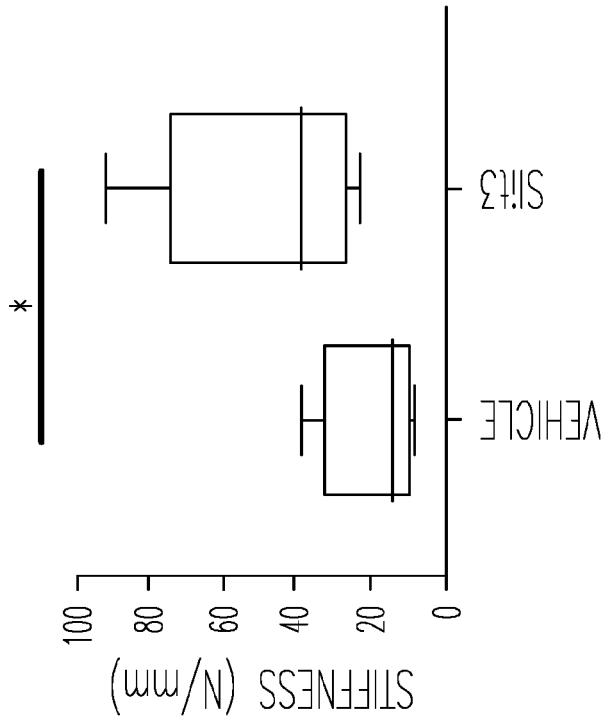

Fig. 6J-2

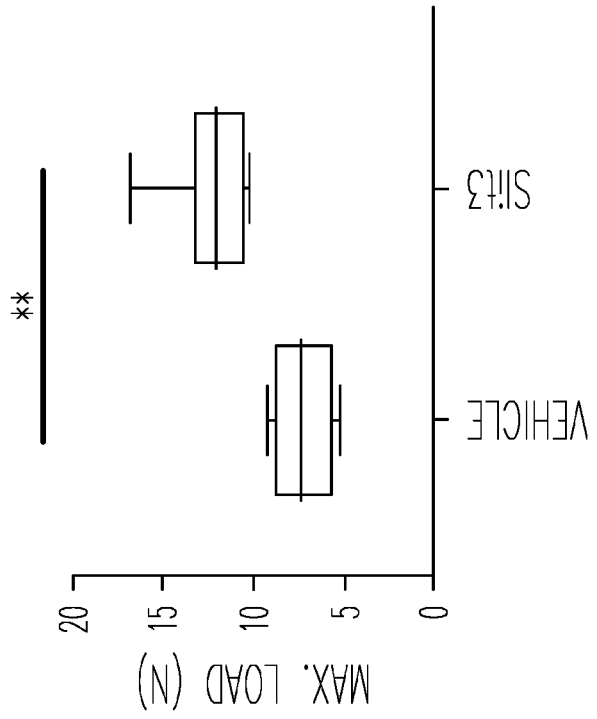

Fig. 6J-1

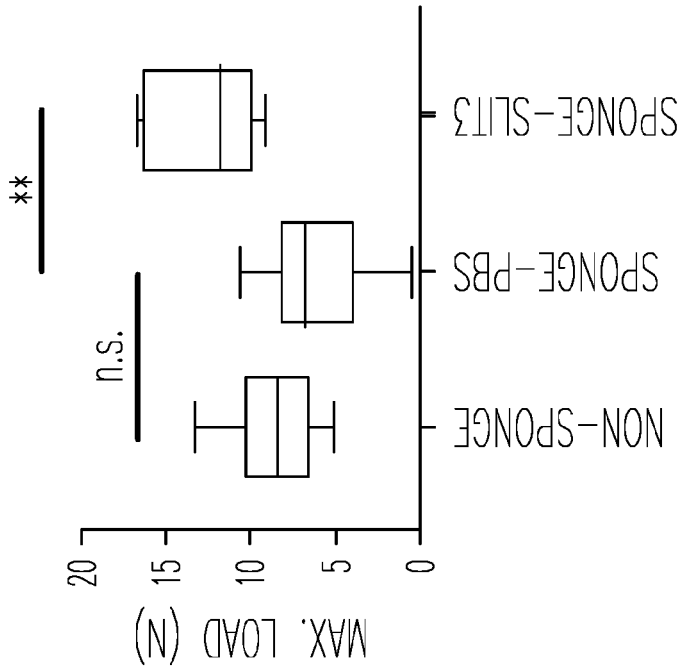

Fig. 6K-2

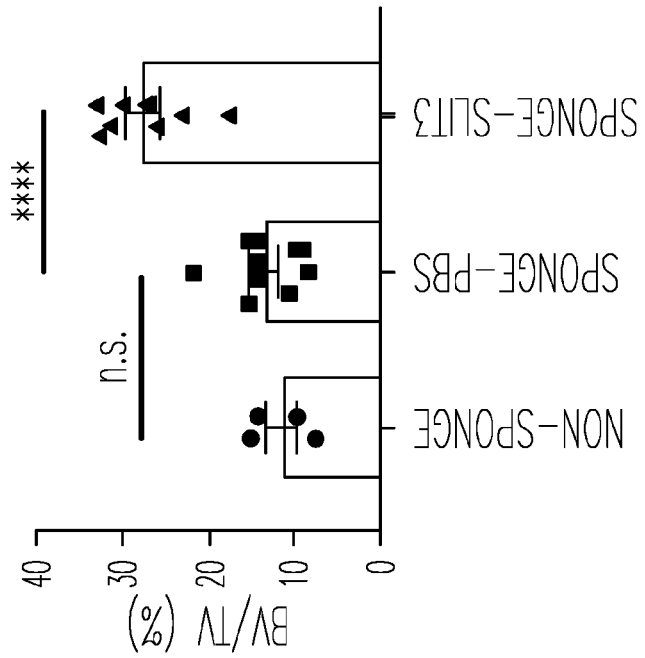

Fig. 6K-1

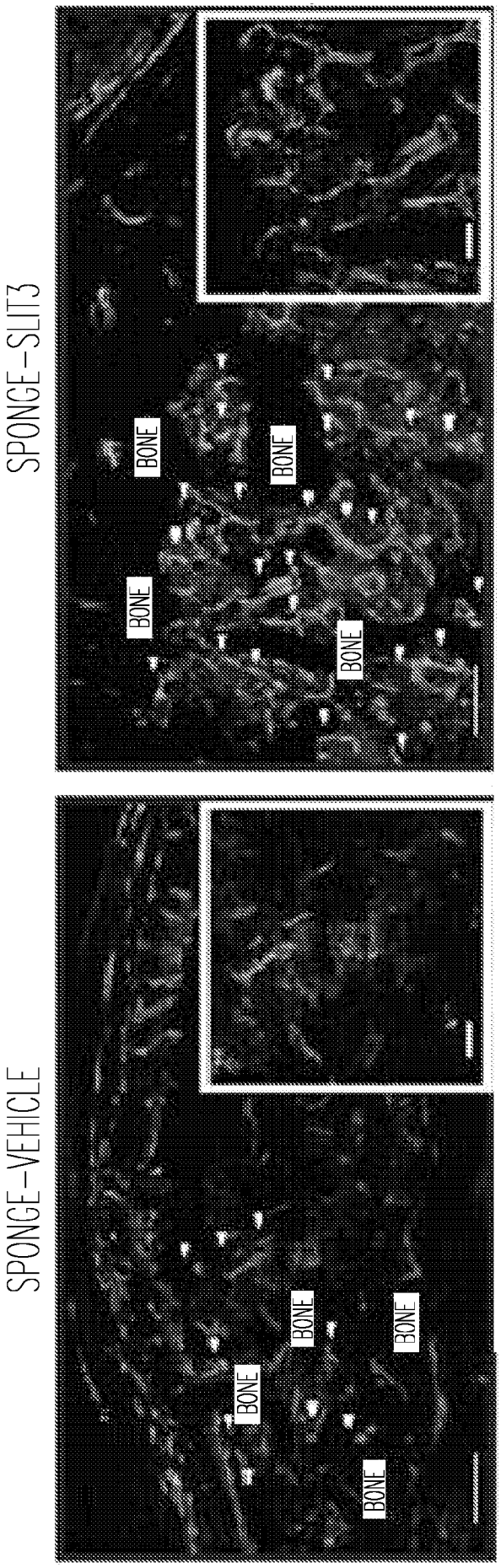
SPONGE-VEHICLE
SPONGE-SLIT3
BONE-FRACTURE CALLUS
BONE
BONE
BONE
BONE
BONE
BONE
CD31 Emcn

Fig. 6L

Fig. 6M

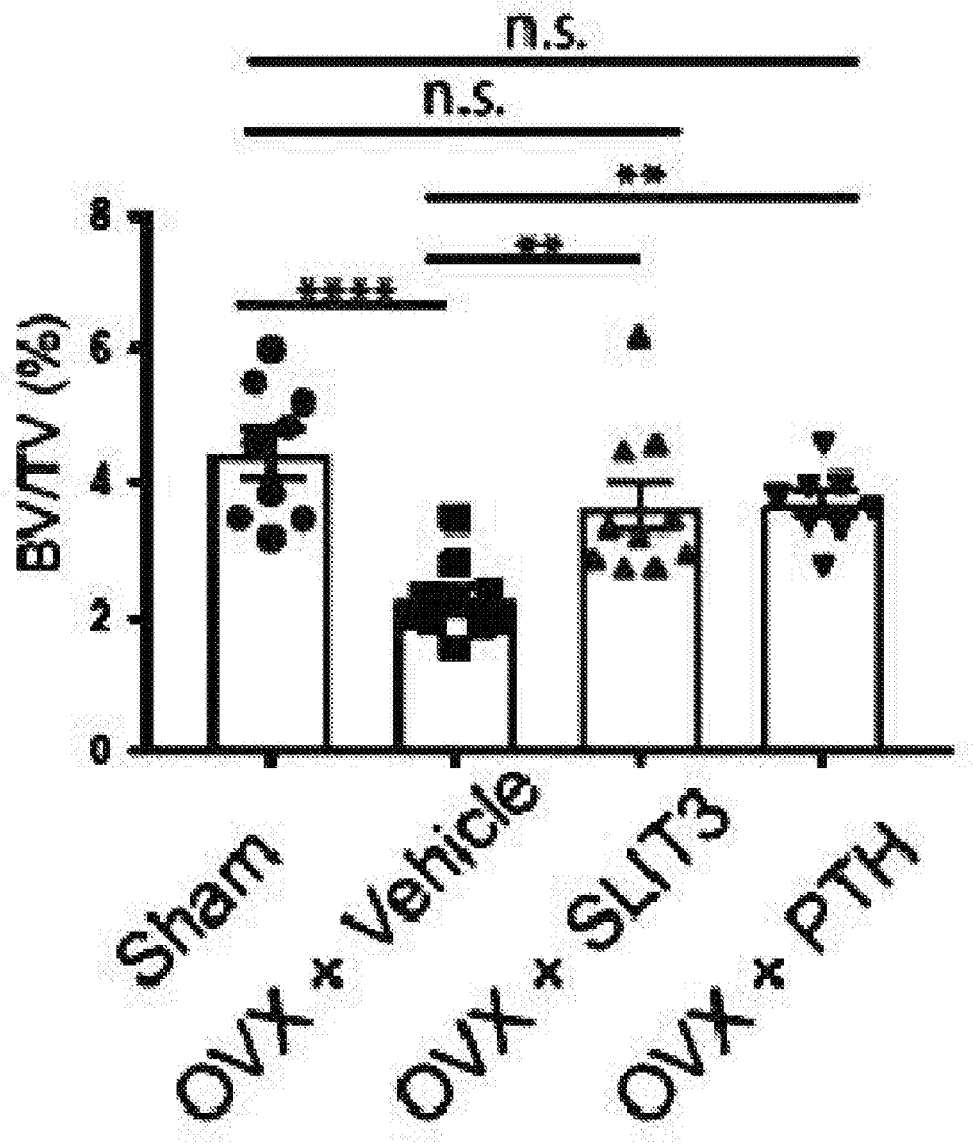

Fig. 6N

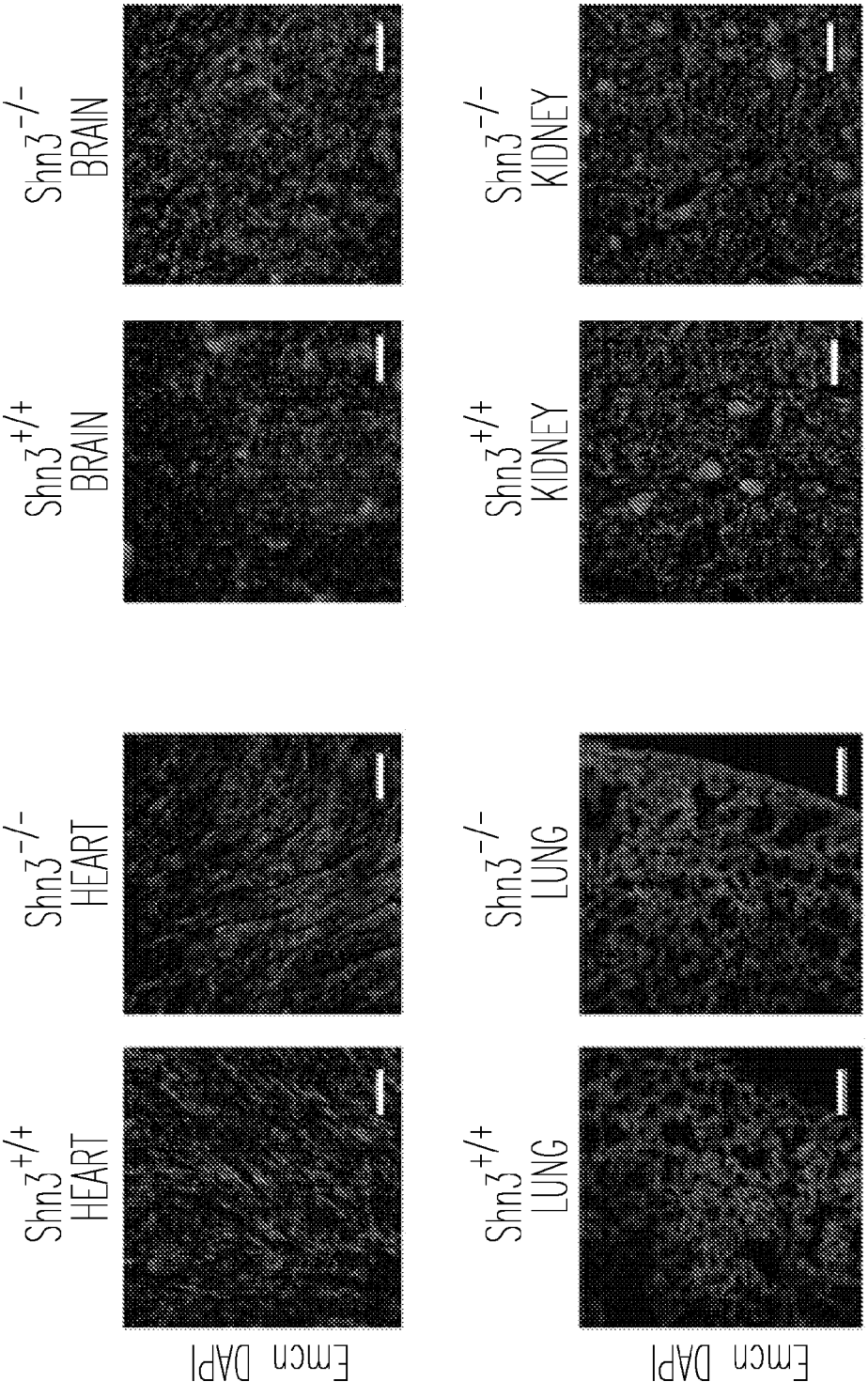
Shn3+/+ HEART
Shn3-/- HEART
Shn3+/+ BRAIN
Shn3-/- BRAIN
Shn3+/+ LUNG
Shn3-/- LUNG
Shn3+/+ KIDNEY
Shn3-/- KIDNEY
Emcn DAPI
Emcn DAPI

Fig. 7A

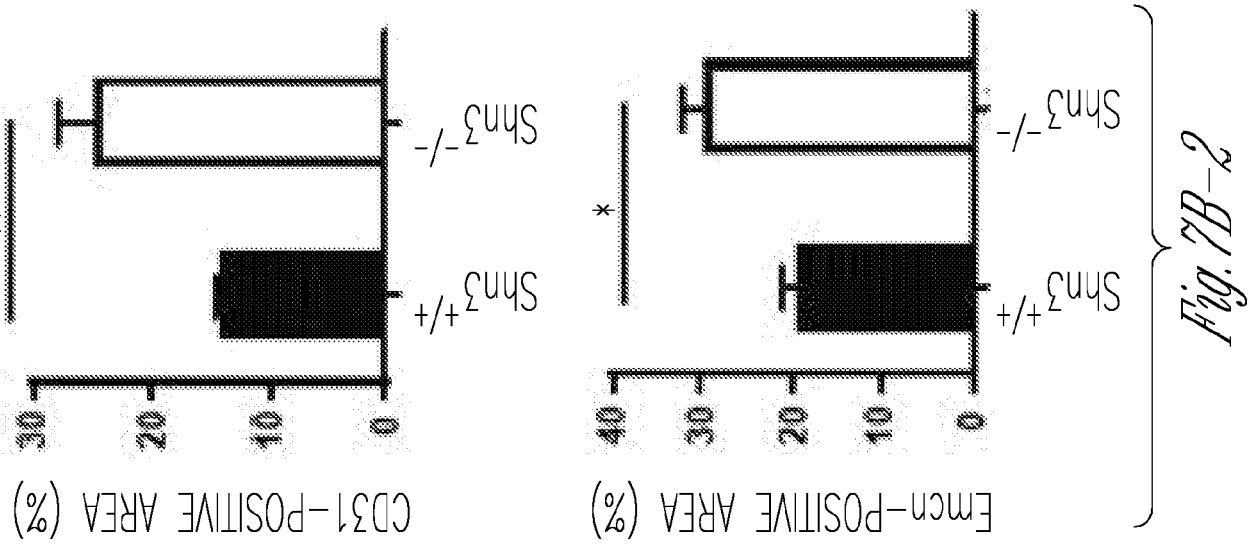

Fig. 7B-2

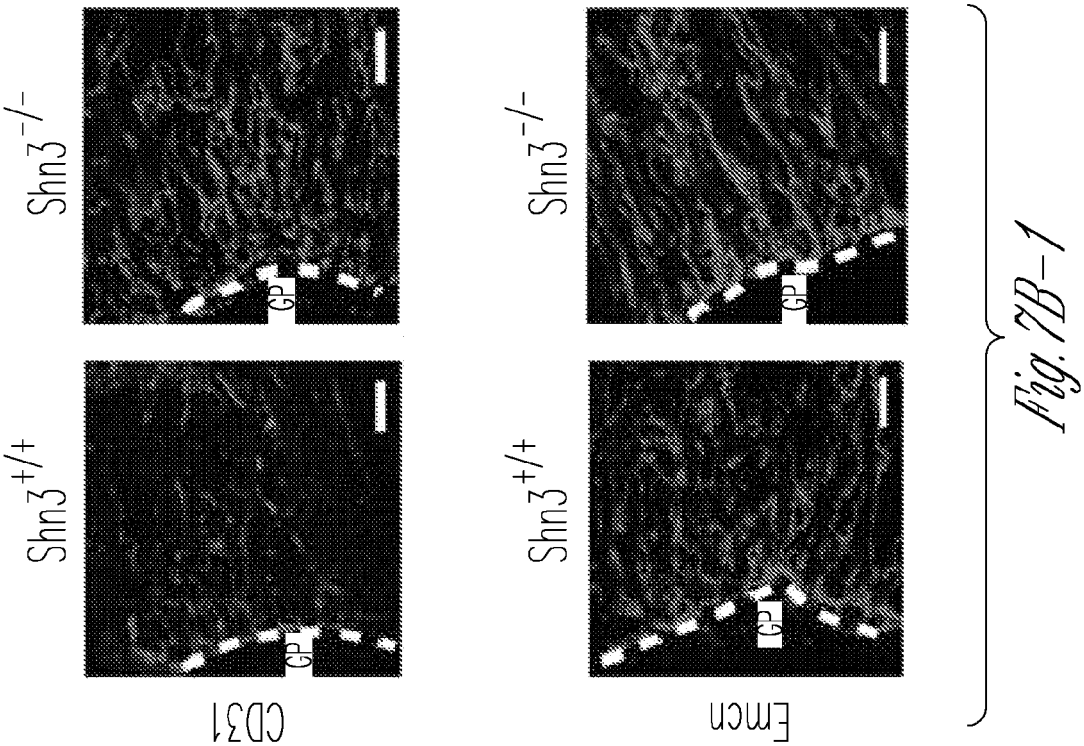

Fig. 7B-1

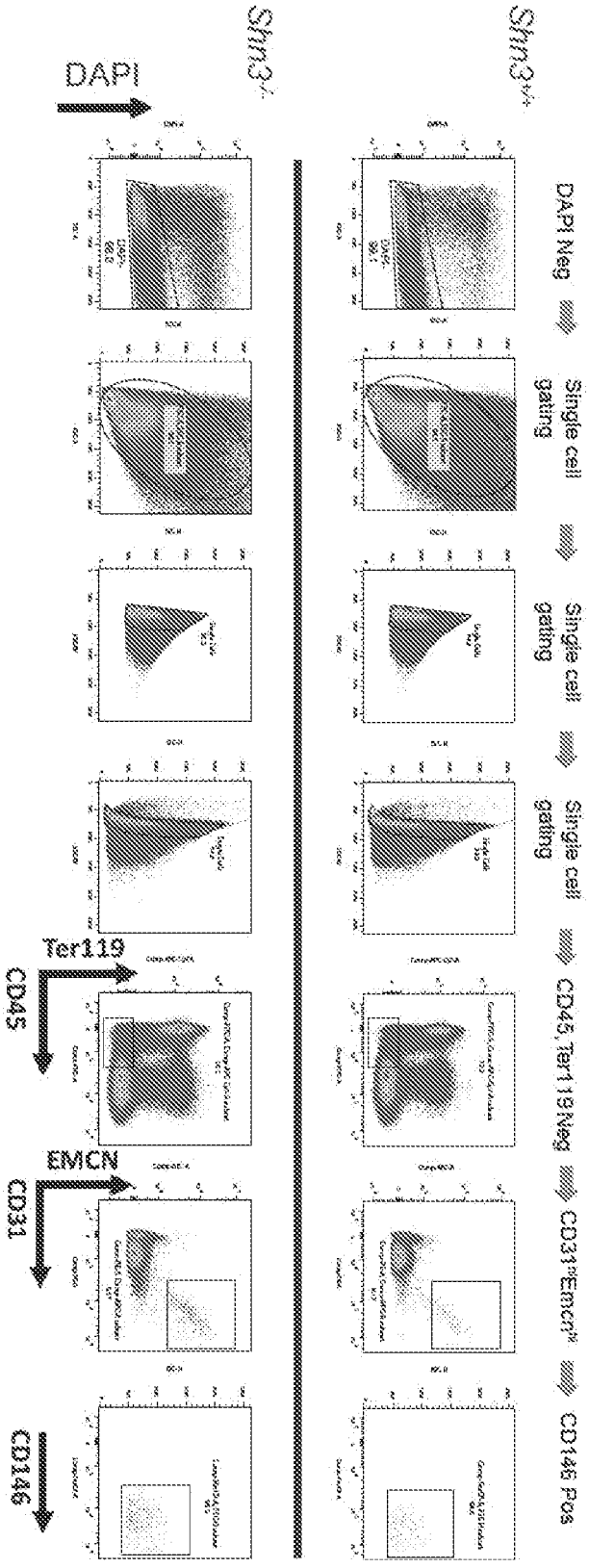
Shn3-/-
Shn3+/+
DAPI
DAPI Neg
Single cell gating
Single cell gating
Single cell gating
CD45,Ter119Neg
CD31+Emcn+
CD146 Pos
Ter119
CD45
EMCN
CD31
CD146

FIG. 7C

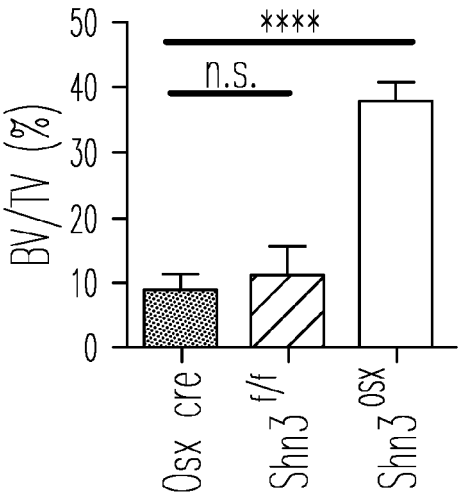

Fig. 8A-1

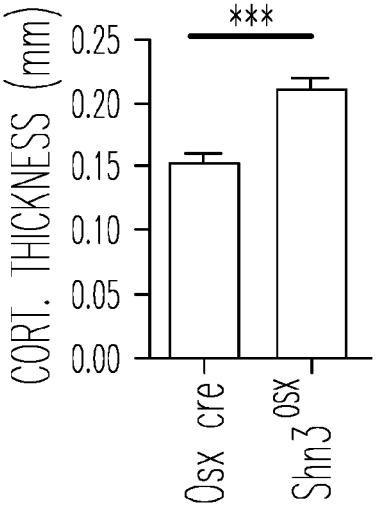

Fig. 8A-2

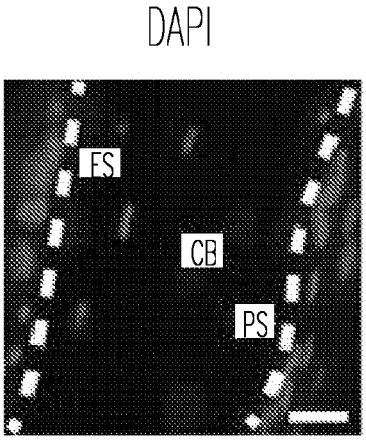

Dmp1-cre mTmG

Fig. 8B-1

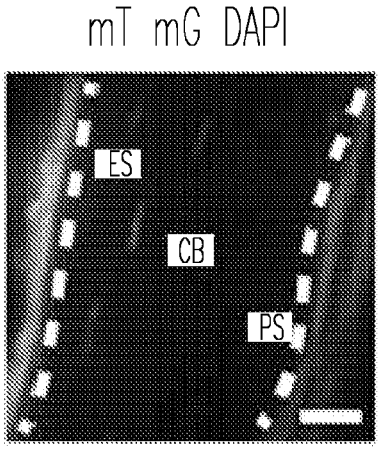

Dmp1-cre mTmG

Fig. 8B-2

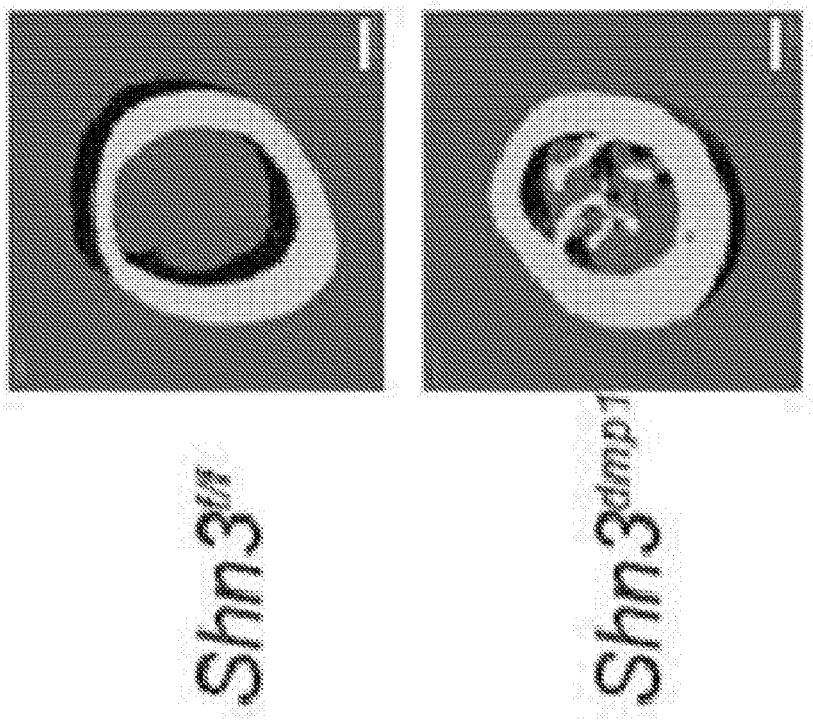

Fig. 8C-1

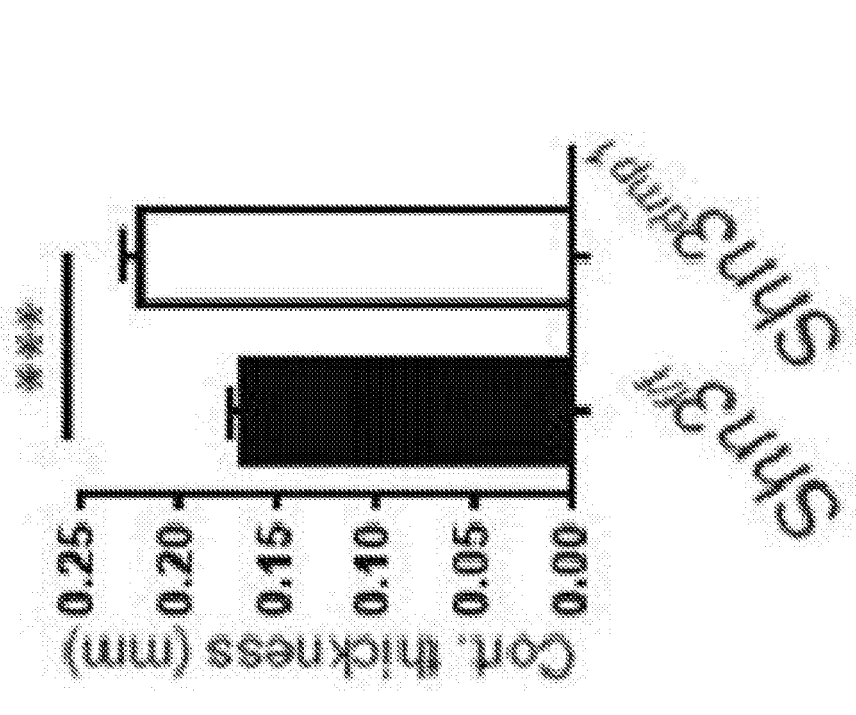

Fig. 8C-2

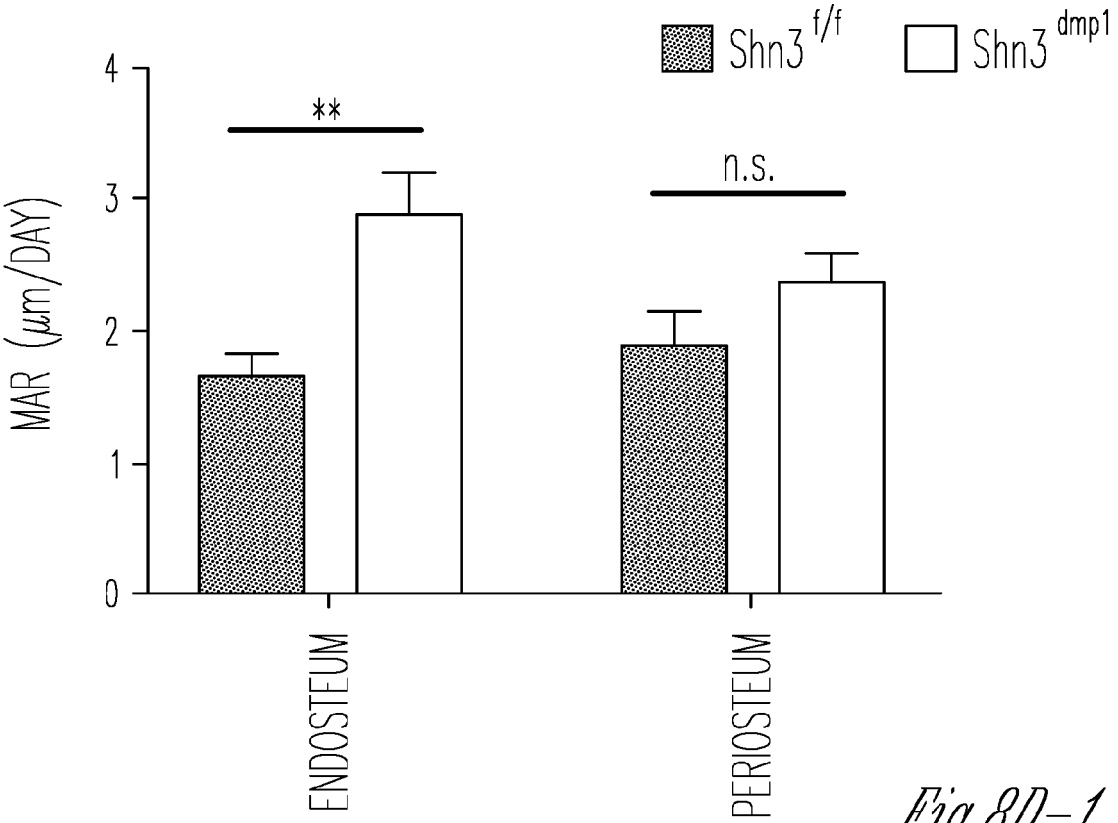

Fig. 8D-1

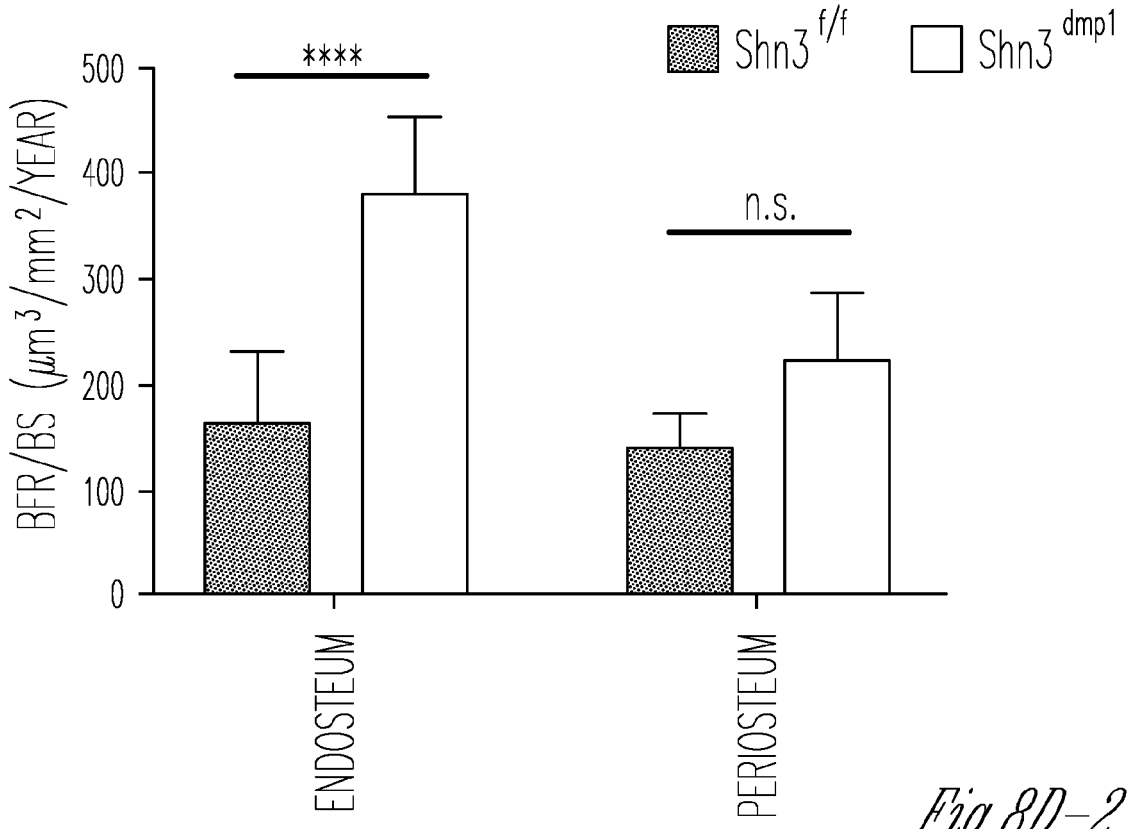

Fig. 8D-2

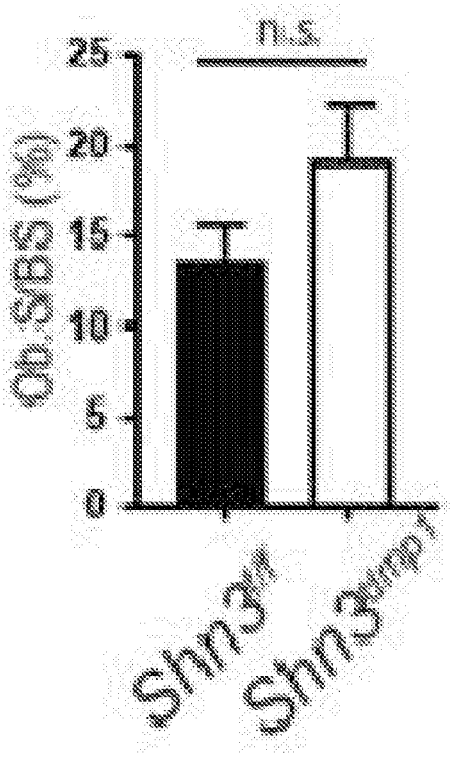

Fig. 8E-1

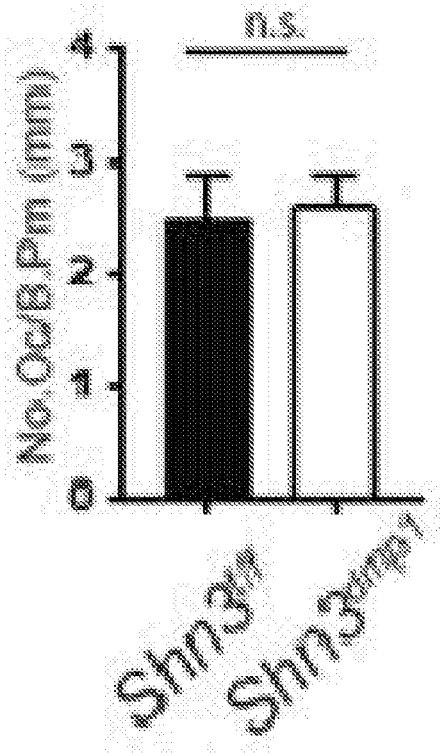

Fig. 8E-2

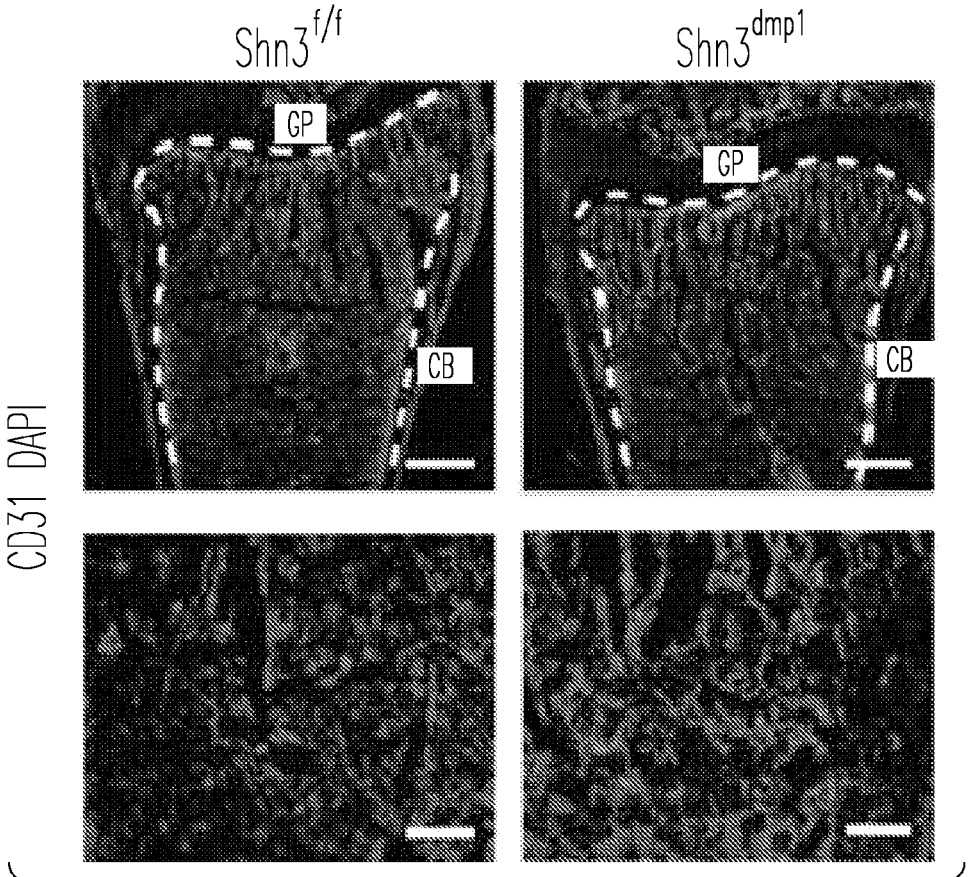

Fig. 8F

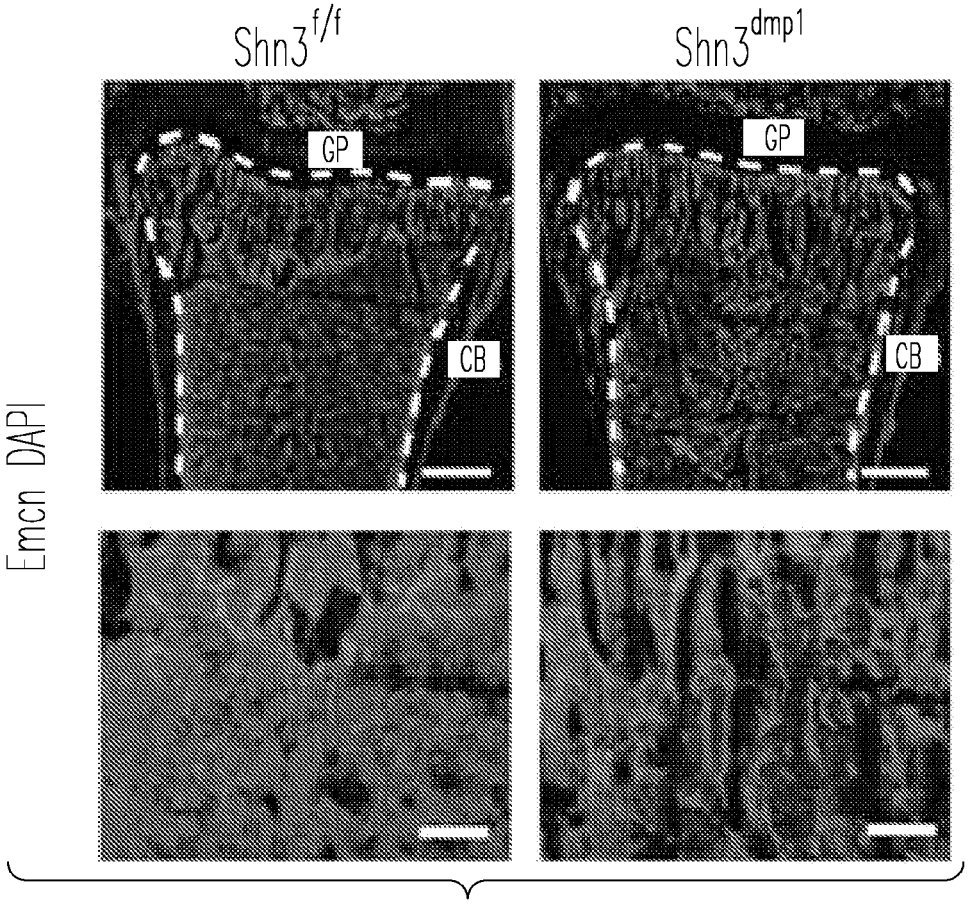

Fig. 8G

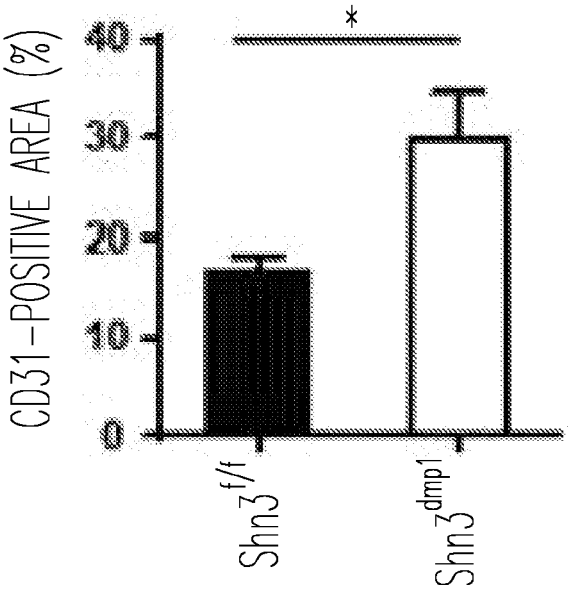

Fig. 8H-1

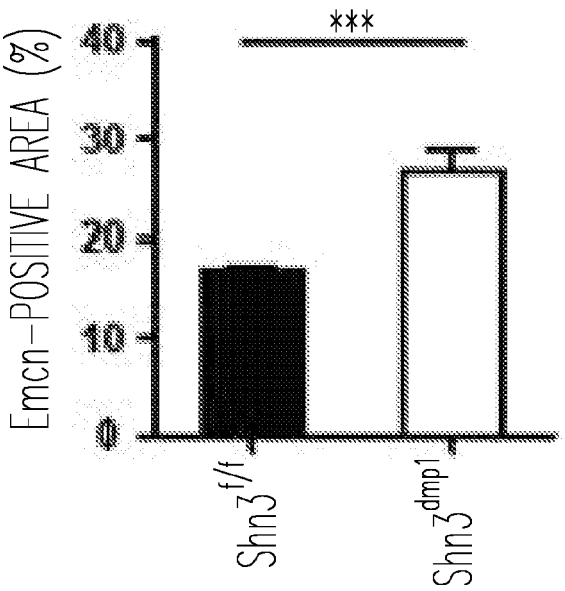

Fig. 8H-2

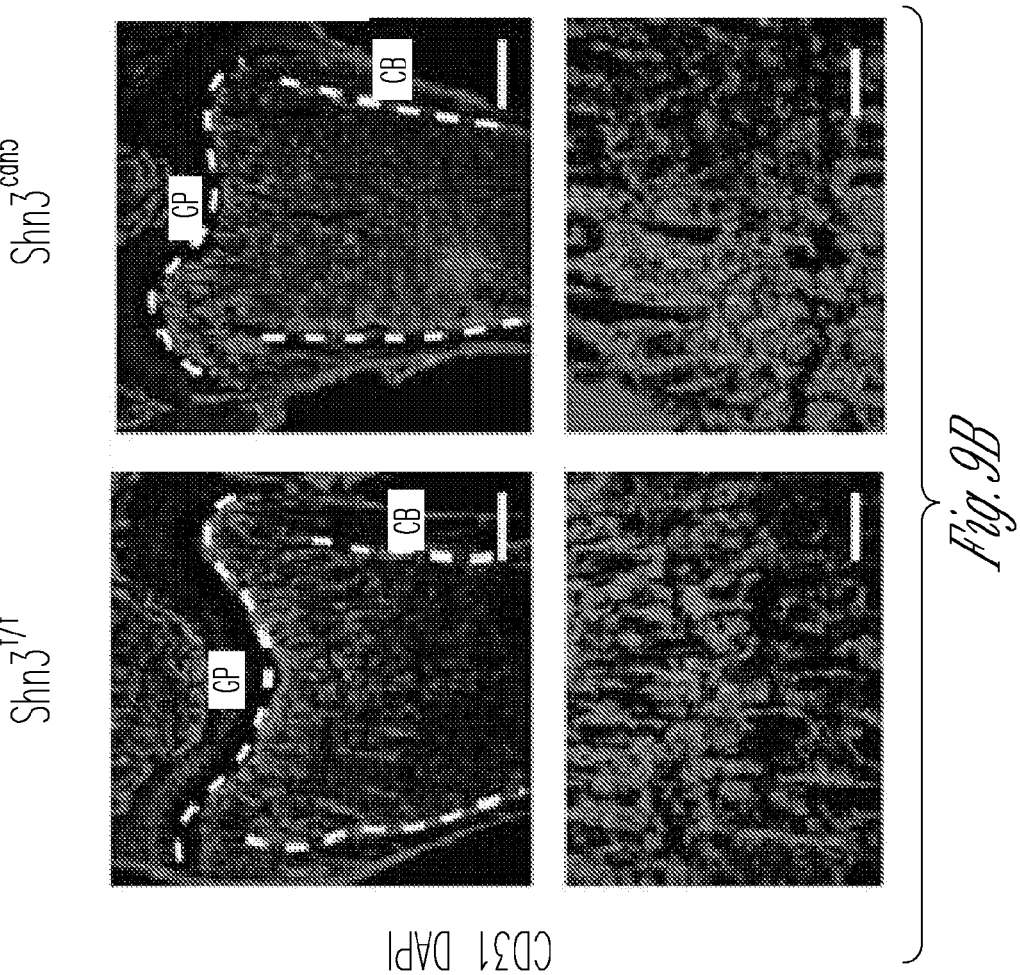
Shn3f/f
Shn3cdh5
CP
CB
CD31 DAPI

Fig. 9B

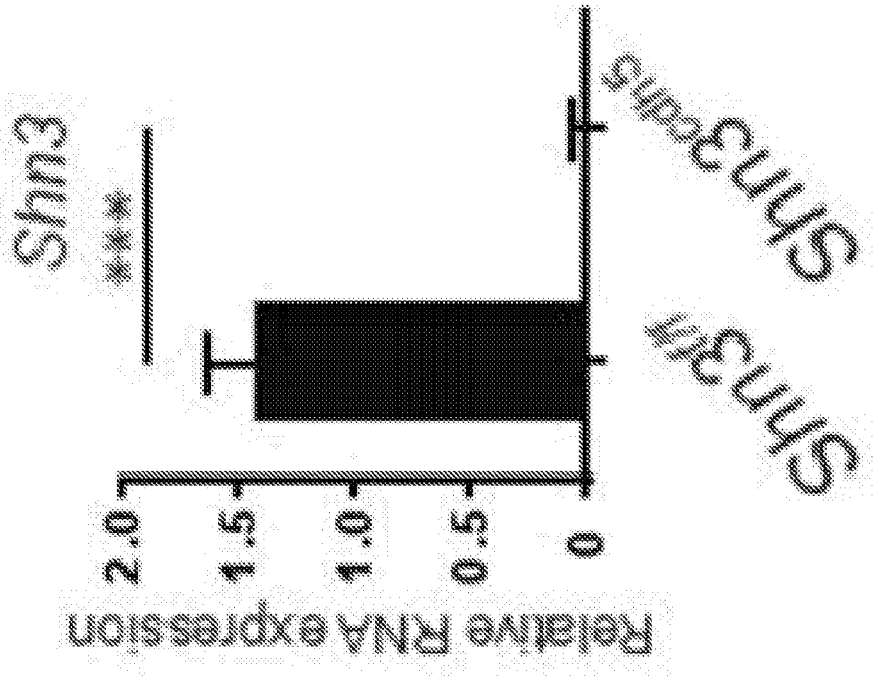
Shn3
***
Relative RNA expression
2.0
1.5
1.0
0.5
0
Shn3f/f
Shn3cdh5

Fig. 9A

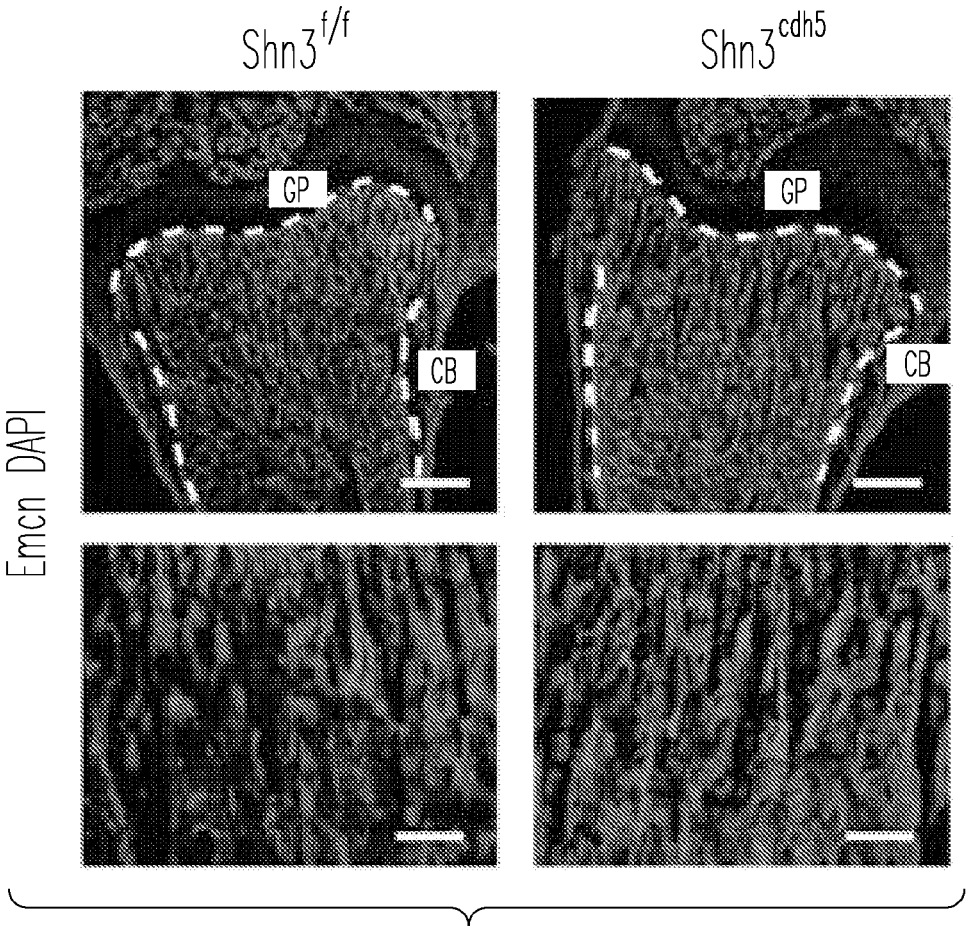

Fig. 9C

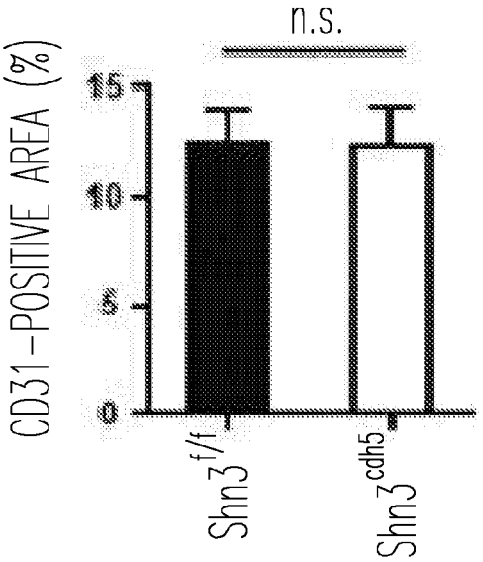

Fig. 9D-1

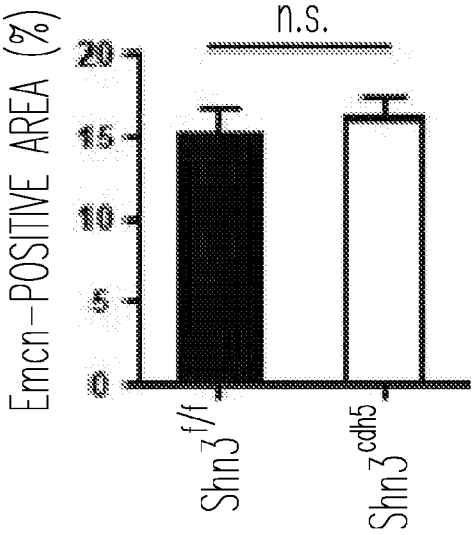

Fig. 9D-2

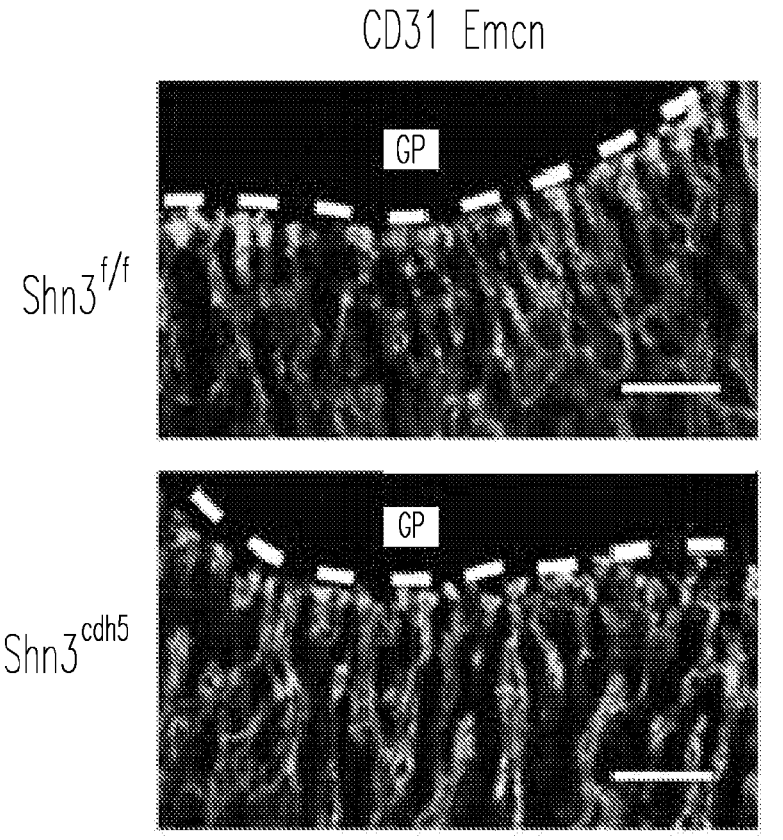

Fig. 9E

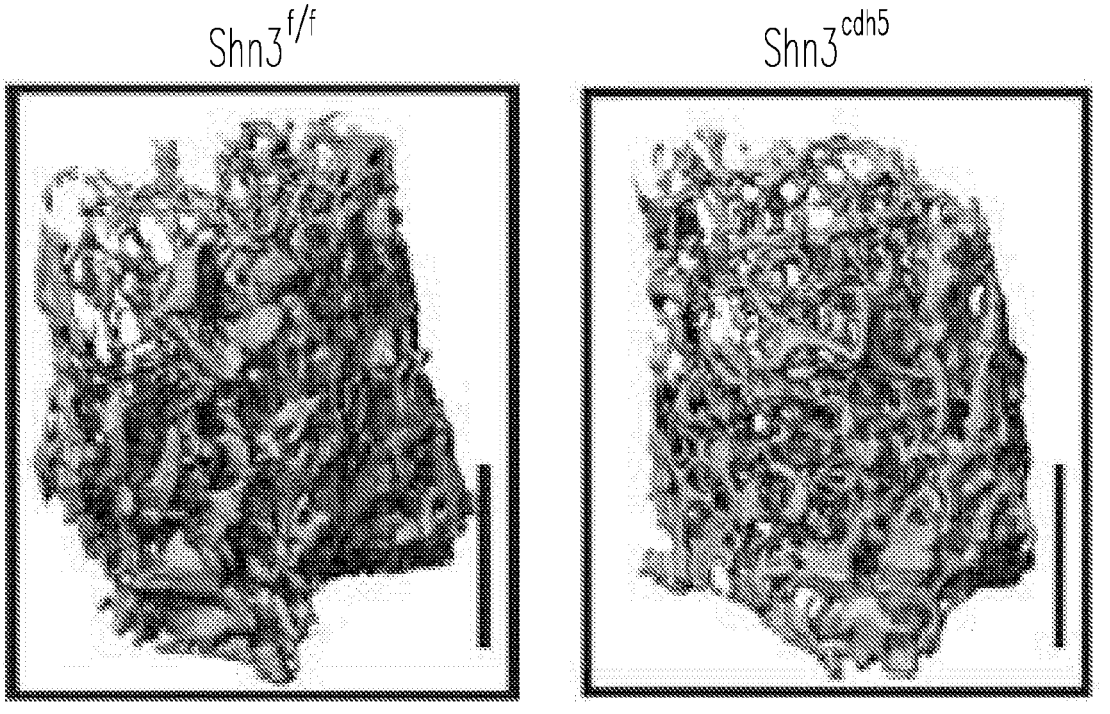

Fig. 9F

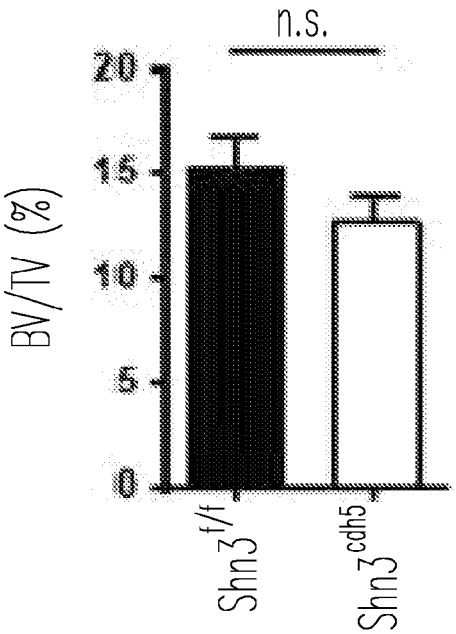
n.s.
BV/TV (%)
20
15
10
5
0
Shn3f/f
Shn3cdh5

Fig. 9C

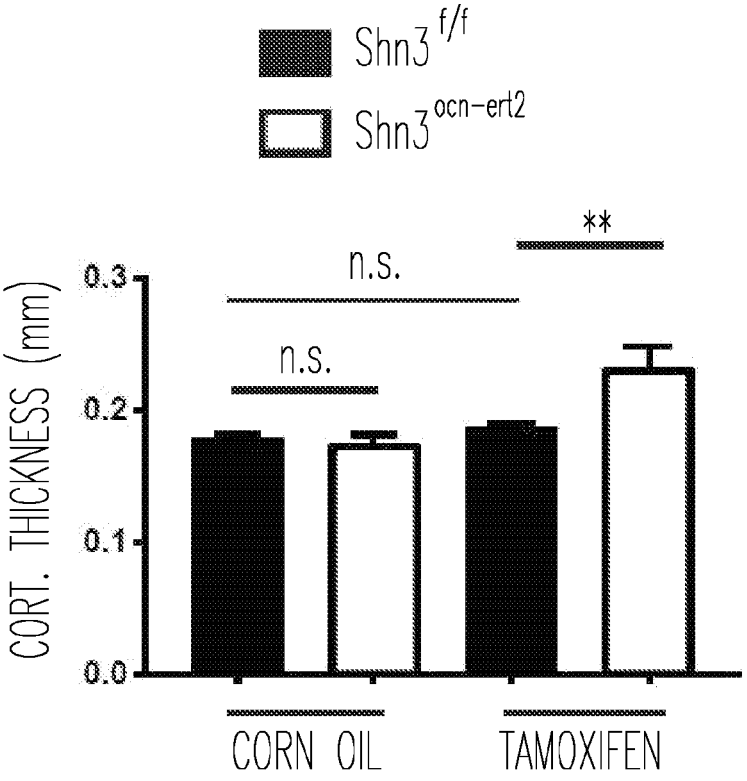
Shn3 f/f
Shn3 ocn-ert2
**
n.s.
n.s.
CORT. THICKNESS (mm)
0.3
0.2
0.1
0.0
CORN OIL
TAMOXIFEN

Fig. 10

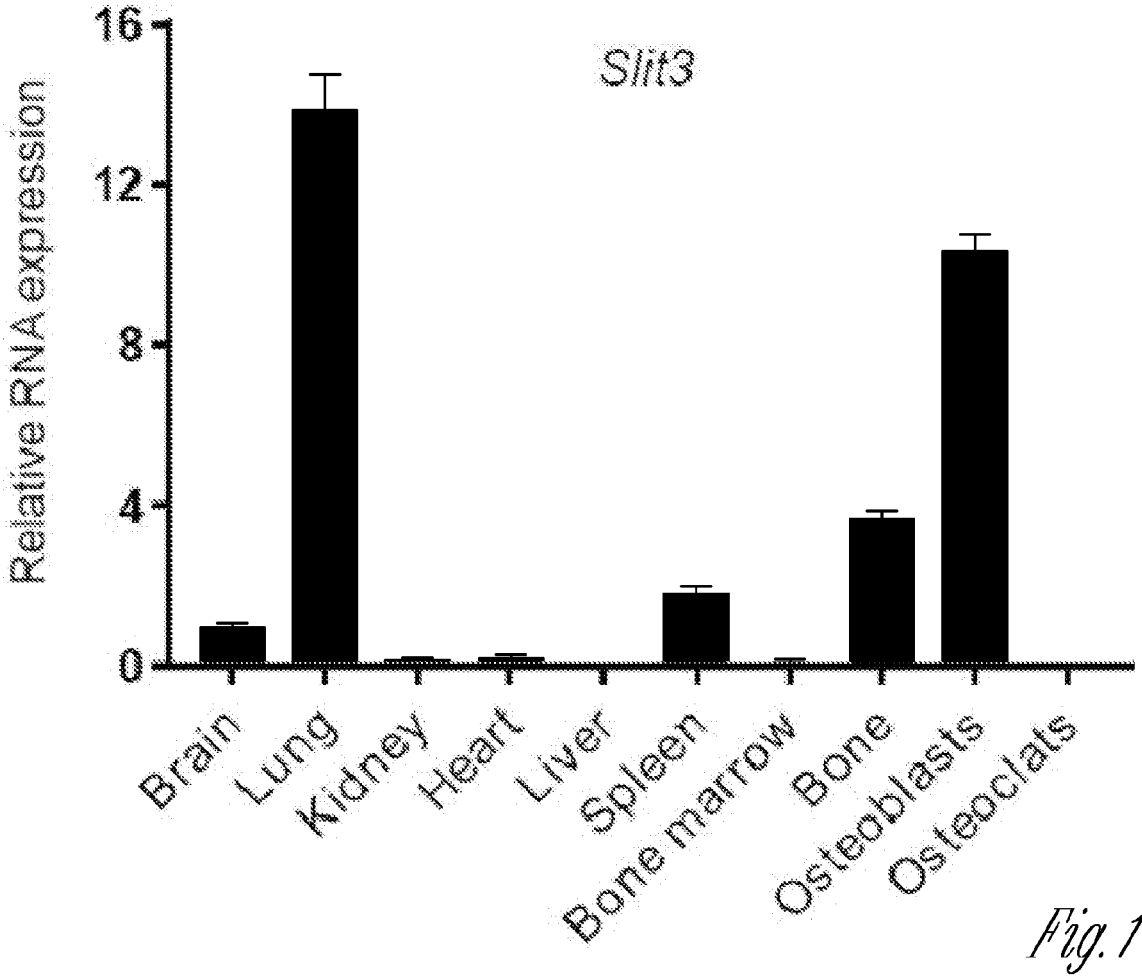

Fig. 11A

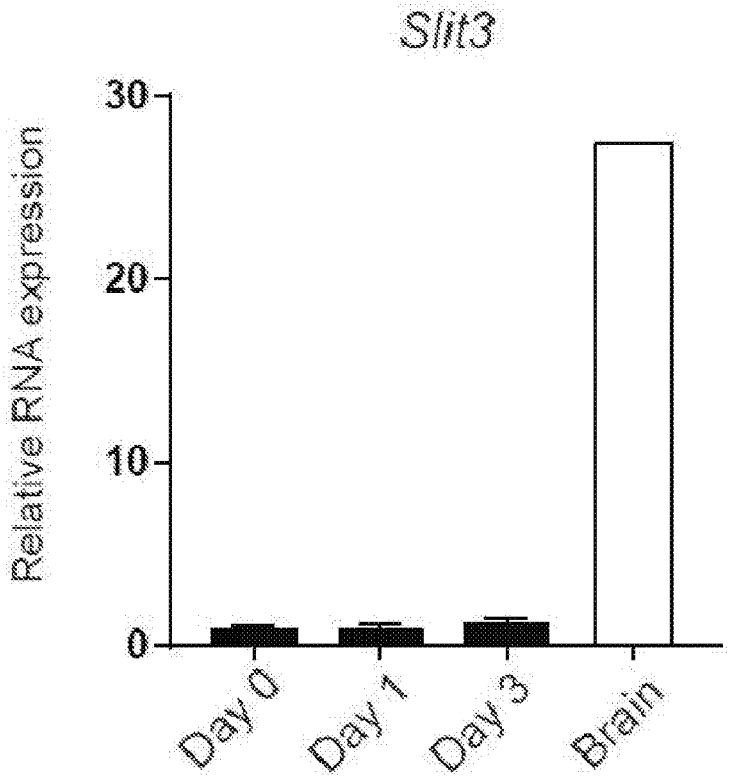

Fig. 11B

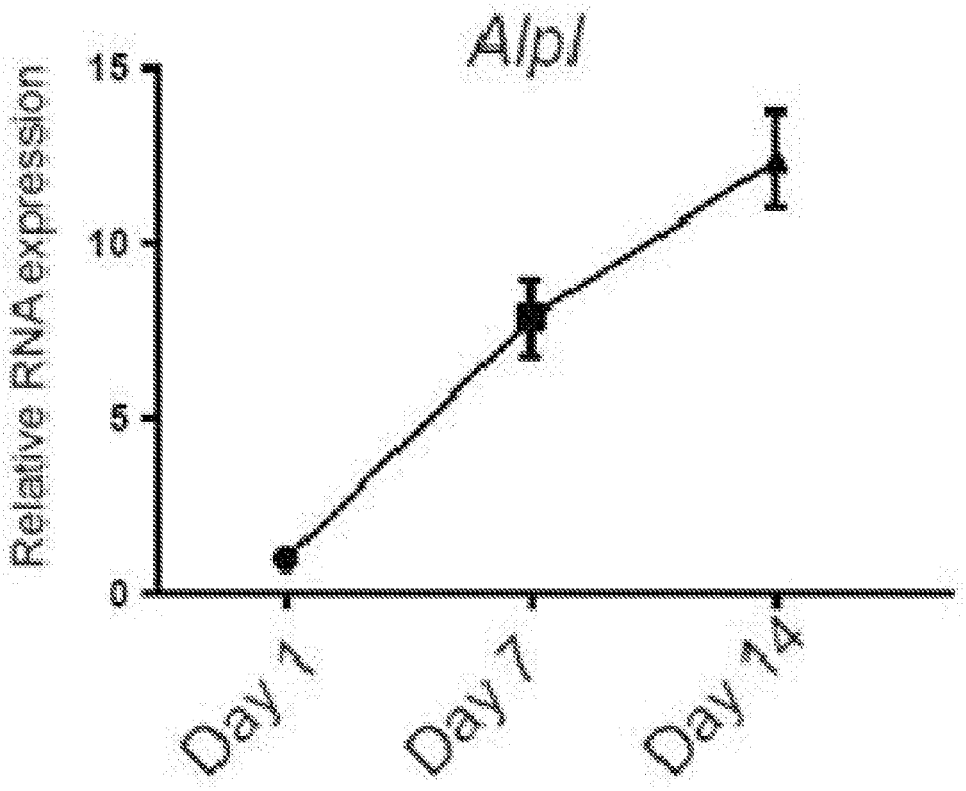

Fig. 11C-1

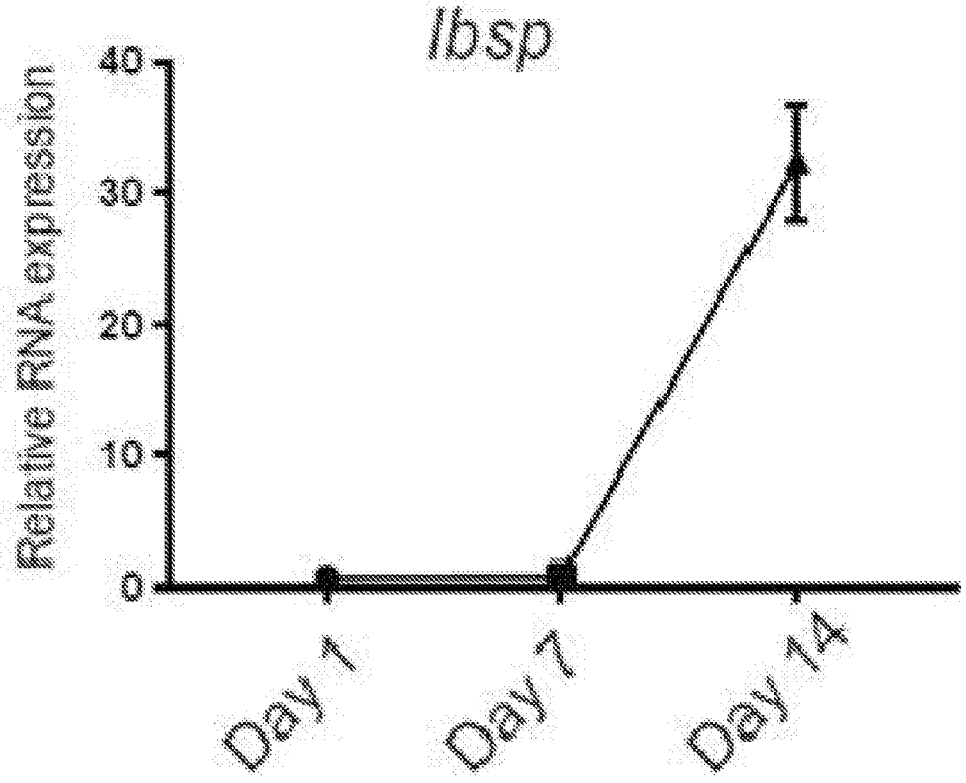

Fig. 11C-2

Fig. 11C-3

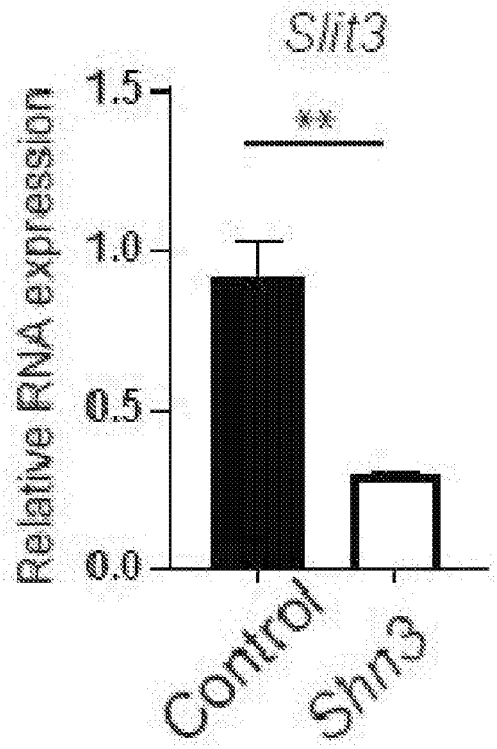

Fig. 11D-1

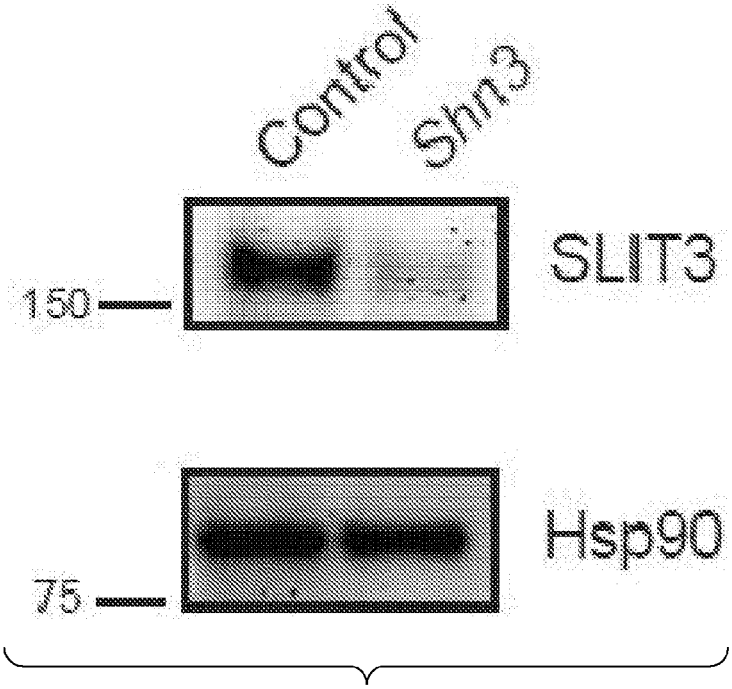

Fig. 11D-2

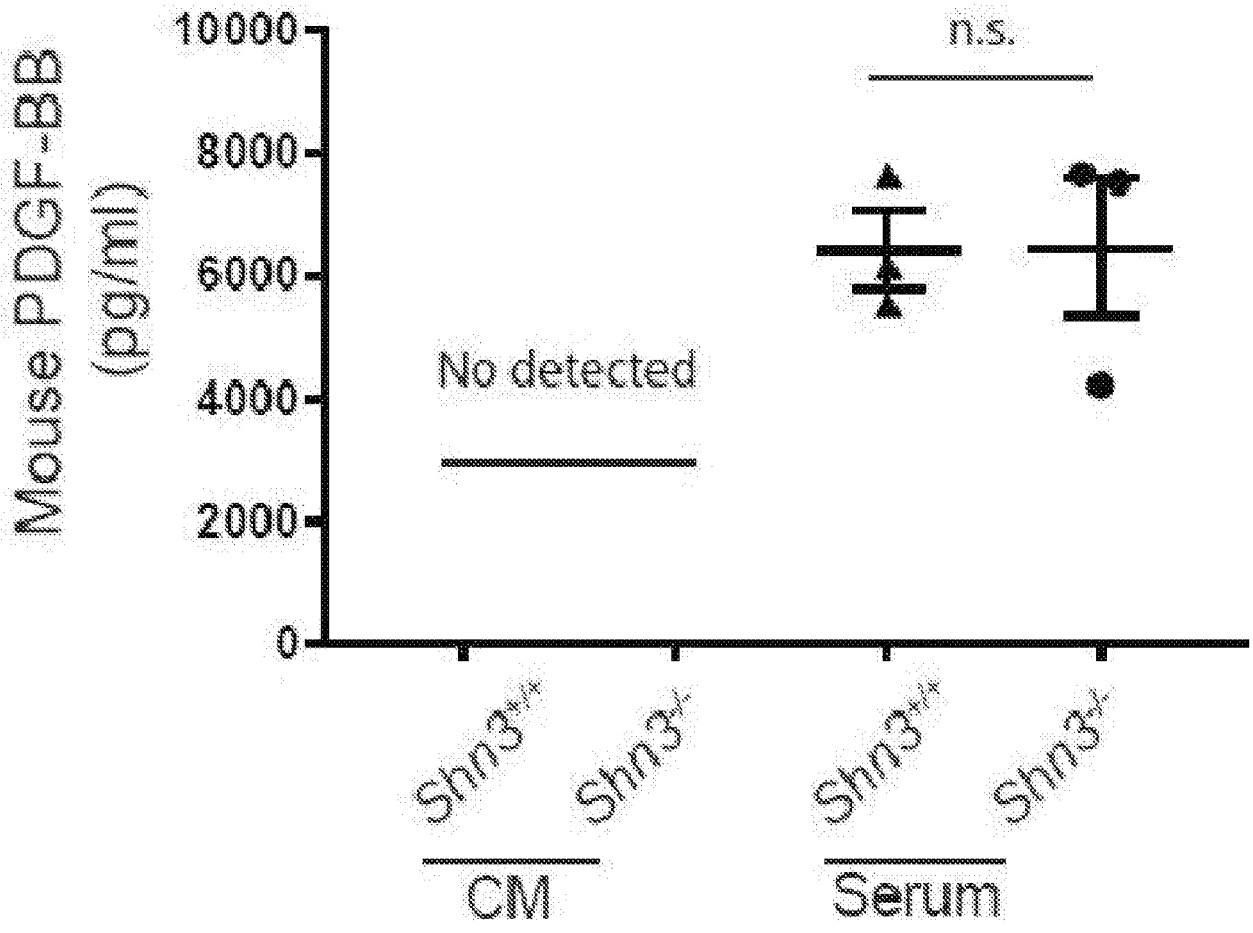

Fig. 11E

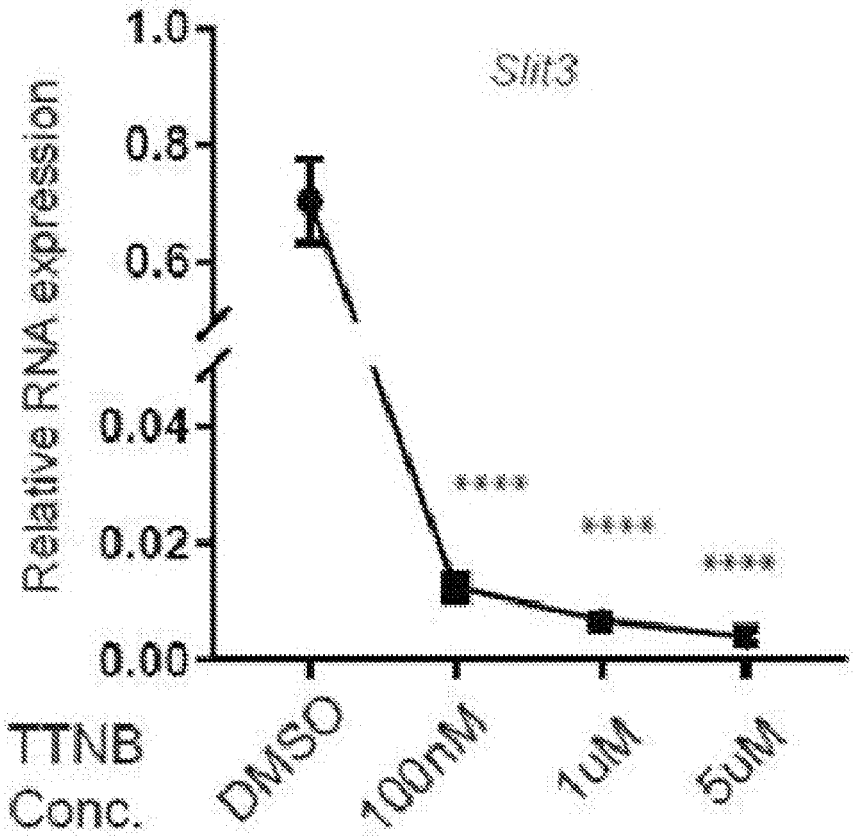
Slit3
Relative RNA expression
1.0
0.8
0.6
0.04
0.02
0.00
****
****
****
TTNB Conc.
DMSO
100nM
1uM
5uM

Fig. 11F

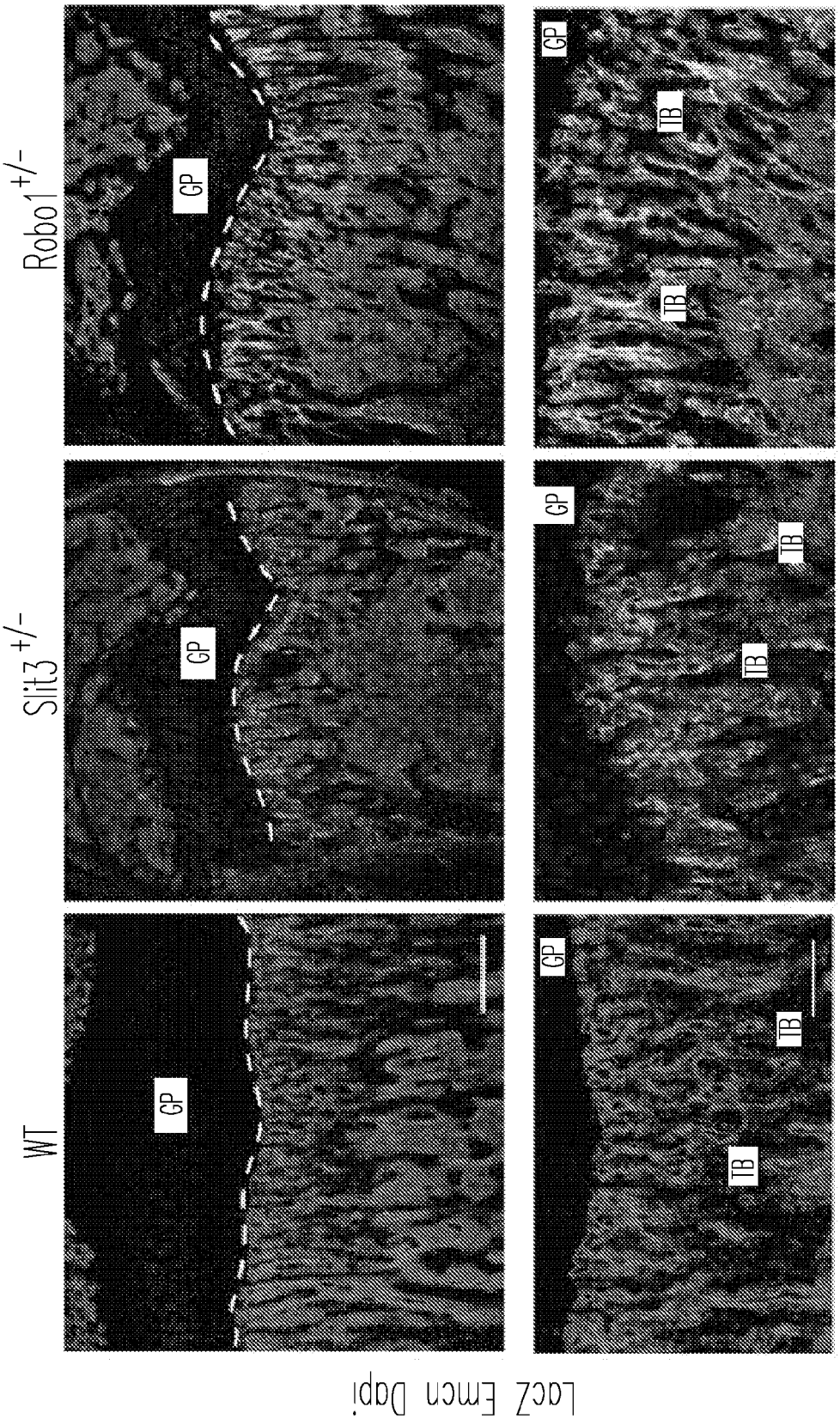

Fig. 12

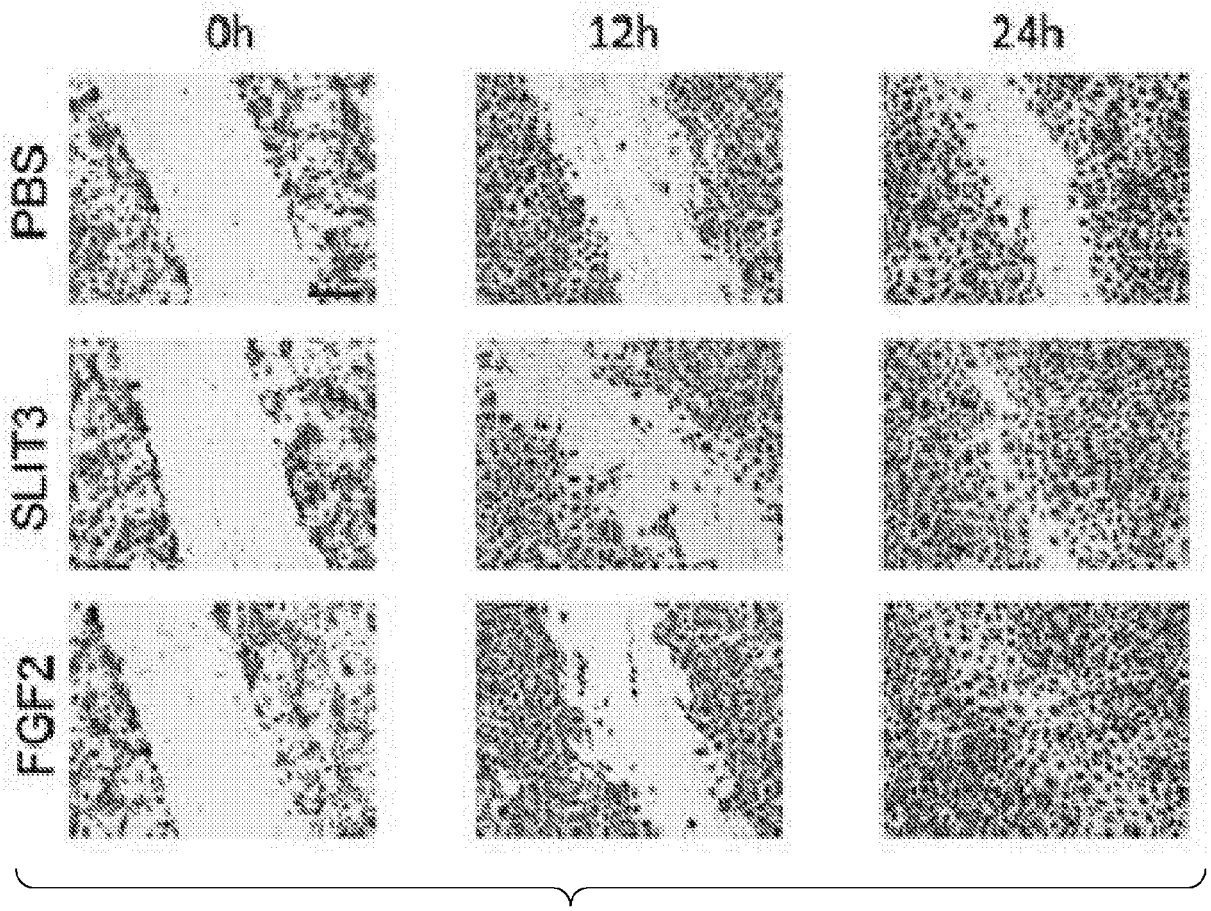

Fig. 13A-1

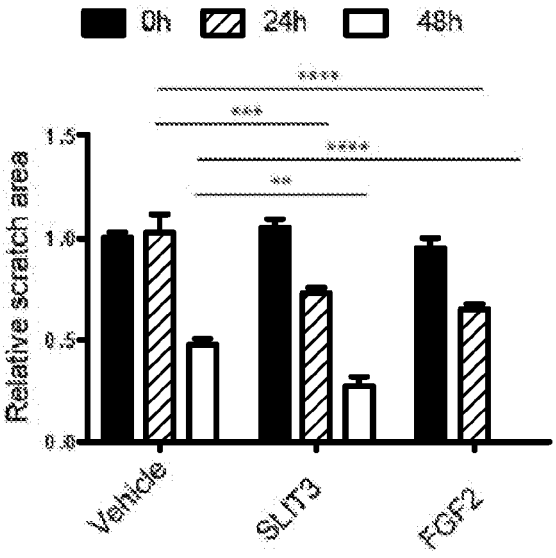

Fig. 13A-2

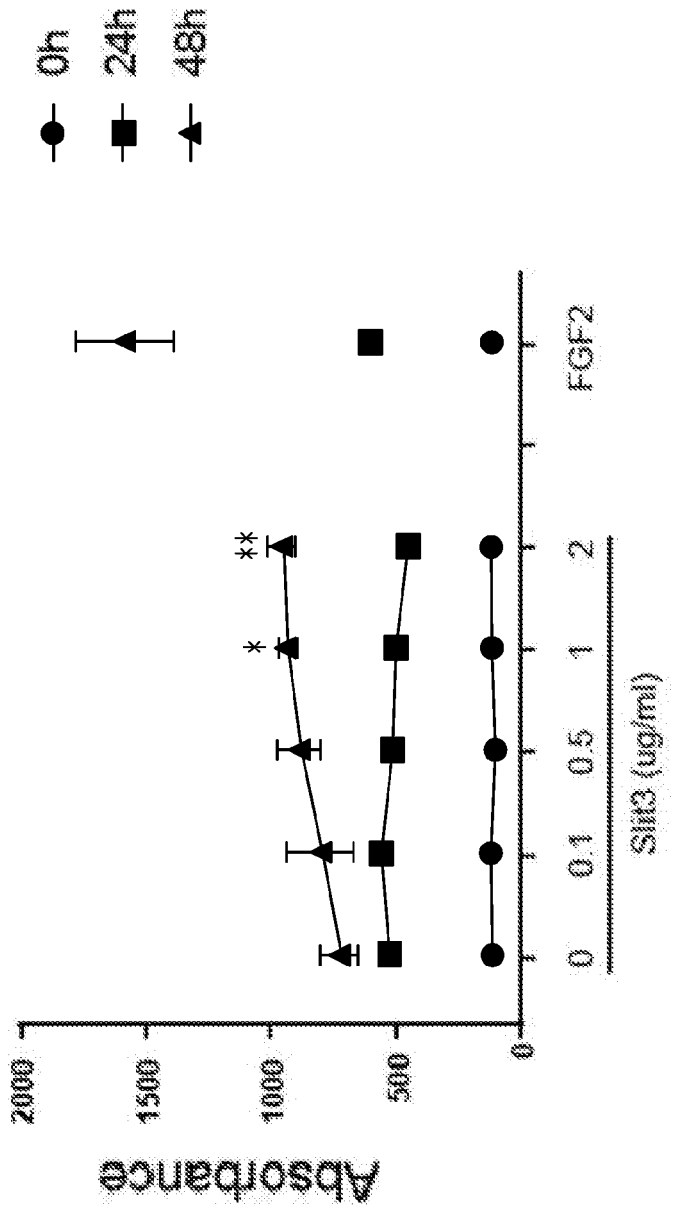
0h
24h
48h
Absorbance
2000
1500
1000
500
0
FGF2
Slit3 (ug/ml)
0
0.1
0.5
1
2
*
**

Fig. 13B

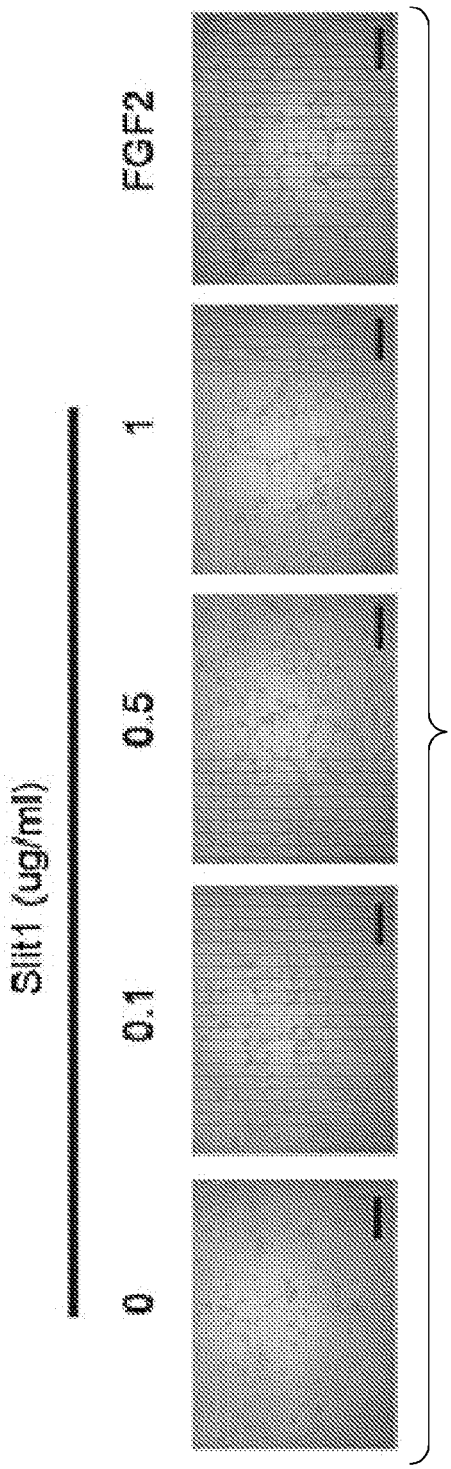

Fig. 14A-1

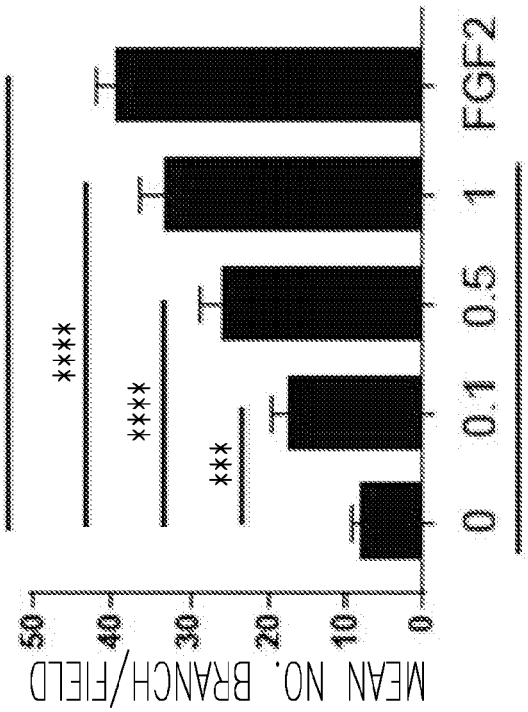

Fig. 14A-2

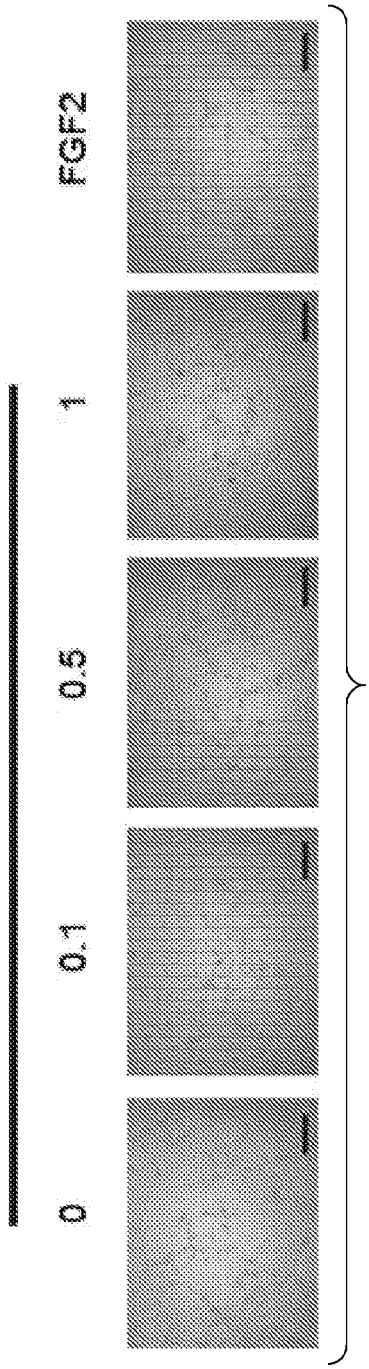

Fig. 14B-1

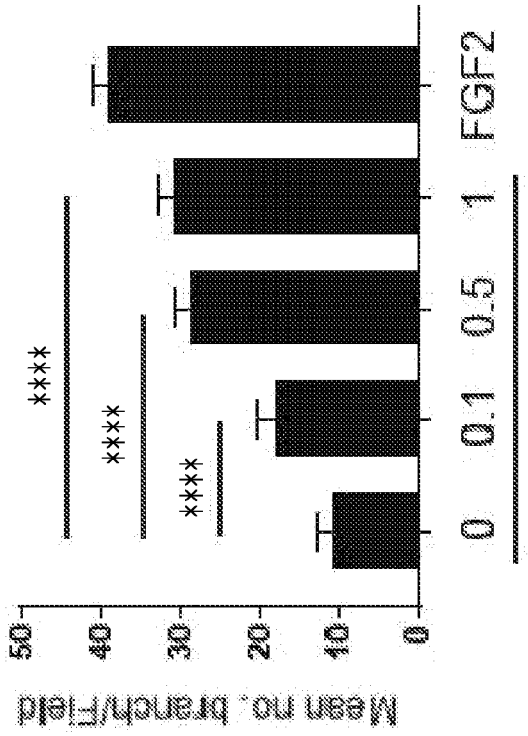

Fig. 14B-2

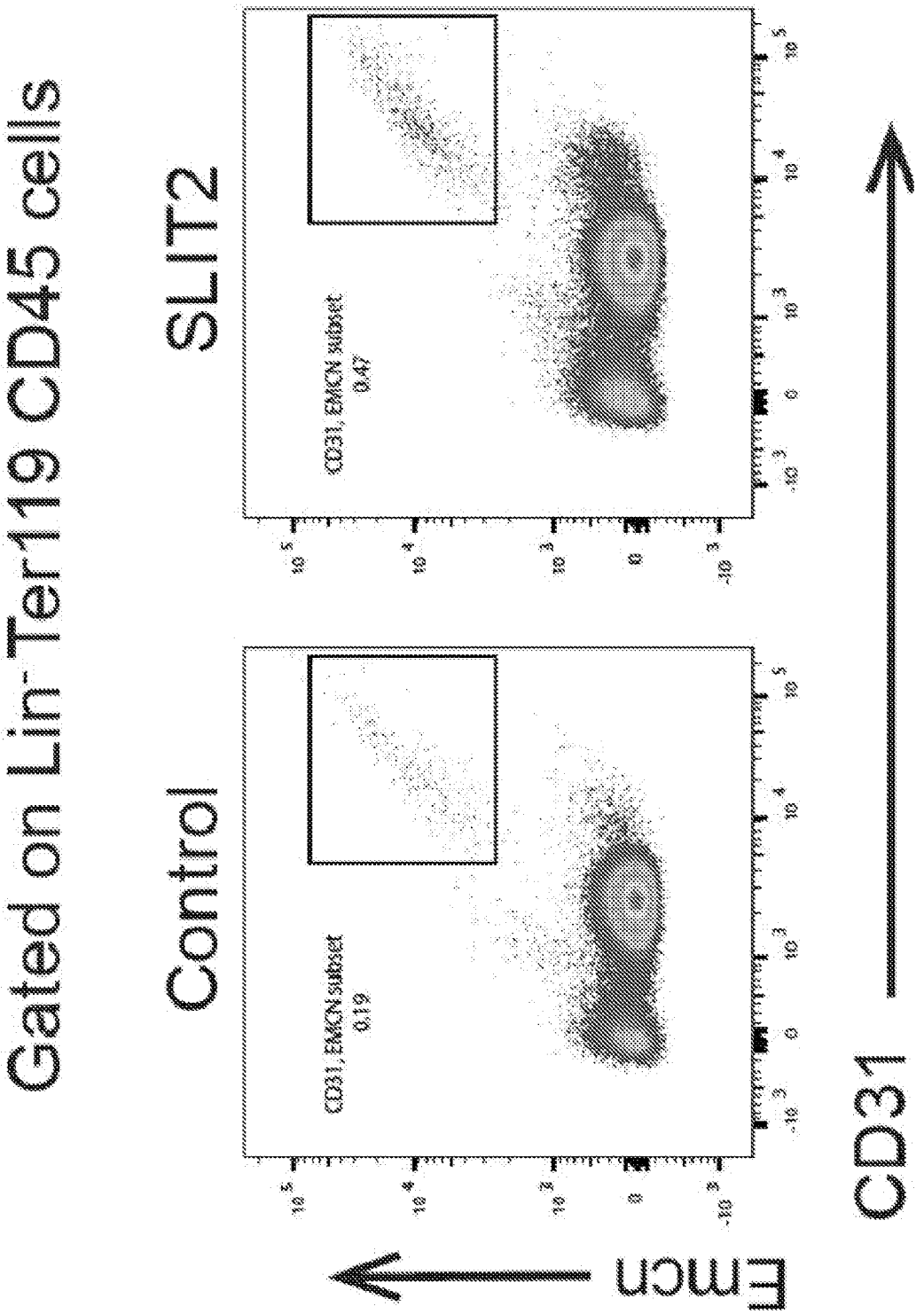
Gated on Lin- Ter119 CD45 cells
Control
SLIT2
CD31, EMCN subset
0.19
CD31, EMCN subset
0.47
Emcn
CD31

Fig. 14C-1

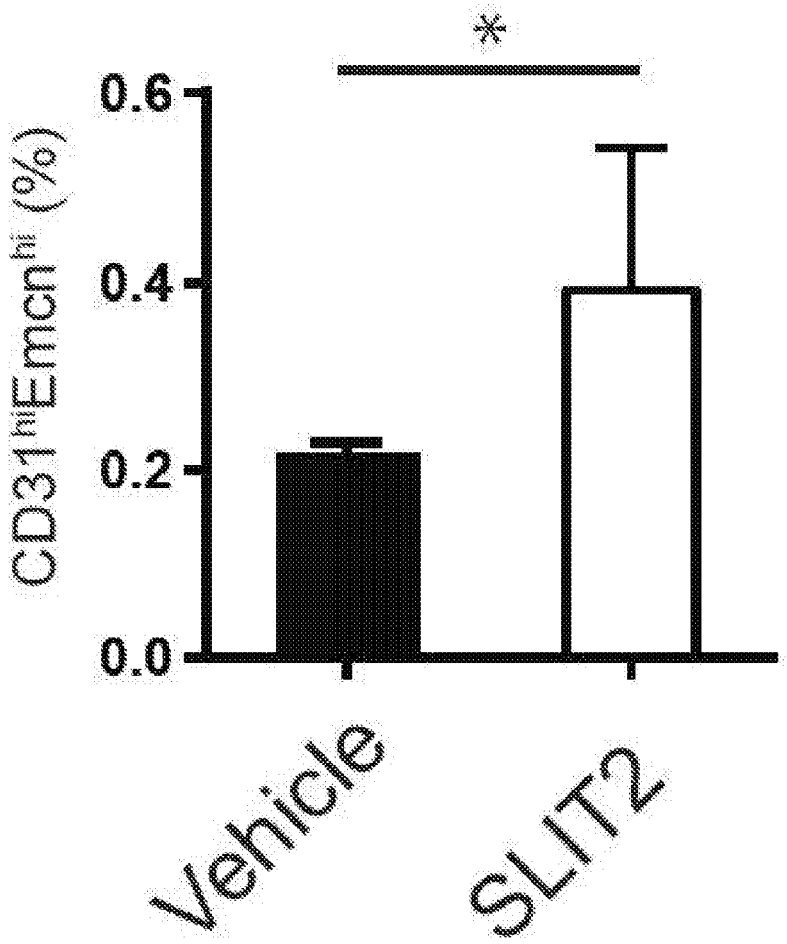

Fig. 14C-2

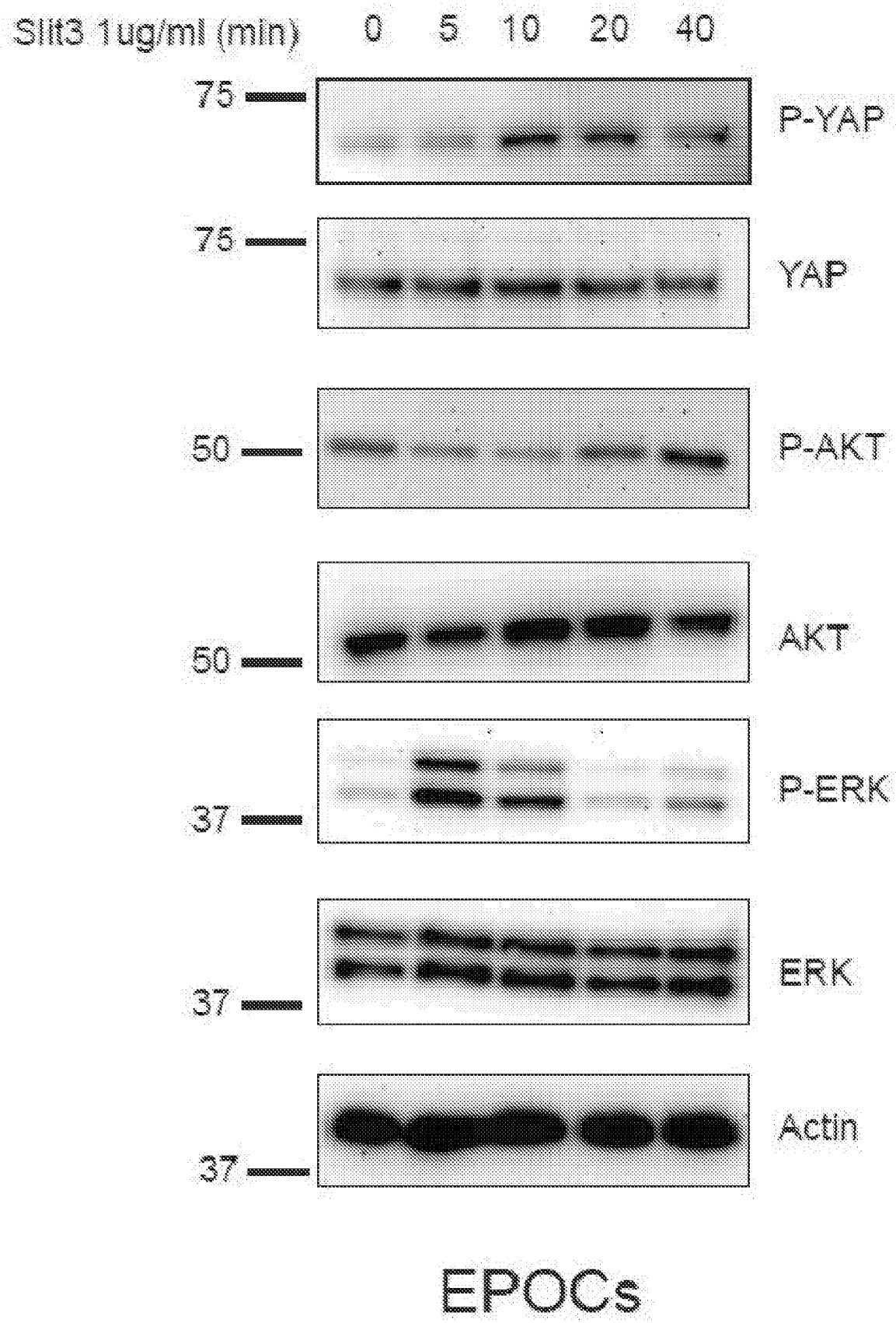
Slit3 1ug/ml (min)
0
5
10
20
40
75
P-YAP
75
YAP
50
P-AKT
50
AKT
37
P-ERK
37
ERK
37
Actin
EPOCs

Fig. 15

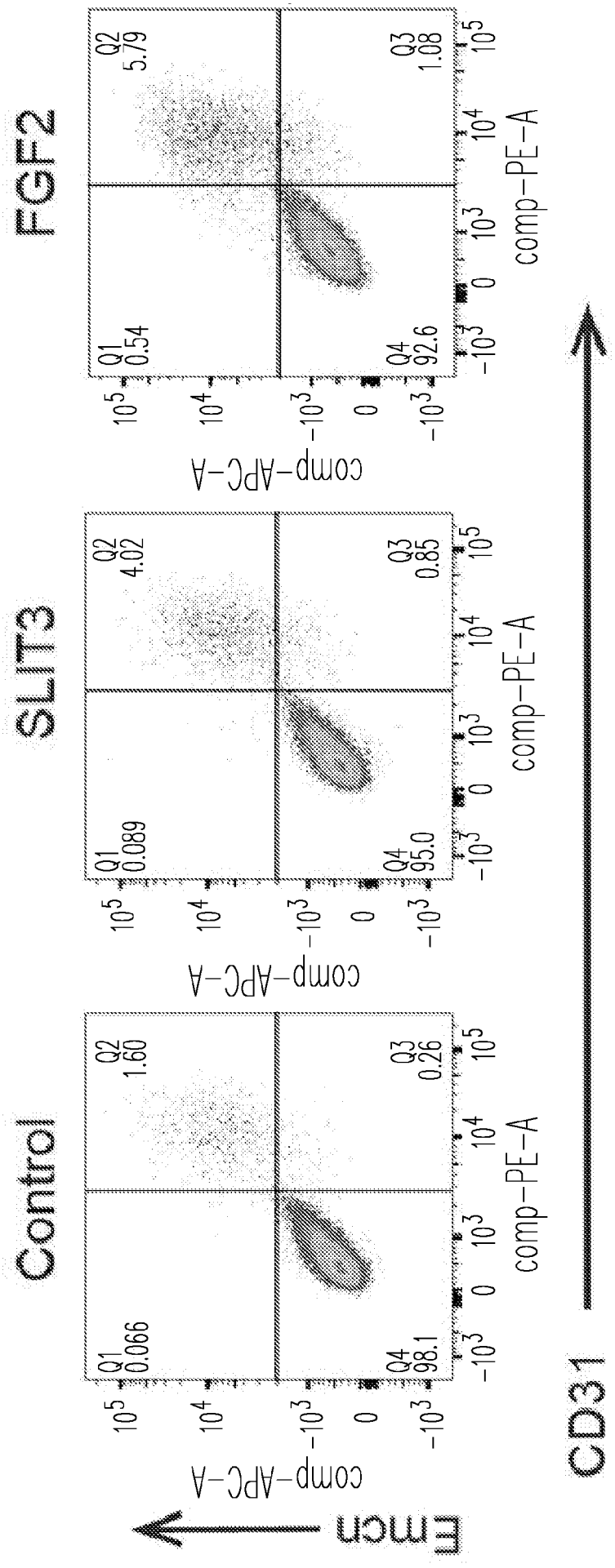
Control
SLIT3
FGF2
Q1 0.066
Q2 1.60
Q3 0.26
Q4 98.1
Q1 0.089
Q2 4.02
Q3 0.85
Q4 95.0
Q1 0.54
Q2 5.79
Q3 1.08
Q4 92.6
comp-APC-A
comp-PE-A
emcn
CD31

Fig. 16A

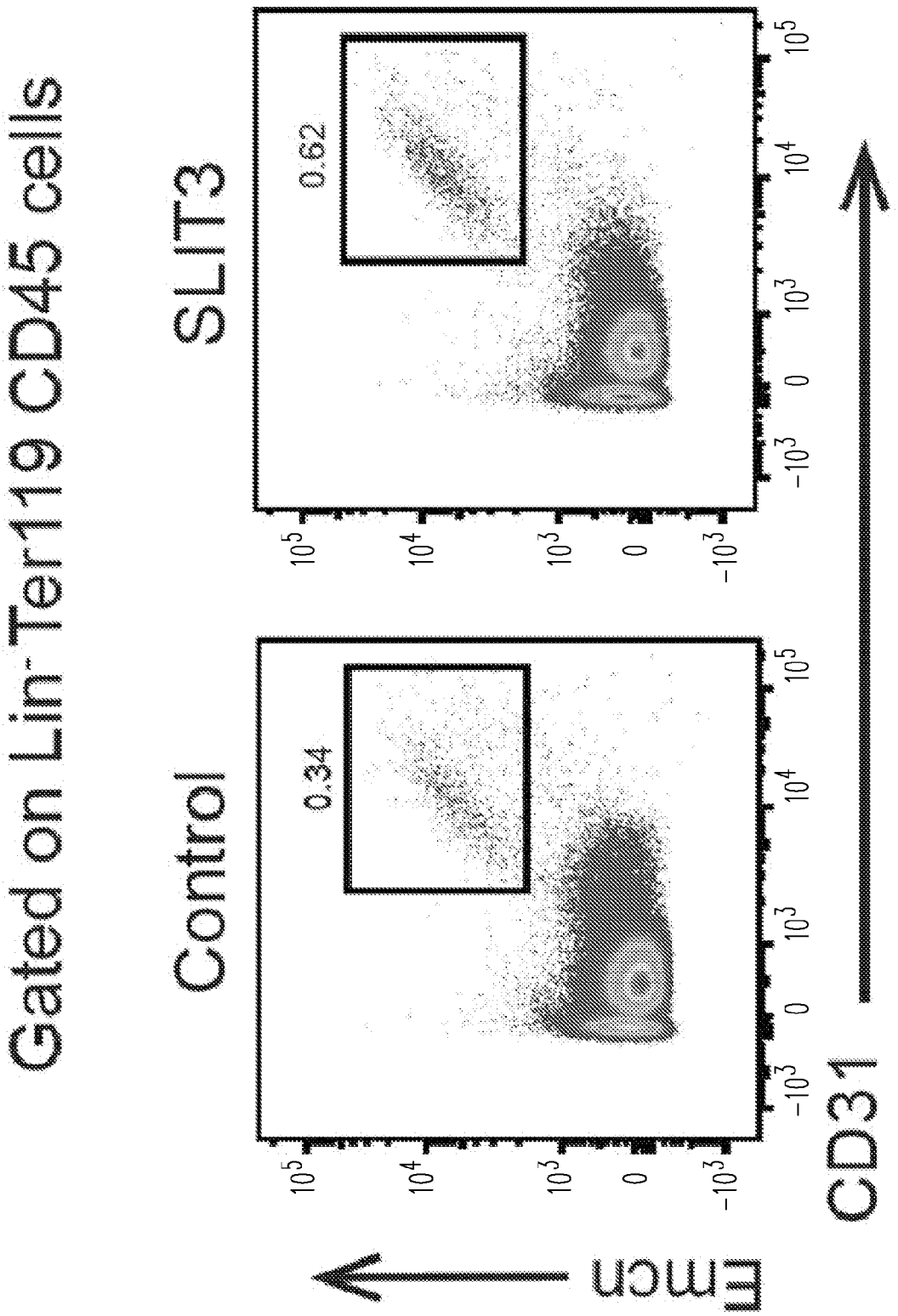
Gated on Lin- Ter119 CD45 cells
Control
SLIT3
0.34
0.62
Emcn
CD31
10^5
10^4
10^3
0
-10^3

Fig. 16B

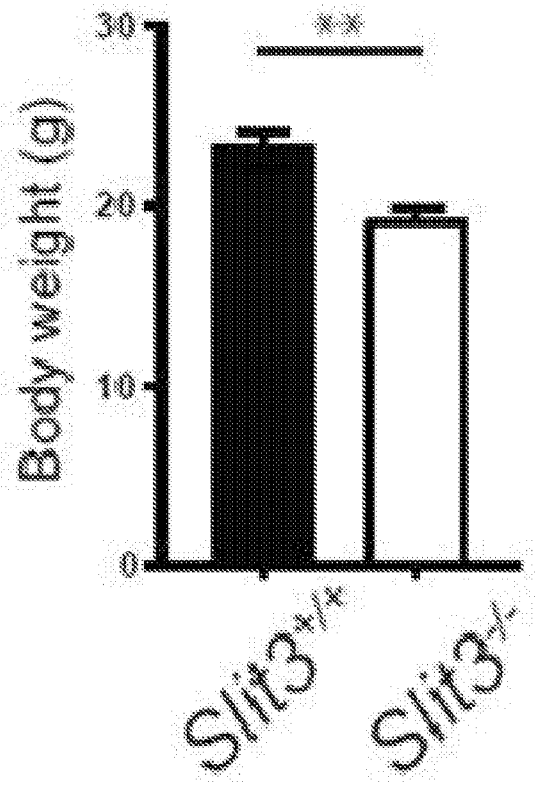

Fig.17A-1

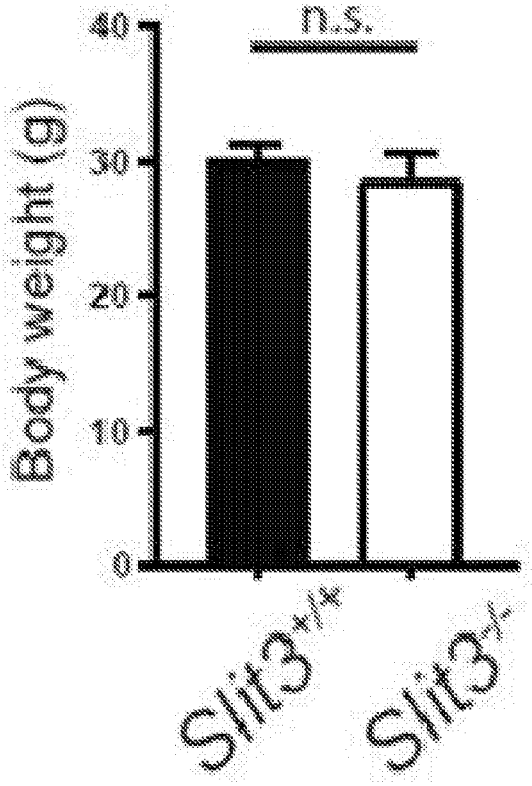

Fig.17A-2

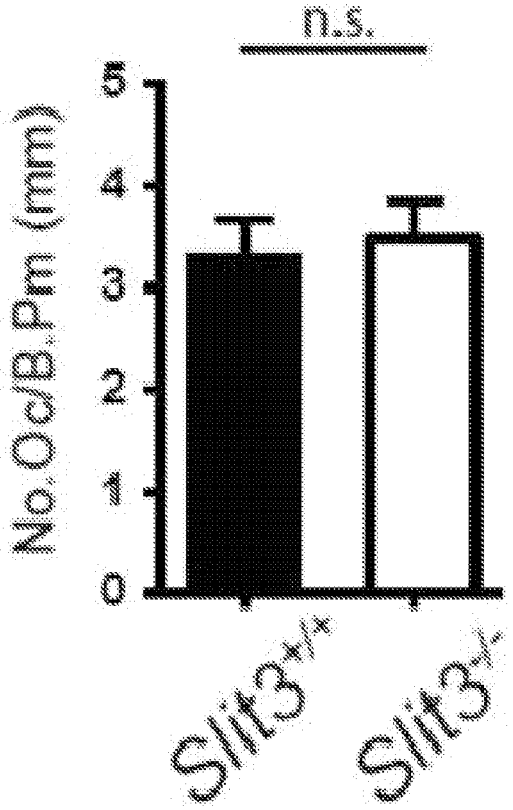

Fig.17B-1

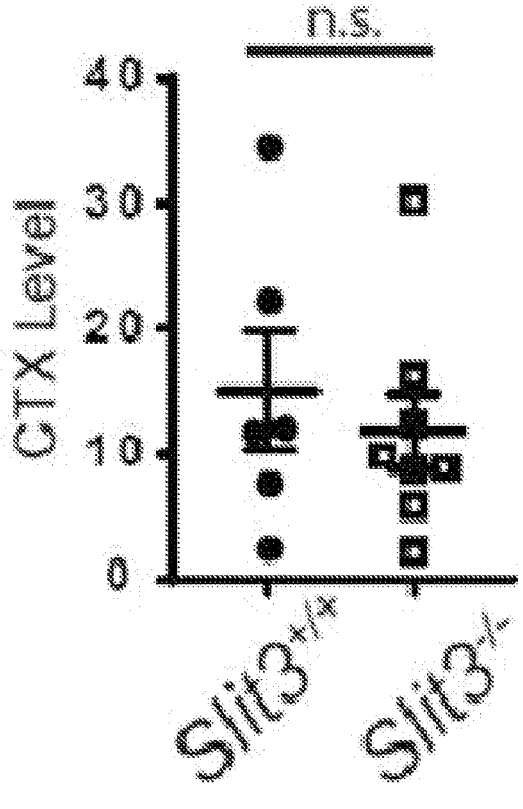

Fig.17B-2

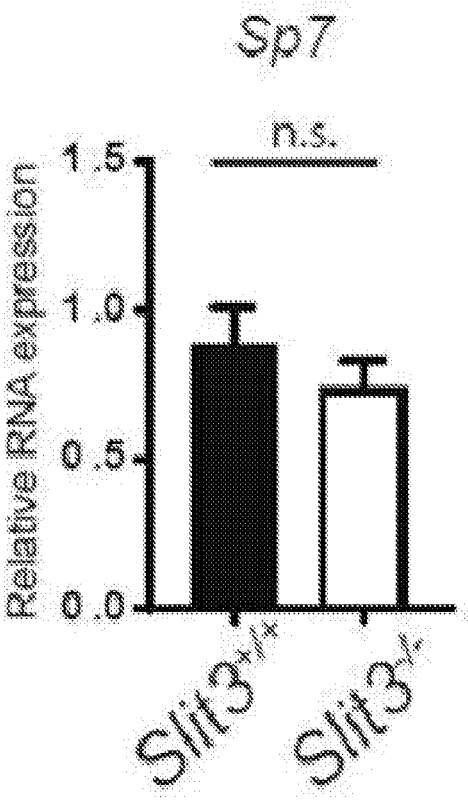

Fig.17C-1

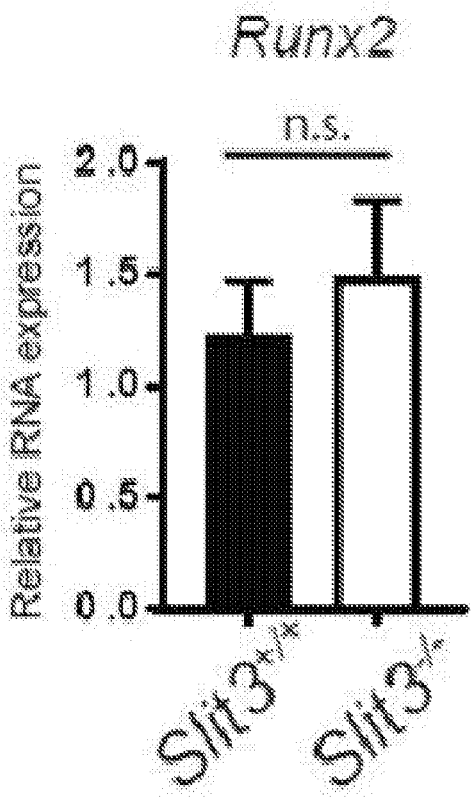

Fig.17C-2

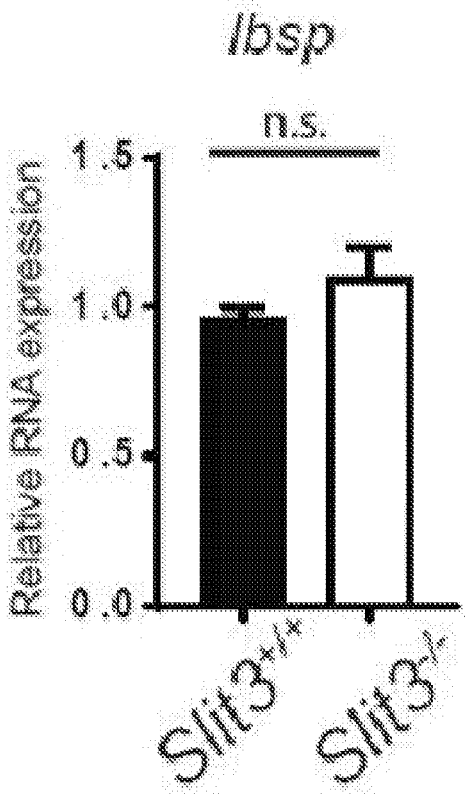

Fig.17C-3

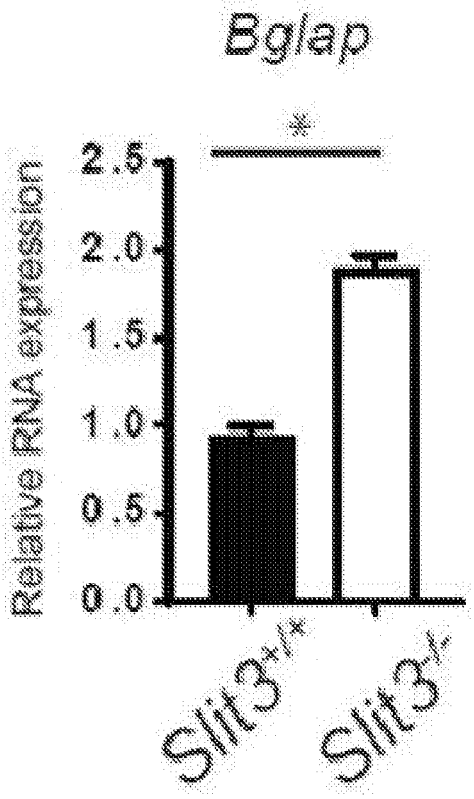

Fig.17C-4

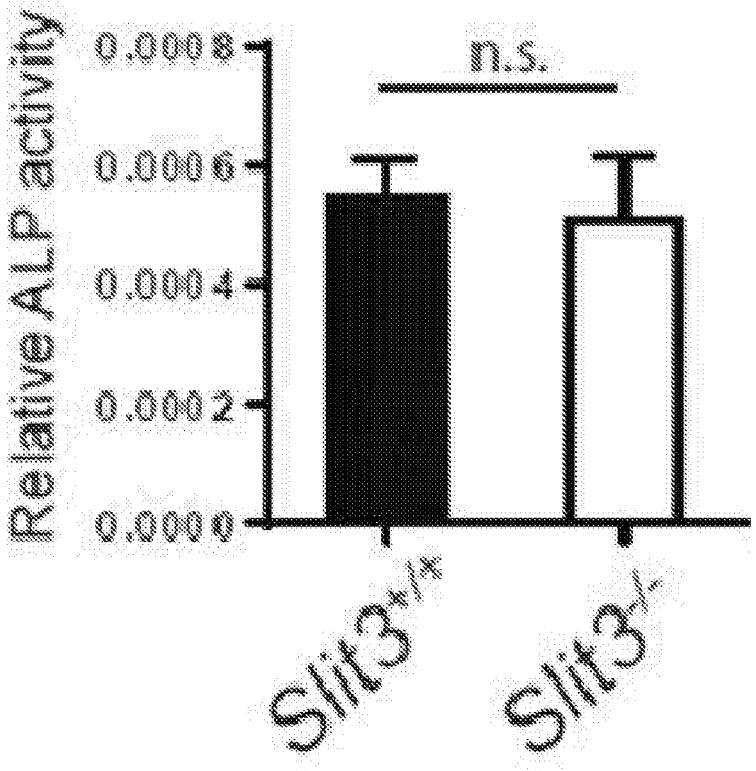

Fig. 17D

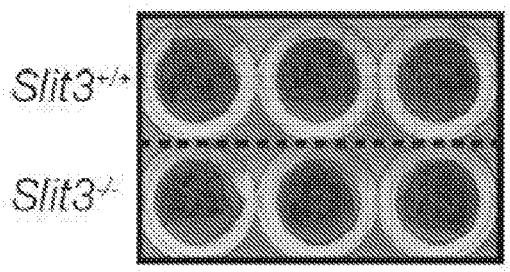

Fig. 17E-1

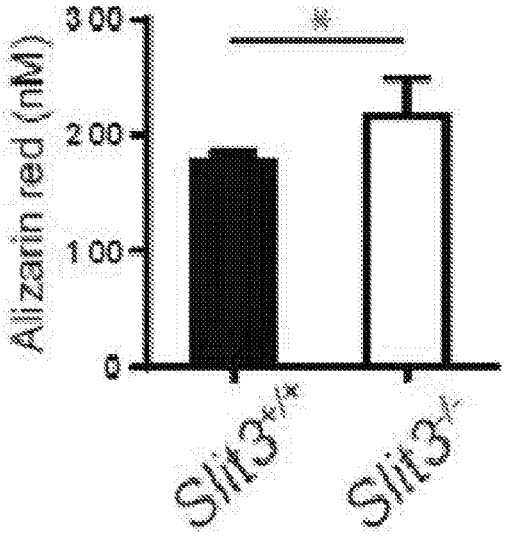

Fig. 17E-2

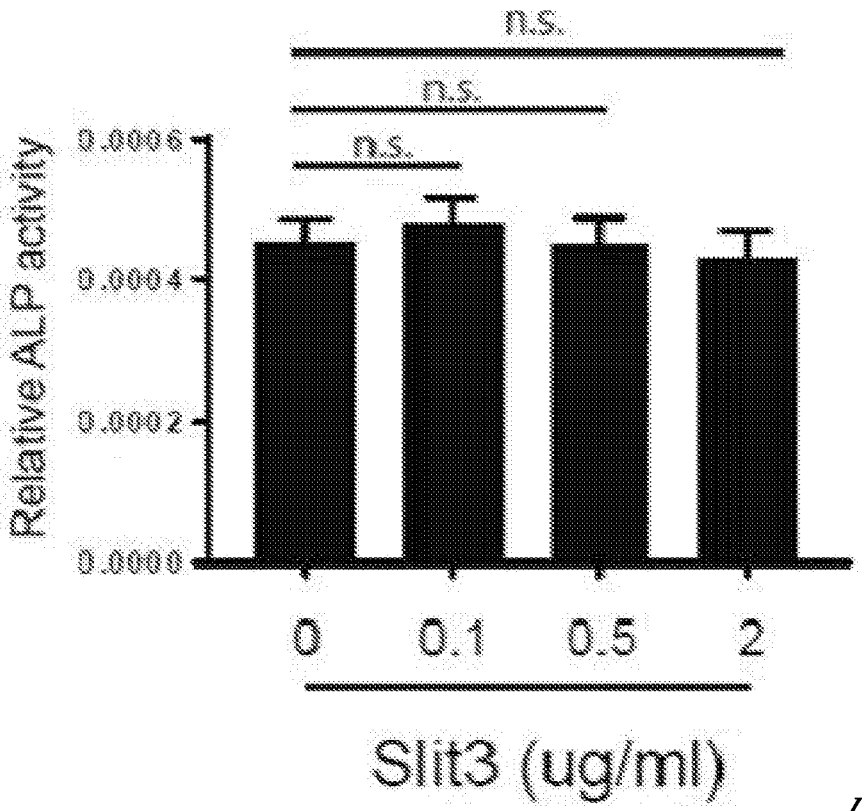

Fig. 17F

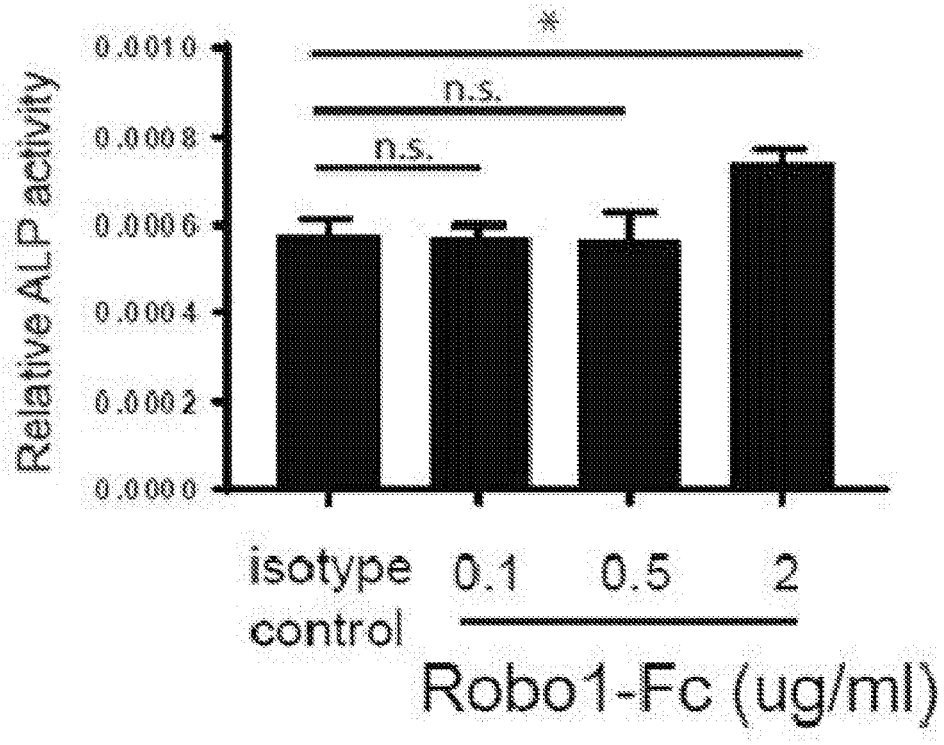

Fig. 17G

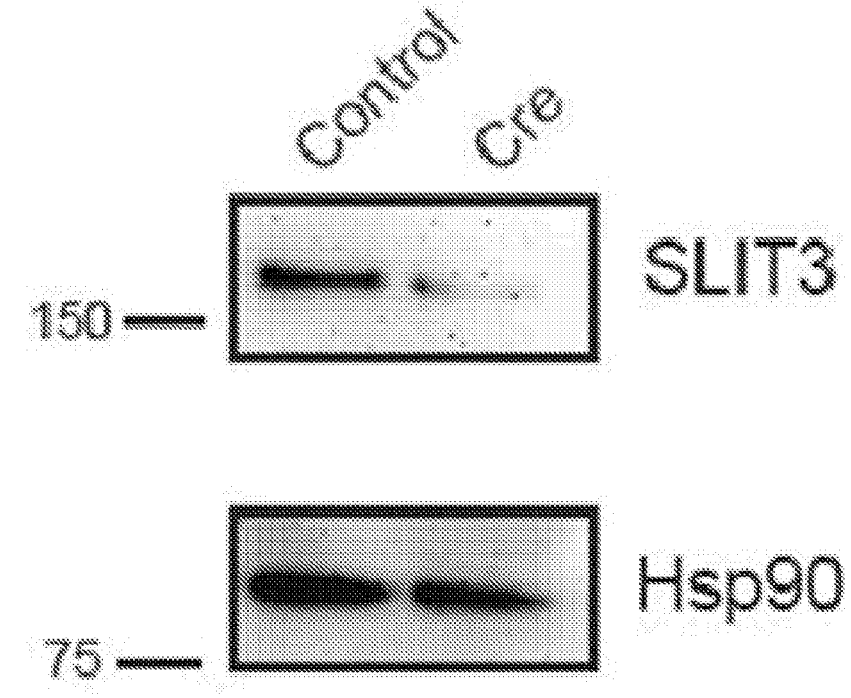

Fig. 18A

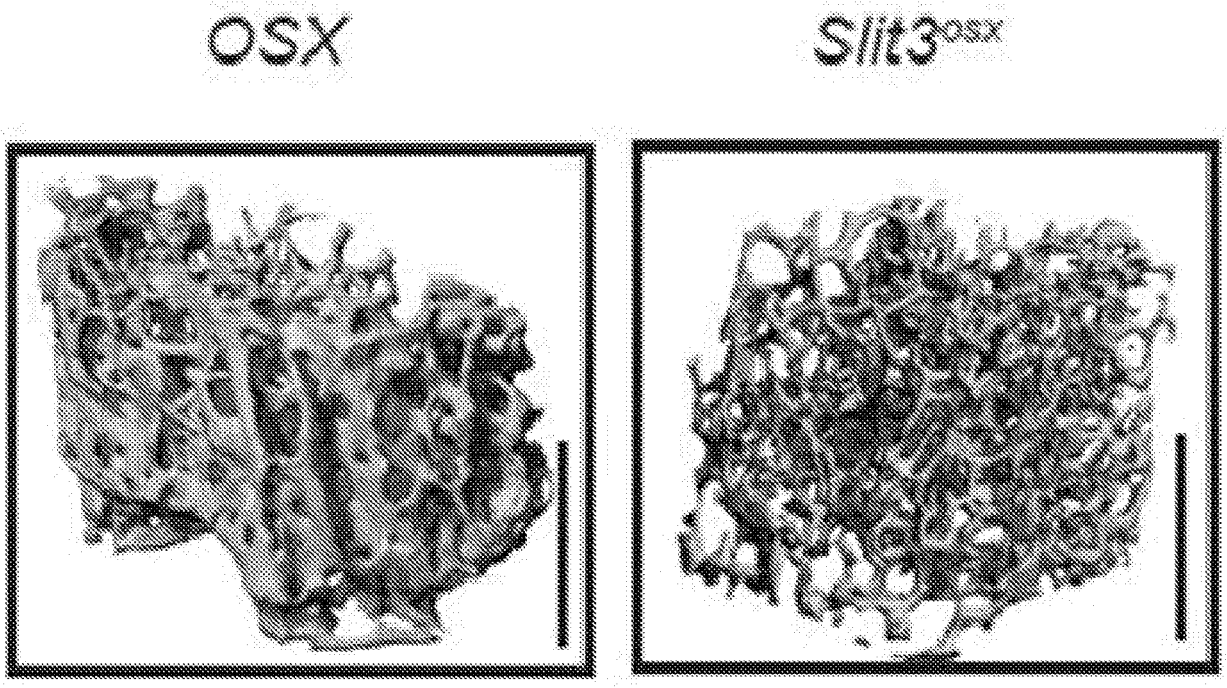

Fig. 18B

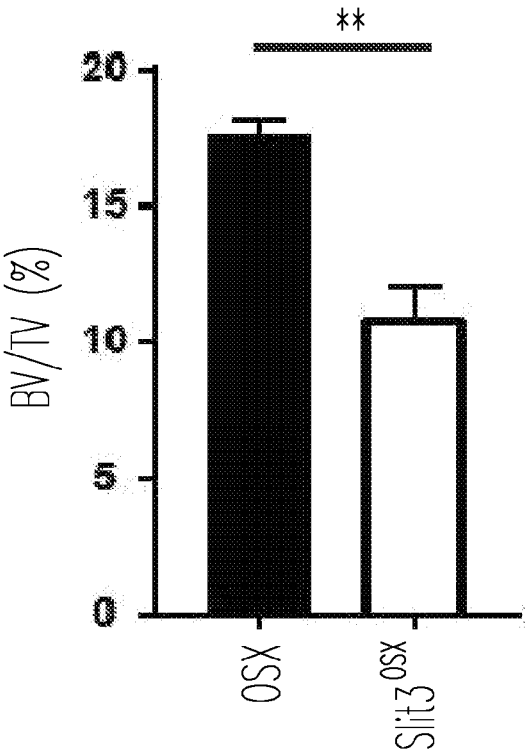

Fig. 18C-1

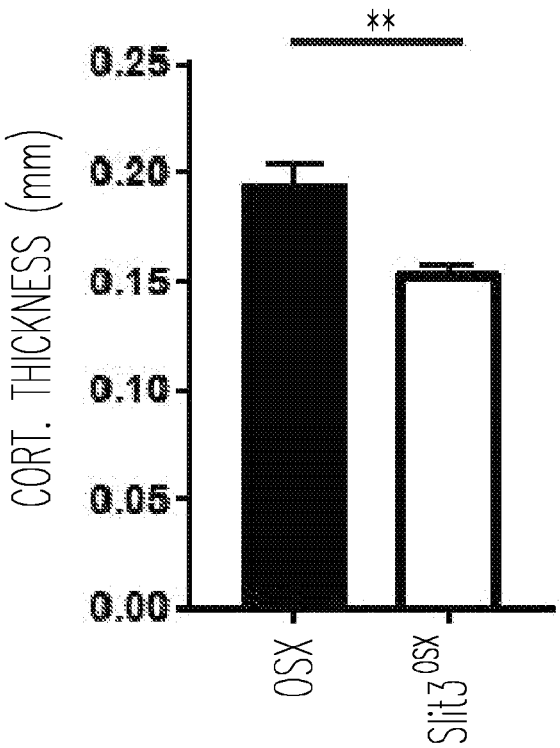

Fig. 18C-2

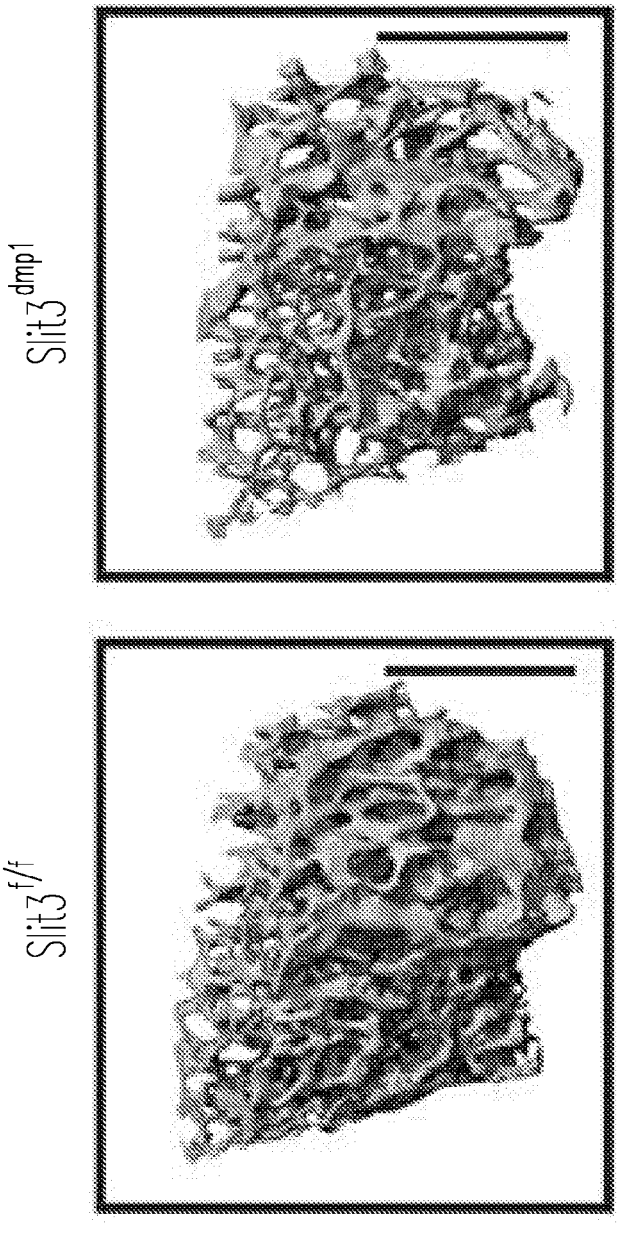

Fig. 18D–1

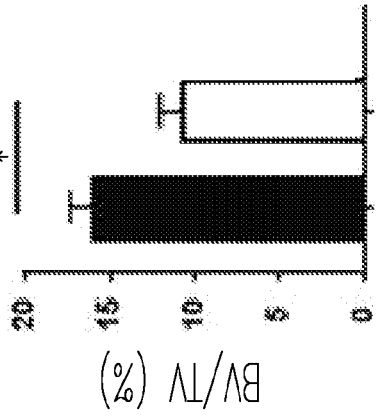

Fig. 18D–2

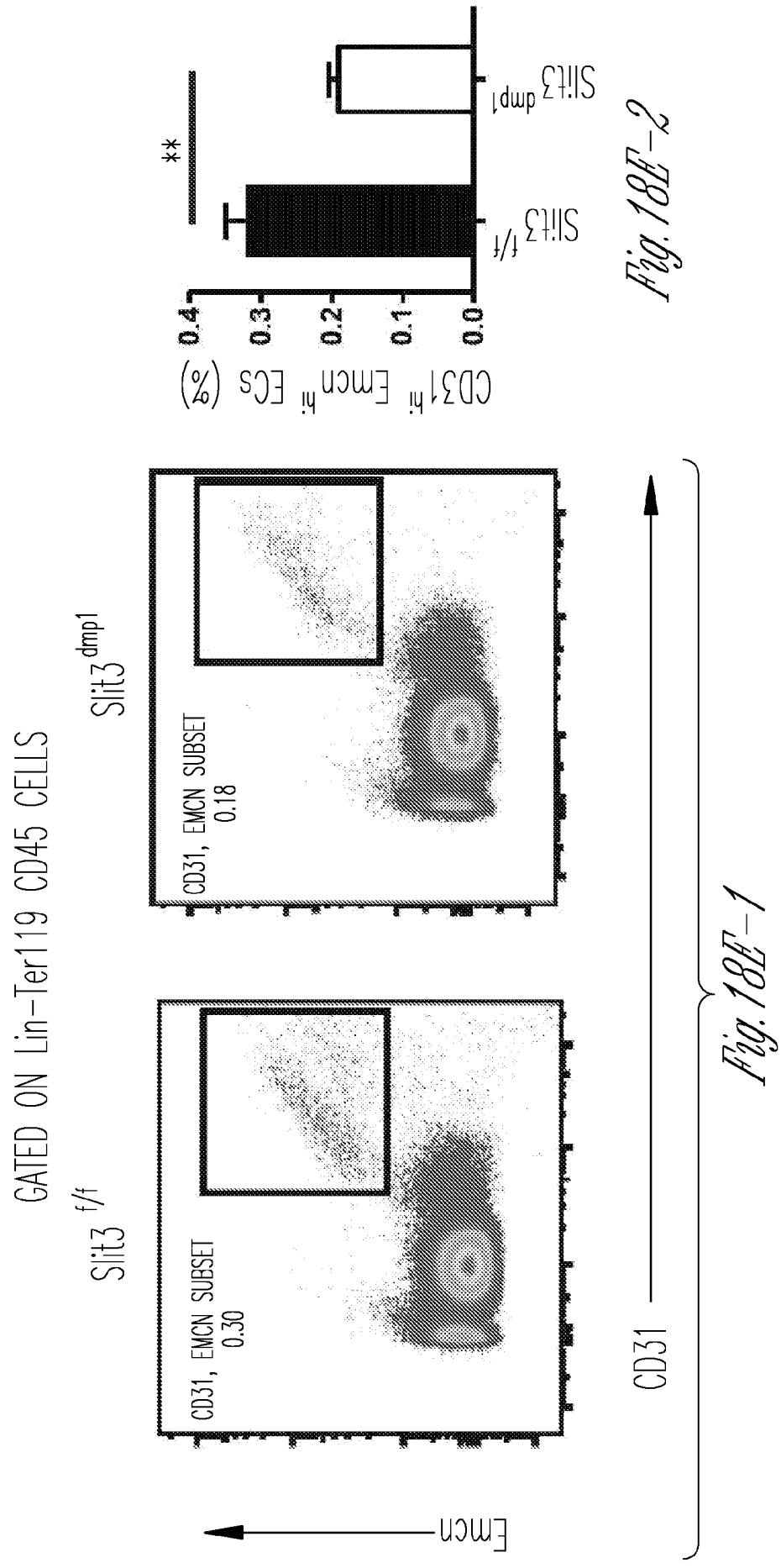

Fig. 18E-1

Fig. 18E-2

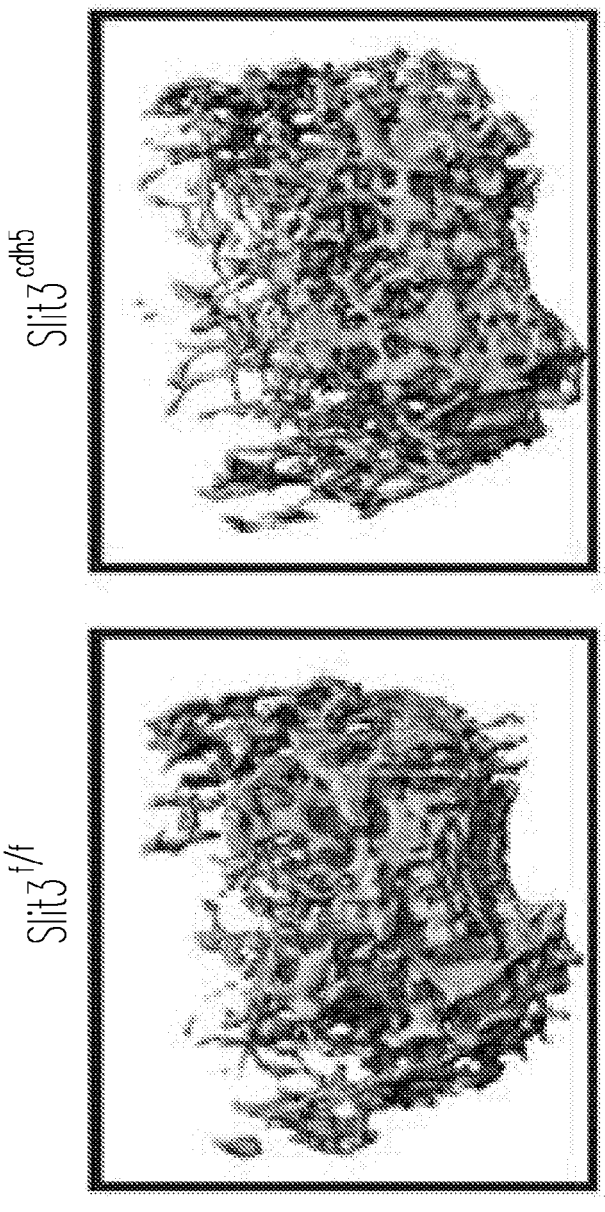

Fig. 19A–1

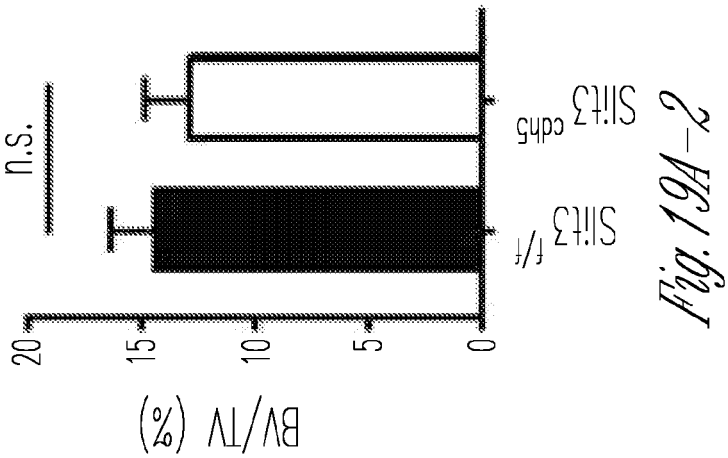

Fig. 19A–2

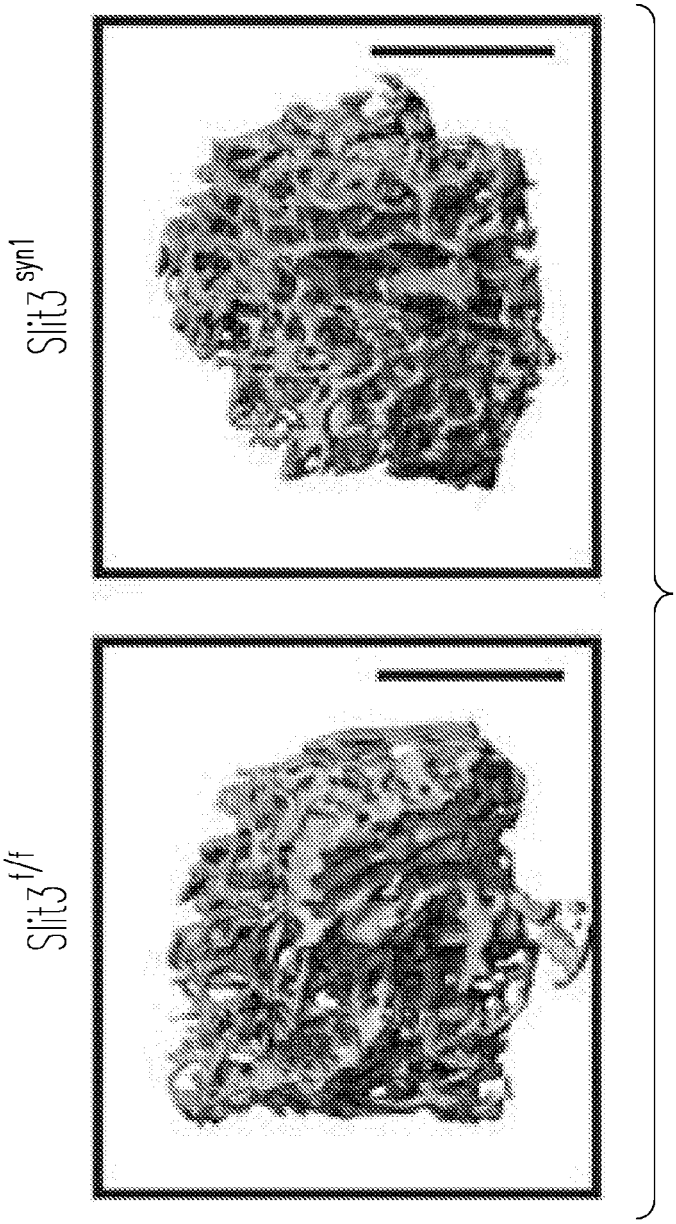

Fig. 19B-1

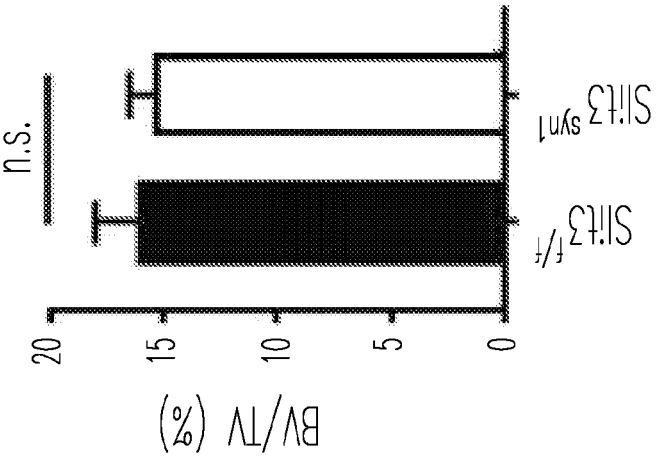

Fig. 19B-2

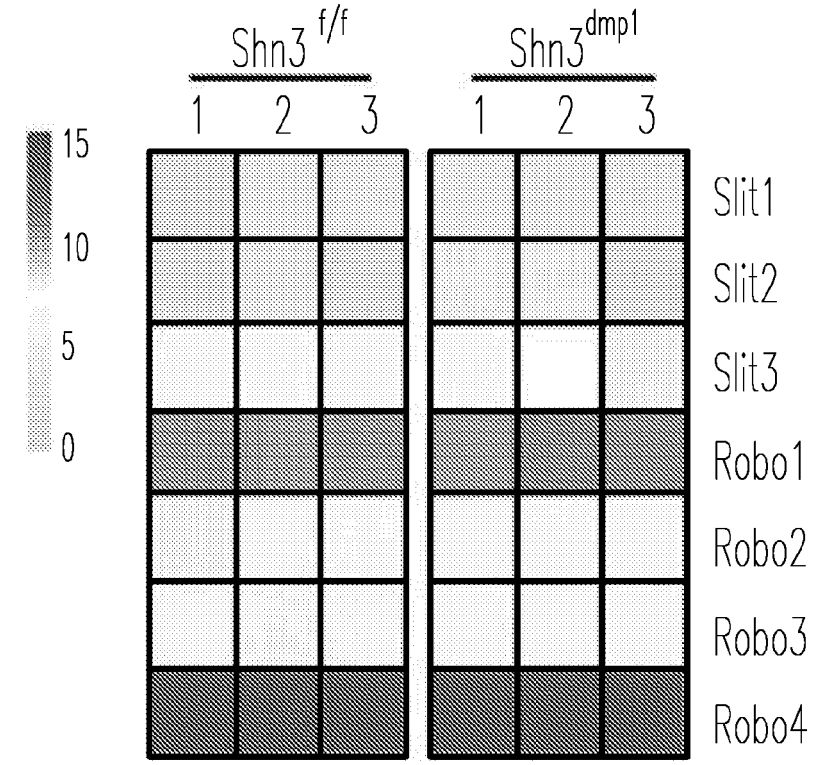

Fig.20A

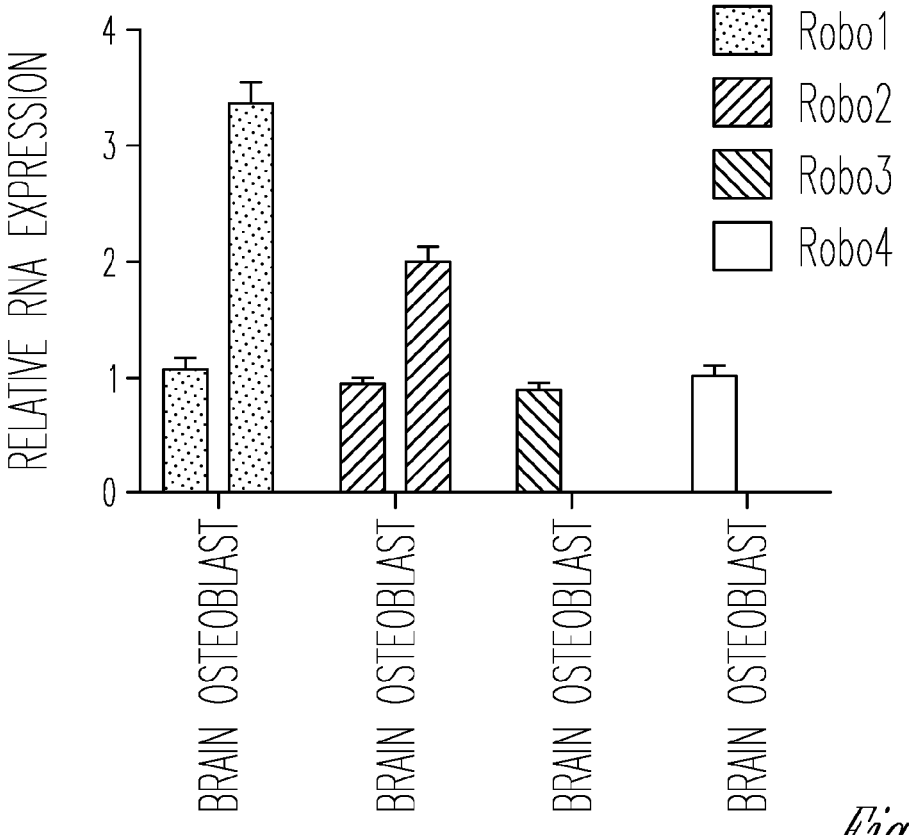

Fig.20B

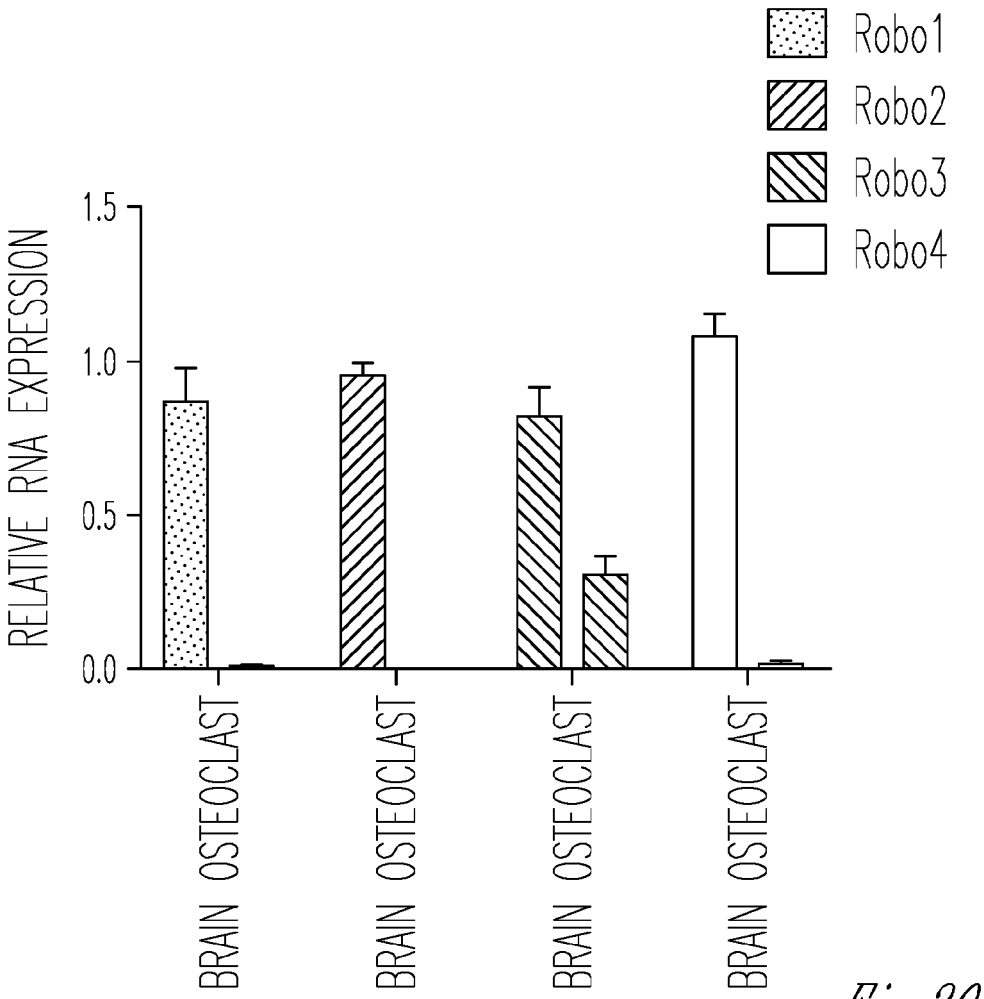
Robo1
Robo2
Robo3
Robo4
RELATIVE RNA EXPRESSION
1.5
1.0
0.5
0.0
BRAIN OSTEOCLAST
BRAIN OSTEOCLAST
BRAIN OSTEOCLAST
BRAIN OSTEOCLAST

Fig. 20C

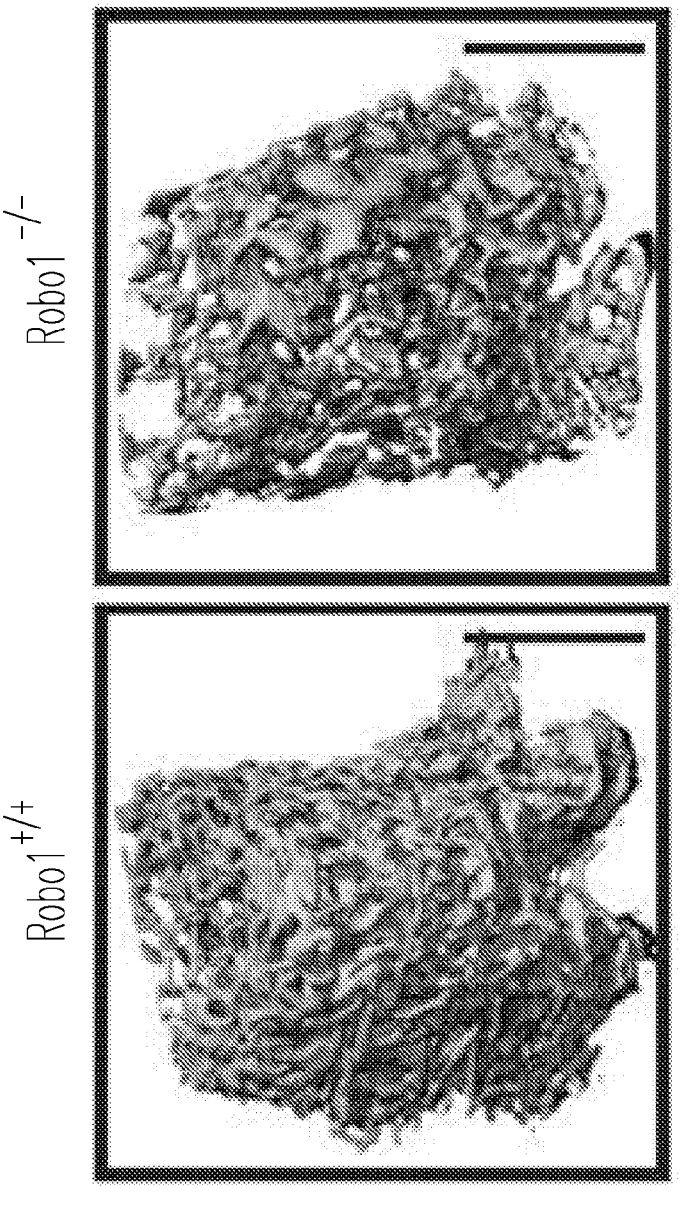

Fig.20D-1

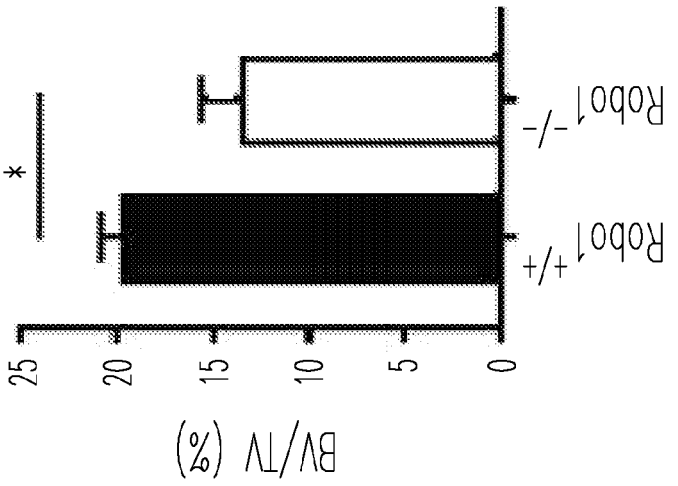

Fig.20D-2

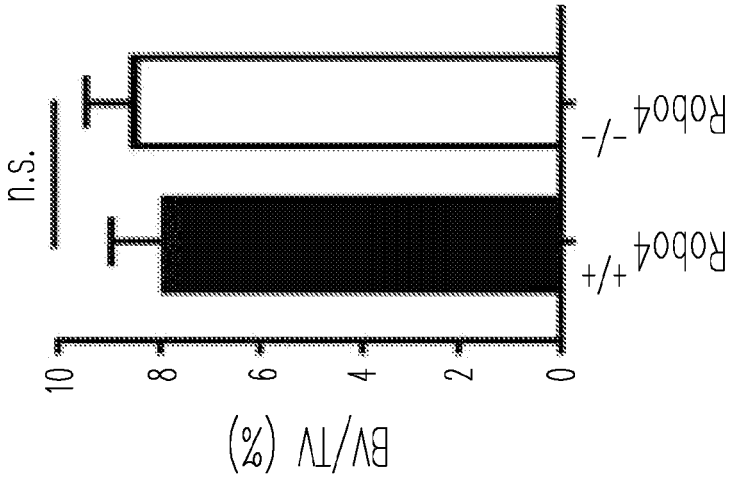

Fig.20E-2

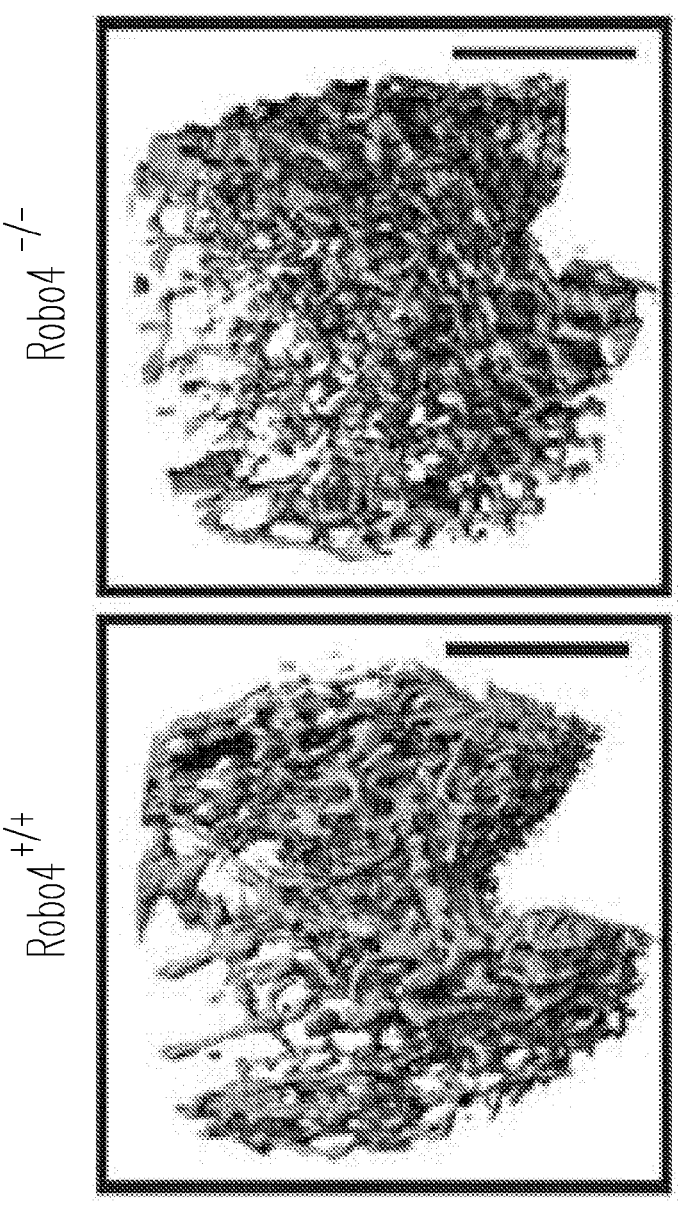

Fig.20E-1

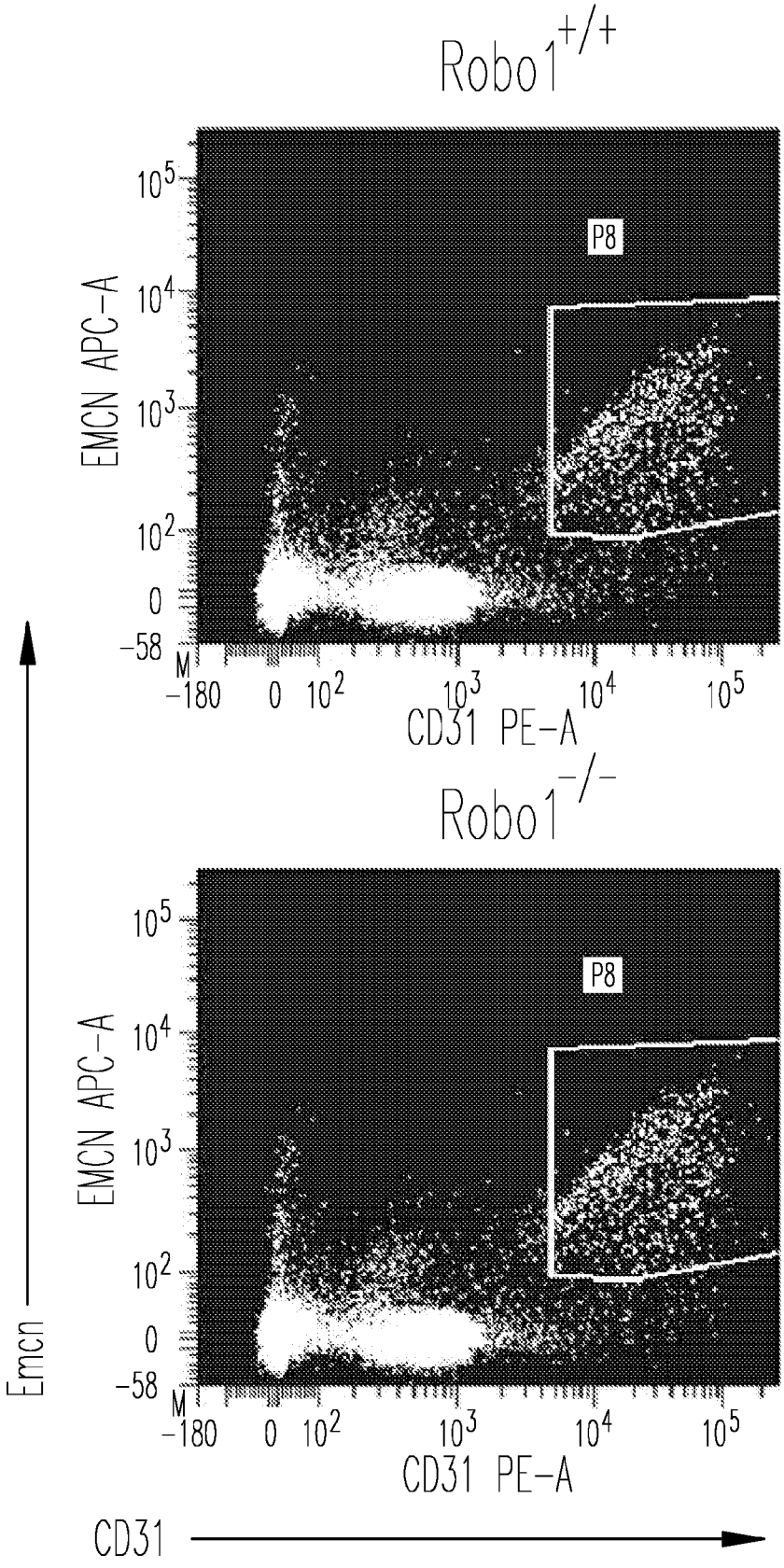
Robo1+/+
P8
EMCN APC-A
CD31 PE-A
Robo1−/−
P8
EMCN APC-A
CD31 PE-A
Emcn
CD31

Fig. 20F

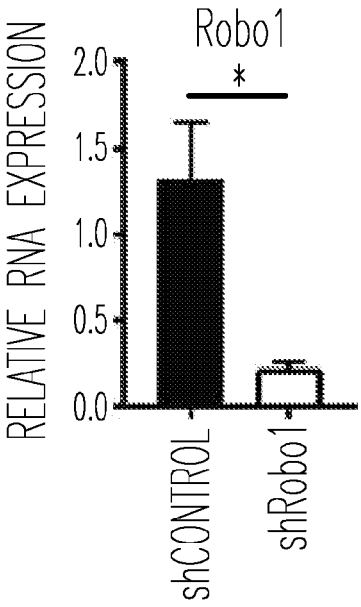

Fig.20G-1

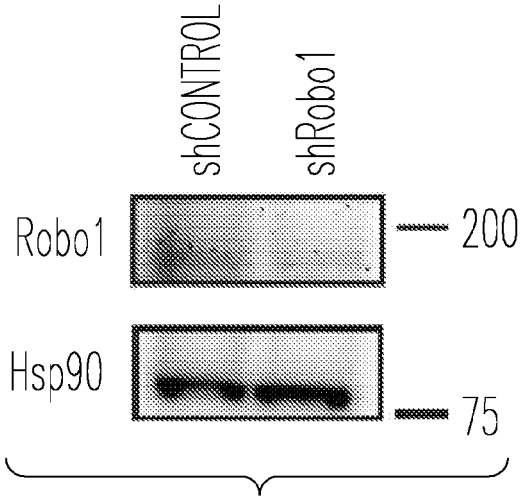

Fig.20G-2

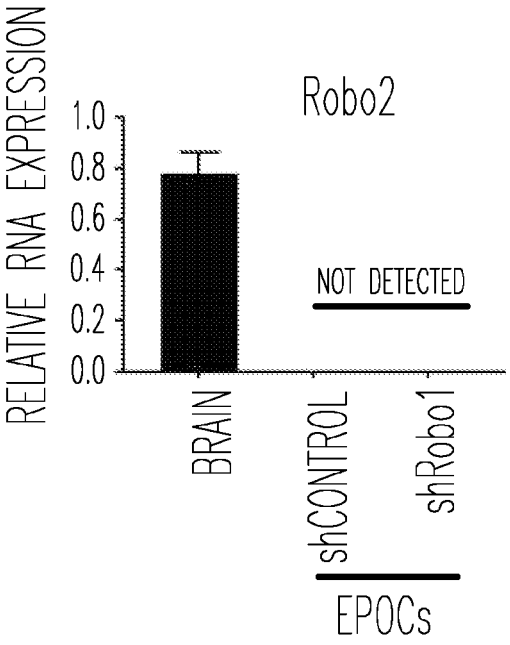

Fig.20H-1

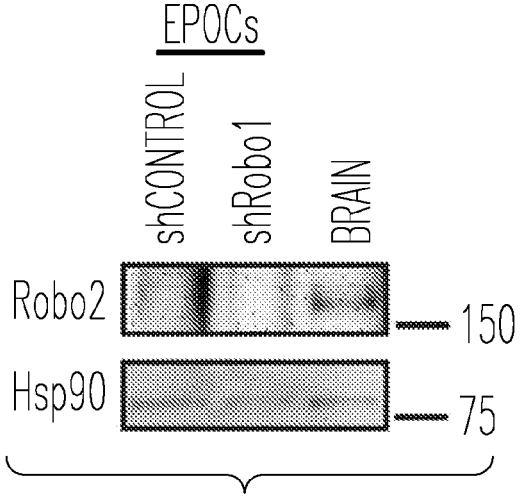

Fig.20H-2

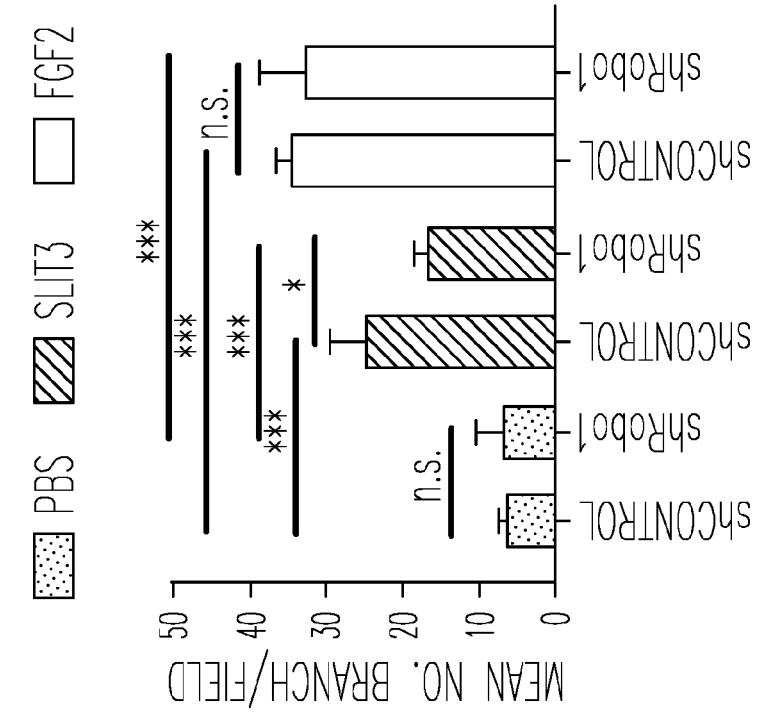

Fig.21A-2

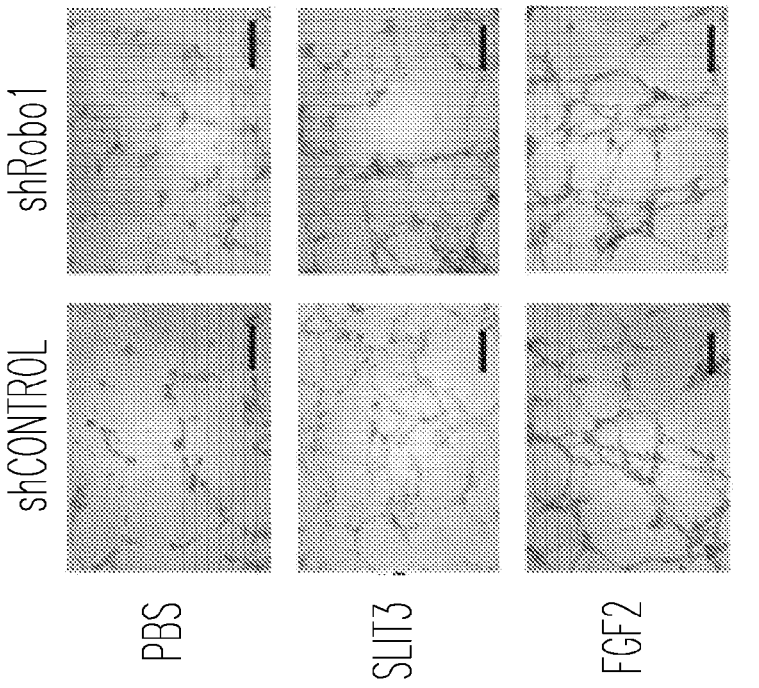

Fig.21A-1

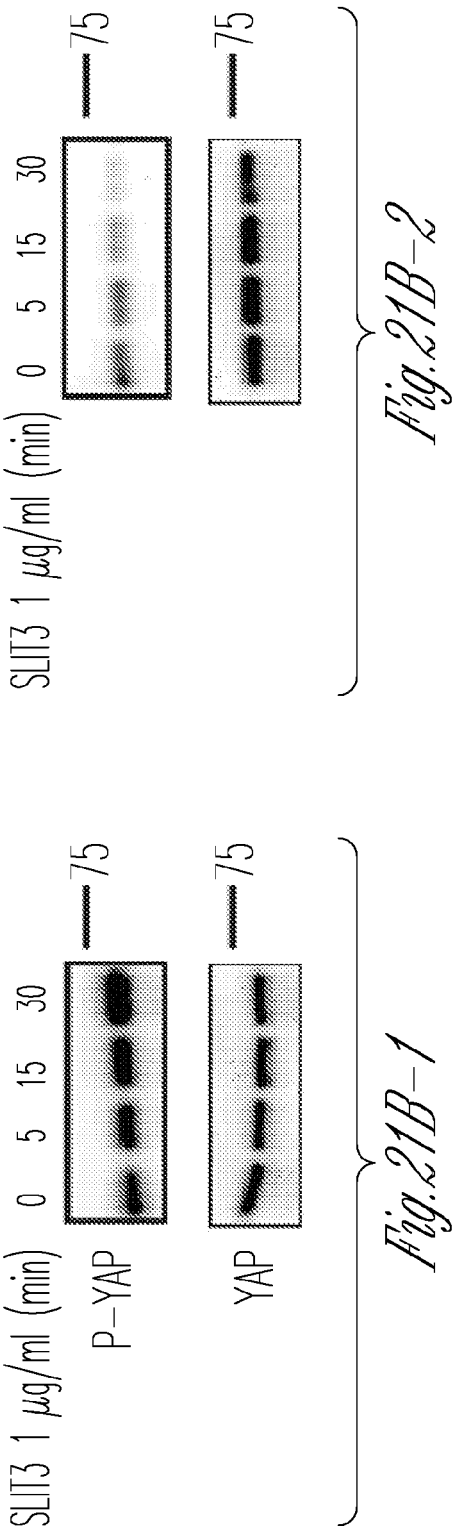

Fig.21B-1

Fig.21B-2

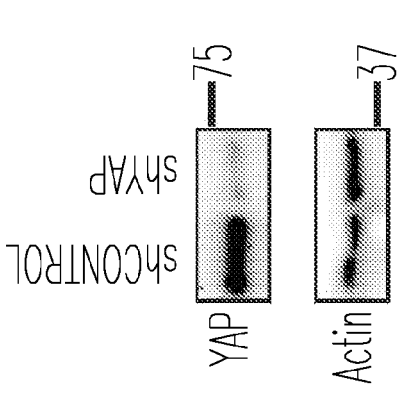

Fig.21C

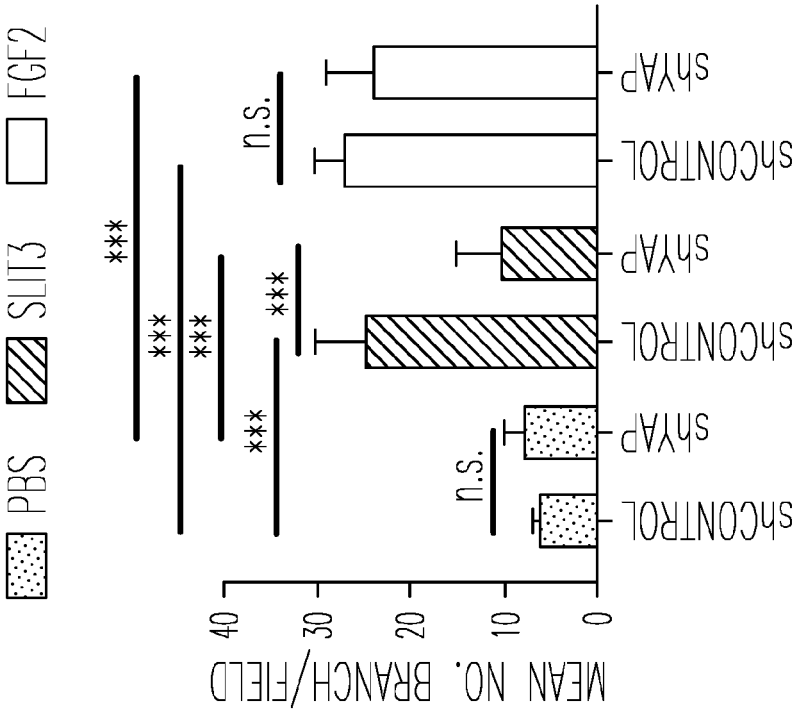

Fig.21D-2

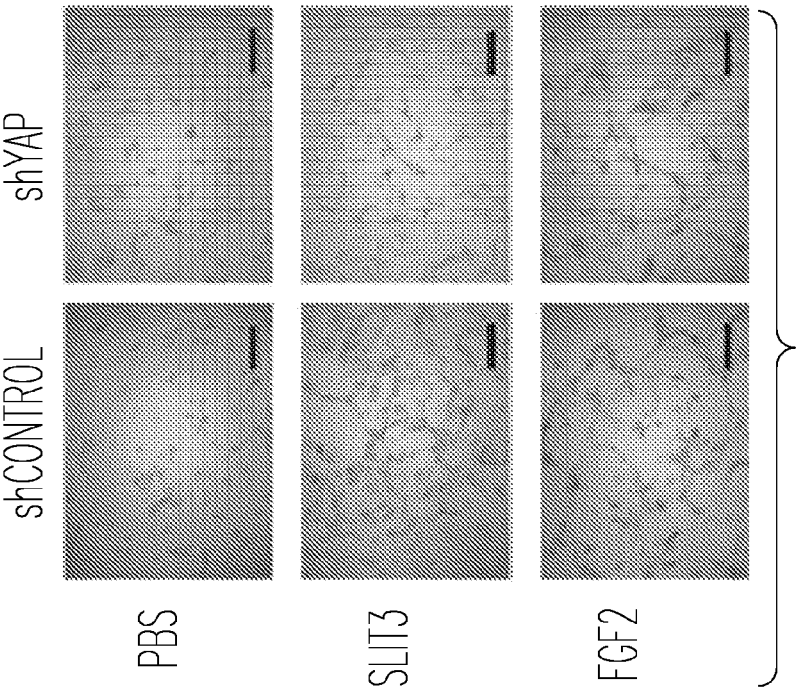

Fig.21D-1

Osx cre

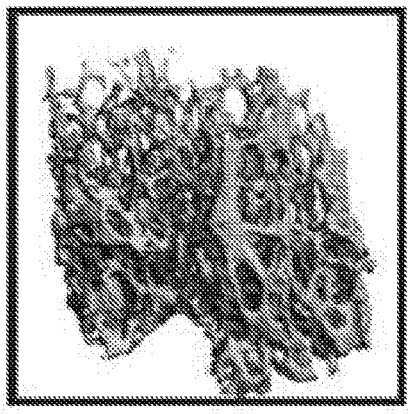

Fig.22A-1

Osx cre Slit3$^{f/+}$

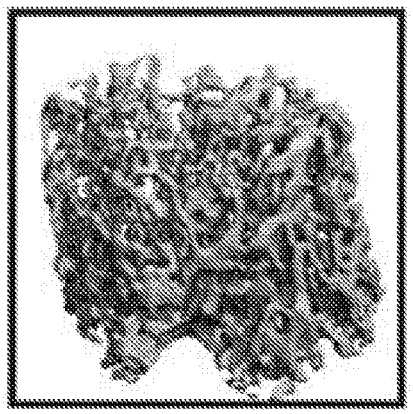

Fig.22A-2

Osx cre Shn3$^{f/+}$

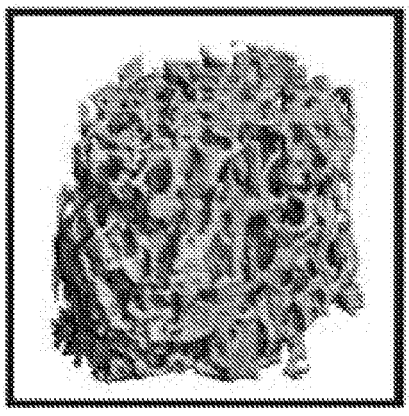

Fig.22A-3

Osx cre Slit3$^{f/+}$Shn3$^{f/+}$

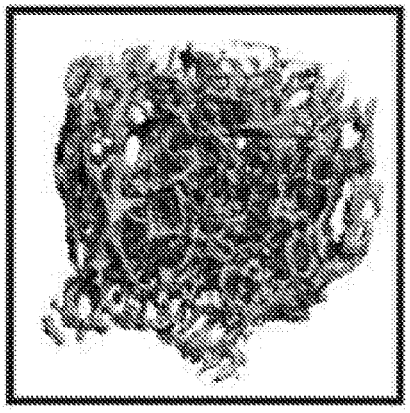

Fig.22A-4

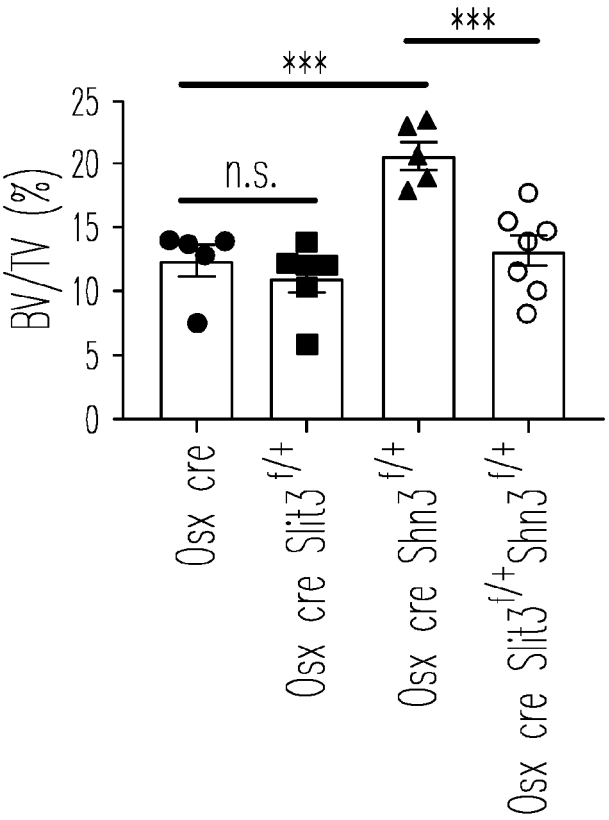

Fig.22B

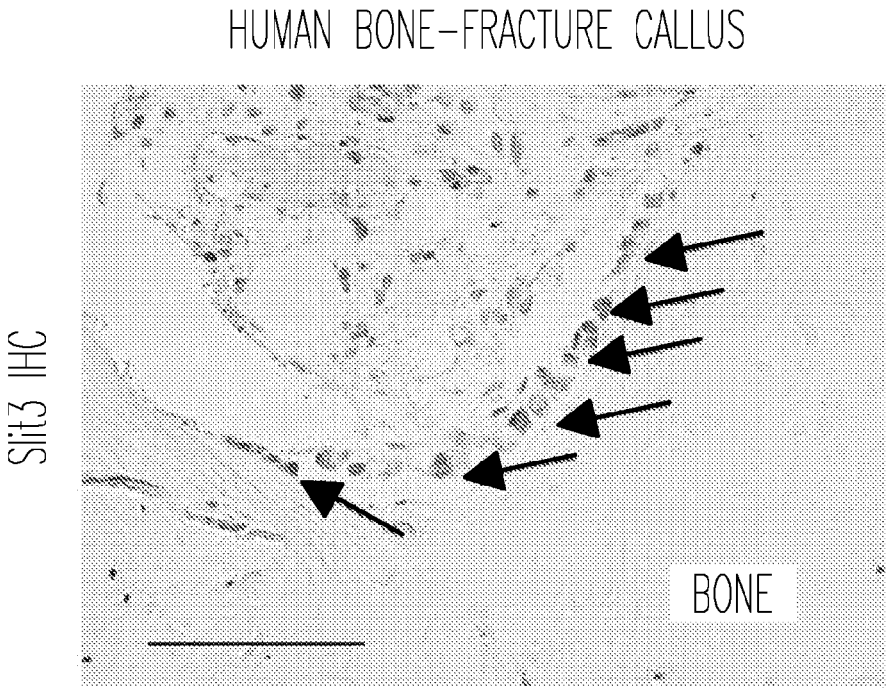

Fig.23A

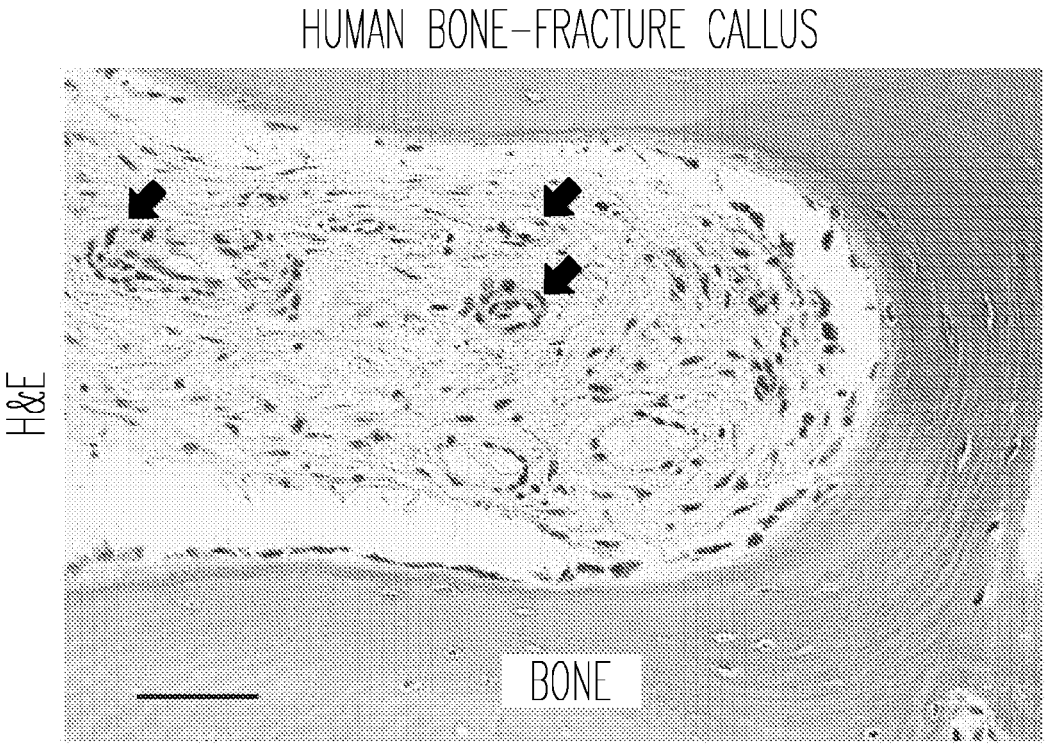

Fig.23B-1

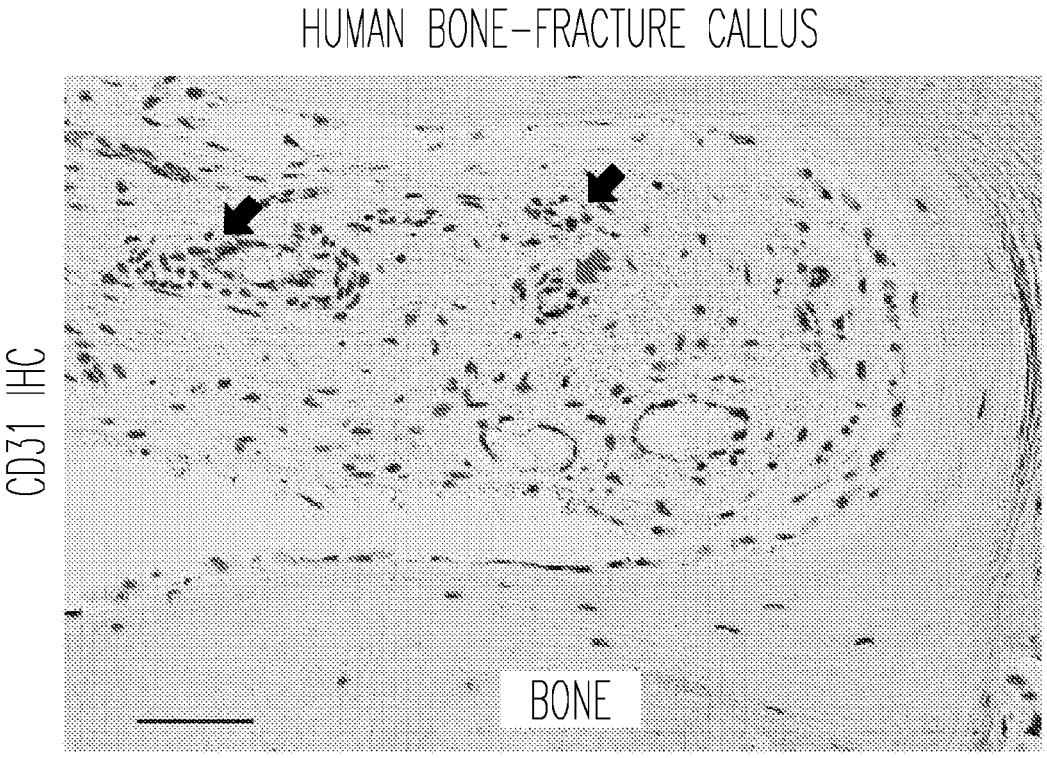

Fig.23B-2

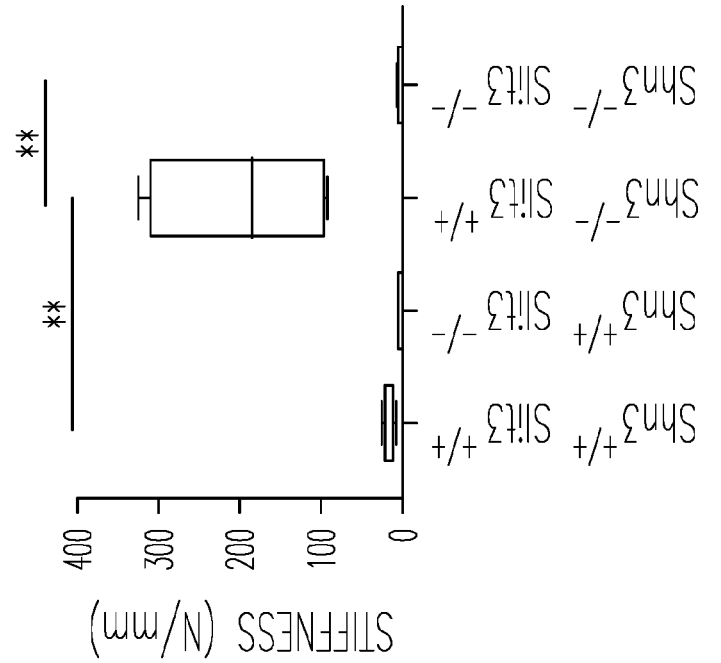

Fig.24B

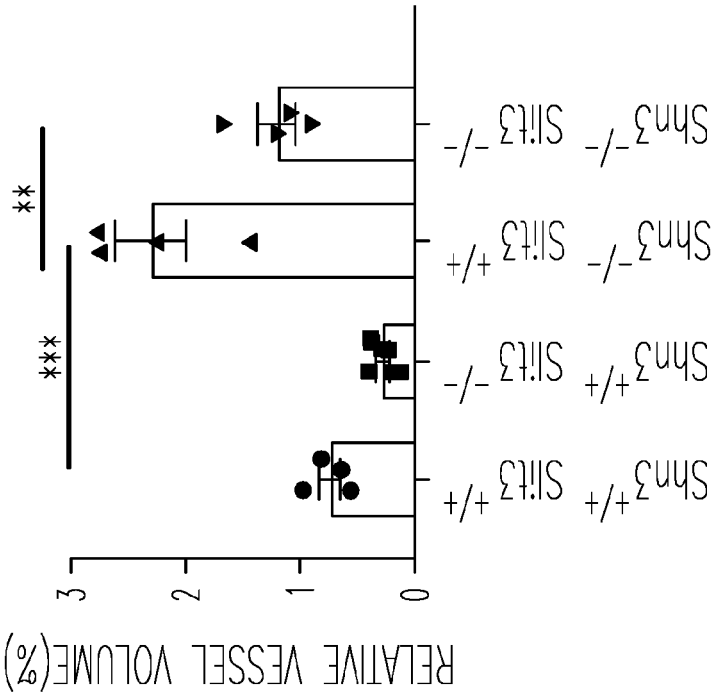

Fig.24A

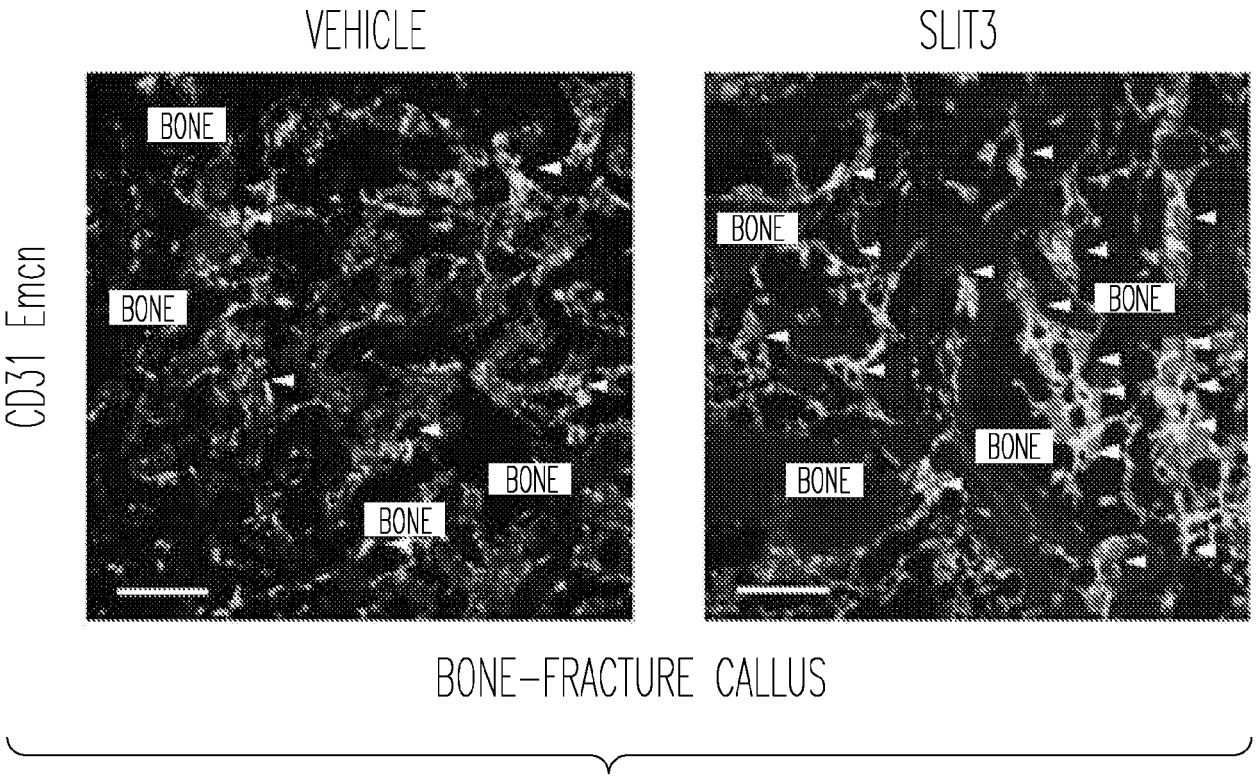

Fig.24C

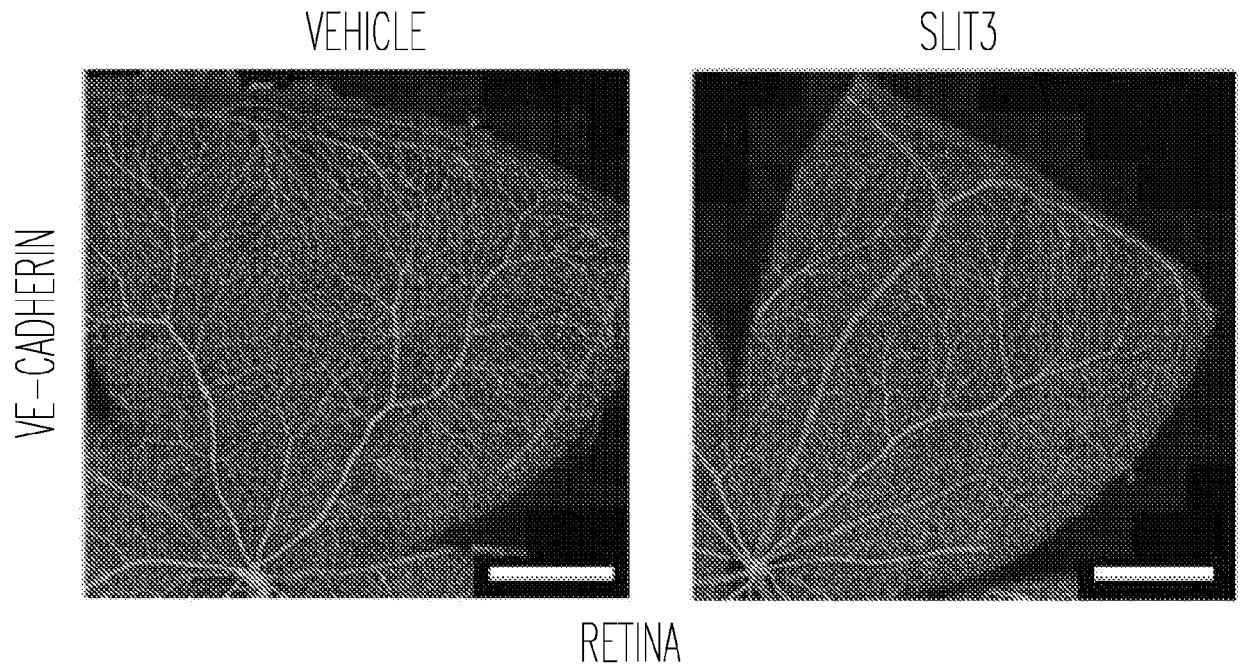

Fig.25A

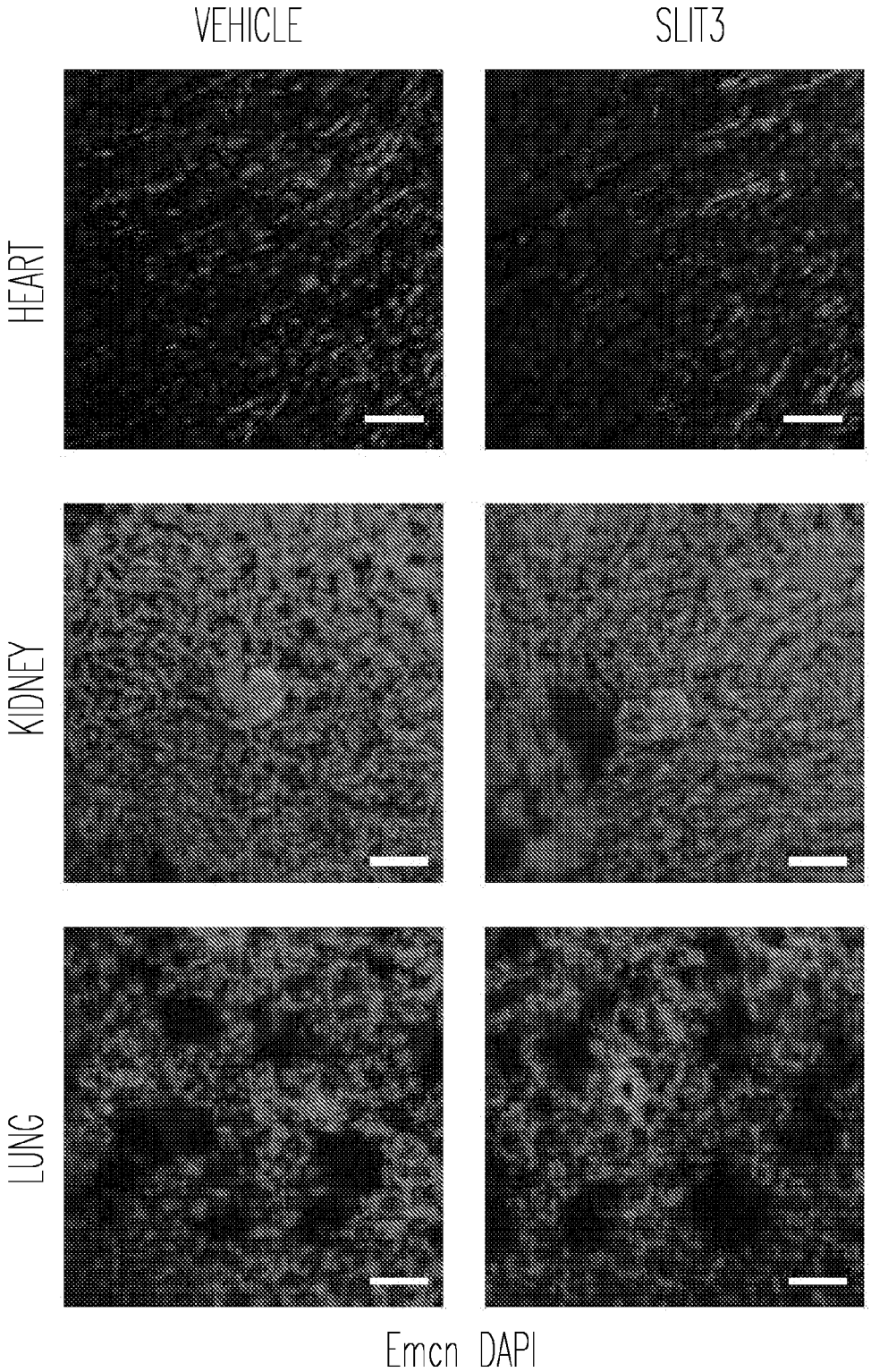

Fig. 25B

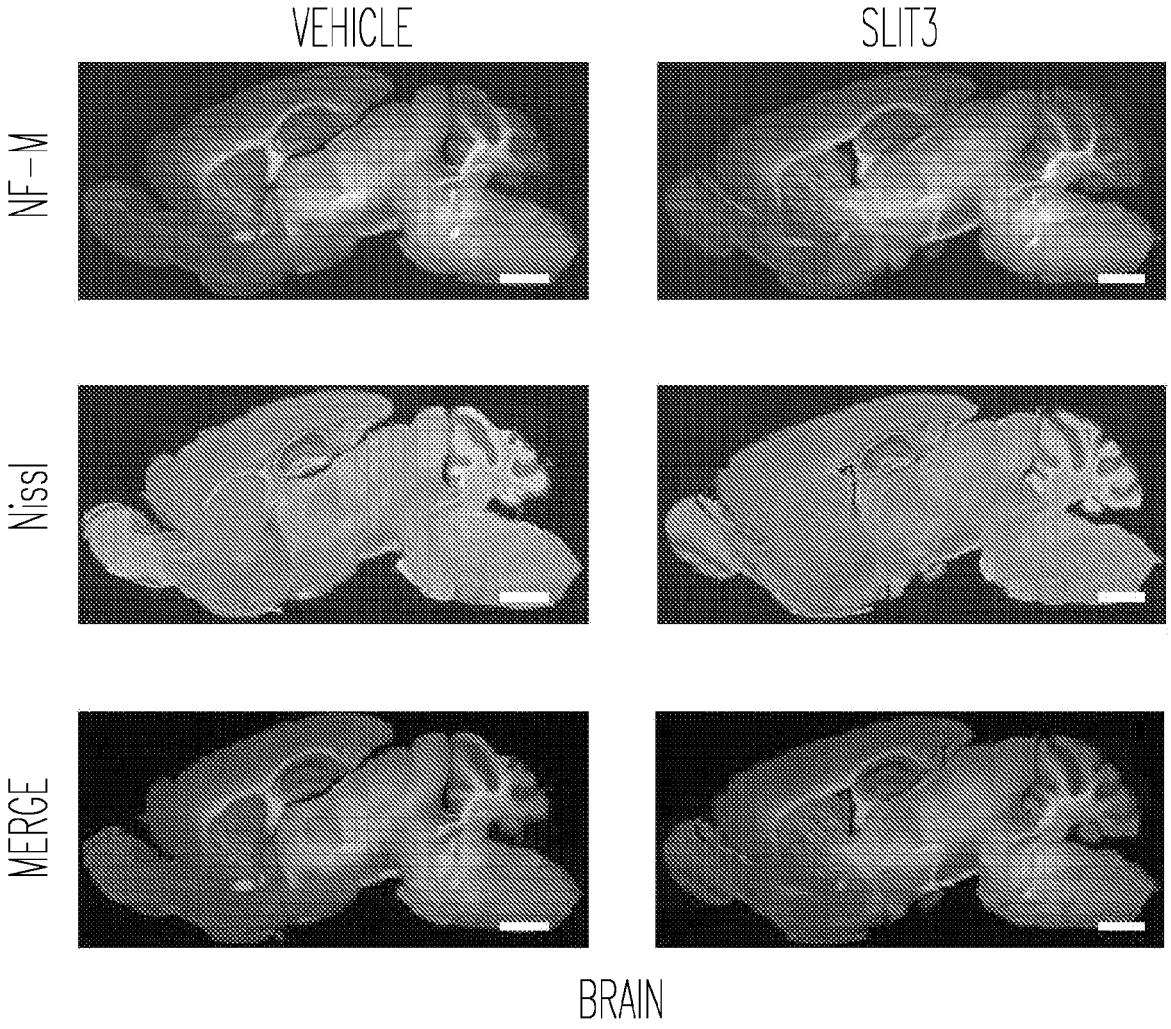

Fig. 25C

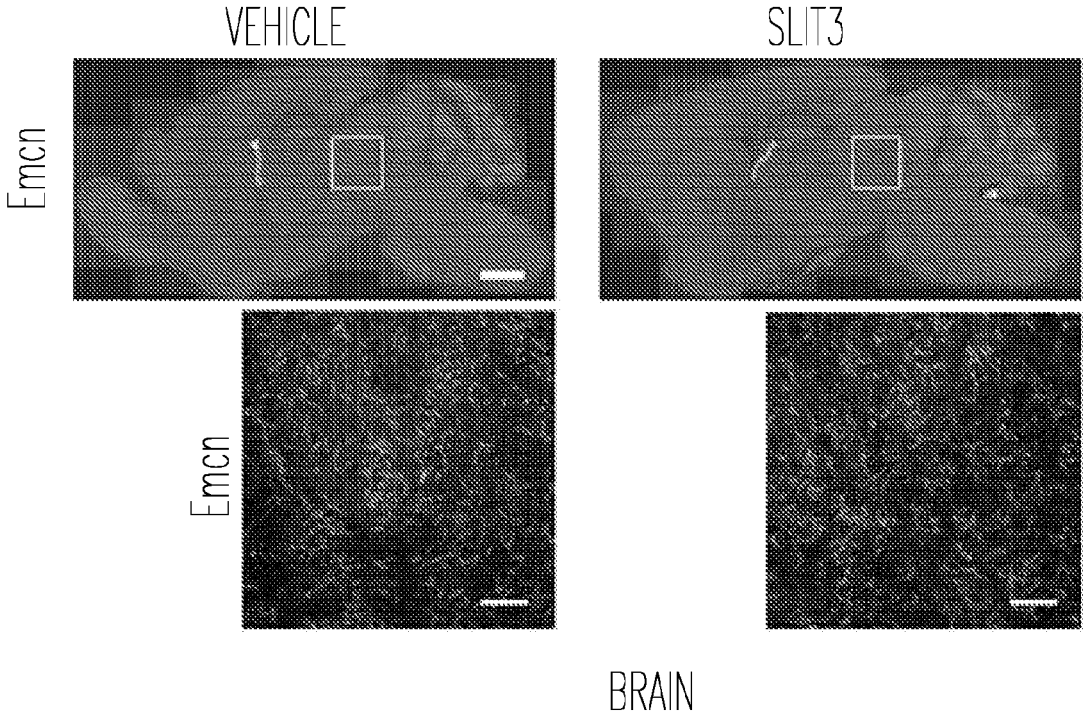

Fig. 25D

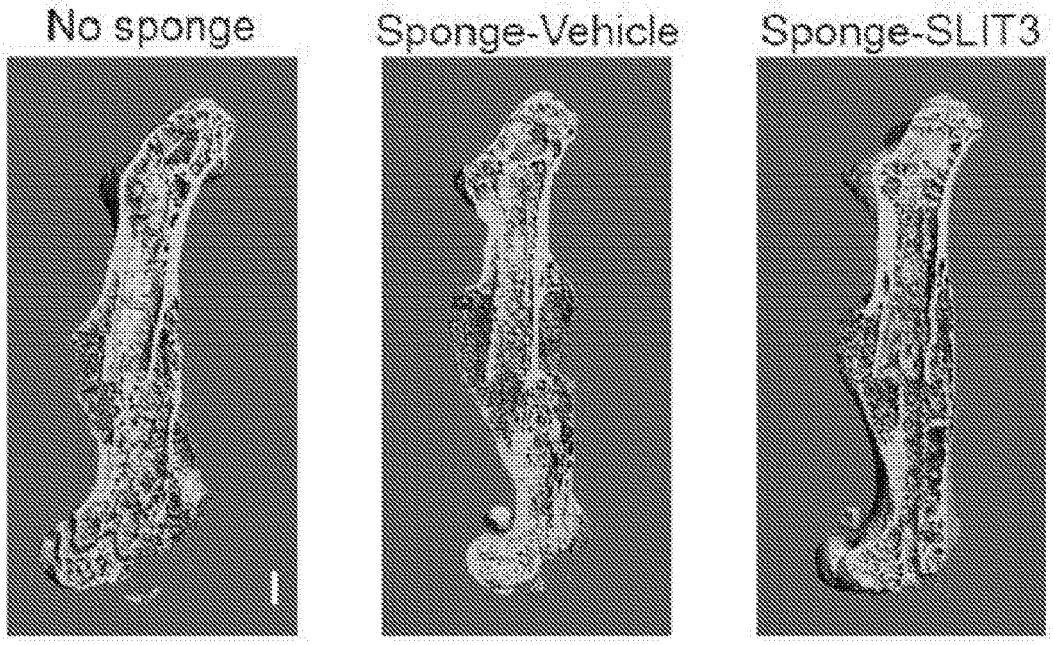

Fig. 26A

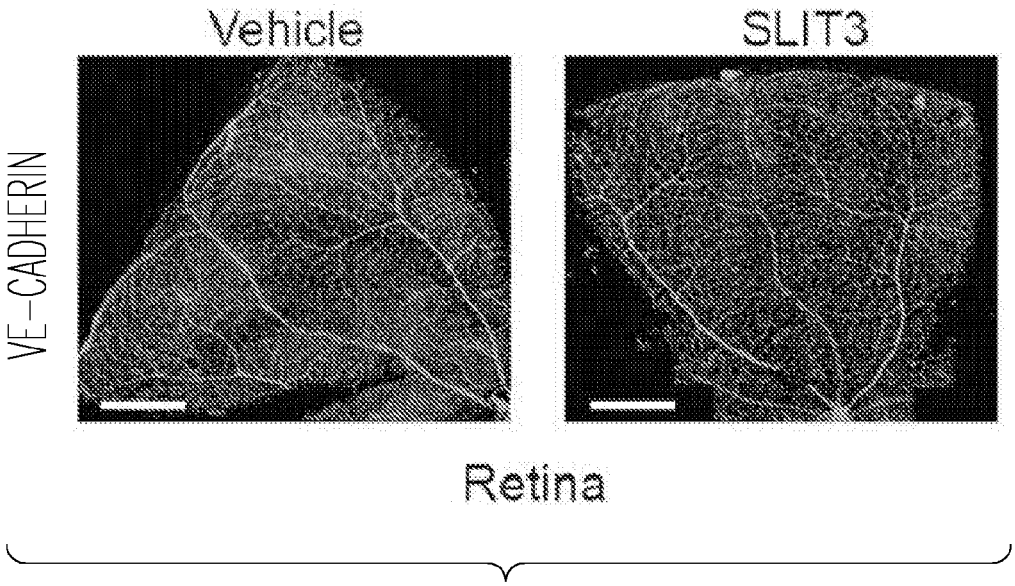

Fig. 26B

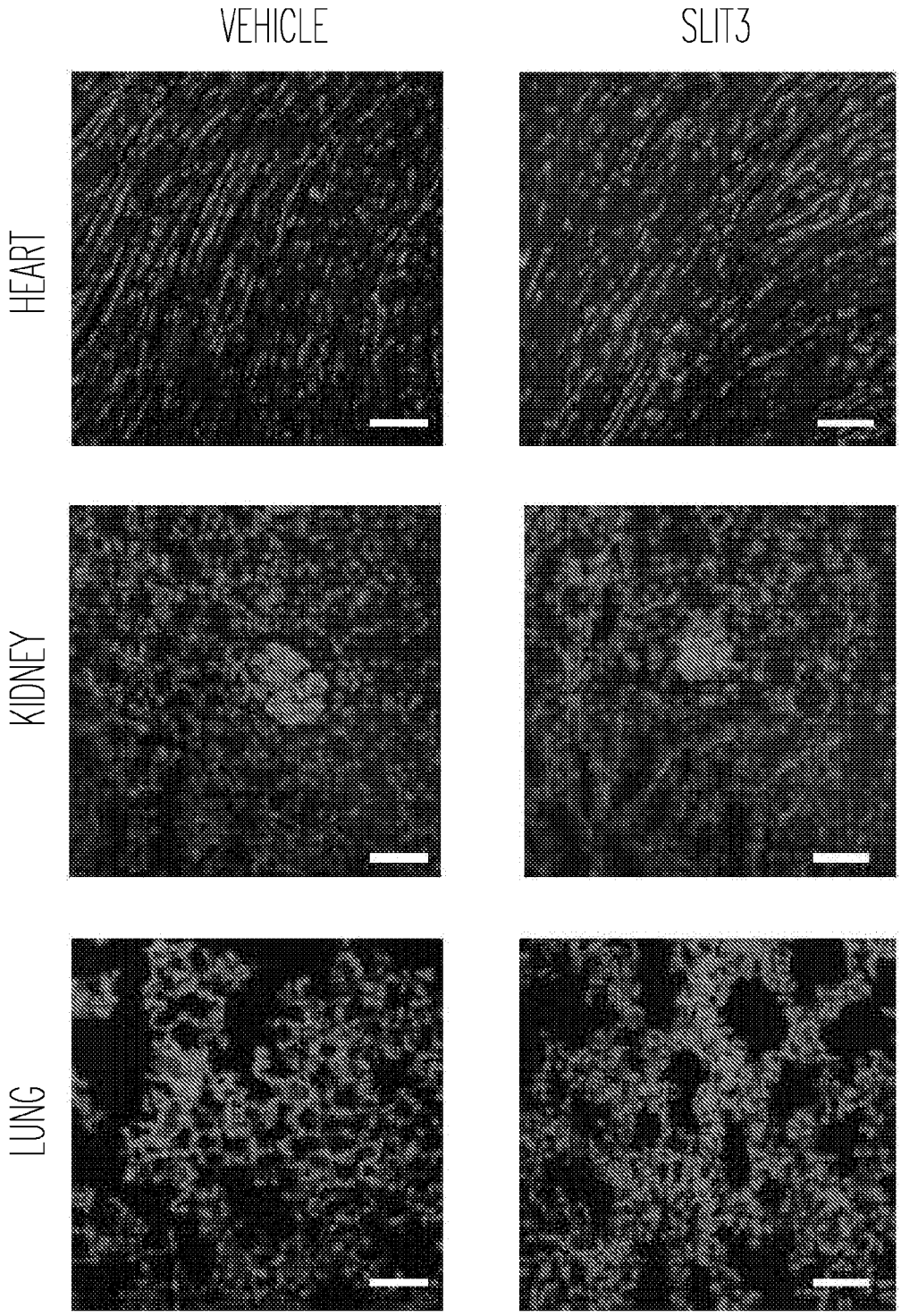

Fig. 26C

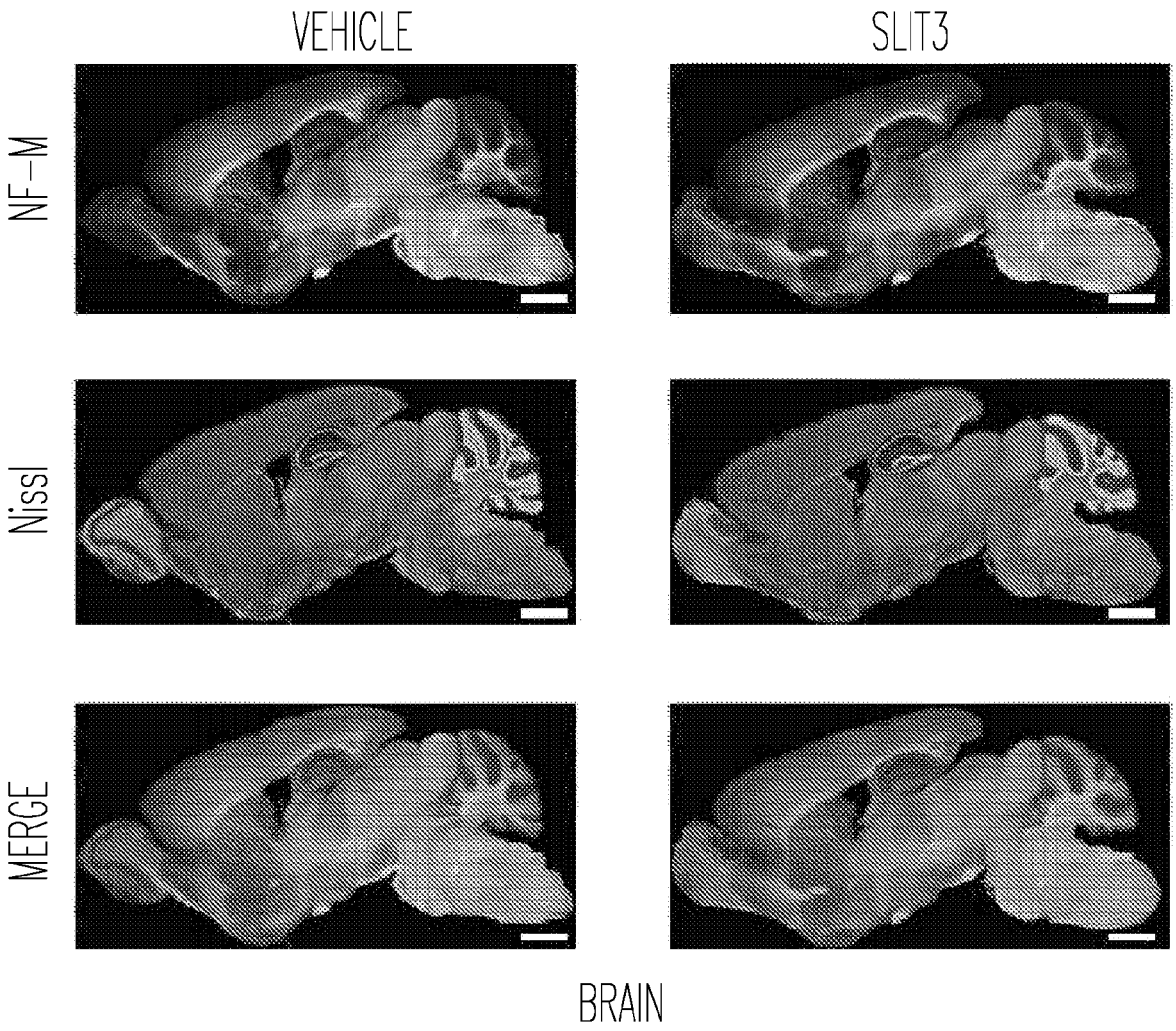

Fig. 26D

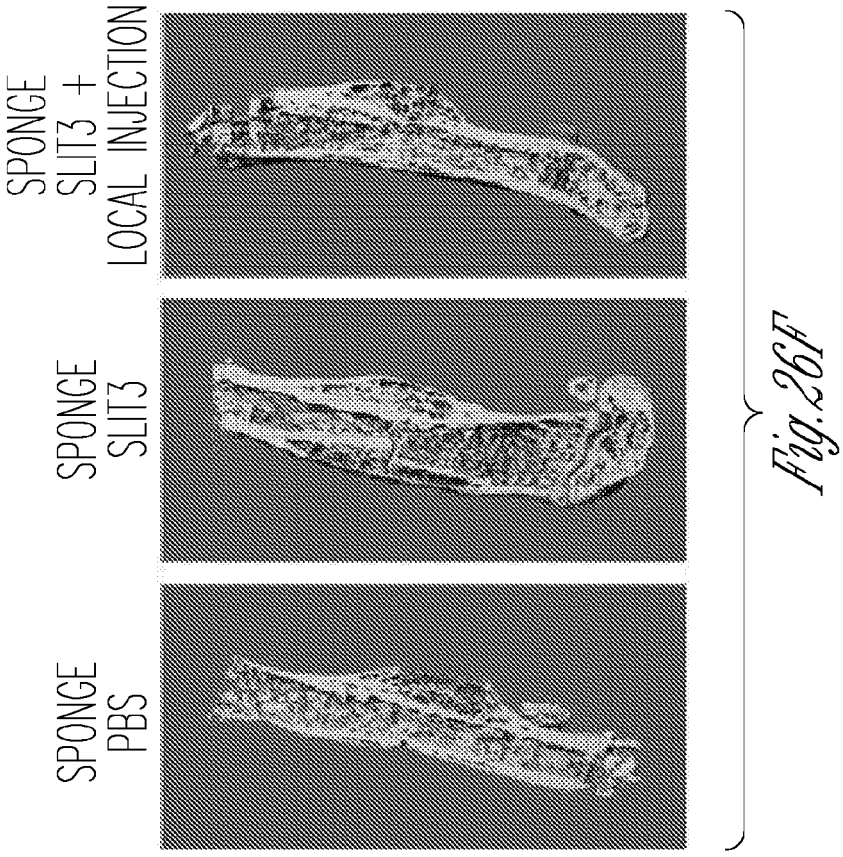

Fig.26F

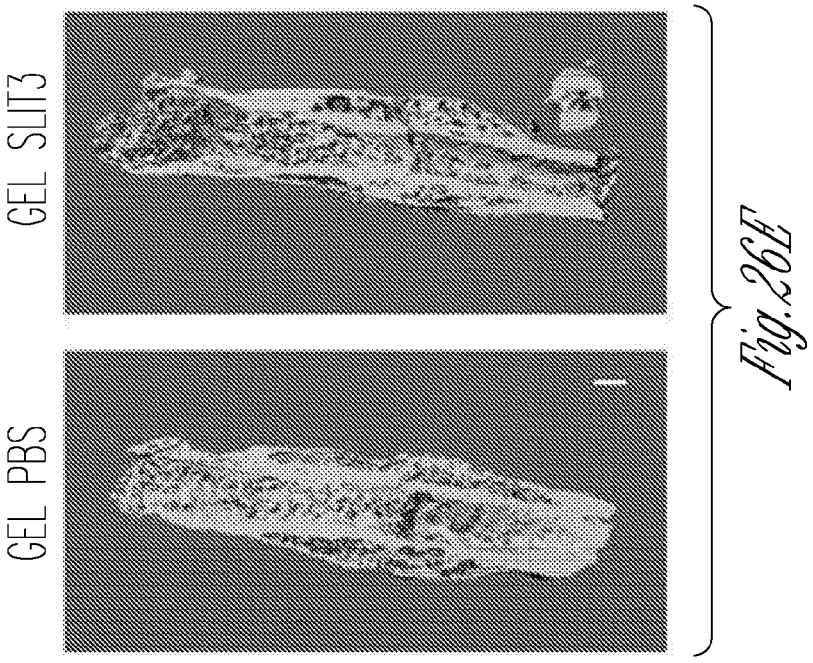

Fig.26E

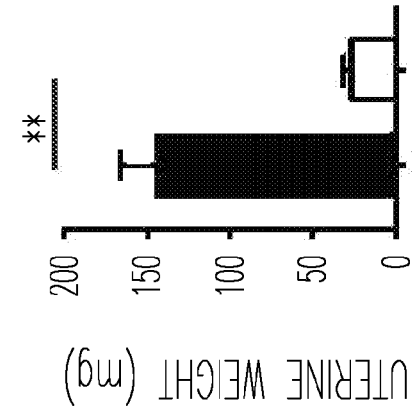

Fig.27B

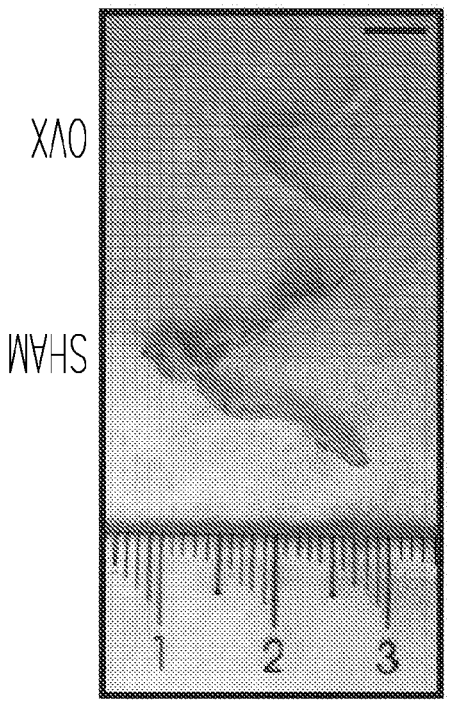

Fig.27A

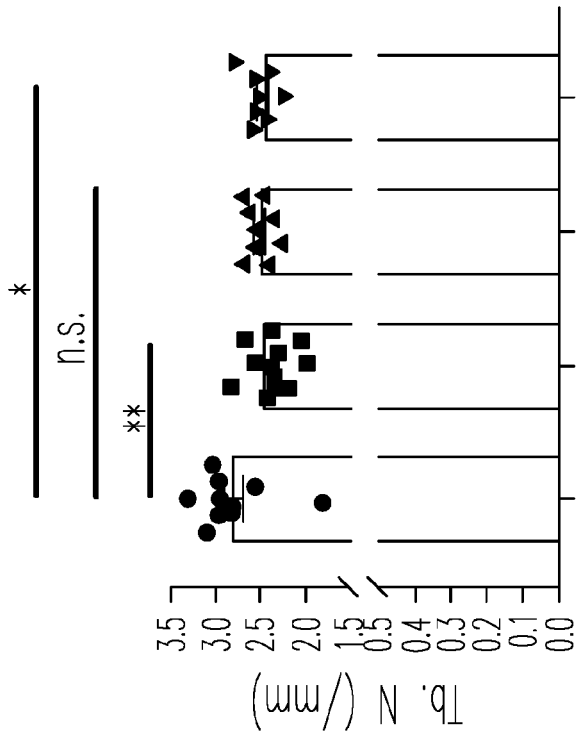

Fig.27C-2

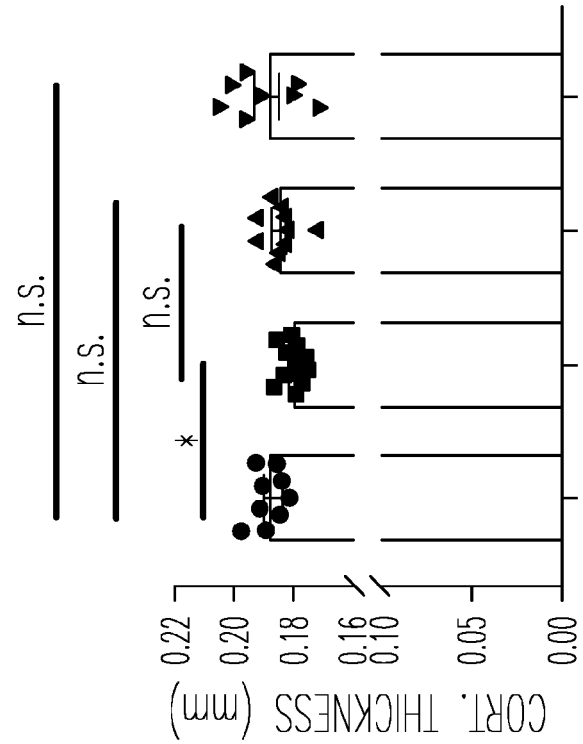

Fig.27C-1

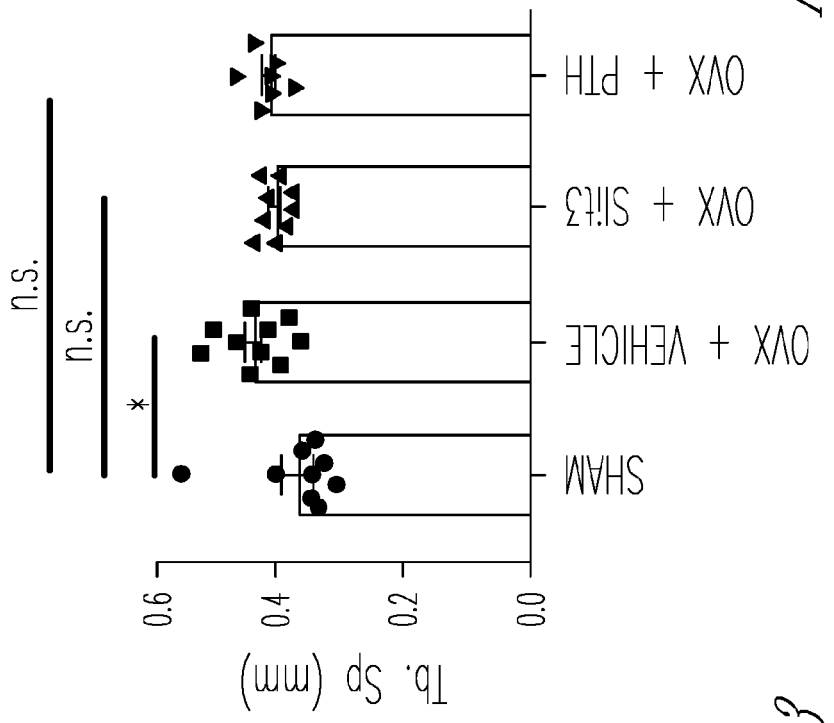

Fig.27C-4

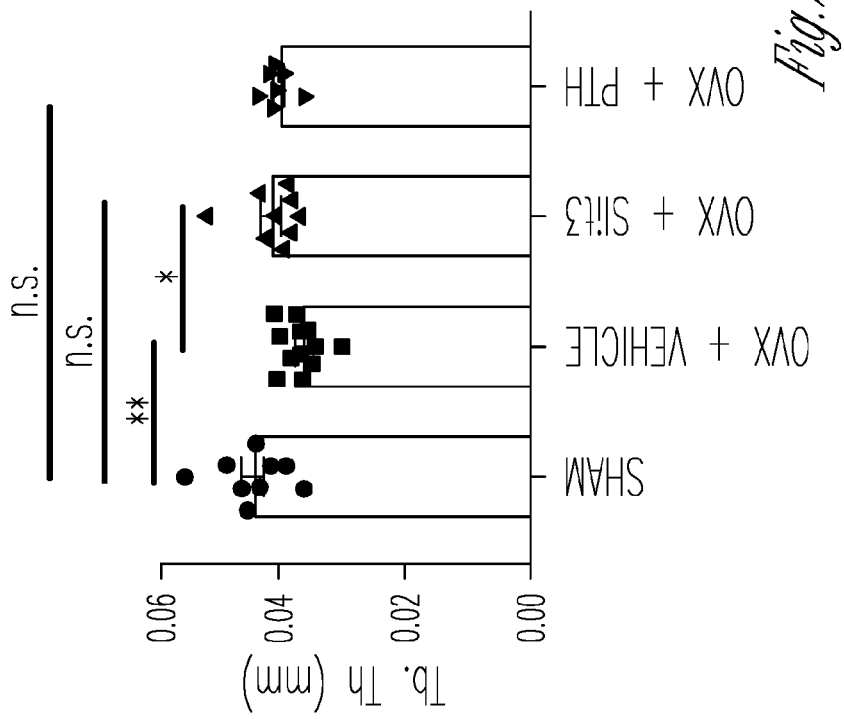

Fig.27C-3

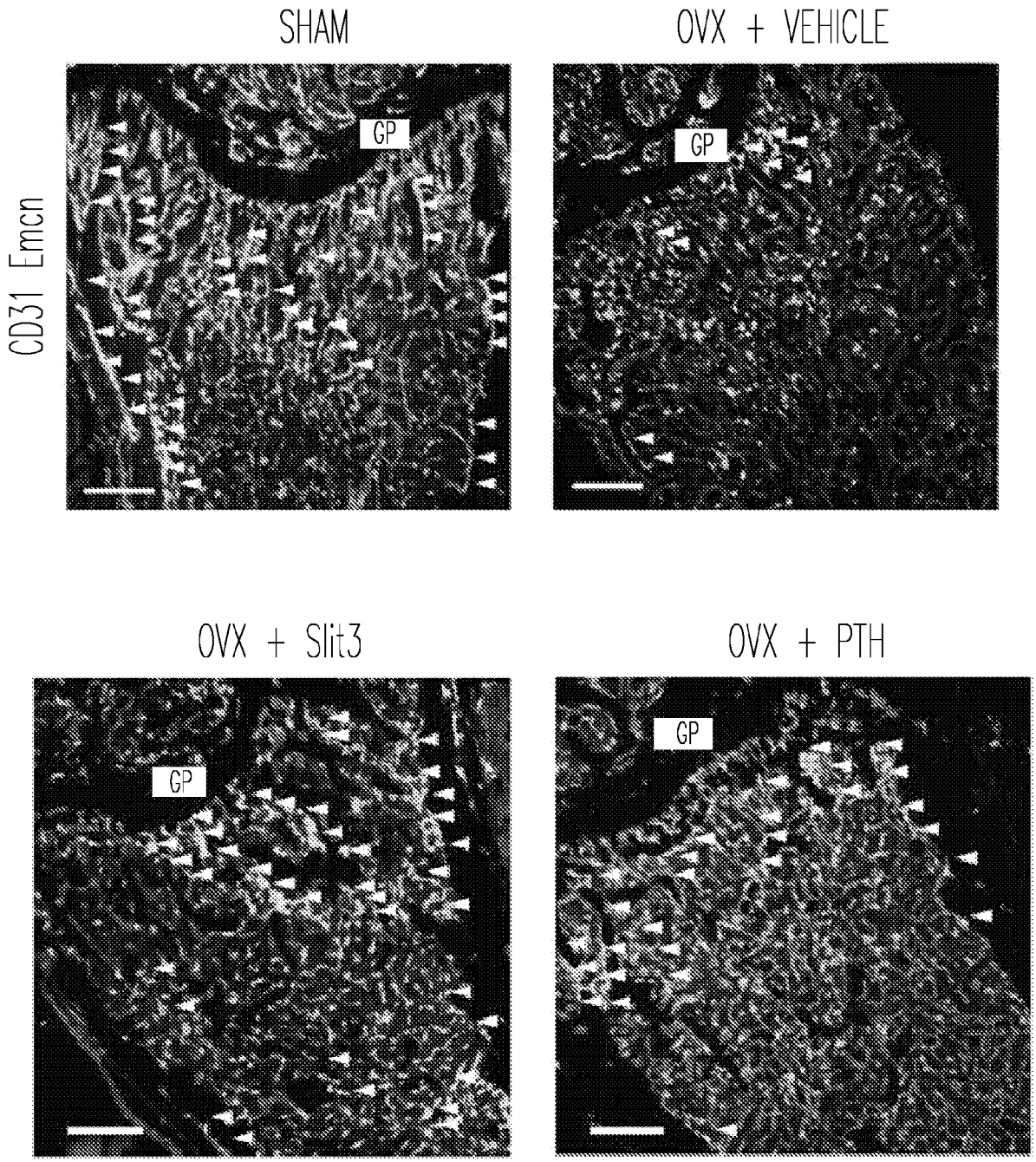

Fig.27D

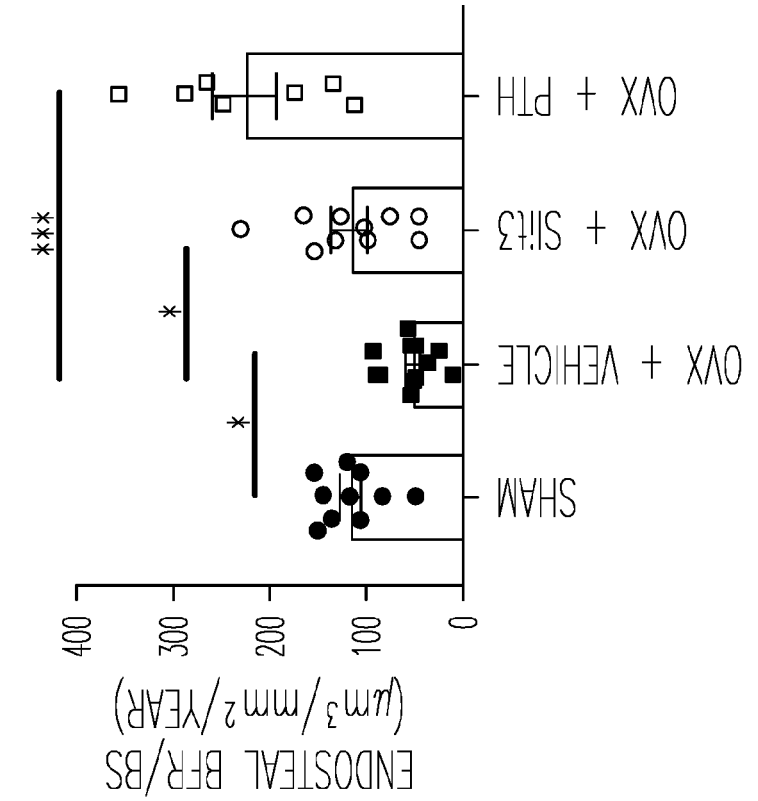

Fig.27E-1

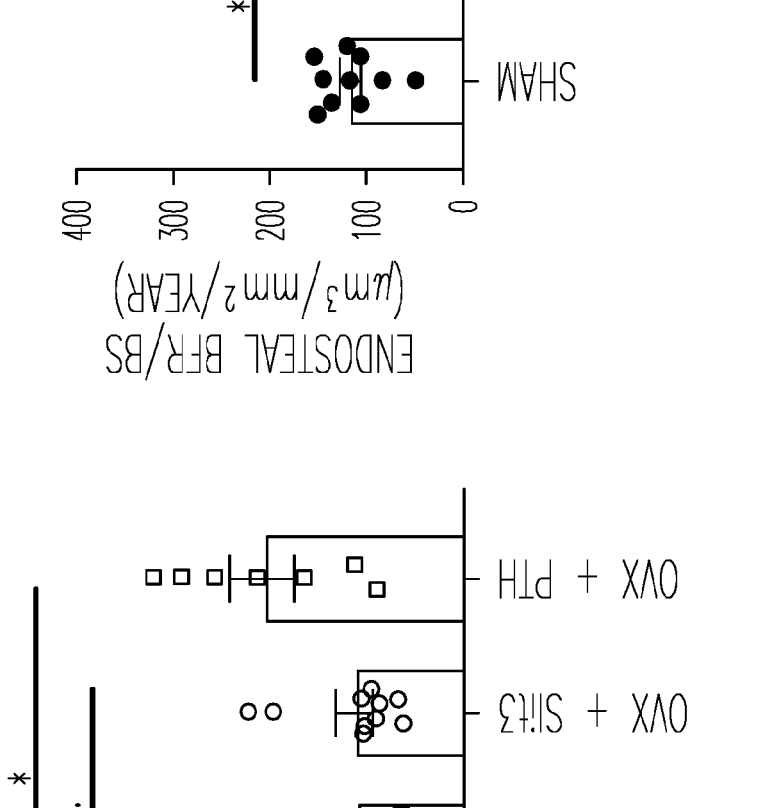

Fig.27E-2

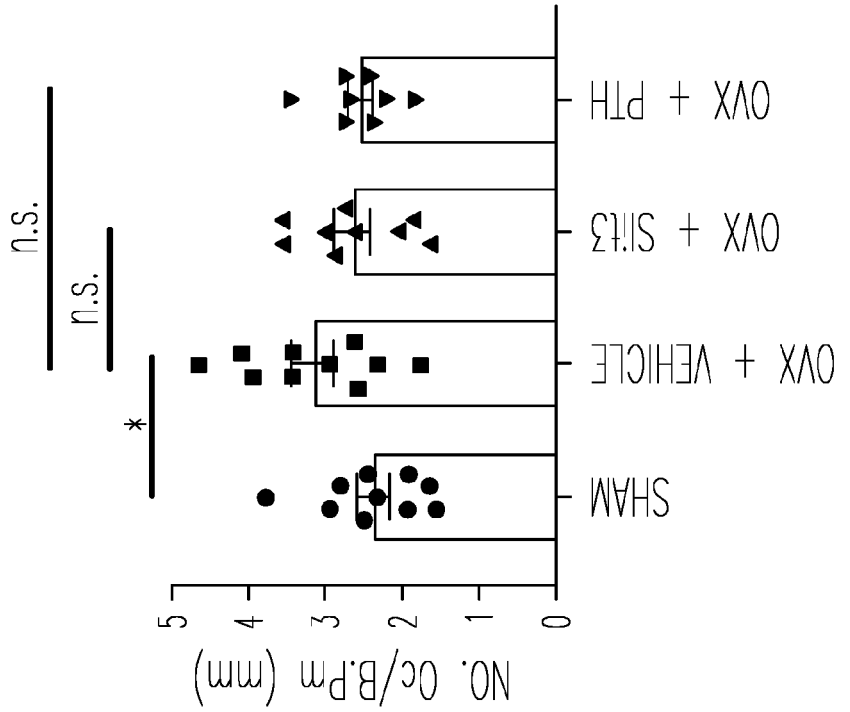

Fig.27F-1

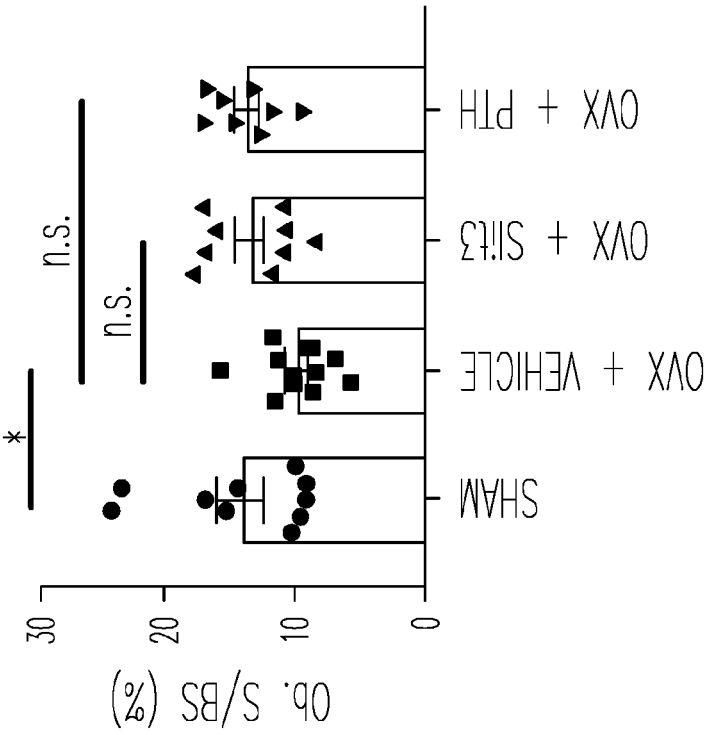

Fig.27F-2

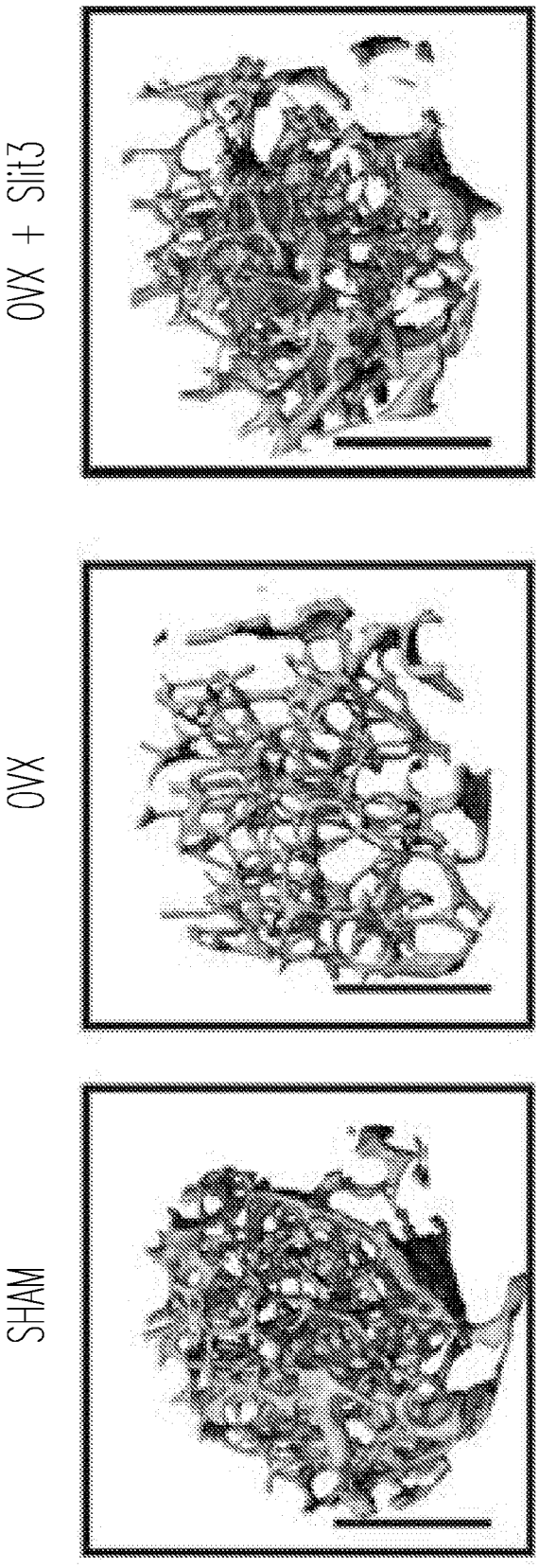

Fig. 28A

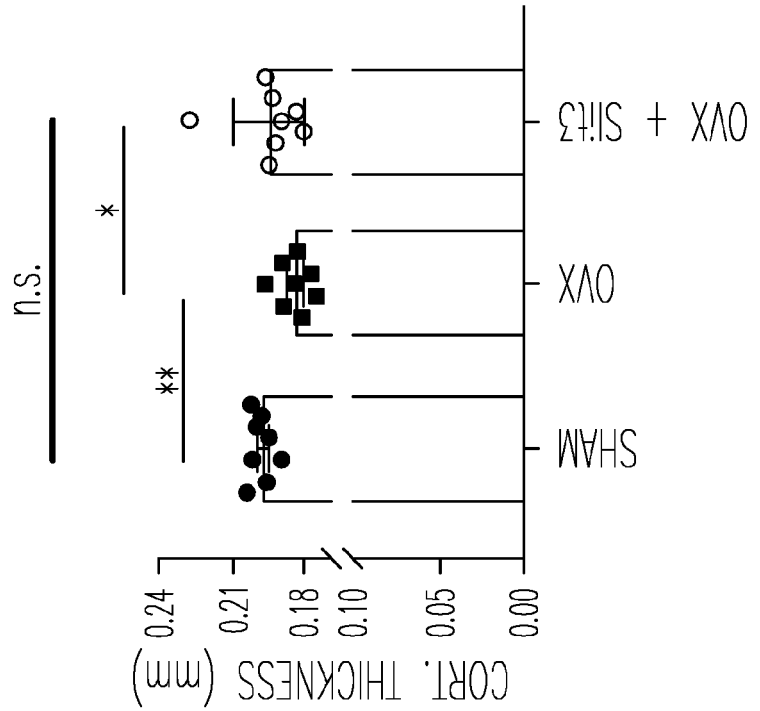

Fig.28B-2

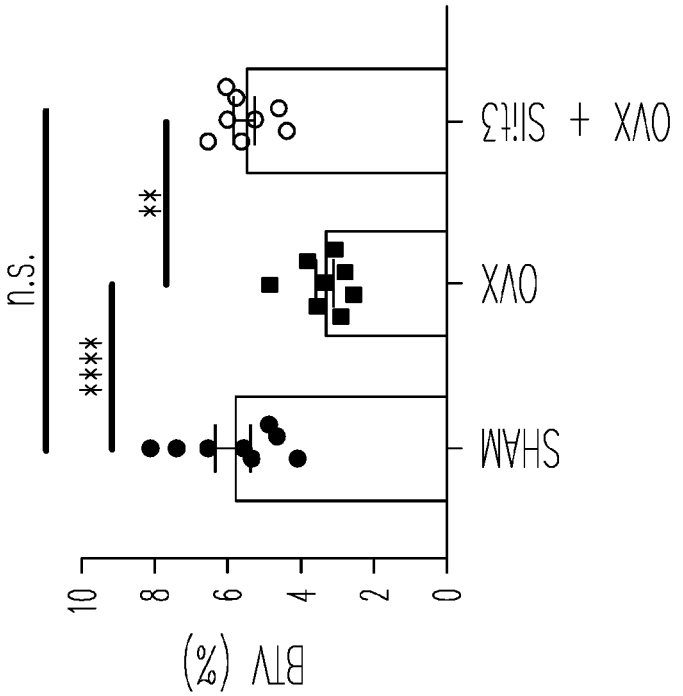

Fig.28B-1

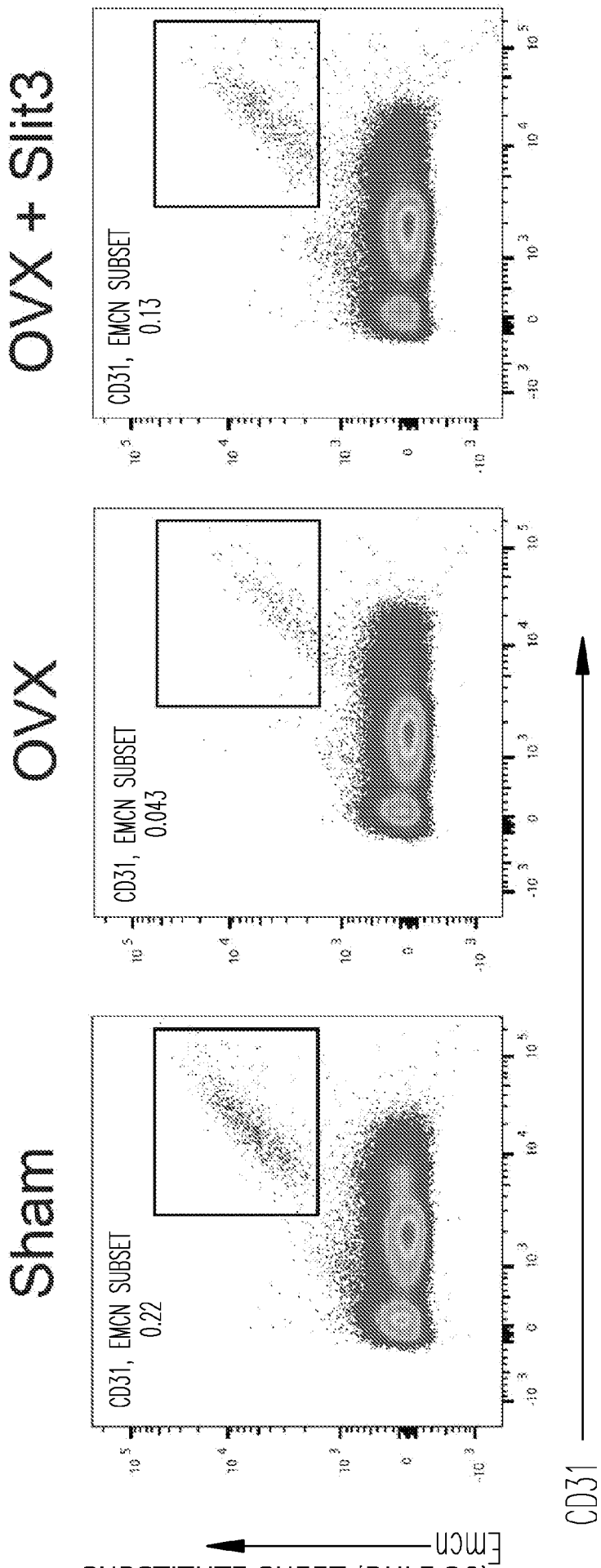
Sham
OVX
OVX + Slit3
CD31, EMCN SUBSET
0.22
CD31, EMCN SUBSET
0.043
CD31, EMCN SUBSET
0.13
EMCN
CD31

Fig.28C

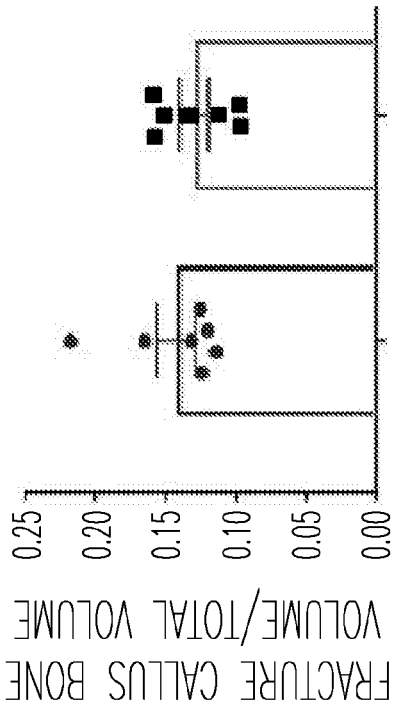

Fig. 29B

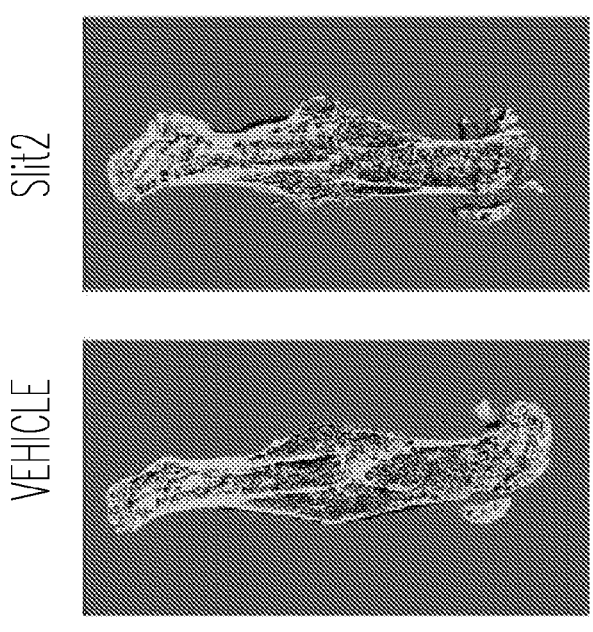

Fig. 29A

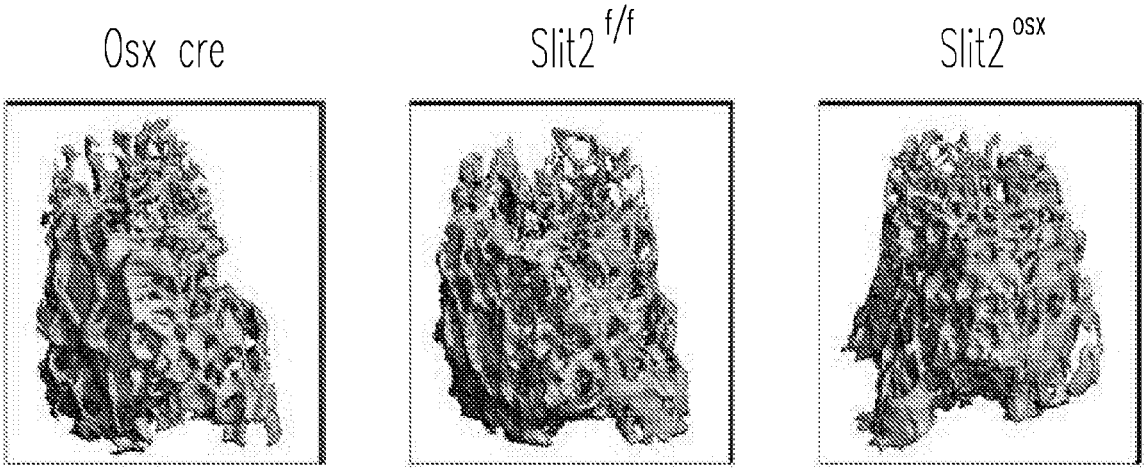

Fig.29C

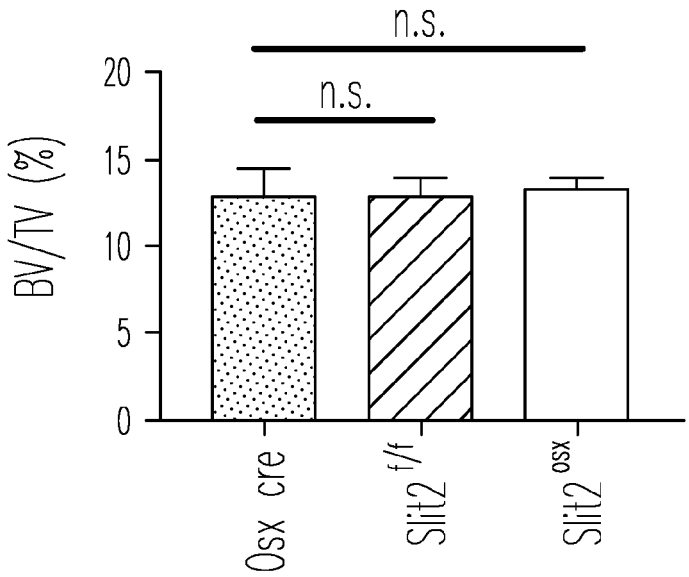

Fig.29D

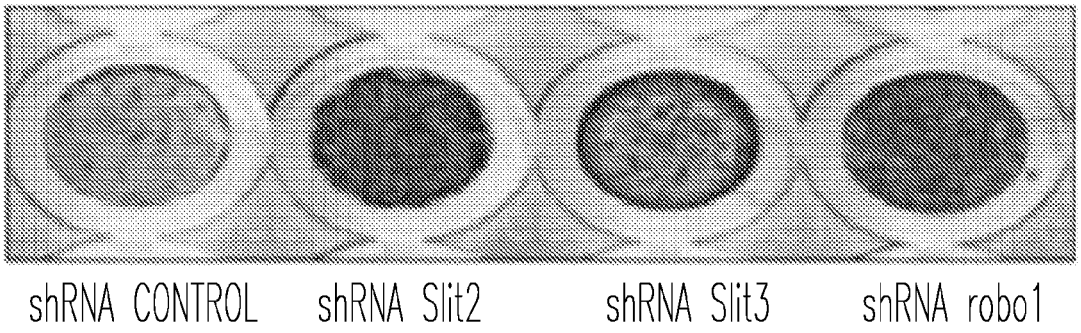

Fig.29E-1

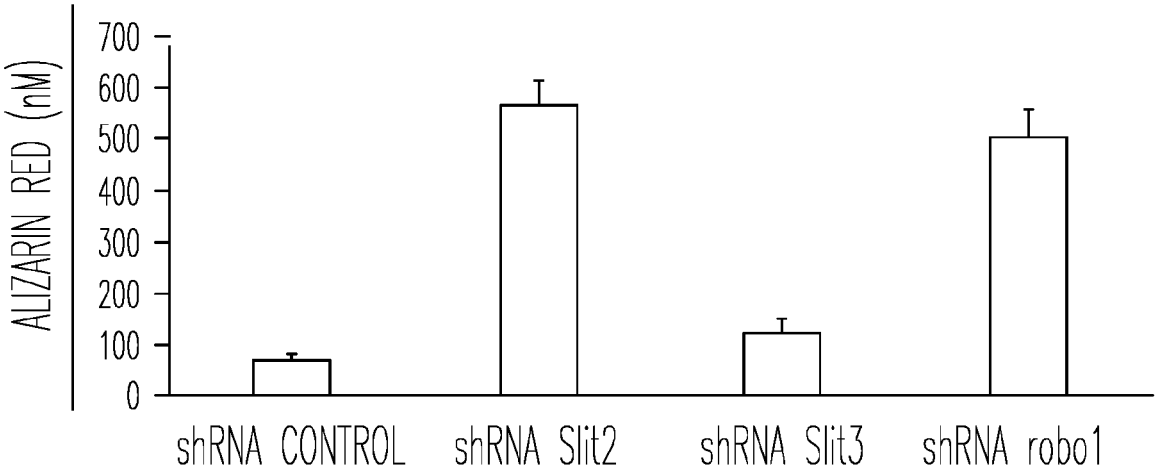

29E-2

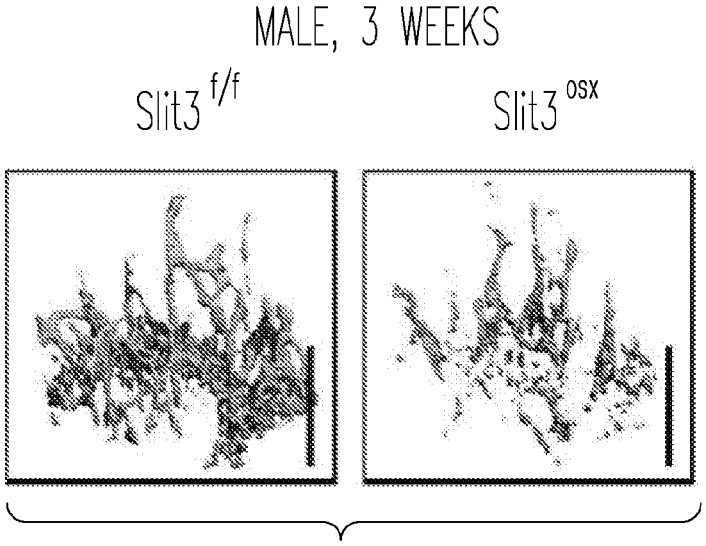

Fig. 30A-1

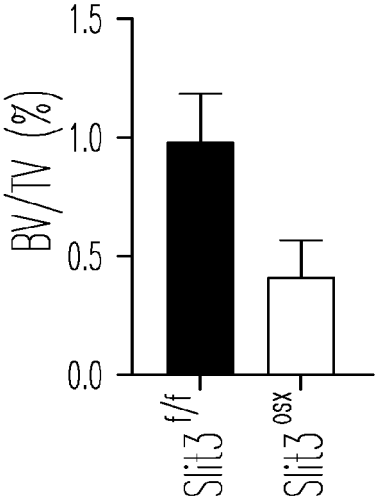

Fig. 30A-2

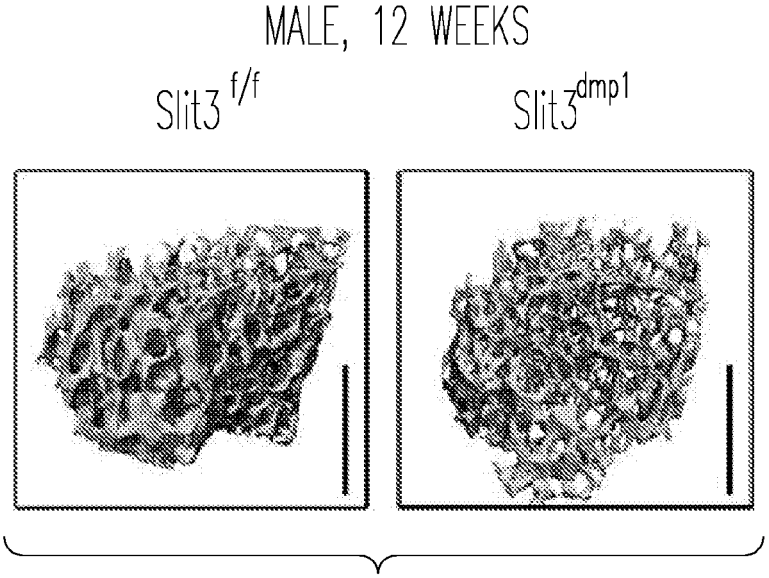

Fig. 30B-1

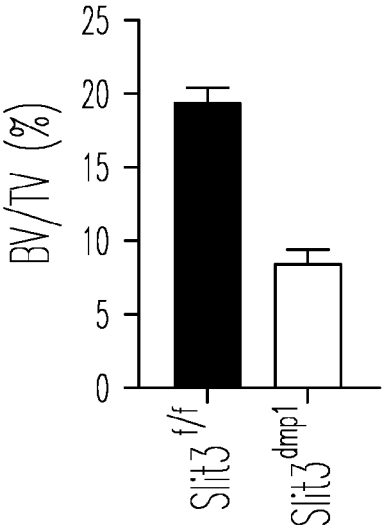

Fig. 30B-2

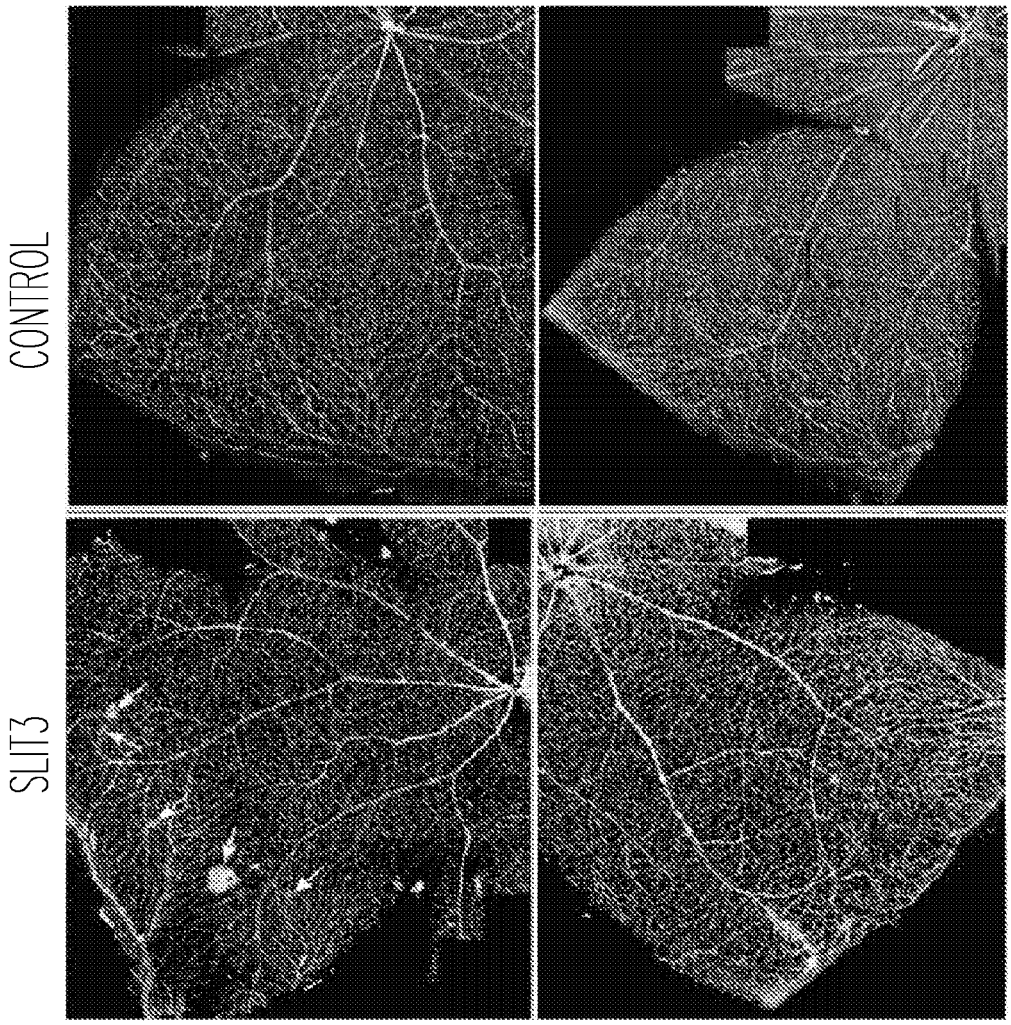

Fig. 31

FIG. 32

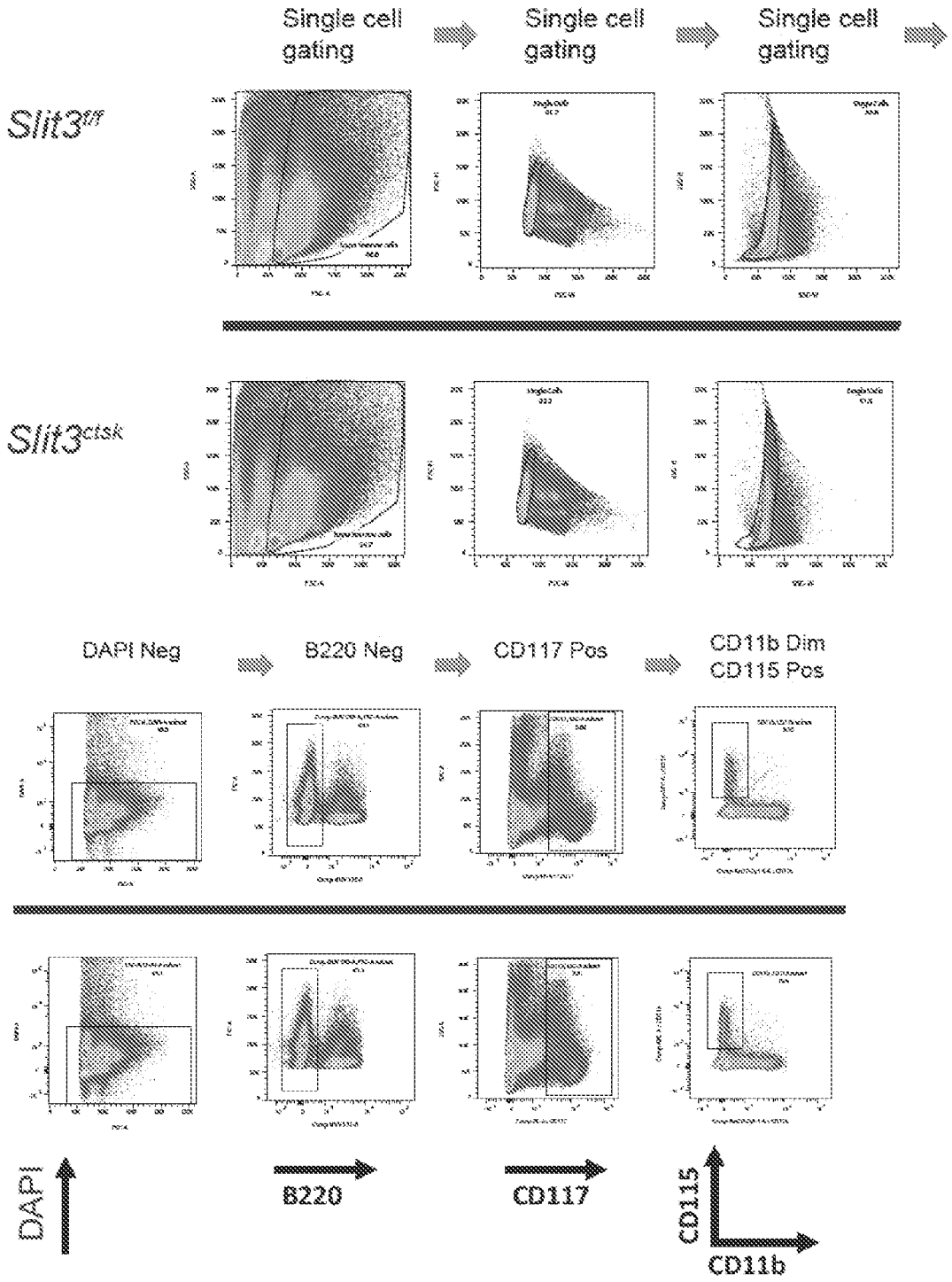
Single cell gating
Single cell gating
Single cell gating
Slit3fl/fl
Slit3ctsk
DAPI Neg
B220 Neg
CD117 Pos
CD11b Dim CD115 Pos
DAPI
B220
CD117
CD115
CD11b

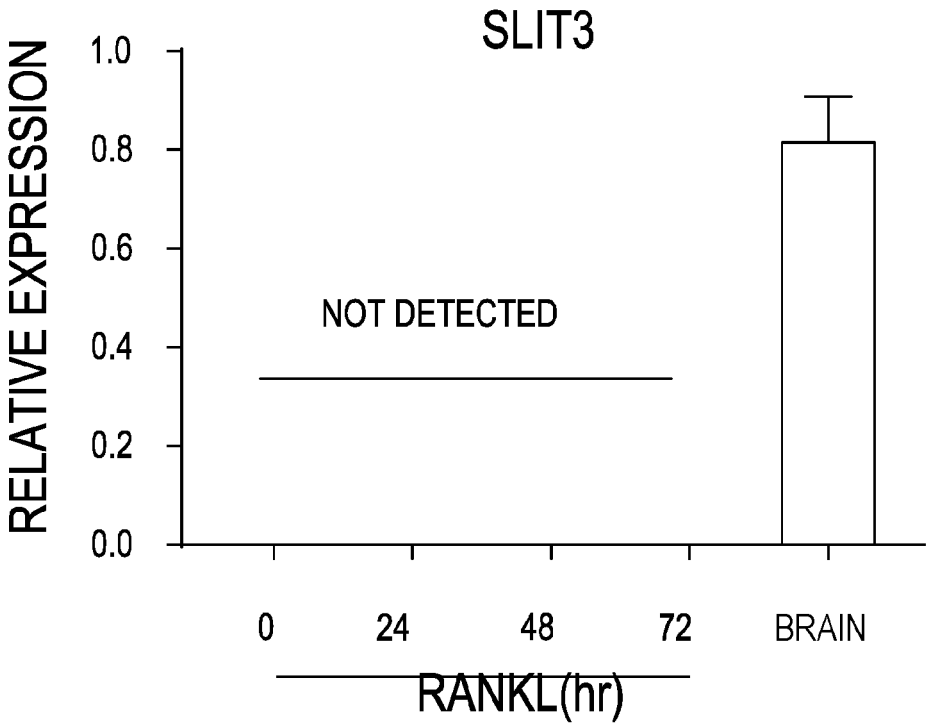

Fig. 33A

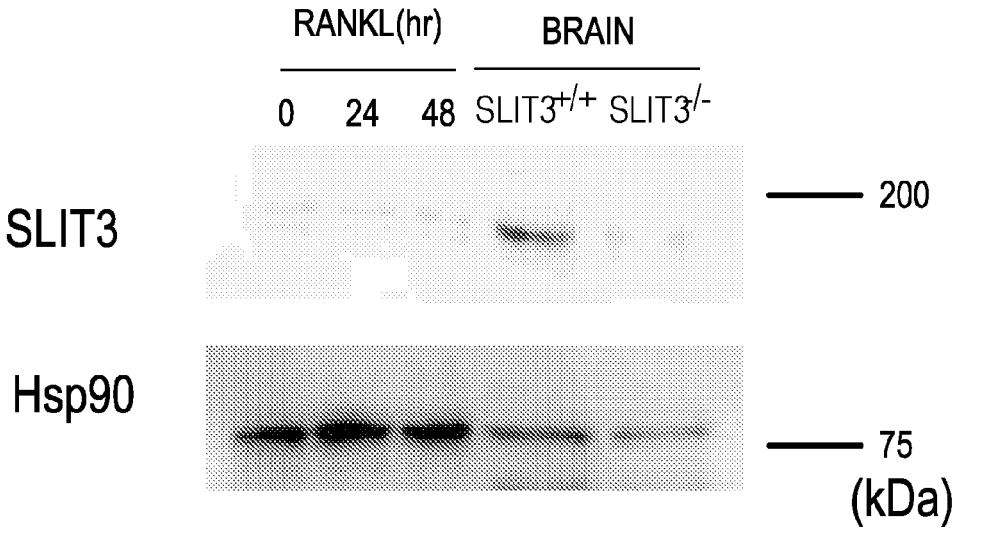

Fig. 33B

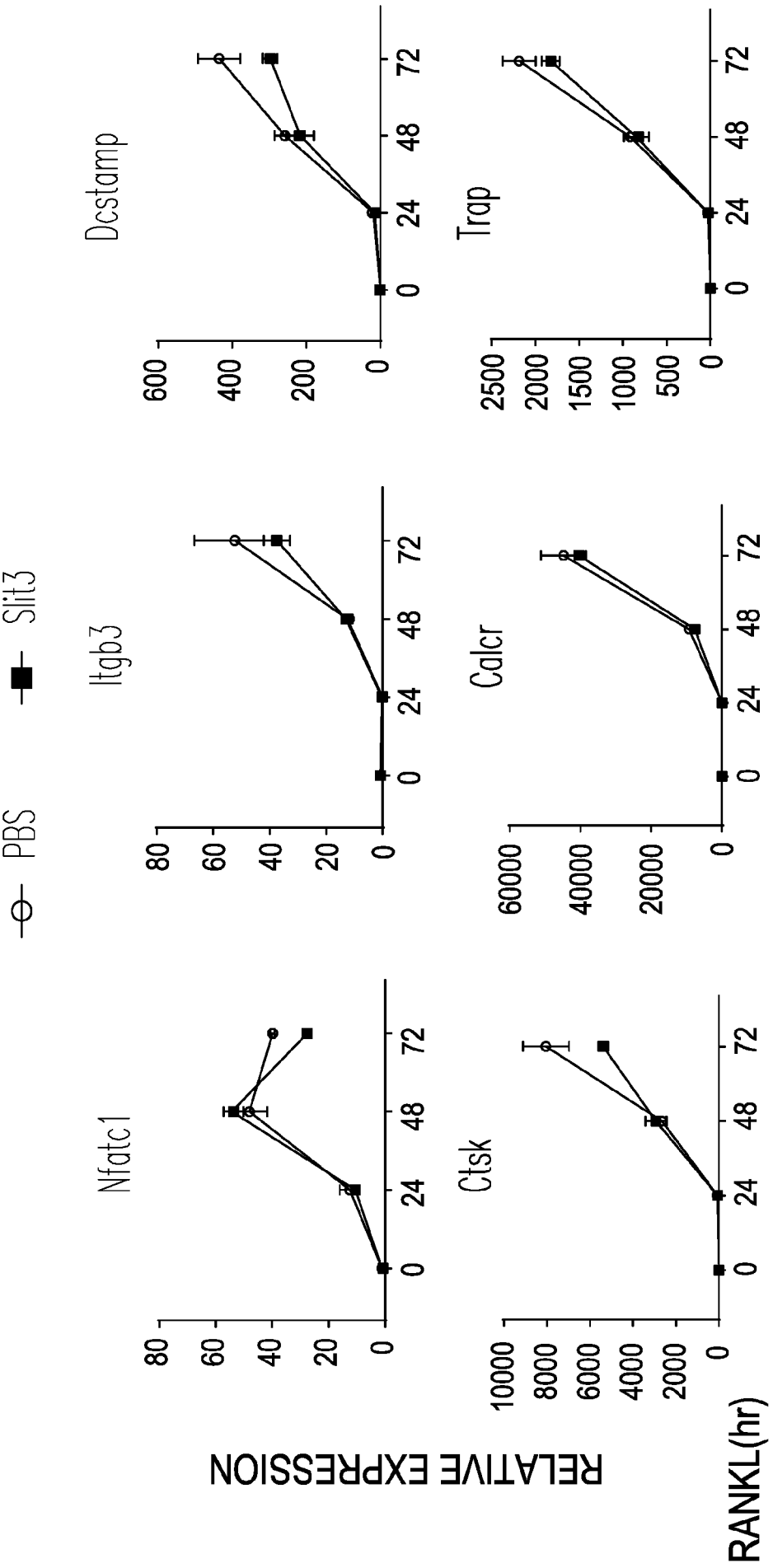
PBS
Slit3
Nfatc1
Itgb3
Dcstamp
Ctsk
Calcr
Trap
RELATIVE EXPRESSION
RANKL(hr)
0
24
48
72
80
60
40
20
10000
8000
6000
4000
2000
60000
40000
20000
600
400
200
2500
2000
1500
1000
500

Fig.33C

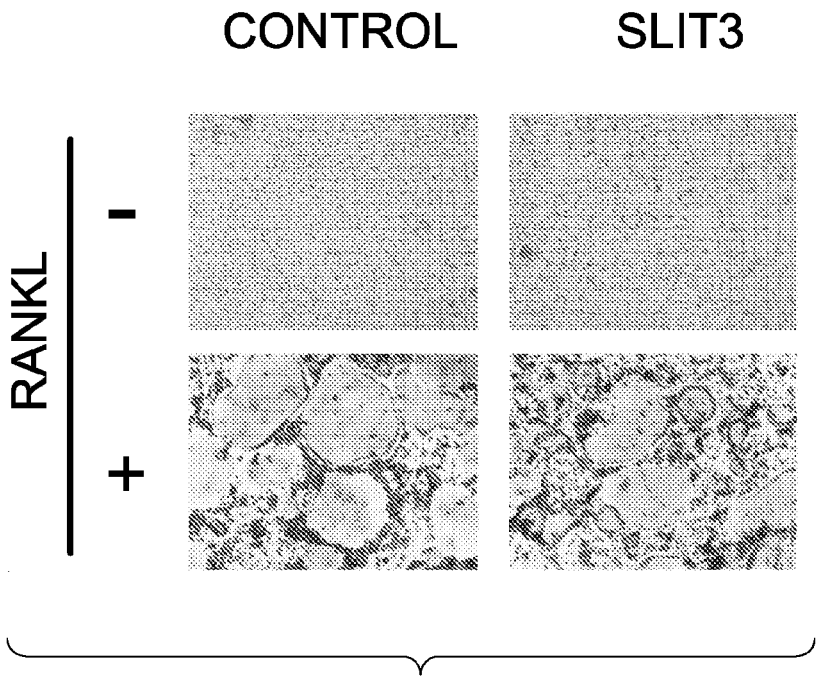

Fig. 33D-1

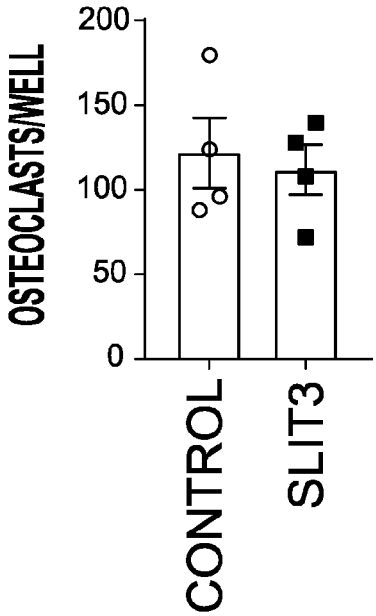

Fig. 33D-2

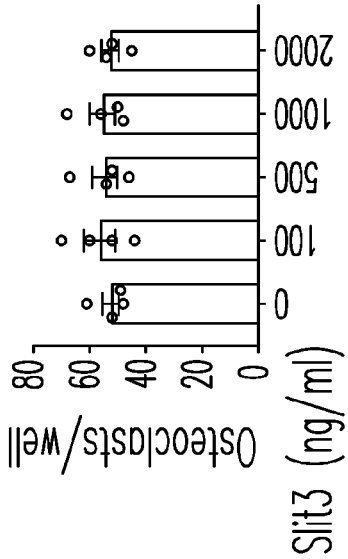

Fig. 33E-2

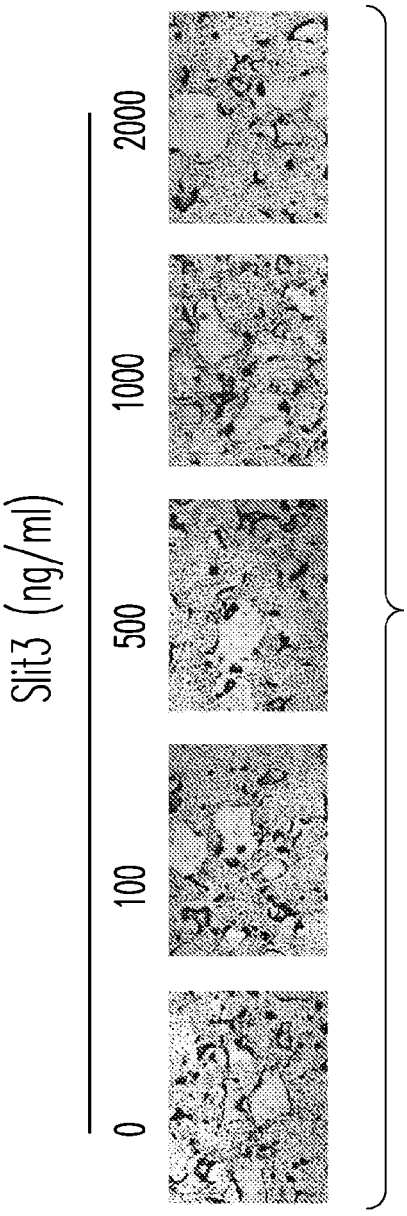

Fig. 33E-1

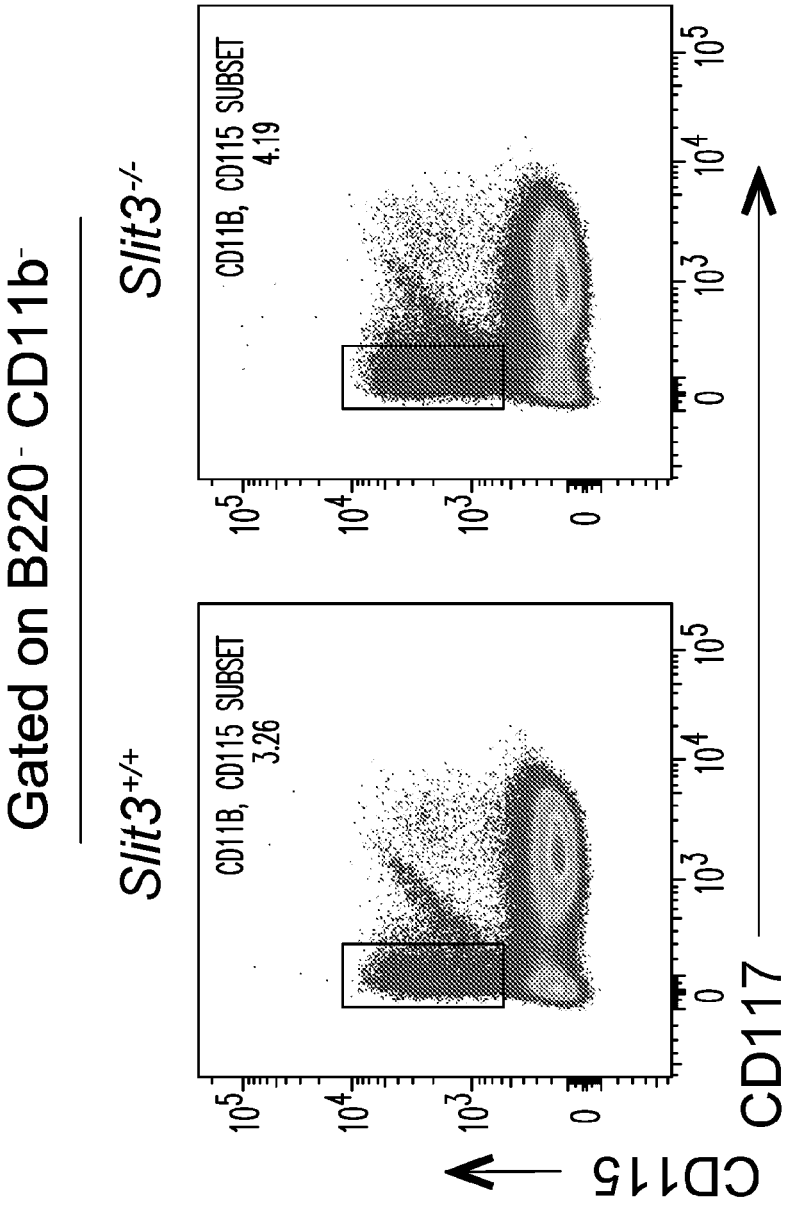

Fig. 34A-1

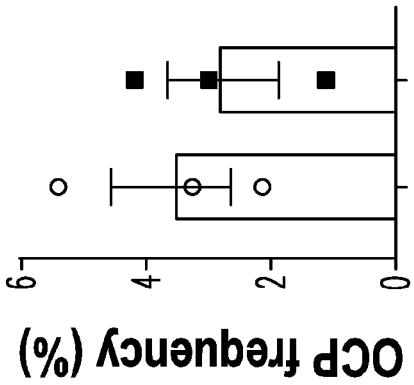

Fig. 34A-2

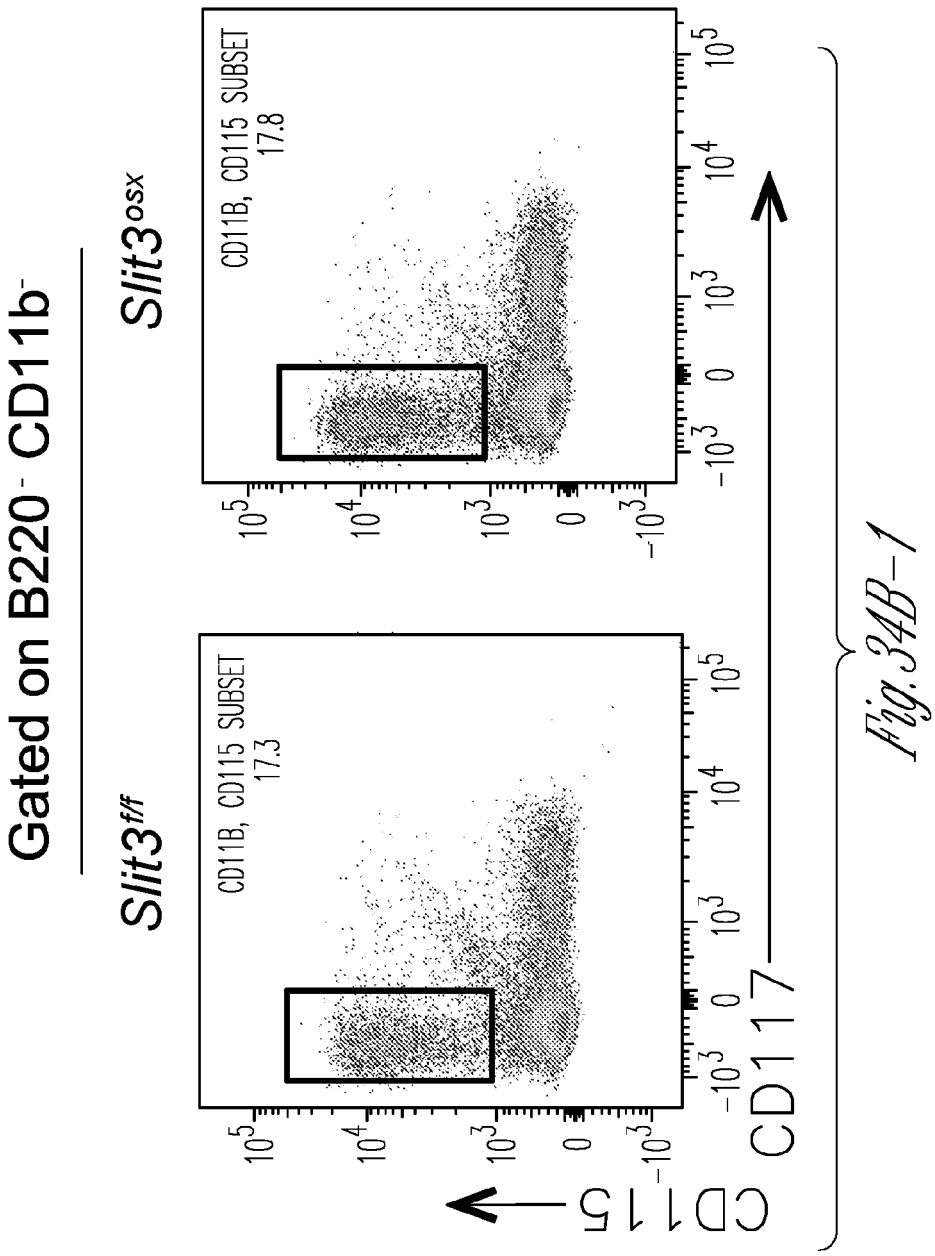

Fig. 34B-1

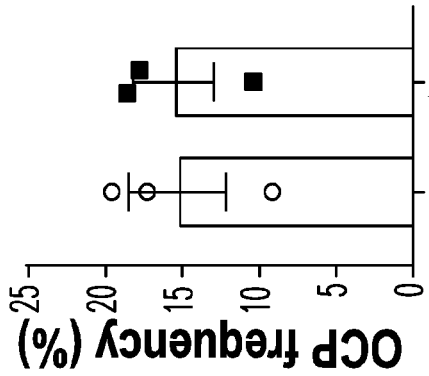

Fig. 34B-2

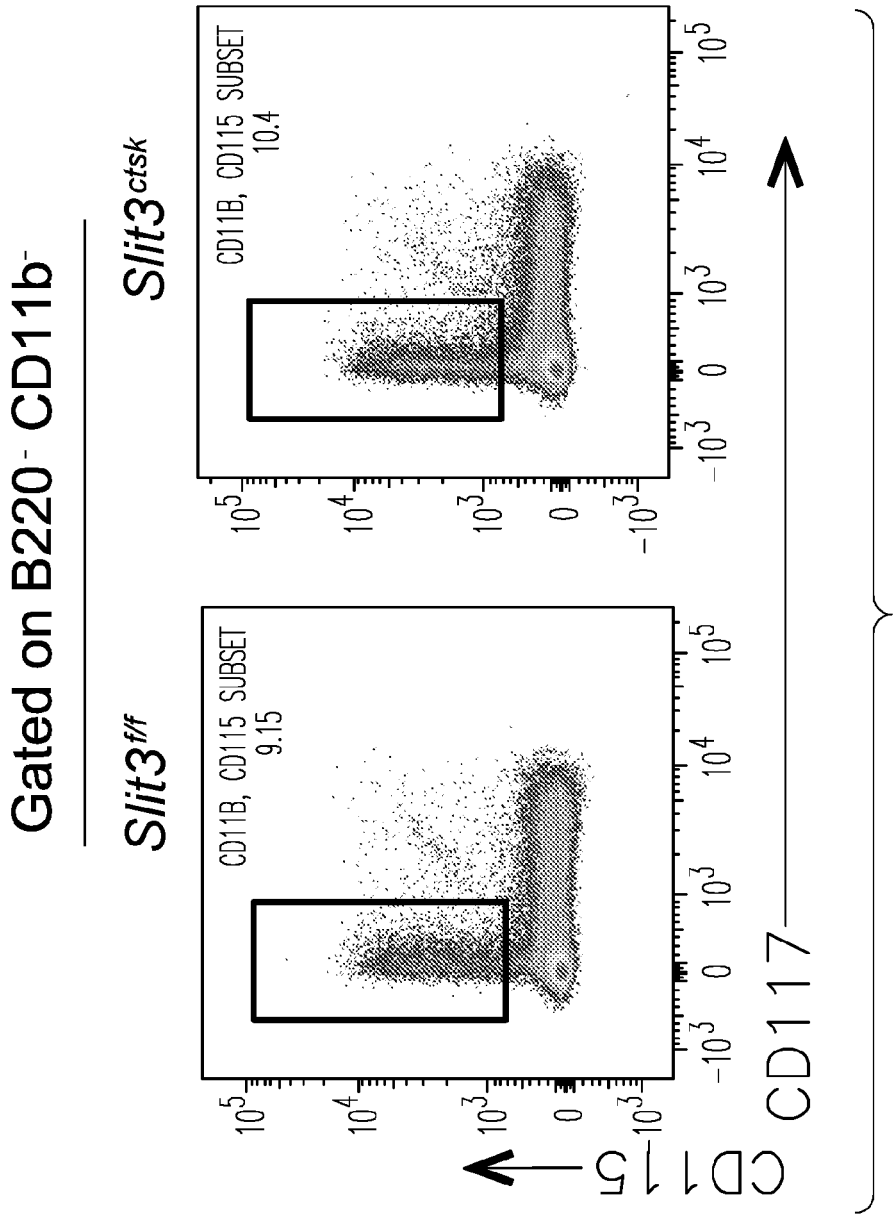

Fig. 34C-1

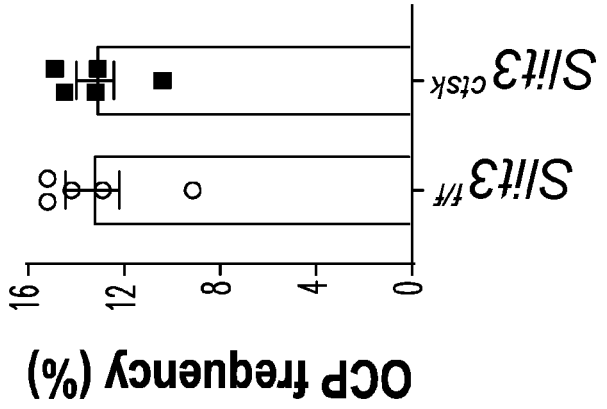

Fig. 34C-2

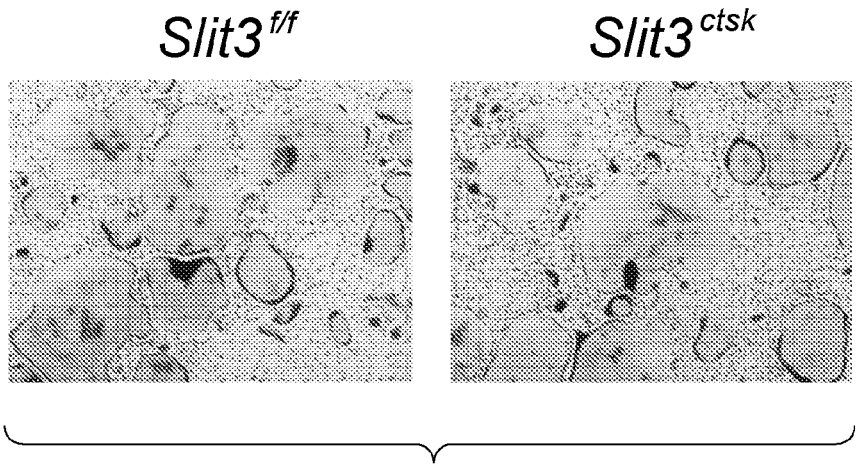

Fig. 34D-1

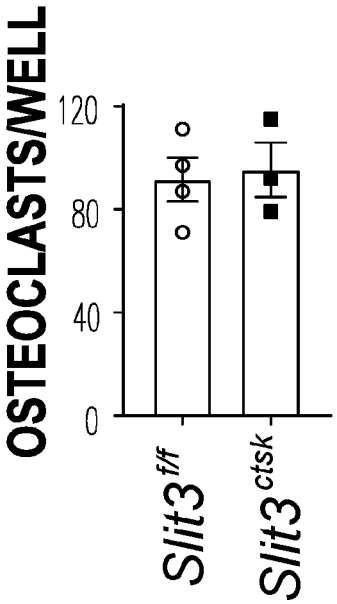

Fig. 34D-2

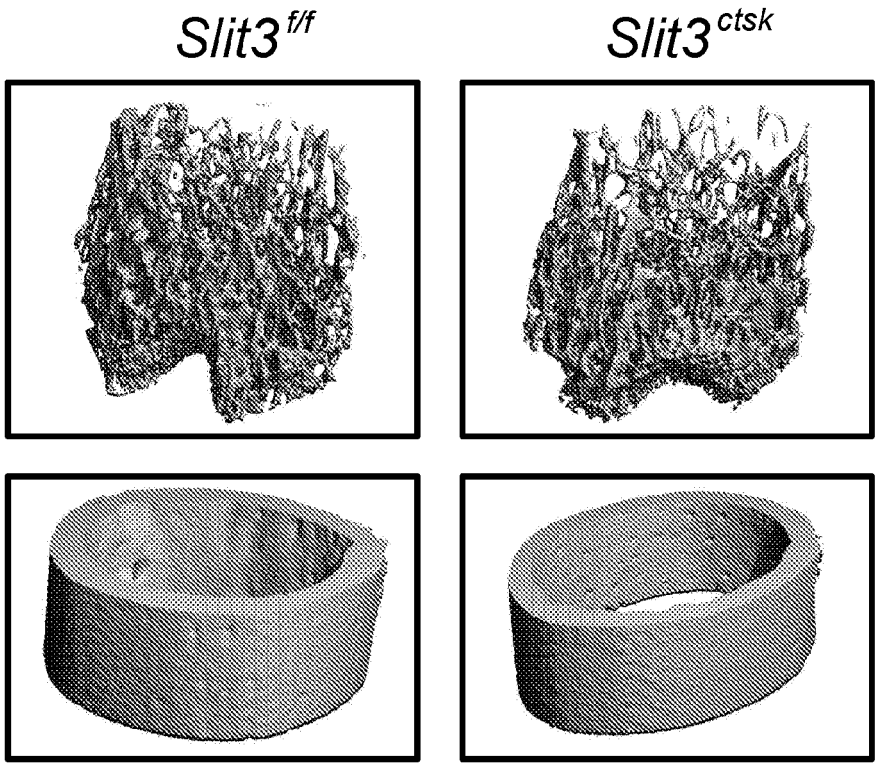

Fig. 34E-1

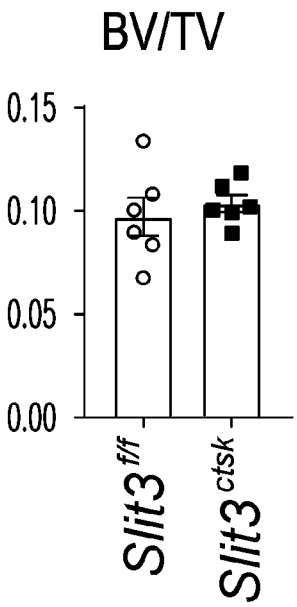

Fig. 34E-2

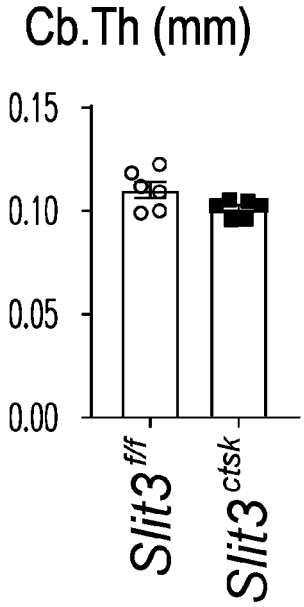

Fig. 34E-3

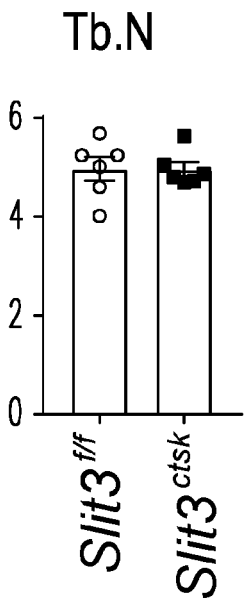

Fig. 34E-4

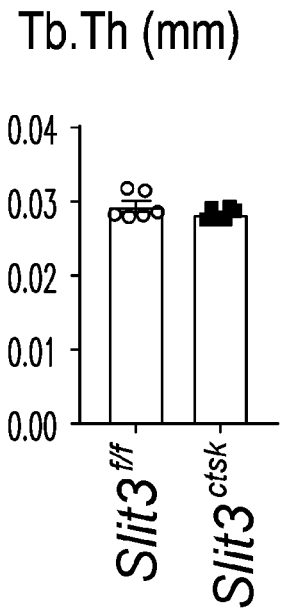

Fig. 34E-5

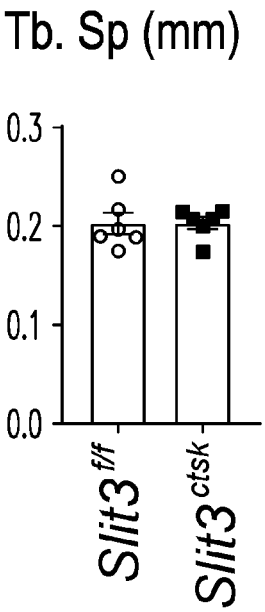

Fig. 34E-6

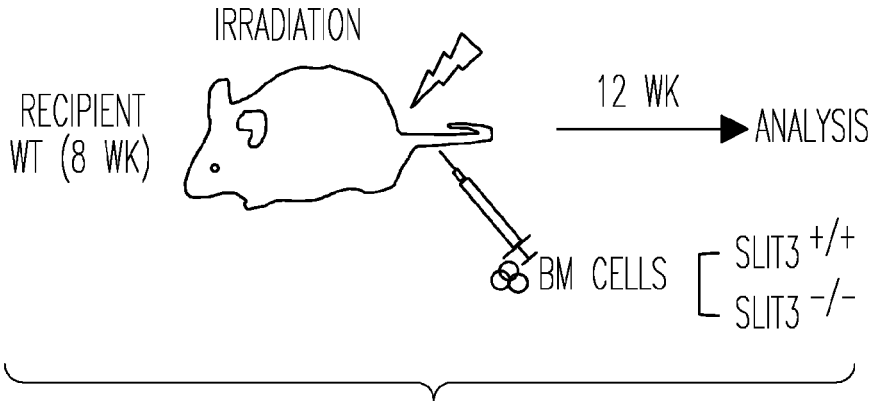

Fig. 35A

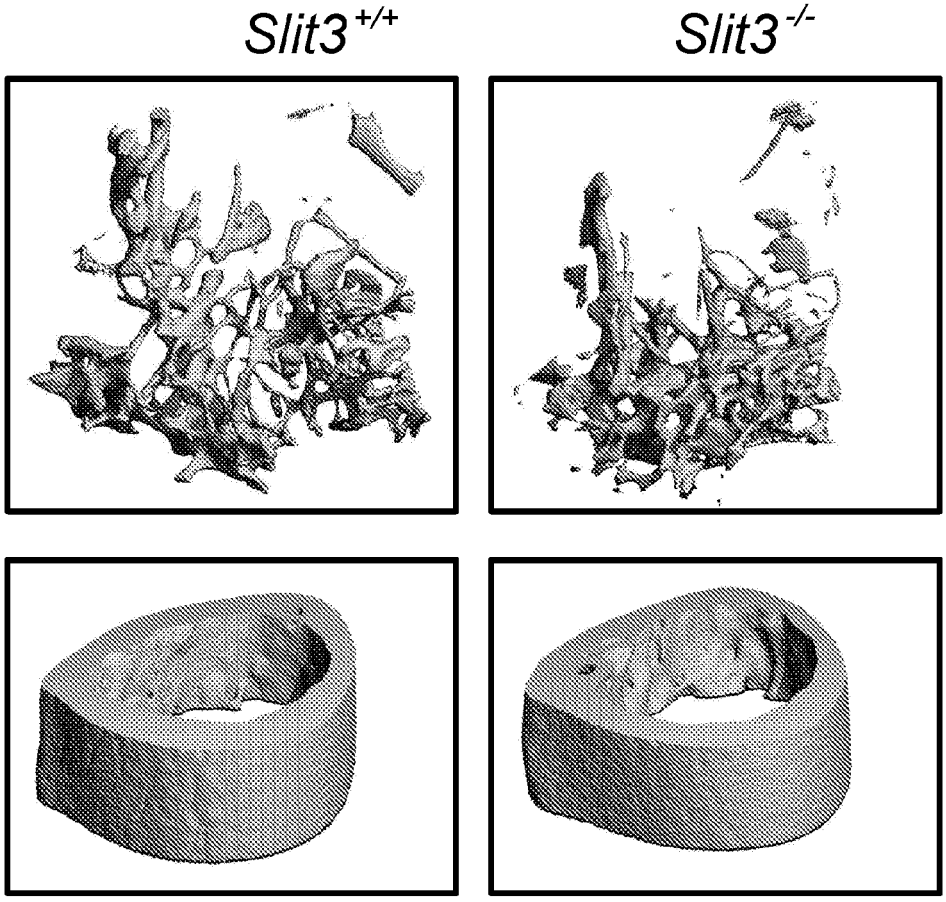

Fig. 35B

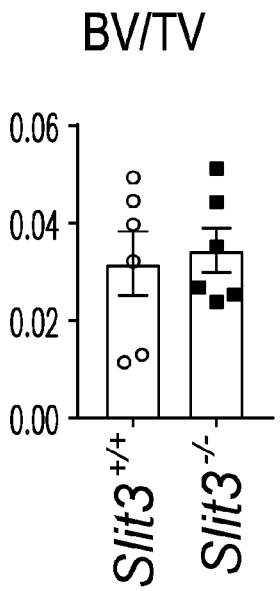

Fig. 35C-1

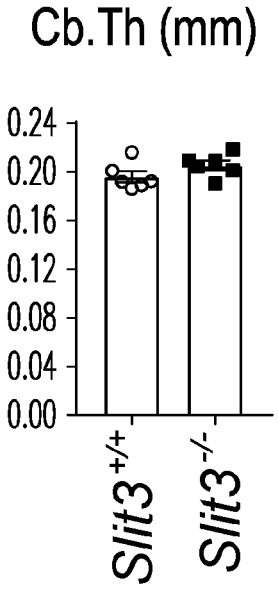

Fig. 35C-2

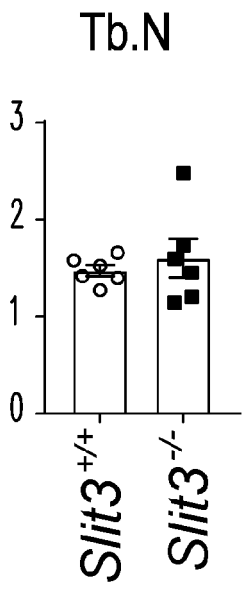

Fig. 35C-3

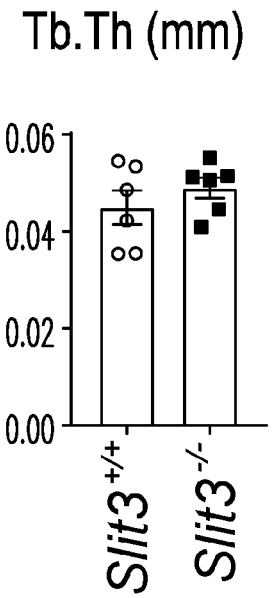

Fig. 35C-4

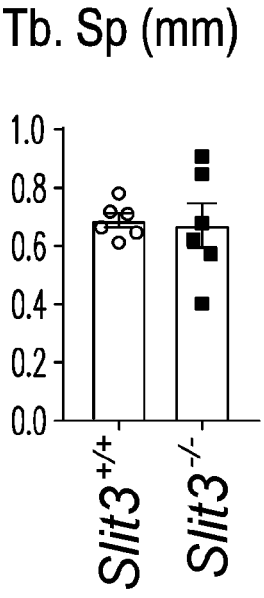

Fig. 35C-5

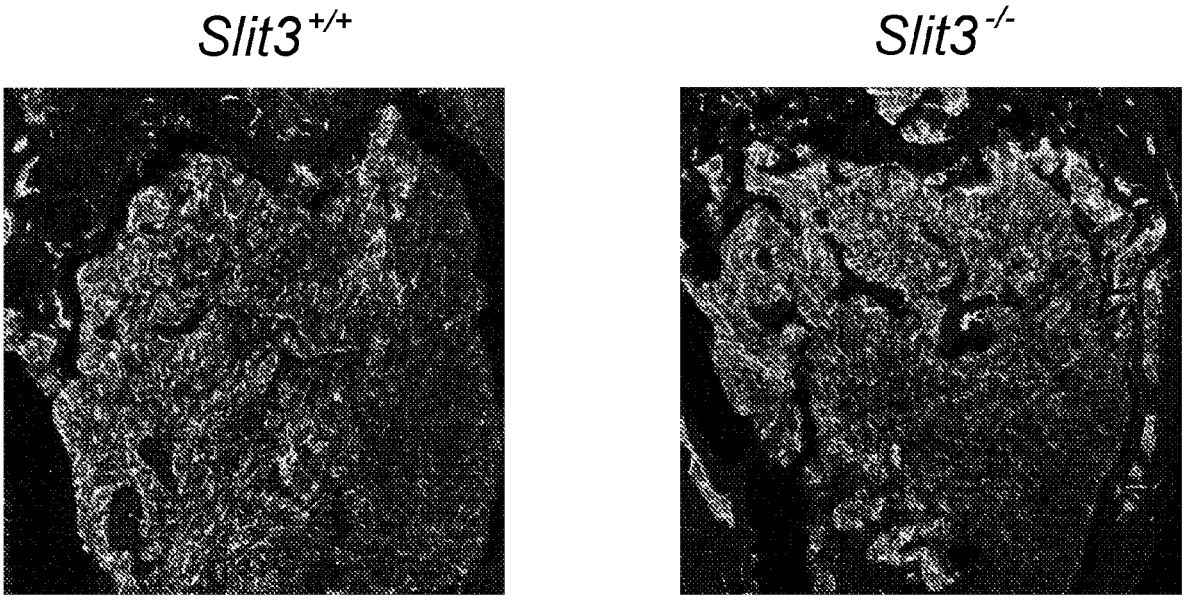

Fig. 35D

INTERNATIONAL SEARCH REPORT

International application No.
PCT/US2019/018115

A. CLASSIFICATION OF SUBJECT MATTER

IPC(8) - A61F 2/28; A61K 35/32; A61K 38/18; A61L 27/00; A61L 27/54; A61P 19/08 (2019.01)
CPC - A61F 2002/2835; A61K 38/18; A61L 27/56; A61L 2430/02 (2019.02)

According to International Patent Classification (IPC) or to both national classification and IPC

B. FIELDS SEARCHED

Minimum documentation searched (classification system followed by classification symbols)
See Search History document

Documentation searched other than minimum documentation to the extent that such documents are included in the fields searched
USPC - 424/423; 514/7.6; 514/16.7; 623/16.11 (keyword delimited)

Electronic data base consulted during the international search (name of data base and, where practicable, search terms used)
See Search History document

C. DOCUMENTS CONSIDERED TO BE RELEVANT

Category*	Citation of document, with indication, where appropriate, of the relevant passages	Relevant to claim No.
X --- Y	US 2017/0000926 A1 (THE RESEARCH FOUNDATION FOR THE STATE UNIVERSITY OF NEW YORK) 05 January 2017 (05.01.2017) entire document	1-3, 5, 7-15 --- 6, 16-19
Y	US 2013/0195863 A1 (CLEZARDIN et al) 01 August 2013 (01.08.2013) entire document	6
Y	US 2009/0028831 A1 (VAN ZANT et al) 29 January 2009 (29.01.2009) entire document	16-19
Y	YANG et al., Intraislet SLIT-ROBO signaling is required for beta-cell survival and potentiates insulin secretion, PNAS, Vol. 110, No. 41, 08 October 2013, Pgs. 16480-16485	18
A	US 2015/0175673 A1 (THE ASAN FOUNDATION) 25 June 2015 (25.06.2015) entire document	1-20
A	US 2011/0002972 A1 (BOSSERHOFF et al) 06 January 2011 (06.01.2011) entire document	1-20
A	US 2010/0129378 A1 (CHAN) 27 May 2010 (27.05.2010) entire document	1-20
P, A	XU et al. Targeting skeletal endothelium to ameliorate bone loss, Nat Med., Vol. 24, No. 6, PMC, 21 November 2018, entire document	1-20

☐ Further documents are listed in the continuation of Box C. ☐ See patent family annex.

* Special categories of cited documents:
"A" document defining the general state of the art which is not considered to be of particular relevance
"E" earlier application or patent but published on or after the international filing date
"L" document which may throw doubts on priority claim(s) or which is cited to establish the publication date of another citation or other special reason (as specified)
"O" document referring to an oral disclosure, use, exhibition or other means
"P" document published prior to the international filing date but later than the priority date claimed
"T" later document published after the international filing date or priority date and not in conflict with the application but cited to understand the principle or theory underlying the invention
"X" document of particular relevance; the claimed invention cannot be considered novel or cannot be considered to involve an inventive step when the document is taken alone
"Y" document of particular relevance; the claimed invention cannot be considered to involve an inventive step when the document is combined with one or more other such documents, such combination being obvious to a person skilled in the art
"&" document member of the same patent family

Date of the actual completion of the international search	Date of mailing of the international search report
08 April 2019	03 MAY 2019
Name and mailing address of the ISA/US Mail Stop PCT, Attn: ISA/US, Commissioner for Patents P.O. Box 1450, Alexandria, VA 22313-1450 Facsimile No. 571-273-8300	Authorized officer Blaine R. Copenheaver PCT Helpdesk: 571-272-4300 PCT OSP: 571-272-7774